



National Library
of Canada

Acquisitions and
Bibliographic Services Branch

395 Wellington Street
Ottawa, Ontario
K1A 0N4

Bibliothèque nationale
du Canada

Direction des acquisitions et
des services bibliographiques

395, rue Wellington
Ottawa (Ontario)
K1A 0N4

Your file Votre référence

Our file Notre référence

NOTICE

The quality of this microform is heavily dependent upon the quality of the original thesis submitted for microfilming. Every effort has been made to ensure the highest quality of reproduction possible.

If pages are missing, contact the university which granted the degree.

Some pages may have indistinct print especially if the original pages were typed with a poor typewriter ribbon or if the university sent us an inferior photocopy.

Reproduction in full or in part of this microform is governed by the Canadian Copyright Act, R.S.C. 1970, c. C-30, and subsequent amendments.

AVIS

La qualité de cette microforme dépend grandement de la qualité de la thèse soumise au microfilmage. Nous avons tout fait pour assurer une qualité supérieure de reproduction.

S'il manque des pages, veuillez communiquer avec l'université qui a conféré le grade.

La qualité d'impression de certaines pages peut laisser à désirer, surtout si les pages originales ont été dactylographiées à l'aide d'un ruban usé ou si l'université nous a fait parvenir une photocopie de qualité inférieure.

La reproduction, même partielle, de cette microforme est soumise à la Loi canadienne sur le droit d'auteur, SRC 1970, c. C-30, et ses amendements subséquents.

Canada

**Aromatization of Light Olefins and Paraffins
on Pure and Hybrid ZSM-5 Catalysts**

Louise A. Dufresne

**A Thesis
in
The Department
of
Chemistry and Biochemistry**

**Presented in Partial Fulfilment of the Requirements
for the Degree of Doctor of Philosophy at
Concordia University
Montreal, Quebec, Canada**

February 1992

©Louise A. Dufresne, 1992



National Library
of Canada

Acquisitions and
Bibliographic Services Branch

395 Wellington Street
Ottawa, Ontario
K1A 0N4

Bibliothèque nationale
du Canada

Direction des acquisitions et
des services bibliographiques

395, rue Wellington
Ottawa (Ontario)
K1A 0N4

Your file Votre référence

Our file Notre référence

The author has granted an irrevocable non-exclusive licence allowing the National Library of Canada to reproduce, loan, distribute or sell copies of his/her thesis by any means and in any form or format, making this thesis available to interested persons.

L'auteur a accordé une licence irrévocable et non exclusive permettant à la Bibliothèque nationale du Canada de reproduire, prêter, distribuer ou vendre des copies de sa thèse de quelque manière et sous quelque forme que ce soit pour mettre des exemplaires de cette thèse à la disposition des personnes intéressées.

The author retains ownership of the copyright in his/her thesis. Neither the thesis nor substantial extracts from it may be printed or otherwise reproduced without his/her permission.

L'auteur conserve la propriété du droit d'auteur qui protège sa thèse. Ni la thèse ni des extraits substantiels de celle-ci ne doivent être imprimés ou autrement reproduits sans son autorisation.

ISBN 0-315-81031-9

Canada

CONCORDIA UNIVERSITY
Division of Graduate Studies

This is to certify that the thesis prepared

By: **Louise A. Dufresne**

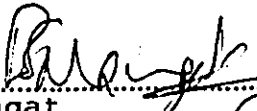
Entitled: **Aromatization of Light Olefins and Paraffins on
Pure and Hybrid ZSM-5 Catalysts**


and submitted in partial fulfilment of the requirements for the degree of


Doctor of Philosophy (Chemistry)

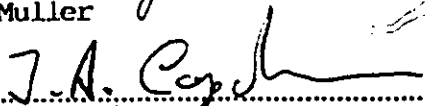
complies with the regulations of this University and meets the accepted standards with
respect to originality and quality.

Signed by the final examining committee:

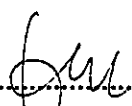

.....
Dr. B. Mangat Chair


.....
Dr. M. Ternan External Examiner

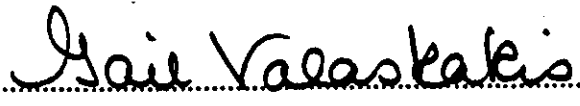

.....
Dr. F. Muller Examiner


.....
Dr. J.A. Capobianco Examiner


.....
Dr. R.H. Pallen Examiner


.....
Dr. R. Le Van Mao Thesis Supervisor


Approved by.....
Chair of Department or Graduate Program Director


May 5 1992
Dean of Faculty

ABSTRACT**Aromatization of Light Olefins and Paraffins
on Pure and Hybrid ZSM-5 Catalysts**

Louise A. Dufresne, Ph.D.
Concordia University, 1992

This dissertation presents the conception, synthesis, optimization and evaluation of a novel class of catalysts used in aromatization of short chain hydrocarbons.

It was found that when an acidic H-ZSM-5 zeolite with Si/Al atomic ratio equal to about 40, was mixed with a ZnO based co-catalyst, aromatization selectivity followed the principles of synergy. For a feed made up of mostly ethylene, as generated in a bench scale propane steam-cracker, ZnO precipitate in the amount of 5wt.-% or ZnO/Al₂O₃ co-precipitate in the amounts of 5-20wt.-%, provided optimum catalytic activity. Furthermore, it was established that for the co-precipitate, a Zn/Al atomic ratio equal to or greater than 1.0 conferred the best performance.

The distance between acid (aromatizing) major component and oxide minor component, was evaluated as being greater than 1 μ m. The increased aromatization selectivity found in hybrid systems was explained by the migration of hydrogen adsorbed species across surface boundaries. A Hydrogen Back-Spillover model was devised.

Sink and scavenging actions on co-catalyst surfaces, resulting in the formation of more important amounts of molecular hydrogen or ethane, were investigated. The differences in intrinsic selectivities of ZnO precipitate and ZnO/alumina co-precipitate (Zn/Al=1.0) were explained. The nature of the active sites was deduced from physico-chemical characterization data correlated with catalytic activity experiments.

The influence of preparation techniques as well as starting reagents was studied. The disordered nature of the co-precipitate, which is favorable to surface restructuration

during induction, was found to be a pre-requisite.

Kinetic studies of ethylene aromatization on a pure H-ZSM-5 zeolite, yielded a negative apparent activation energy, indicative of intracrystallite diffusional limitations. Thermogravimetric studies of used catalysts indicated that soluble coke was trapped inside the zeolite pores when the catalyst was used in its pure form at high temperatures. Migration of C_9^+ aromatic coke precursors out of ZSM-5 channels is induced by the co-catalyst, which gives rise to synergy in hybrid systems. A model based on transport barriers was proposed to explain hydrogen and coke migration.

Acknowledgements

I would like to acknowledge Dr. Raymond Le Van Mao for his guidance and encouragement during these graduate studies. Specifically, I would like to thank him for having taught me the importance of a synthetic and innovative approach to real problems.

I would also like to thank the members of my research committee, Dr. John A. Capobianco and Dr. Robert H. Pallen.

I would like to express my gratitude to Ms. Jianhua Yao and Mr. Riccardo Carli for their help and especially their scientific curiosity. Many new ideas have taken shape through our dynamic discussions. I would also like to acknowledge my friends and colleagues in the lab and the department.

I would like to thank my husband for his immense understanding, support and help, during both experimental and redaction stages of this work. His drive and continuous quest for knowledge have been exemplary.

At last, I would like to thank my family for believing in me.

Table of Contents

Table of Contents	vi
List of Figures	ix
List of Tables	xi
List of Abbreviations	xii
Chapter	
1.0	Introduction 1
1.1	Energy and crude oil 2
1.2	Catalysis: general 8
1.3	Catalysis: zeolites 15
.1	Zeolite synthesis 18
.2	Acidity in zeolites 19
.3	Bonding and catalytic activity 22
.4	Shape selectivity 24
1.4	Steam-cracking process 28
1.5	Ph.D. thesis presentation 31
Chapter	
2.0	Aromatization of light olefins and paraffins: catalyst development, optimization and evaluation of the catalytic reaction 33
2.1	Introduction 34
2.2	Experimental 37
.1	ZSM-5 zeolite synthesis 37
.2	Synthesis of the co-catalysts 40
.3	Acidity measurements 40
.4	Preparation of the catalysts 41
.5	Catalytic testing 41
.6	Product calculations 45
2.3	Results and discussion 48
2.4	Conclusions 72

Chapter	3.0	Evidence for the involvement of Hydrogen Back-Spillover in the aromatization of light olefins and paraffins on hybrid zeolite catalysts.	73
	3.1	Introduction	74
	3.2	Hydrogen effects in catalysis and hydrogen spillover	76
	3.3	Experimental	81
	.1	ZSM-5 zeolite synthesis	81
	.2	Synthesis of the co-catalysts	81
	.3	Acidity measurements	81
	.4	Hydrogen chemisorption measurements	83
	.5	Preparation of the catalysts	83
	.6	Catalytic testing	84
	.7	Product calculations	85
	3.4	Results and discussion	86
	3.5	Conclusions	110
Chapter	4.0	Physico-chemical characterization of catalytic components and correlation with the chemical reactivity of pure and hybrid systems.	112
	4.1	Introduction	113
	4.2	Experimental	116
	.1	ZSM-5 zeolite synthesis	116
	.2	Synthesis of the co-catalysts	116
	.3	Preparation of the catalysts	118
	.4	Catalytic testing	118
	.5	Product calculations	119
	4.3	Results and discussion	120
	4.4	Conclusions	145

Chapter	5.0	Kinetic study of ethylene aromatization on pure and hybrid catalysts	146
	5.1	Introduction	147
	5.2	Theoretical principles of kinetic studies.	150
	.1	Mechanism of contact catalysis	150
	.2	Catalyst evaluation	152
	.3	Measuring the properties of catalysts: catalytic reactors	154
	.4	Arrhenius equation	157
	5.3	Experimental	160
	.1	ZSM-5 zeolite synthesis	160
	.2	Synthesis of the co-catalysts	160
	.3	Preparation of the catalysts	160
	.4	Catalytic testing	162
	.5	Investigation of mass transfer limitations	164
	.6	Resume of chosen experimental conditions for kinetic studies	167
	.7	Product calculations	167
	.8	Data acquisition for kinetic studies	167
	5.4	Results and discussion	169
	5.5	Conclusions	197
Chapter	6.0	Conclusions	198
Chapter	7.0	References	202

List of Figures

1.1	Scheme of a modern refinery	4
1.2	Energetic pathways of catalyzed/uncatalyzed reactions	9
1.3	Energetic pathway of a catalyzed reaction	12
1.4	Arrangement of SBU and framework for a ZSM-5 zeolite	17
1.5	Chemical arrangement of the zeolite backbone	20
1.6	Geometric shape selectivity in zeolites	26
2.1	XRD powder pattern of H-ZSM-5(37)	38
2.2	Variation of total acidity content for co-precipitates	43
2.3	Experimental set-up for catalytic testings	44
2.4	Comparison of catalytic activity between pure and chemically modified ZSM-5 catalysts	49
2.5	Product yield variation as a function of the catalyst	51
2.6	Effect of ZnO content in co-precipitate on aromatic yield	54
2.7	Identification of aromatization and dehydrogenation components	55
2.8	Proposed reaction mechanism for olefin aromatization	57
2.9	Optimization of catalyst composition	58
2.10	Catalytic cycle on hybrid catalysts	60
2.11	Effect of catalytic reactor temperature on product yields	62
2.12	Comparison of total aromatic yields for pure and hybrid catalysts	63
2.13	Comparison of total aromatic yields for pure and hybrid catalysts	66
2.14	Optimization of catalyst composition	67
2.15	SEM photographs of co-catalysts	70
3.1	Hydrocracking tendency for pure and hybrid catalysts as a function of Si/Al ratio in zeolite	89
3.2	Hydrogen chemisorption of co-catalysts	97
3.3	Effect of distance between catalytic components	100
3.4	Effect of added hydrogen feed on catalytic activity	104
3.5	SEM photographs of hybrid catalyst extrudates (fresh/used)	106
3.6	Schematic representation of HBS action	111
4.1	BET plots (isotherm and pore size distribution)	122
4.2	Effect of preparation reagents on aromatization activity	126
4.3	SEM photographs of co-precipitates	130

4.4	Induction periods of ZnO-N at different temperatures	133
4.5	Induction periods of ZnO-N with different pretreatments	134
4.6	Induction periods of Zn/Al-S=1.0 at different temperatures	136
4.7	Induction periods of Zn/Al-S=1.0 with different pretreatments	137
4.8	Induction periods of Zn/Al-S=1.0 with different preparation methods	138
4.9	Stability of hybrid catalysts	139
4.10	Thermograms of alumina precipitates	140
4.11	Thermograms of ZnO precipitates	141
4.12	Thermograms of ZnO/alumina co-precipitates	144
5.1	Diffusion in contact catalysis	151
5.2	Chemical phenomena in contact catalysis	153
5.3	Dynamic concentration gradient reaction system	156
5.4	Experimental set-up for catalytic testings	163
5.5	Evaluation of mass transfer limitations for kinetic studies	165
5.6	Ethylene conversion on H-ZSM-5(43)	170
5.7	Ethylene conversion on ZnO hybrid catalyst	171
5.8	Ethylene conversion on ZnO/alumina hybrid catalyst	172
5.9	Ethylene conversion on ZnO precipitate	177
5.10	Ethylene conversion on ZnO/alumina co-precipitate	178
5.11	Arrhenius plot	179
5.12	Arrhenius plot	180
5.13	Product selectivities as a function of ethylene partial pressure	188
5.14	Thermograms for used H-ZSM-5(43) and hybrid catalysts	194

List of Tables

1.1	1987 estimated refining catalysts associated with fuels processing	7
1.2	Dimensions of zeolite pores and kinetic diameter of molecules	25
2.1	Physico-chemical characterization of zeolites	39
2.2	Acidity characterization of co-precipitates	42
2.3	Total product distribution from a propane steam-cracker	46
2.4	Catalytic activity of pure catalytic components	50
2.5	Effect of catalytic composition on catalytic activity of hybrids	53
2.6	Comparison of product distributions for pure and hybrid catalysts	64
2.7	Comparison of product distributions from pure feedstocks	68
3.1	Physico-chemical characterization of hybrid individual components	82
3.2	Effect of zeolite Si/Al ratio in n-butane aromatization	87
3.3	Hydrocracking tendency for hybrid catalysts	88
3.4	Conversion of n-butane on ZnO	90
3.5	Comparison of product yields for pure and hybrid catalysts	93
3.6	Aromatization activity and hydrogen yields	94
3.7	Results of hydrogen chemisorption experiments	98
3.8	Influence of distance on catalytic activity of hybrids	101
3.9	Influence of oxygen feed on aromatization for pure zeolite	103
4.1	Results of co-precipitate preparation calibration	117
4.2	BET total surface areas for co-catalysts from different reagents	121
4.3	Porosity of co-catalysts	123
4.4	Porosity of co-catalysts	125
4.5	Residual sulphate content	128
4.6	EDAX chemical analysis results of co-precipitates	132
5.1	Physico-chemical characterization of H-ZSM-5(43)	161
5.2	Effect of catalyst weight on mass transfer	166
5.3	Product selectivity for H-ZSM-5(43)	173
5.4	Product selectivity for ZnO hybrid catalyst	174
5.5	Product selectivity for ZnO/alumina hybrid catalyst	175
5.6	Apparent activation energies and pre-exponential factors	181
5.7	Product selectivities for pure and hybrid catalysts	185
5.8	Aromatic product distribution	192
5.9	Aromatic product distribution extracted from used H-ZSM-5(43)	196

Abbreviations

BET	Brunauer Emmett and Teller
BTX	Benzene, Toluene, Ethylbenzene, Xylenes and Styrene
CPMAS NMR	Cross Polarization Magic Angle Spinning Nuclear Magnetic Resonance
DTA	Differential Thermal Analysis
EDAX	Energy Dispersive Absorption X-ray
EGA	Evolved Gas Analysis
ESR	Electron Spin Resonance
ethylene_{ads}	Adsorbed Ethylene
FCC	Fluid Catalytic Cracking
FID	Flame Ionization Detector
FTIR	Fourier Transform Infrared Spectroscopy
GC	Gas Chromatography
GC-MSD	Gas Chromatography Mass Selective Detector
H_{ads}	Adsorbed Hydrogen
HC	HydroCarbon
H_{sp}	Spillover Hydrogen Species
HREM	High Resolution Electronic Microscopy
I.D.	Internal Diameter
IR	Infrared Spectroscopy
LPG	Liquefied Petroleum Gases
MAS-NMR	Magic Angle Spinning Nuclear Magnetic Resonance
MAS-SSNMR	Magic Angle Spinning Solid State Nuclear Magnetic Resonance
MSI	Metal Support Interaction
MTBE	Methyl TerButyl Ether
MTG	Methanol-To-Gasoline
O.D.	Outer Diameter
OPEC	Organization of Petroleum Exporting Countries
PFG NMR	Pulsed Field-Gradient Nuclear Magnetic Resonance
PNAH	PolyNuclear Aromatic Hydrocarbons
RON	Research Octane Number
SA	Silica Alumina
SACR	Spillover Assisted Catalytic Reactions

SBU	Secondary Building Units
SEM	Scanning Electron Microscopy
SIMS	Secondary Ion Mass Spectrometry
SMSI	Strong Metal Support Interaction
STEM	Scanning Transmission Electron Microscopy
TCD	Thermal Conductivity Detector
TGA	ThermoGravimetric Analysis
TPD	Temperature Programmed Desorption
TPD/MS	Temperature Programmed Desorption Mass Spectrometry
TPO	Temperature Programmed Oxidation
TPR	Temperature Programmed Reduction
WHSV	Weight Hourly Space Velocity (weight feed/weight catalyst)
WMSI	Weak Metal support Interaction
XPS	X-ray Photoelectron Spectroscopy
ZSM	Zeolite Socony Mobil

1.0 Introduction

1.1 Energy and crude oil

Energy is one of the most critical resources (1): without it life would cease. Food is our energy source. Through photosynthesis, the plant life we consume depends on energy from the sun. The materials we use to produce goods, are extracted from the earth's crust then transformed into finished products with expenditure of energy.

Since the industrial revolution and the invention of the steam engine, industrialized countries have come to depend more and more heavily on oil and natural gas for most of their energy needs. Besides its chemical diversity, liquid crude oil has the added advantages of easy extraction and transportation (2). Economically (1), it is considered a renewable natural resource, although its origin lies even before the appearance of the first men on earth.

Fossil fuel is an organic based material. Hydrocarbons with chemical structures similar to chlorophyll or heme (porphyrin) have been identified, which points to its biological beginnings.

The transformation of organic matter in petroleum and gas was a long and delicate process that took place in an *underground refinery*. Descent of the sediments was due to the weight of the earth's upper strata and increasing conditions of temperature and pressure with depth induced the genesis of hydrocarbons. Crude oil as known today, is the result of 60 million years of chemical transmutations, assuming a constant temperature of 100°C (2).

Depending on the reaction conditions (temperature, pressure, synthesis time), the intrinsic properties of a crude may vary sharply. For example, if the time is long or the temperature high, the oil will be light or less viscous. Its contaminant concentration will be low since every period of chemical transformation also acts as a purification step, favoring the enrichment in carbon and hydrogen. The commercial value of the resulting oil will be high because of easy extraction and less intensive refining operations. However, if the temperature is excessive or the time too long, all hydrocarbon molecules will be cracked to natural gas. The attractiveness of this raw material will be lower.

Heavy petroleum crude will be generated if the reaction conditions are not optimal (low temperature, shorter time). In this case, the characteristics of the crude will be:

- (1) very high viscosity;
- (2) high contaminant content (S, N, O, Ni, V, Fe, Na..);
- (3) high coking tendency conferred by polynuclear aromatic hydrocarbons (PNAH), asphaltenes, etc.

The commercial value of this material will be lower because it involves intensive refining operations.

Most of the world's oil is produced by a cartel (1) called the Organization of Petroleum Exporting Countries (OPEC). An advantage of petroleum crude produced in the Persian area is its low viscosity which results in low extraction costs i.e. a lower price per barrel, and low processing costs i.e. higher return on investment. In general, crude oil extracted in the Americas is heavier and more contaminated by metals and heteroatoms.

It is estimated (4) that world crude oil intake may grow from about 2.2b tonnes in 1985 to about 2.6b tonnes by the year 2000, mainly as a result of increased consumption in third world countries. Due to many factors, including political unrest in the Persian Gulf, the tendency for use of heavier crude as the world's reserves are dwindling, coupled with more stringent pollution laws, refining efficiency has become the major goal of petroleum companies. Great efforts are now directed toward perfecting the chemical technology associated with petroleum refining and transformations (3).

Because of its diversified origin and synthesis procedure, an untreated barrel of crude contains a wealth of fractions that can be separated by fractional distillation as the first step. Fig. 1.1 shows a typical oil barrel breakdown as well as a simplified version of a modern refinery. As seen, most processing steps of the refinery deal with the transformation of a feed into lighter products. *Whitening* or *lightening* of the barrel (4) is a world wide phenomenon which results from a higher demand for transportation fuels.

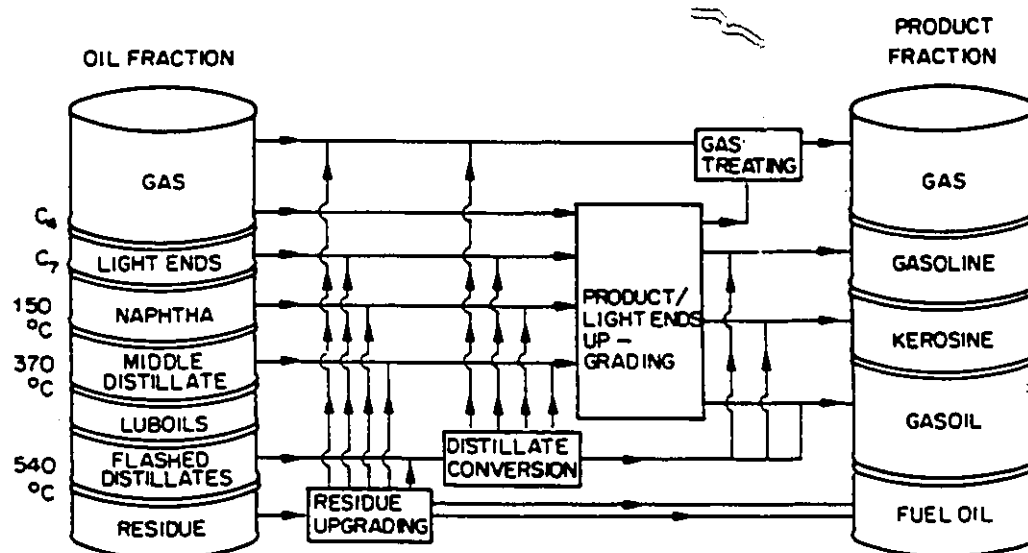


Figure 1.1 Simplified scheme of a modern refinery (from reference 4).

The aim of petroleum companies is to efficiently increase conversion to desired products, while coping with more contaminated feedstock and more severe smoke stack pollution laws. Refiners are also challenged by newly emerging regulations on car exhaust and noise (4). Lead phase out legislation and vapor pressure reduction (6) put the emphasis on finished product quality specifications. The result is the development of very selective processes that are also 'utilization intensive' of the crude oil barrel.

Optimization of existing processes is one solution for coping with socio-economic pressures for change. As discussed by Moukhlenov (3), the inter-related principal directions of chemical technology developments are:

- 1) increase of the reactor's dimensions to take advantage of its full capacity while improving work conditions;
- 2) optimization/intensification of the reaction system without changing the reactor size but rather its conception, for example;
- 3) mechanization/robotization in support of 2) while reducing the personnel;
- 4) automation, a step above 3);
- 5) replacement of batch operations with continuous ones that are inextricably linked with intensification and amelioration of product quality;
- 6) recycling the heat of reaction to achieve better energy efficiency and lower operation costs;
- 7) creation of new processes without waste by-products to simultaneously solve the environmental problem and the added cost of waste treatment.

All the above solutions deal mostly with optimization of the parameters as seen by a process engineer. The second route to be explored is tailoring of a reaction by the development of a catalyst.

The development of a novel or modified catalyst is a long process that requires chemists and engineers to work in tandem. Chemists are responsible for the conception, elaboration, formulation and the initial catalytic testings. Engineers model the reaction from a kinetic approach, diffusion approach, etc. They then determine the optimal reaction conditions, optimize the performance of the catalyst and the catalytic reactor and are responsible for scale-up procedures. Synergy must exist between chemists and

engineers so an idea can become reality, just as synergy may exist between a reaction and its catalyst or between the components of a specific catalyst.

It is estimated (5) that approximately 90% of the currently used chemicals and refinery processes are catalytic in nature. Three main areas of application can be identified: catalysts for the manufacture of chemicals (34%), petroleum refining (37%), and emission control (29%). Table 1.1 reports the breakdown of estimated refining catalyst consumption associated with fuels processing.

Catalysts are considered specialty chemicals sold mostly on the basis of performance rather than costs. Therefore, the catalyst industry or catalysis research within a refining industry, is highly intensive since profit margins are driven mostly by performance. Technology continues to advance rapidly due to the strong economic pressures to improve the selectivity, activity, lifetime and costs of catalysts (7-8). In turn, this has a large impact on feedstock utilization and plant overall capital and operating costs.

Table 1.1 1987 Estimated refining catalysts associated with fuels processing (adapted from reference 4).

Refining processes	Capacity millions of bpcd	Typical U.S. averages			1987 Estimated catalyst market, millions of U.S. dollars			
		Catalyst consum. lb/bbl	Usage millions of lb	Unit price \$/lb	U.S.	W. Europe	Others	World
Cat. cracking	4.9	0.2	380	0.7	250	76	131	457
Hydrotreating	8.4	0.005	28	3.0	84	42	63	189
Alkylation, H_2SO_4	0.50	18	3300	0.03	99	1	6	106
Hydrocracking	1.0	0.013	4.7	10.0	47	9	42	98
Cat. reforming	3.5	0.0033	4.5	6.5	27	15	21	63
Alkylation, HF	0.40	0.15	22	0.7	15	3	5	23
Isomerization	0.25	0.015	1.4	6.0	8	4	2	14
Oligomerization	0.05	-	-	-	-	-	-	-
Total					530	150	273	950

1.2 Catalysis: general

A catalyst is a chemical substance capable of directing and accelerating a thermodynamically feasible reaction (9) by providing an alternate reaction pathway. The energy barriers to chemical reaction with and without a catalyst are shown in Fig. 1.2. Since the velocity of the reaction is expressed as:

$$-\frac{d[A]}{dt} = k[A]^n[B]^m \quad (1-1)$$

where $k = A \exp(-\Delta E_a/RT)$ (11), the reaction rate at a given temperature will be increased by reducing ΔE_a or increasing the concentration of A and/or B. In the presence of a catalyst, which might chemically interact with A and/or B, the system will follow a new reaction path with a lower activation, ΔE_a . In effect the system passes through a new transition state.

Catalysts are observed to change while acting upon chemical species (10) and can be recovered with modifications after the reaction. In particular, the surface of heterogeneous catalysts is very sensitive to the reaction environment and undergoes changes due to sintering, coking, surface restructuring, etc.

Catalysts fall into two classes - homogeneous and heterogeneous.

Homogeneous catalysts are present in the same phase as the reactants and products, usually the liquid phase. Their main advantage is one of high selectivity or specificity because of tailoring possibilities via ligand selection or solvent effects, for example. Although selectivity is an important issue in catalytic chemistry, problems of reactor corrosion, separation and expensive catalyst recovery operations result in a low utilization of homogeneous catalysts in high volume chemical processes.

Heterogeneous catalysis applies to reactions where the catalyst is in a separate phase. These reactions may be gas/solid, liquid/solid and gas/liquid. Solid catalysts are widely used because of their attractiveness for continuous operation, easy regeneration

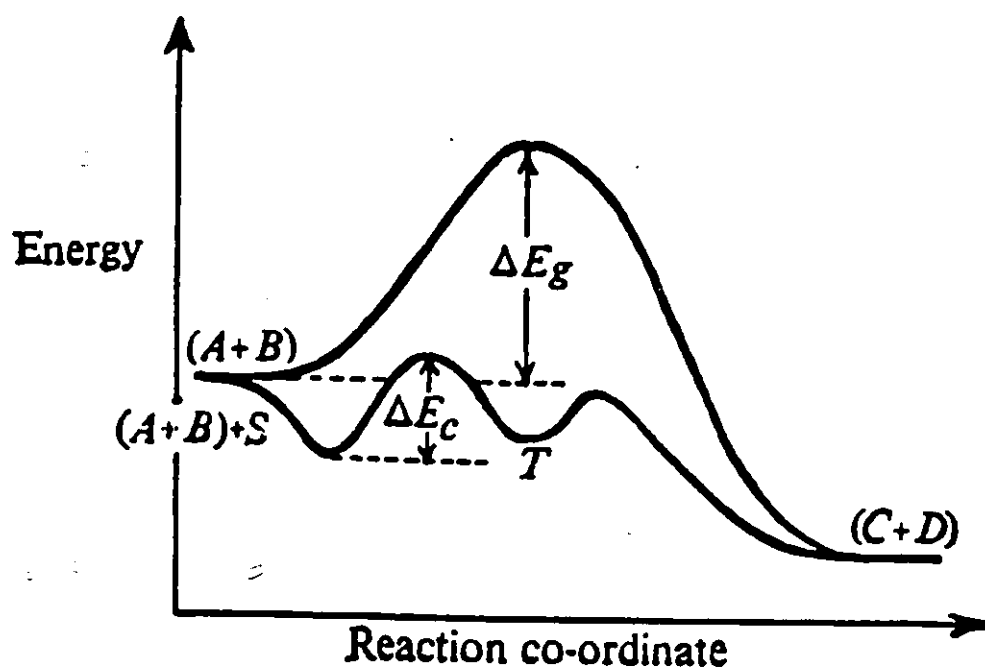


Figure 1.2 Energetic pathways of uncatalyzed and catalyzed reactions (from reference 11).

even during the reaction, facile separation, absence of reactor corrosion, long lifetime, endurance with respect to reaction conditions (high temperature and pressure) and flexibility in the reactor design. It is estimated (9) that more than 80% of the molecules in the >2.2b tonnes of crude oil processed annually worldwide, meet with a solid catalyst at one time or another during their trips through refineries.

In either case, homogeneous or heterogeneous catalysis, the catalytic act may be represented by five essential steps (10):

- (1) Diffusion to the catalytic site (reactant);
- (2) Bond formation at the catalytic site (reactant);
- (3) Reaction of the catalyst-reactant complex;
- (4) Bond rupture at the catalytic site (product);
- (5) Diffusion away from the catalytic site (product).

In the case of a homogeneous catalyst, steps (2)-(4) represent the formation and decay of the reactive intermediate. In heterogeneous catalysis, they represent the surface-adsorption and desorption with reaction of the surface intermediates.

Frontier areas and mechanistic relationships exist between homogeneous and heterogeneous catalysis. On the one hand, knowledge of the reaction mechanisms of many homogenous catalysts has been growing steadily(12), due to developments in molecular chemistry, especially organometallic chemistry. Proposed explanations for a variety of elementary steps has followed. In contrast, progress in the knowledge of detailed mechanisms on solid catalysts still remains more limited. One of the difficulties encountered in heterogenous catalysis is the almost unknown structure of the solid at the atomic level, including the active site. The frontier now being explored in an attempt to bridge the two domains is surface organometallic chemistry. An understanding of the mechanisms occurring on supported organometallics may increase the comprehension of the intrinsic workings of heterogeneous catalysts, while extending homogenous catalysis into new areas.

The surface of a heterogenous catalyst is energetically non-uniform (10), in contrast to the uniform nature of supported organometallics in terms of active site

geometry, electronic properties, etc.,. The surface atoms of heterogeneous catalysts are exposed to varying degrees of coordinative unsaturation, so it is possible that adsorbed reactants are too strongly bonded to undergo further reaction on some active centers. Equally, adsorption may be too weak on others to allow a sufficiently reactive intermediate to form. Therefore, optimum conditions for adsorption and desorption as well as a certain prerequisite of surface uniformity exist for any particular reaction.

The process of adsorption on the surface of a heterogeneous catalyst is exothermic, while desorption is endothermic. Two types of adsorption can be identified: physisorption and chemisorption.

The forces of attraction involved in physical adsorption are similar to non-ideal gases: van der Waals (13). The temporal fluctuations in the electron density about the nucleus of the reactant and atoms in the surface region of the solid, cause the creation of instantaneous dipole moments. In turn, they create very weak van der Waals attraction forces (13). The process is unactivated and multilayers of adsorbate molecules can be formed. Physisorption is usually a prerequisite in the formation of a chemisorbed species.

Since a chemical bond is formed with the surface, the second type of adsorption is known as chemisorption. Energy of activation may be required for a molecule to chemically bond to the surface and only a monolayer of adsorbate molecules is possible.

Fig. 1.3 A shows the formation of a chemisorbed species, associatively or dissociatively, in the form of Lennard-Jones potential energy curves. If the solid line pathway representing associative chemisorption is followed, chemisorbed species undergo a reaction that involves an activation energy, E_{ads} . It also can be seen that as reactant molecules approach the solid surface, they must first pass through the van der Waals envelope and so begin their activation as physisorbed species. In associative chemisorption, the activated complex will have a potential energy that is decreased by the heat of chemisorption, ΔH_c (Fig. 1.3 B). In other words, chemisorption supplies some of the energy required to form the activated complex, which otherwise would have to depend solely on temperature as the energy source. Transformation of the activated complex gives the chemisorbed product which then endothermally desorbs.

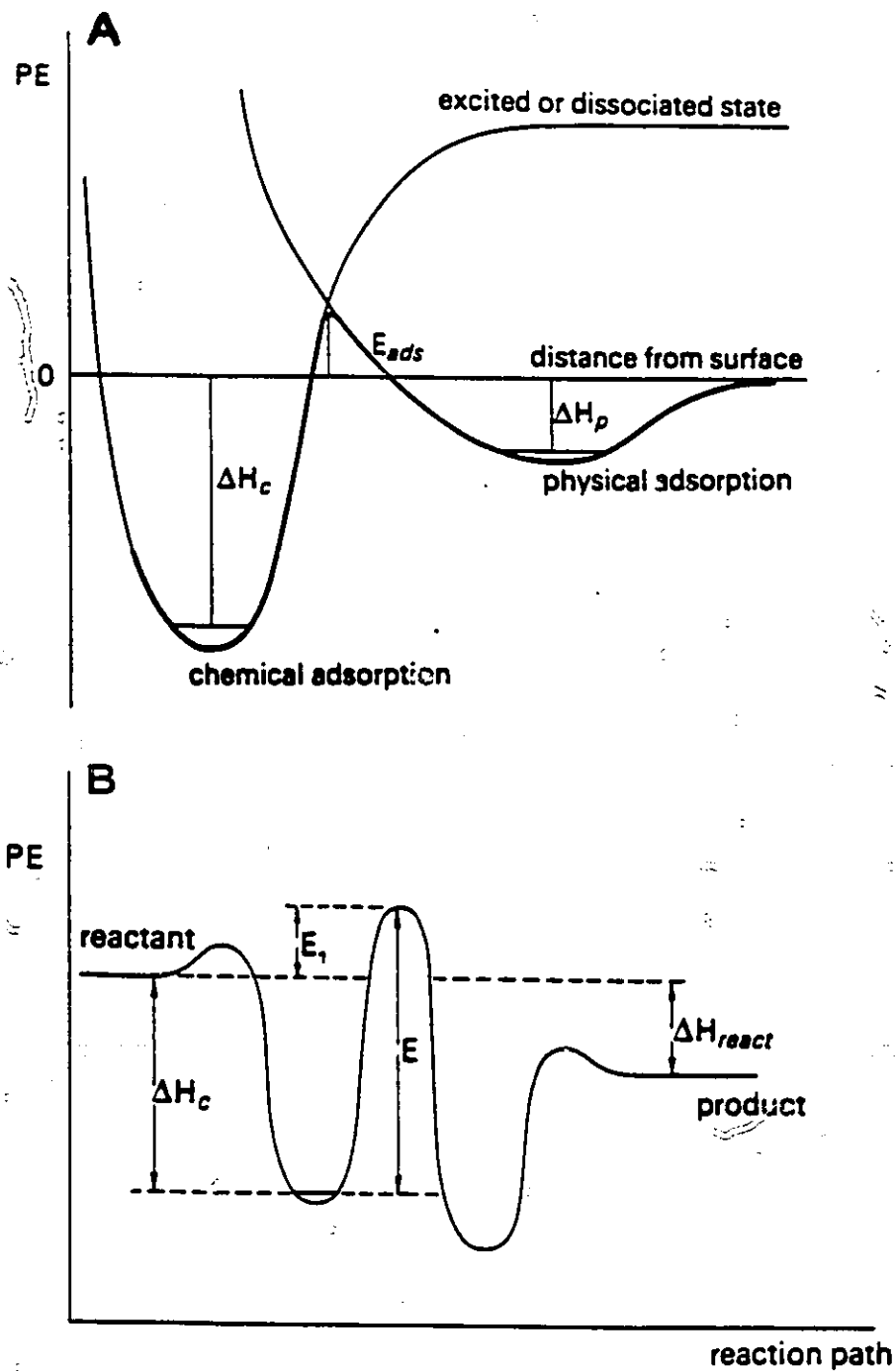


Figure 1.3 Energetic pathway of a catalyzed reaction. (A) Lennard-Jones potential energy curves showing physisorption and chemisorption on a surface; (B) Energy associated with a catalyzed reaction (from reference 10).

Fig. 1.3 B demonstrates how a catalytic surface may lower the activation energy of a chemical reaction. The same reaction taking place in the gas phase would have an activation energy E . On the catalyst surface, the required energy has been lowered by ΔH_c , so E_1 now represents the activation energy of the reaction. Therefore, the reaction rate will be greater for the same temperature, if the reaction is catalytic. Activity is defined by the above principles.

Catalytic selectivity is not as easily explained. It is a function of the heat of desorption, but more importantly it depends on the nature of the interaction between the reactant molecules and the active centers on the catalyst surface. Furthermore, the nature of the active centers will determine the type of activated complex formed and ultimately the products of the reaction.

The difficulty in calculating surface energetics points to the reason why catalysts are discovered by extensive experimental screening. In fact the development of a new or improved catalyst (5) is a tedious, time consuming process involving a combination of good science, hard work, experience and considerable serendipity. Catalyst development is not however totally empirical, as a great deal of preselection is now employed.

Fluid Catalytic Cracking (FCC) is an example of catalytic process adaptation to increased selectivity demands. FCC is a process for the formation of gasolines (4). It started in 1936 (14) as a fixed bed technology on acid treated clays. At the end of WWII, because of increasing gasoline demand, an amorphous synthetic aluminosilicate replaced montmorillonites and hallosites. In early 1960, synthetic faujasite was discovered and the domination of FCC by zeolites began. This discovery was paralleled by the development of a rising reactor that allowed regeneration of the catalyst during reaction, although continuous FCC processes included regenerators were in use for many years before riser reactors were utilized. Rare earth exchange of zeolites X, Y and ultrastabilization of the framework resulted in a large increase of cracking activity and gasoline yield. Today, strong economic pressures to process more abundant, less expensive metal contaminated crudes and resids prevail. The new generation of FCC catalysts will be designed to incorporate metal resistance, octane enhancing and pollution curtailing functions.

Zeolites and other molecular sieves are finding widespread application in a diversity of areas. They are unique catalysts because their pores are uniform and are of sizes comparable with small molecules (15). Zeolites are called molecular sieves because they can discriminate between molecules on the basis of size. Molecules smaller than the aperture size are internally adsorbed, while the larger ones are not. Therefore, zeolites offer an immense selectivity advantage over amorphous analogs, thus explaining their growing importance in the chemical industry (16-17).

1.3 Catalysis: zeolites

The term zeolite was coined by Cronstedt in 1756 as a name for an extraordinary aluminosilicate mineral that appeared to boil when heated (18). Since that time more than 40 naturally occurring zeolites have been identified (15, 18, 25). The scope of zeolite structural chemistry has been broadened by the success of laboratory syntheses that have yielded many structures and compositions with no natural counterparts. The diversity of interest in zeolite chemistry has been fuelled by:

- (1) economic rewards of industrial applications of zeolites in such fields as petroleum processing, petrochemicals, chemicals synthesis, pollution control (19) and as detergent builders (15);
- (2) developments in synthetic procedures;
- (3) application of new techniques to zeolite characterization (20-24).

Zeolites are hydrated, crystalline tectoaluminosilicates (15, 18) formed under hydrothermal conditions (26). They have a framework structure constructed from TO_4 tetrahedra (T = tetrahedra atoms, e.g., Si, Al) that share vertices (18). The individual tetrahedra are always close to regular. Because the shared oxygen linkage can accommodate T-O-T angles between 130° and 180° , they can combine into a variety of framework topologies.

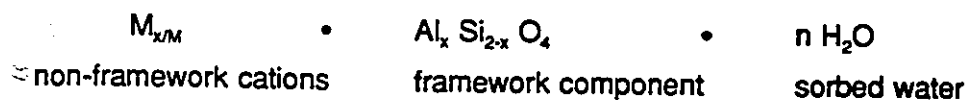
Several groups of zeolite structures exist, differentiated by the nature of the secondary building units (SBU) which compose them. SBU can be made up of 4-16 tetrahedra (25). The number and spacial organization of the SBU, determine the type of configuration of the zeolite's microporous network (dimension aspect) and the internal volume (channel density and level of interconnection between channels). The apertures of the pores are polygons, which can be separated in four categories:

- (1) hexagonal (aperture $\approx 0.3\text{nm}$);
- (2) octagonal (aperture $\approx 0.5\text{nm}$);
- (3) 10-ring (aperture $\approx 0.6\text{nm}$);
- (4) 12-ring (aperture $\approx 0.8\text{nm}$);

The aperture dimensions control accessibility into the zeolite's internal volume, so the common name: molecular sieves.

For example (Fig. 1.4), SBU of the ZSM-5 zeolite are 5-1 or a normal five membered ring to which is attached another TO_4 . The SBU are linked to form chains and the irreducible pattern (repeating unit) in a chain is made up of eight 5-ring cycles. The chains are organized to form a tridimensional network with parallel channels in one direction and zig-zag channels in the other. The aperture is defined by a 10-ring opening ($\approx 5.5\text{\AA}$) (25). This zeolite is considered to be a medium pore size type, a member of the pentasil family.

A general formula for aluminosilicate zeolites can be written as:



Because the chemical composition may vary within a zeolite structure, framework topology is used as an identification method for any particular zeolite.

Aluminium atoms isomorphously replace silicon atoms in the zeolite framework and they adopt a tetrahedral coordination with four oxygens. The net charge on aluminium is (-1) since it carries a (+3) valence charge. When tetrahedra containing Si and Al are linked to form the zeolite backbone, the negative charge associated with each aluminium atom is balanced by a positive ion to preserve electrical neutrality (cations of alkali metals, alkali earth metals and the proton). If H^+ is used as the counter ion, acid properties are generated on the surface of the solid, which cause acid catalysis on zeolites. This aspect will be discussed more thoroughly in section 1.3.2.

In general, tectoaluminosilicates do not have Si/Al ratios < 1 , so an aluminium atom does not have another aluminium atom in its second coordination shell. The framework stability would not benefit from this arrangement because of the octahedral forming tendency of aluminium with sorbed water molecules. The aluminium avoidance rule is commonly called Lowenstein's rule (15) and holds true for the majority of zeolites (20, 25-27) although some exceptions have been identified using IR and MAS ^{29}Si -NMR (29).

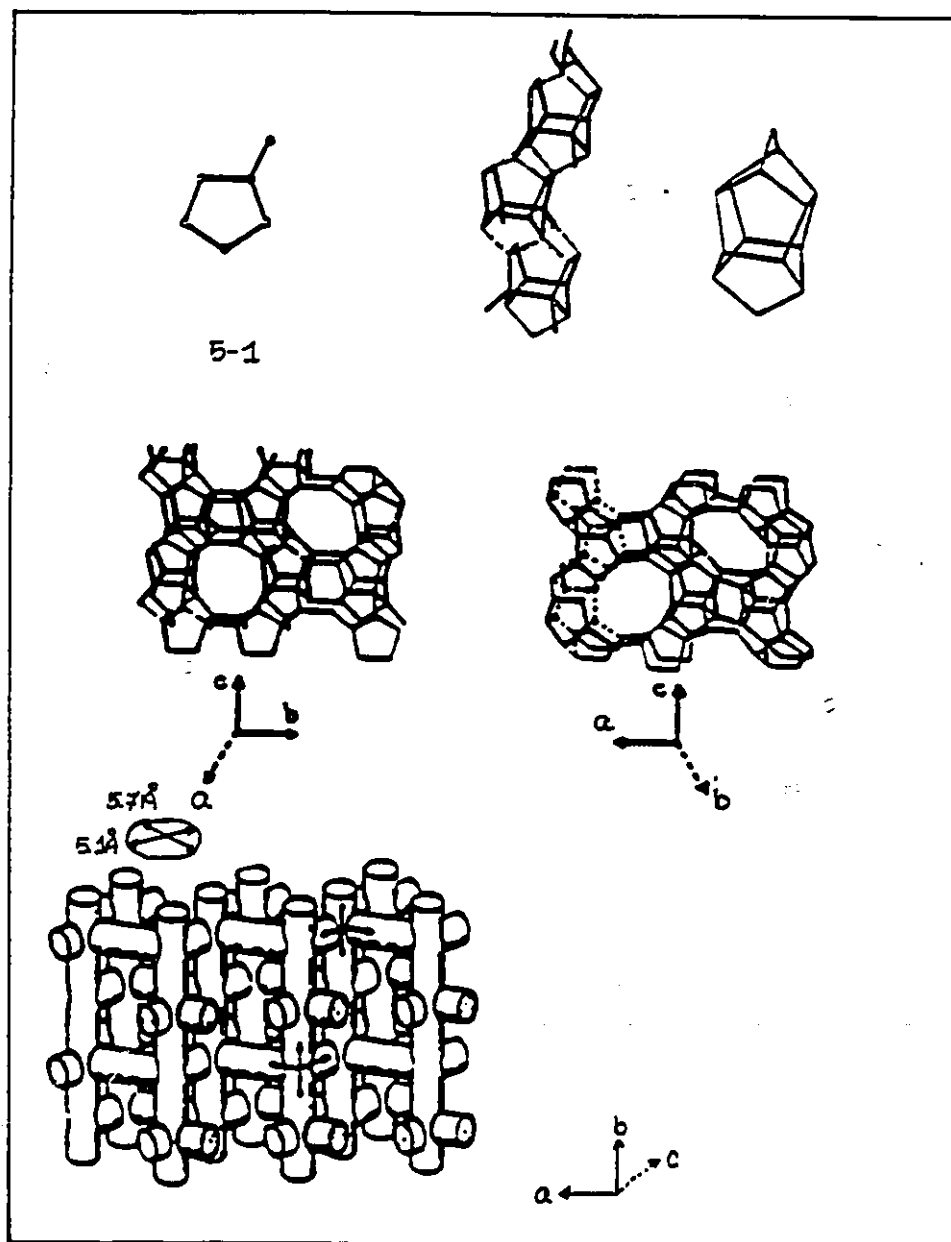


Figure 1.4. Arrangement of the secondary building blocks (SBU) in a ZSM-5 zeolite framework in a step by step approach (from reference 28).

1.3.1 Zeolite synthesis

Hydrothermal synthesis of aluminosilicates refers to the crystallization of zeolites from aqueous systems that contain the necessary chemical components. A zeolite synthesized rapidly (several days) and at low temperature, may exhibit differences with respect to its mineral analog because of a lack of ordering in the synthetic structure. In fact, most of the synthetic zeolites are produced under non-equilibrium conditions and are considered thermodynamically metastable phases. According to the simplicity principle of Goldsmith (26), synthesized zeolites exhibit high simplicity which is synonymous with disorder, structural simplicity or high entropy. Since growth of the crystalline phase first requires the formation of a nucleus, the precursors of a structurally disordered form most likely favor nucleation and the development of a metastable phase (maybe several of them). As a result, zeolite crystallization is fairly easy, but care must be taken to control all synthesis conditions accurately in order to avoid the formation of intertwined zeolite structures.

The general conditions used for synthesis are (26):

- (1) reactive starting materials such as a freshly co-precipitated gel produced by the co-polymerization of the individual silicate and aluminate species, by a condensation/ polymerization mechanism;
- (2) relatively high pH introduced in the form of an alkali metal hydroxide or other strong base to allow complete dissolution of silicate species initially and depolymerization of the synthesis gel later (28);
- (3) low temperature (RT-175°C) hydrothermal conditions with concurrent low autogenous pressure at saturated water vapor pressure;
- (4) high degree of supersaturation of the components in the gel leading to the nucleation of a larger number of crystallites.

The gel synthesis of zeolites from aluminosilicate gels of alkali or alkali-earth metals is common, especially to reproduce natural analogs synthetically. The laboratory synthesis of alkylammonium-based or nitrogenous zeolites is also possible. However, zeolites crystallized from N-systems require the presence of an alkali hydroxide, particularly Na^+ , in nearly every case. Traces of sodium (26) appear to help in the

nucleation step, and the rate of crystallization has been shown to depend on the $[\text{Na}^+]$ for type N-A. Synthesis from N-systems for zeolite A results in different characteristic properties. In particular, comparison of the aperture size of Na-A and N-A shows a smaller dimension for N-A.

Tetrapropylammonium cation (TPA^+) is used in the synthesis of the ZSM-5 zeolite. TPA^+ acts as the template during the aging step and is directly involved in the resulting directionality of the framework and the medium pore size. However, ZSM-5 zeolites have also been synthesized in the absence of a template (30-31).

1.3.2 Acidity in zeolites

As discussed in Sections 1.3 and 1.3.1, the isomorphous substitution of Si by Al results in the formation of a negatively charged framework, and a cation must be introduced to preserve electrical neutrality. Synthesis in the presence of alkali metal (e.g., Na^+), yields the sodium form of the zeolite (Fig. 1.5 A).

The most interesting applications of zeolites are based on zeolites acting as solid acid catalysts (19, 24, 32-34). To obtain the acid form of the zeolite, sodium ions are replaced by protons by ion-exchange with an ammonium salt, followed by heating to decompose the NH_4^+ into NH_3 and H^+ (Fig. 1.5 B). Pfeifer *et al.* (23) have shown using proton MAS-NMR, that ammonium ions can still be present in HY zeolite up to 450°C and contribute to the measured acid density but are not active in catalysis.

After ammonia evolution, the protons bond with lattice oxygens to give OH groups. Some sites represent Brønsted acid sites in the bridging position between Al and Si atoms (Fig. 1.5 C). They are identified by IR as low frequency (LF) bands at 3650 and 3545 cm^{-1} in zeolite HY (35) and 3602 cm^{-1} in H-ZSM-5 (24). The bridging OH groups are active in acid catalysis and are sites of carbenium ion formation (36). A high frequency (HF) band at $\sim 3740\text{ cm}^{-1}$ is also observed by IR and has been ascribed to terminal OH groups (24, 35). Spectroscopic evidence for the presence of internal silanols (Si-OH) in ZSM-5 (aluminium independent cation exchange) has been demonstrated by Woolery and co-workers (37). Terminal and internal silanols have been shown to be inactive in acid catalysis (24, 35, 37).

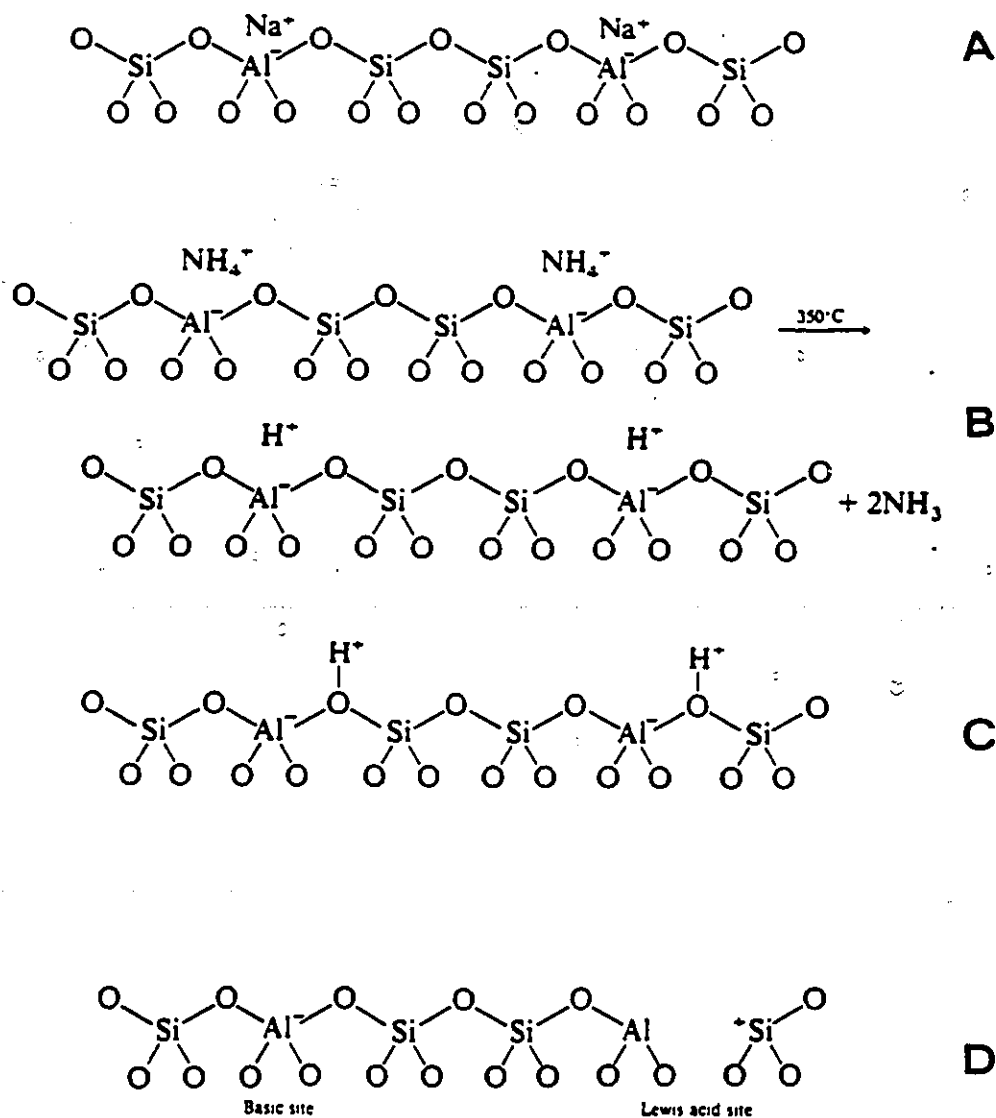


Figure 1.5 Chemical arrangement of the zeolite backbone. (A) Sodium form of the zeolite after synthesis; (B) Ammonium form after ion exchange and evolution of ammonia at high temperature; (C) Acid form of the zeolite with the generation of Brønsted acid sites; (D) After heating at higher temperature, dehydroxylation of the surface and generation of Lewis acid and basic sites (from reference 36).

Upon further heating ($>475^{\circ}\text{C}$) (27, 35), reversible Lewis acid and basic sites can be formed progressively (Fig. 1.5 D) as adsorbed water is removed.

As discussed by Barthomeuf (32), Védrine *et al.* (24) and Pfeifer and co-workers (23), although several methods exist to characterize the acid density and strength, as well as the nature of the active sites, it is very difficult to elaborate a static model predicting the exact configuration of the zeolite surface. Protons have been shown to be mobile during a catalytic reaction (23, 32) so a rigorous model should consider zeolite dynamics in attempting a complete description of acid properties.

The superficial electric fields generated in decationized or acid zeolites (27), when they are submitted to high temperature (increased proton mobility), have been shown to be sufficiently high to polarize the C-H bonds of n-paraffins and to result in the formation of an instantaneous dipole, which is a prerequisite to physisorption (13).

Choudhary *et al.* (33-34) have associated the acid strength distribution of the zeolite surface to site energy distribution in studies of pyridine adsorption and temperature programmed desorption. Upon comparison of the total acidity vs site energy distribution of catalytically important zeolites, they have established the following orders (34):

- (1) for total acidity: $\text{CeNaX} > \text{HKL} > \text{HY} > \text{CeNaY} > \text{H-ZSM-5} > \text{H-ZSM-11}$
- (2) when ordered as a function of strong acid sites (i.e. acid sites which can chemisorb pyridine at 623K): $\text{HY} > \text{CeNaX} > \text{CeNaY} > \text{H-ZSM-5} > \text{HKL} > \text{H-ZSM-11}$
- (3) when further compared on the basis of the number of strong acid sites per active aluminium (i.e. $q_{\text{I(pyridine 623K)}} / (C_{\text{Al}} - C_{\text{Na}})$): $\text{H-ZSM-5} > \text{HY} > \text{CeNaY} > \text{H-ZSM-11} > \text{CeNaX} > \text{HKL}$.

In H-ZSM-5 having a Si/Al ratio of ~ 40 , 50% of the active aluminium atoms were found to be strong acid sites (34).

The acid strength distributions on zeolites and the observed differences in strong acid sites, acidity distributions and number of strong acid sites per active Al, have been attributed by Choudhary *et al.* (34) to the presence of structural Al⁺ in different

environments/ configurations, depending on Si/Al ratios, exchanged cations and channel structures. In highly siliceous zeolites such as ZSM-5, it was demonstrated that the quality of Brønsted Al sites was high (strong acid/ active Al), as expected because of a wide separation of framework Al⁺.

1.3.3 Bonding and catalytic activity

Using XPS, Barr and co-workers (20) demonstrated that the properties of a zeolite surface are a function of framework structures, relative compositions, nature of cations and exchange levels. Using a series of zeolites and pure oxides as reference, they showed that the relative covalency/ ionicity character of the mixed oxides followed a progressive change in bonding properties (20).

- (1) the Si-O bond of SiO₂ is much more covalent than the Al-O bond in an aluminate system;
- (2) in zeolites, upon increasing the Si/Al ratio (decreasing the aluminium content NaA → NaX → NaY → Na-mordenite → Na-ZSM-5), the system gradually evolved to the natural covalency of the Si-O units in pure SiO₂, while driving up the ionicity of the Al-O bond and Na-O bond. Similarly, progressive acid strength increase was observed with increases in the Si/Al ratio.

Barr *et al.* state (20) that probably the most important single conclusion of these studies is that the oxide in a zeolite is a highly *polarizable* unit that may provide a *variable*, largely ionic field or one that is much more covalent.

The activity of a zeolite surface toward hydrocarbon activation is therefore a collective property of the zeolite framework (20, 29). The Si/Al ratio has a direct influence on the strength of the Brønsted acid sites and is related to the covalency/ ionicity of the TO₄ units. Ultimately, it is connected to electronegativity in zeolites with the presence of local electrostatic fields in the channel network (38).

According to Clément (39), the activity and selectivity of molecular sieves are related to an electrostatic factor that depends on the type of zeolite used and on the

polarity of a diffusing molecule (in or out). In fact, the Si/Al ratio and the nature of exchanged cations can result in the creation of a perpendicular electric field at the pore openings. This field can initially interact with the dipole moment of a reactant molecule in a Coulomb type interaction, to either create a potential barrier or favor inward diffusion of sterically unfavored species.

The framework topology and structure of zeolites have been suggested to be factors which influence the specific energy of framework atoms and adsorbed species, perhaps implying the presence of an internal crystal field (40-41). In fact, using $n\text{-C}_7$, $n\text{-C}_8$ and $n\text{-C}_{10}$ alkanes and a variety of zeolite structures, selectivity was demonstrated to depend on the cage structure and was not related to any geometric effect. The variables affecting the cracking mechanism of the above alkanes were rationalized using a field gradient approach. The strength of this field gradient was related to the nature of the zeolite surface: a low density of AlO_4^- tetrahedra in a given zeolite framework and the presence of long narrow channels were said to increase the field gradient due to greater distances between charges.

Polarization of molecules inside the reaction loci by London dispersive forces of attraction (13), induces the creation of multipole moments that make the adsorbate molecules dependent on the field gradient. The resulting selectivity in n -alkane cracking (40-41) could not be explained by purely geometric effects.

1.3.4 Shape selectivity

Shape selectivity has received new and intensive attention since the discovery of ZSM-5 type zeolites, because the channel dimensions are approximately the same as the molecular dimensions of many aromatic molecules (table 1.2), and favor the formation of *para*-substituted benzenic species (42-49).

Three main and inter-related factors influence shape selectivity (39):

- (1) a geometric factor which depends on the molecule geometry and the configuration of the solid;
- (2) an electrostatic factor as discussed in section 1.3.3, which can influence the in-/ out- diffusion of sterically bulky molecules;
- (3) a diffusivity factor which depends on the textural properties of the solid (particle size, pore dimension) and the diffusivity coefficients of molecules.

This factor is superimposed on (1). In fact, ZSM-5 and ZSM-11 zeolites can be produced with intrinsic activities and diffusion properties extending over a wide range of magnitudes, by systematically varying the number of active centers (Si/Al ratio, chemical modification...) and/or crystal size (50).

Three main types of geometric molecular shape selectivities have been identified (Fig. 1.6) (51):

- (1) Reactant selectivity;
- (2) Product selectivity;
- (3) Restricted transition state selectivity.

Reactant selectivity is observed when only a selected reactant or a class of reactants is able to enter and diffuse freely in the intracrystalline free void volume of the zeolite network (Fig. 1.6 A). Dwyer and co-workers (52) have demonstrated the effect of reactant selectivity on the basis of molecules converted during dewaxing of waxy distillate chargestocks on ZSM-5. They showed that *n*- or methyl-branched alkanes were converted but at least 1/3 of the more highly branched alkanes remained after the reaction. Their conclusion was that ZSM-5 actually discriminates on the basis of

Table 1.2 A Dimensions of zeolite channels and apertures (adapted from references 40-41).

Zeolite	Pore type	Cage size (nm)	Aperture (nm)
H-ZSM-5	Channel		0.54 X 0.56
	Intersection	0.9	0.52 X 0.58
Erionite	Cage	1.3 X 0.63	0.36 X 0.52
Mordenite	Channel		0.67 X 0.7
Faujasite	Intersecting Cavities	1 to 1.3	0.74
H-NaX	Supercage	1 to 1.3	0.74

Table 1.2 B Dimensions of molecules (adapted from references 26, 39).

	Kinetic diameter (Å)
H₂	2.89
Methane	3.8
Ethylene	3.9
Propane	4.3
Propylene	4.5
n-Butane	4.3
iso-Butane	5.0
1-Butene	4.5
n-Hexane	4.6-4.9
Cyclohexane	6.0 (26)
	6.9 (39)
Benzene	5.85 (26)
	4.8 (39)
o-Xylene	7.4
m-Xylene	7.4
p-Xylene	6.8
Naphthalene	7.4

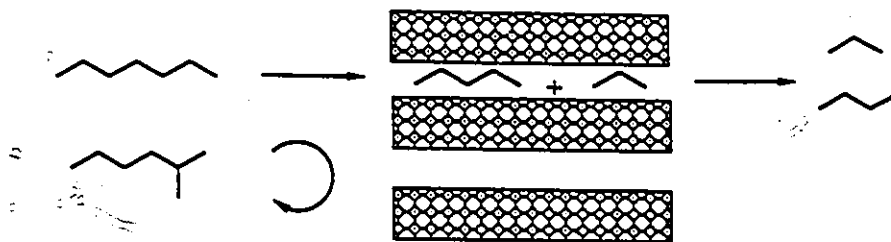
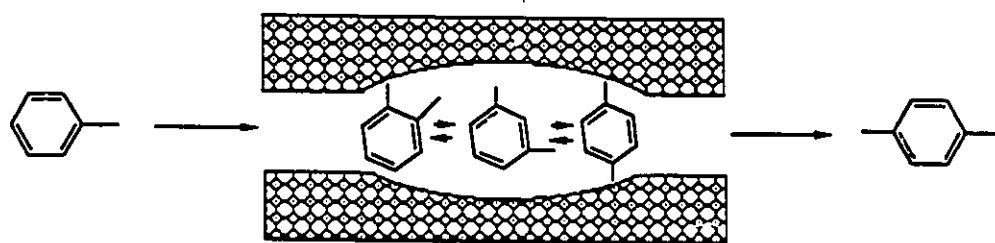
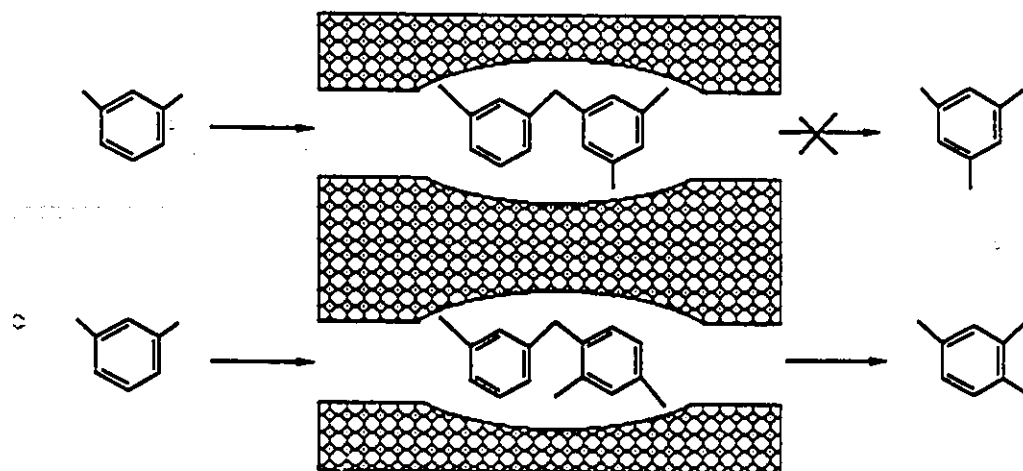
A: Reactant selectivity**B: Product selectivity****C: Restricted transition state selectivity**

Figure 1.6 Illustration of different geometric shape selectivities occurring in zeolites.

molecular shape as well as size in catalytic conversions (52).

Product selectivity is obtained when some of the product molecules are too bulky to freely diffuse out of the zeolite and are then converted to smaller product molecules by cracking or rearrangement, or to bulkier products that deactivate the material (coke deposit). Notable examples of product selectivity are the isomerization of xylenes and the alkylation of toluene by methanol (53-54). Both reactions strongly favor the formation of the *para*- isomer in ZSM-5 (Fig. 1.6 B). Butter *et al.* (55) have shown *para* selectivity with chemically modified ZSM-5 in the formation of xylenes on alkylation of toluene with methanol. They report greater than 90% *para* isomer in the xylene product.

Restricted transition state selectivity occurs when certain reactions are inhibited because of local steric configuration constraints imposed by the environment of the active sites (cage, channel intersection, etc) (Fig. 1.6 C). This type of shape selectivity is attached to a modification of reaction kinetics rather than limits to the diffusivity of molecules (39). An example of restricted transition state selectivity was demonstrated in the cracking of paraffins (50).

Catalyst deactivation is industrially a very important problem. The aging characteristics of zeolites are a function of pore structure and acid site distribution for pore blockage, pore size (shape selectivity constraints) and site poisoning (51). It was shown that restricted transition state shape selectivity was responsible for limiting the amount of coke formation in the ZSM-5 zeolite (39).

The success of zeolites in the petrochemical / refining industry is attributed to their activity, selectivity, regular structure and stability. Since the discovery of the ZSM-5 by Mobil workers, many processes dealing with dehydrogenation, isomerization, aromatization, etc., have been 're-invented', with product yields and selectivities never thought possible with conventional amorphous aluminosilicates, chromia/alumina or platinum/alumina catalysts. The conception of selectivity in hydrocarbon processing has undergone an irreversible transformation. Not all petrochemical processes are based on zeolites however, or are even catalytic in nature. A notable example of an uncatalyzed reaction is the steam- cracking process, the starting point of this research.

1.4 Steam-cracking process

Steam-cracking is an example of a non-catalyzed, high volume petrochemical process, that would benefit from product up-grading to meet today's market demands, while minimizing energy costs (56-57).

Steam-cracking evolved from thermal cracking. In 1890, the addition of steam was shown to orient the product distribution of an oil thermal cracker, favoring lighter fractions (58). Today, steam-cracking is responsible for the production of most light olefins: ethylene, propylene, butenes, butadiene, the building blocks of the modern world (polymerization to plastics, rubber...). A by-product of the process is the formation of pyrolysis oils. They are composed of benzene, toluene, ethylbenzene, xylenes, styrene (BTX compounds with high commercial value) and polynuclear condensated aromatic hydrocarbons. BTX compounds are extracted using a solvent and up-graded further by alkylation, disproportionation or isomerization, catalytically (59).

In Europe and Japan, most processes are based on naphtha feedstock because of the low availability and high cost of lighter feedstocks (60). In the U.S. and Canada, gaseous feeds (ethane, propane, butane) separated from natural gas are abundant and at reasonable costs, so plants mostly operate with light paraffin feeds (called LPG-Liquefied Petroleum Gases, more specifically nC_3 - nC_4).

Highly severe conditions prevail in a typical steam-cracker (high temperature: 800-900°C; short residence time: 0.1-0.4 sec) for the selective production of light olefins, while minimizing aromatic yields. The water partial pressure is controlled according to the desired product spectrum (0.5- 0.9 atm) (61).

The mechanism governing the steam-cracking product distribution is a free radical one (61-64). The values of hydrocarbon initial partial pressures and the presence of steam favor monomolecular processes and so increase ethylene selectivity (61). The formation of aromatic compounds is attributed to secondary reactions (63). In the pyrolysis of paraffins, aromatics are formed during the synthesis reactions of lower hydrocarbons. In the case of oligocyclic naphthene feeds, degradation reactions dominate aromatic formation. The tendency for aromatization is unavoidable under industrial

conditions, resulting in the formation of pyrolysis oils or coke deposit in the reactor.

Because of the free radical mechanism in a steam-cracker, the product spectrum is dependent on the severity in the cracker. Increased severity results in increased ethylene yield and lower aromatic forming tendency. However, in today's market an important selectivity parameter is the propylene/ethylene (P/E) ratio. When industry trends are studied, it becomes apparent that the propylene yield must be increased (65,87), while naphtha steam-crackers reorient themselves toward LPG feedstocks (66-68).

Propylene is produced mainly from saturated hydrocarbons by primary reactions. It is also produced by secondary reactions via thermal decomposition of C_4 or higher olefins (87). When the process temperature is high, the rate of propylene disappearance exceeds the rate of formation. The maximum propylene yield from propane feed is about 65-70% conversion (P/E:0.32/pass; propylene yield 28wt.-%). The maximum economical P/E ratio (at 65% conversion) is 0.69, including recycle of ethane and propane to extinction. The choice of feedstock is an important parameter controlling the production of propylene. For example, when ethane is used as feedstock only 2-4 pounds of propylene are produced for every 100 pounds of ethylene (P/E: 0.2-0.4) as compared with the yields obtained from propane feedstock (P/E: 0.32-0.69).

A method that would increase the propylene yield and control the P/E ratio would be desirable. Also, any improvement of the steam-cracking process should keep in mind a desired high selectivity to BTX products. Presently, a typical BTX/total aromatic ratio in the pyrolysis oils of a propane steam-cracker can vary between 10-65 wt.-% depending on the temperature.

Some catalysts have been used in steam-cracking. To improve ethylene and ethane yields, Koltz and Delzer (69) have used a calcium-promoted MgO supported catalyst. Lemonidou and Vasalos (70) have shown that a $12CaO-7Al_2O_3$ catalyst can increase the ethylene production of a laboratory scale n-hexane steam-cracker operated under mild conditions. Although the results show increased ethylene selectivity or potentially lower energy costs, the P/E ratio is not favorably modified. Also, the composition of the pyrolysis oils remained heavy.

In a novel approach designed by Le Van Mao (71), a catalyst composed of Cr_2O_3 /alumina mixed with Zn-ZSM-5 zeolite or Zn-ZSM-5 asb-zeolite was shown to significantly increase the C_2 - C_4 olefin yield of a propane steam-cracker, while increasing the BTX/total aromatic ratio to more than 80wt.-%. In its initial conception, a catalytic reactor was placed in series with a bench scale horizontal steam-cracker. All effluents (including vaporized pyrolysis oils and steam) were allowed to pass over the bicomponent catalyst for up-grading.

In the present project, the same approach was pursued. A propane steam-cracker was operated under typical conditions (high severity; short residence time) and a normal product spectrum was obtained (Specifications of Pétromont Inc. Qc). A catalytic reactor operated between 500-550°C was placed in series and a H-ZSM-5 or modified/ bicomponent-ZSM-5 catalyst was used. The main difference between this and the previous work was the incorporation of a condensing flask between the cracker and the catalytic reactor to trap water and heavy hydrocarbons. At high temperature, steam has the ability to promote zeolite dealumination and the creation of extraframework aluminium species. With time, a destabilization of the zeolite framework is observed. In order to avoid this form of zeolite deactivation, water was condensed prior to the up-grading step. Only the gaseous effluents were allowed to come in contact with the catalyst.

The selectivity of an unmodified H-ZSM-5 depends on the Si/Al ratio of the framework and the resulting acid density and strength. It was found that the use of a pure zeolite did not significantly change the product spectrum obtained in the uncatalyzed steam-cracking process. Therefore, chemical modification of the zeolite internal framework or use of bicomponent catalysts prepared by admixing, were investigated as a means of modifying C_2 - C_4 olefin yields and P/E ratios. Economically, the price of bicomponent catalysts containing less expensive co-catalyst components, is more advantageous than using the ZSM-5 alone. This is especially true if the product distribution is favorably manipulated.

A great variety of oxide based co-catalysts were tried with minimal improvement of the C_2 - C_4 olefinic fraction after the condensing flask was installed. However, the mixed catalytic system composed of Cr_2O_3 /alumina ($\text{Cr}/\text{Al}=0.15$) (40wt.-%) prepared by incipient wetness impregnation mixed with a H-ZSM-5 ($\text{Si}/\text{Al}=20$) (40wt.-%) and reduced prior to

the reaction, resulted in an increased total aromatic yield of more than 13.5wt.-% compared with the uncatalyzed product spectrum obtained at 840°C. A jump in the BTX/total aromatic ratio was also recorded for the uncatalyzed and catalyzed reactions (10wt.-% vs 86wt.-%).

Since the aromatization propensity was present in several other experimental runs using different catalytic systems, it was decided to follow the natural tendency of the reaction and to aim to produce BTX aromatics from the downstream gases of a propane steam-cracker.

1.5 Ph.D. thesis presentation

The best catalysts identified in this work have been bicomponent catalysts where the co-catalyst can be pure ZnO or a ZnO/Al₂O₃ co-precipitate, admixed with an unmodified H-ZSM-5 (Si/Al≈40) zeolite.

In Chapter 2, following an initial literature review, the results of catalytic screening, catalyst evaluation and optimization will be discussed. The factors influencing catalytic activity will be presented. An explanation will be offered for the synergy existing between the two components based on a Hydrogen Back-Spillover approach.

Chapter 3 will develop the spillover hypothesis by presenting more probing evidence, including monitoring of hydrogen evolution during reactions and the effects of added hydrogen partial pressure.

Chapter 4 will deal with the characterization aspect of the zeolite and co-catalyst. The influence of catalyst preparation and pretreatment will be correlated with reaction data. Physico-chemical results including BET, TGA, SEM/ EDAX will be discussed. In a before/after approach (since *in situ* analysis was not available), an attempt will be made to correlate the intrinsic properties of the materials with the activities of pure and mixed catalytic systems.

Chapter 5 will be concerned with the evaluation of the kinetic parameters. Comparison of the individual behaviors and product distributions of pure and hybrid systems tested under identical conditions, will be used to gain information about the mechanistic pathways. The feedstock used for kinetics studies will be pure ethylene as a simplification step. When appropriate, differences between ethylene and n-butane reactions on bicomponent catalysts will be pointed out.

This work presents the discovery of a first generation of ZnO based hybrid catalysts that exhibit synergy in aromatization of light olefins and paraffins. A hydrogen spillover explanation is at the heart of the improved aromatization processes. The concept of long-distance modification of catalytic activity has been firmly established in the course of this Ph.D. research work.

2.0 Aromatization of light olefins and paraffins:
Catalyst development, optimization and evaluation of the catalytic reaction

**Partially presented at the 3rd Chemical Congress of North America, Toronto
Canada, June 5-10 1988.**

Partly published in ref. 72, 73.

2.1 Introduction

Aromatic hydrocarbons are important commodity chemicals in the petroleum industry. The most commercially valuable aromatics are the BTX compounds (benzene, toluene, ethylbenzene and xylenes), which also can be used as octane enhancing additives for motor gasolines (74) (although Methyl- TerButyl Ether or MTBE (RON 115) and other oxygenated compounds are increasingly used because of their clean burning properties (75-76)).

Aromatics are currently produced by catalytic cracking of naphtha and catalytic reforming of various petroleum-derived feedstocks, etc (10,14,36,76). Aromatics can also be produced by catalytic conversion of light alcohols (particularly methanol), olefins or paraffins. The Methanol-To-Gasoline process or MTG (78), as well as the olefins- and/or paraffins-to-gasoline-and-distillate processes or MOGD, M2-Forming and M-Forming (79-83) were all developed by Mobil Oil. They are based on a catalyst which belongs to the pentasil zeolite family: ZSM-5. As discussed in the first chapter, this synthetic zeolite is a tridimensional crystalline aluminosilicate with acid sites of varied strengths depending on the location of Al atoms and the Si/Al molar ratio. Its intermediate pore size (ca. 5.5Å) and intersecting channel network, result in specific transition state and product shape selectivities due to the configurational constraints of the reaction loci, which favor the production of monoaromatics or p-substituted dialkylbenzenes.

In the MOGD, M2-Forming and M-Forming processes (79-83), the acidic form of ZSM-5 zeolite, or H-ZSM-5, having a Si/Al₂O₃ ratio of 70, is used alone to convert olefinic or paraffinic feeds into liquid hydrocarbons of highly aromatic content. The desired products of M2-Forming are the BTX aromatics with an average hydrogen content of about 8.7wt.-% (80). When a feedstock such as propane is used with an 18.3wt.-% hydrogen content, the excess hydrogen must be rejected in the form of hydrogen rich products such as H₂, CH₄, C₂H₆ and C₃H₈. A stoichiometric limitation is thus established for the aromatization propensity of the reactant. Only a small amount of molecular hydrogen gas (1.0- 1.9wt.-%) is produced using pure H-ZSM-5. The hydrogen production is believed to be an acid site-mediated transfer reaction as proposed by Haag and Dessau (84).

Other processes commercially available for converting light petroleum gases (LPG) to aromatics include:

- (a) Thermal/ Catalytic Pyroform process from Kinetics Technology International Corp./ Pyrotec (85) for the aromatization of C_2 and/or C_3 paraffins under high severity conditions;
- (b) British Petroleum's CYCLAR process (86, 88) which is aimed at the dehydrocyclo-dimerization of C_3 and C_4 paraffinic gases over a gallium-containing zeolite catalyst (Ga introduced by reflux). In this case, a hydrogen yield of 5.6wt.-% has been observed when 100% propane feed is used (55.9wt.-% total aromatics);
- (c) Phillips's STAR process (STeam Active Reforming) (89-90) which employs Pt and Sn supported on zinc aluminate (gahnite) to catalytically dehydrogenate isobutane and propane with more than 85% selectivity to isobutene and propylene. The Phillips' STAR process utilized with an isobutane feed, can be coupled with an MTBE or alkylation unit to generate high octane additives.

El Tanany *et al.* (91) have described the phenomenon of hydrogen spillover when a H-erionite zeolite is activated by a platinum/ alumina catalyst and flowing hydrogen gas prior to its catalytic reaction with n-heptane. The Pt/ Al_2O_3 component is at the source of the surface migration of adsorbed hydrogen species or spillover hydrogen, which activates the erionite lattice.

Previous studies have demonstrated that chemically modified zeolites such as zinc-bearing ZSM-5, have enhanced aromatizing activity in alcohol conversion (92-93). The incorporation of group VIII, IIB, IB elements (94), of gallium and of platinum (95-96) into ZSM-5 zeolites, or of platinum into a modified gallosilicate of the same porous structure (97), can also lead to significantly greater aromatics production from light paraffins when compared with a pure H-ZSM-5.

From the previous information, it is apparent that two distinct modes of zeolite activation exist: activation of a zeolite (e.g., H-erionite) by hydrogen spillover (91), and activation of a zeolite toward aromatic production by incorporation of certain metals in the framework (94-96).

In the first case, the *activator* ($\text{Pt}/\text{Al}_2\text{O}_3$) in a reducing atmosphere, is put in contact with the zeolite catalyst for a predetermined period preceding the catalytic reaction. Using a special reactor, the *activator* is removed before $n\text{-C}_7$ feed introduction. During activation, the distance between both components (erionite and *activator*) is considerable ($\geq 1\mu\text{m}$). It is the spillover hydrogen species (H_{sp}) which migrate across the boundary of two distinct surfaces and are responsible for activation of the zeolite. Long- distance remote control of catalytic activity can then be implied with zeolite catalysts.

In the second case, it has been seen that for olefinic and paraffinic feeds, the incorporation of metals such as gallium, zinc or platinum into the zeolite framework results in a significantly increased aromatization activity. The high aromatic selectivity has been ascribed to bifunctional catalysis between zeolite acid sites and metal (metallic or ionic) functions, presumably because dehydrogenation of reaction intermediates on metal sites is faster than hydrogen transfer on the acid sites (98). Therefore, production of aromatics and consequently hydrogen in the gas phase is enhanced. The inconvenience of having the two catalytic sites close by in the zeolite lattice, is that the catalyst needs to be regenerated frequently. In the absence of added hydrogen, the production of coke in the reaction loci is very significant. Consequently, catalytic decay is accelerated by the action of pore blocking. For bicomponent $\text{Ga}_2\text{O}_3/\text{H-ZSM-5}$ catalysts where the dehydrogenating function is located outside the zeolite channels, changes in stability and resistance to coking have been observed (101, 114). The increased stability was directly related to the size of the gallium species with an almost atomic dispersion being shown to be a prerequisite for sustained catalytic activity and selectivity (114).

In this work, catalytic performance obeying the principles of synergy has been observed using for historical reasons, a mixture of olefins and paraffins. This catalysis originates when a redox and acidic/ basic component (99), such as a zinc oxide-based precipitate, is put in proximity to a H-ZSM-5 zeolite acid catalyst. It is believed (72-73) that the co-catalyst behaves as a hydrogen porthole, intercepting the hydrogen species released during the aromatization sequence of olefinic or paraffinic compounds inside the zeolite channels. The aims of this chapter are to compare the activity and selectivity of the parent pure H-ZSM-5 zeolite or chemically modified zeolite, with those of hybrid catalysts, to evaluate the catalysts and the catalytic reaction using pure and mixed feeds and to attempt an initial description of the promoting effects induced by the co-catalyst.

2.2 Experimental

2.2.1 ZSM-5 zeolite synthesis

Several zeolites were synthesized according to the method of Argauer and Landolt (100). The composition of the synthesis gel and the parameters were selected so the resulting zeolites had a Si/Al atomic ratio ranging between 25 and 55.

The acid form, or H-ZSM-5(Si/Al ratio), was obtained by ion- exchange with a 5wt.-% ammonium chloride solution in deionized water at 80°C, under mild stirring. The ion- exchange solution was replaced every hour with a fresh supply, for at least eight consecutive times. The solid was then filtered, washed with deionized water and dried overnight at 120°C. Subsequently it was activated in air at 550°C for about 10 h.

Gallosilicate and alumino- gallosilicate having the ZSM-5 tridimensional structure were also synthesized. In the synthesis gel, the required amounts of gallium nitrate were introduced instead of sodium aluminate. Synthesis and treatment of the zeolite powder was identical to that described above.

In the case of an acid zeolite which was modified by zinc ions, ion- exchange was used. A 5wt.-% zinc nitrate solution in deionized water and the H-ZSM-5(20) powder were stirred at 80°C for 1h. The solid was then filtered, washed with deionized water and dried overnight at 120°C. Subsequently it was activated in air at 550°C for about 10 h. An amount of 0.63wt.-% Zn^{2+} was introduced by this operation.

The zeolite powder in its acid form was characterized by X-ray powder diffraction for qualitative identification of the ZSM-5 structure (Fig. 2.1)(100) and for measurement of its degree of crystallinity. NaCl was used as an internal standard and H-ZSM-5(20)/NaCl mixture as an external standard, as described by Le Van Mao *et al.* (102). Atomic absorption determined the exact chemical composition. BET measurements using an ASAP 2000 apparatus from Micromeritics yielded the total surface area. Adsorption and temperature programmed desorption (TPD) of ammonia studies provided the acid density properties. Scanning electron microscopy (SEM) showed an average particle size for the zeolite powders of 2-3 μm . Table 2.1 reports the results of the above characterization

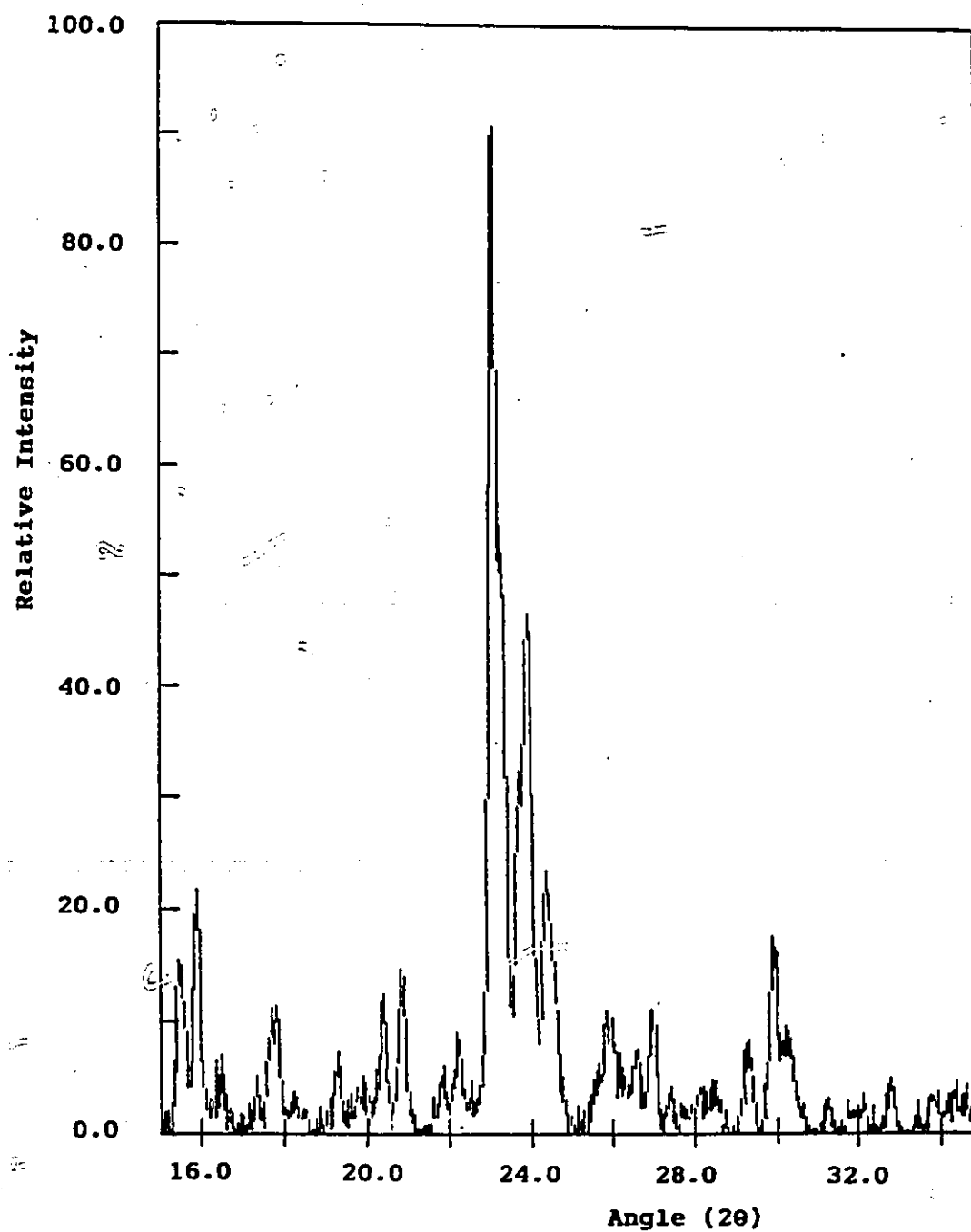


Figure 2.1 XRD powder pattern of H-ZSM-5(37).

Table 2.1 Physico-chemical characterization of the H-ZSM-5 zeolites (pure and modified) used in the exploratory studies.

	Catalyst Identification			
	H-ZSM-5 (37)	H-ZSM-5 (34)	H-Ga-ZSM-5	H-GaAl- ZSM-5
Si/Al ratio	37.7	34.0	-	40.5
Si/Ga ratio	-	-	5.2	10.2
Si/(Ga + Al) ratio	-	-	-	8.1
Na ₂ O content (wt%)	0.08	0.17	0.14	0.26
DC	102.3	94.0	95.7	104.0
BET Surface Area (m ² /g)	360	384	-	-
Acidity by Temperature Programmed Desorption (TPD) of Ammonia				
Catalysts	Temperature ^a (°C)	Acid Density (mol/g)(x10 ⁴)	Total (mol/g) (x10 ⁴)	
H-ZSM-5(37)	93	13.97		
	218	10.72		
	366	3.25		
	508	3.12	31.06	
H-ZSM-5(34)	151	9.82		
	224	7.71		
	370	2.60		
	520	2.50	22.63	
H-Ga-ZSM-5	120	11.35		
	220	7.69		
	368	2.23		
	516	2.24	23.51	
H-GaAl-ZSM-5	121	9.33		
	225	7.65		
	363	2.49		
	510	2.16	21.63	

DC: Degree of crystallinity with respect to H-ZSM-5(20).

(a): Temperature of desorption peak maximum.

experiments.

Prior to using a new zeolite, standard catalytic tests for pure and hybrid catalysts were conducted to ensure uniformity and reproducibility with previously synthesized batches.

2.2.2 Synthesis of the co-catalysts

The co-catalysts were prepared by heterogeneous co-precipitation. A liquid mixture of soluble zinc nitrate (hexahydrate) and aluminium sulfate (decahydrate) for the $\text{ZnO}/\text{Al}_2\text{O}_3$ co-precipitates, or pure soluble salts to yield the pure oxides, was prepared. The solution, kept at 50°C , was adjusted to $\text{pH } 7.5 \pm 0.5$ by the dropwise addition of ammonium hydroxide (28vol.-%) under vigorous stirring conditions. The gel-like substance was further stirred for 2h at 50°C and aged without agitation for 70h at room temperature. The resulting polymeric hydroxides were washed thoroughly to remove most of the soluble ammonium salts, evaporated to dryness and activated in air at 550°C for about 10h. Mixed oxides or pure oxides were obtained.

The co-catalysts were crushed and sieved (80-100 mesh). They were characterized by atomic absorption, X-ray powder diffraction, BET surface area, SEM and TPD of ammonia.

2.2.3 Acidity measurements

For the zeolite and co-precipitate surfaces, the technique of temperature programmed desorption (TPD) of ammonia was used to determine the acid site density and relative acid strengths (102). The operative procedure was similar to that described by Derouane *et al.* (103).

The catalyst extrudates (0.8g) were loaded in a quartz reactor and pretreated at 550°C under flowing He overnight. *In situ*, NH_3 was adsorbed at room temperature for 1h. After thorough flushing with He (1.5 h) to remove most free or physisorbed ammonia molecules, the *chemisorbed* ammonia was desorbed by linearly increasing the temperature at a rate of $15^\circ\text{C min}^{-1}$, from room temperature to 530°C . A SRI student GC

equipped with a thermal conductivity detector (TCD) and set on-line with the system was used to detect the desorbed ammonia in the eluted gas stream. The NH_3 uptake was estimated by integration of the TPD trace as a function of time. Known amounts of NH_3 were injected into the GC as a volumetric calibration procedure, so the TCD responses could be reported as acid densities (mol/g). Furthermore, knowing the time of the desorption peak maximum, the temperature of desorption was determined. In principle, as desorption temperature increases, so does the strength of the acid sites (102).

Table 2.2 reports the acidity characteristics of the different co-precipitates and commercial ZnO(BAKER) used in the present work. Fig. 2.2 is a graphical representation of total acid densities obtained. However, since it was shown by Tanabe *et al.* (99) that the surface of $\text{ZnO}/\text{Al}_2\text{O}_3$ prepared by heterogeneous co-precipitation contains both acidic and basic sites using Hammett indicators, it is possible that the ammonia TPD uptake curves incorporate some deviation because of dissociation of the ammonia molecules.

2.2.4 Preparation of the catalysts

To prepare the final catalysts, the H-ZSM-5 powder (mesh size higher than 60) and the alumina, zinc oxide- aluminium oxide or zinc oxide precipitate powders (mesh size higher than 60) were mechanically mixed at room temperature. Bentonite clay (20-60wt.-%) was then incorporated and intimately mixed with the solid catalyst. Deionized water was added dropwise until a malleable paste was obtained. The latter was extruded into 1.5mm O.D. *spaghettis*. They were dried at 120°C overnight and activated in air at 550°C for about 10h. The final length of the catalyst extrudates was $5 \pm 0.5\text{mm}$.

2.2.5 Catalytic testing

Figure 2.3 shows the schematic experimental set-up. The extruded catalyst was loaded in a quartz tubular reactor (R_2) and heated by a digitally controlled electrical furnace. Control of temperatures, as well as feed and carrier gas (nitrogen) flow rates was done through automatic devices as shown. The feed was composed of gaseous olefinic and paraffinic hydrocarbons, as generated in a bench scale steam- cracker (R_1 and V1), or pure feedstocks (ethylene, propylene, propane and n-butane) (V2 introduction).

Table 2.2 Acidity characteristics of co-catalysts as measured by temperature programmed desorption (TPD) of ammonia.

Mixed Oxides			
Zn/Al molar ratio	Temperature ^a (°C)	Acid Density (mol/g) (x10 ⁴)	Total (mol/g) (x10 ⁴)
0.16	118	4.60	
	162	5.61	
	335	2.39	
	370	5.46	18.06
0.39	108	5.47	
	172	4.70	
	218	7.78	
	396	8.27	26.22
1.0	126	6.34	
	176	14.41	
	378	6.06	26.81
2.4	162	4.44	
	289	11.59	16.03
Pure Oxides			
Al ₂ O ₃ -S ^b	120	4.48	
	169	3.49	
	330	3.94	
	375	5.46	17.38
ZnO precipitate	104	1.32	
	210	1.54	
	500	0.27	3.13
ZnO(BAKER)	101	1.91	
	504	0.48	2.39

(a): Temperature of desorption peak maximum.

(b): Al₂O₃ precipitate from Al₂(SO₄)₃.

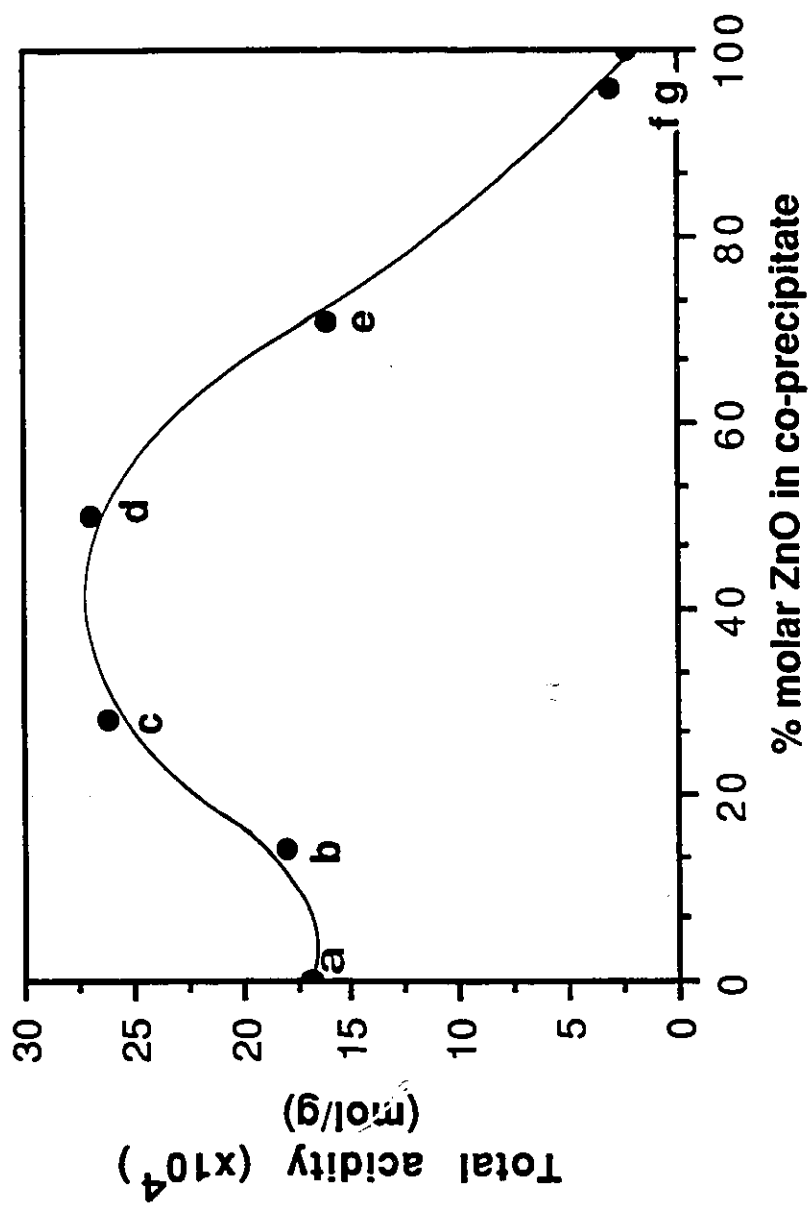


Figure 2.2 Variation of total acidity of co-precipitate with ZnO content.

Co-precipitate identification:

- (a) $\text{Al}_2\text{O}_3\text{-S}$
- (b) $\text{Zn}/\text{Al} = 0.16$
- (c) $\text{Zn}/\text{Al} = 0.39$
- (d) $\text{Zn}/\text{Al} = 1.0$
- (e) $\text{Zn}/\text{Al} = 2.4$
- (f) ZnO precipitate
- (g) ZnO(BAKER)

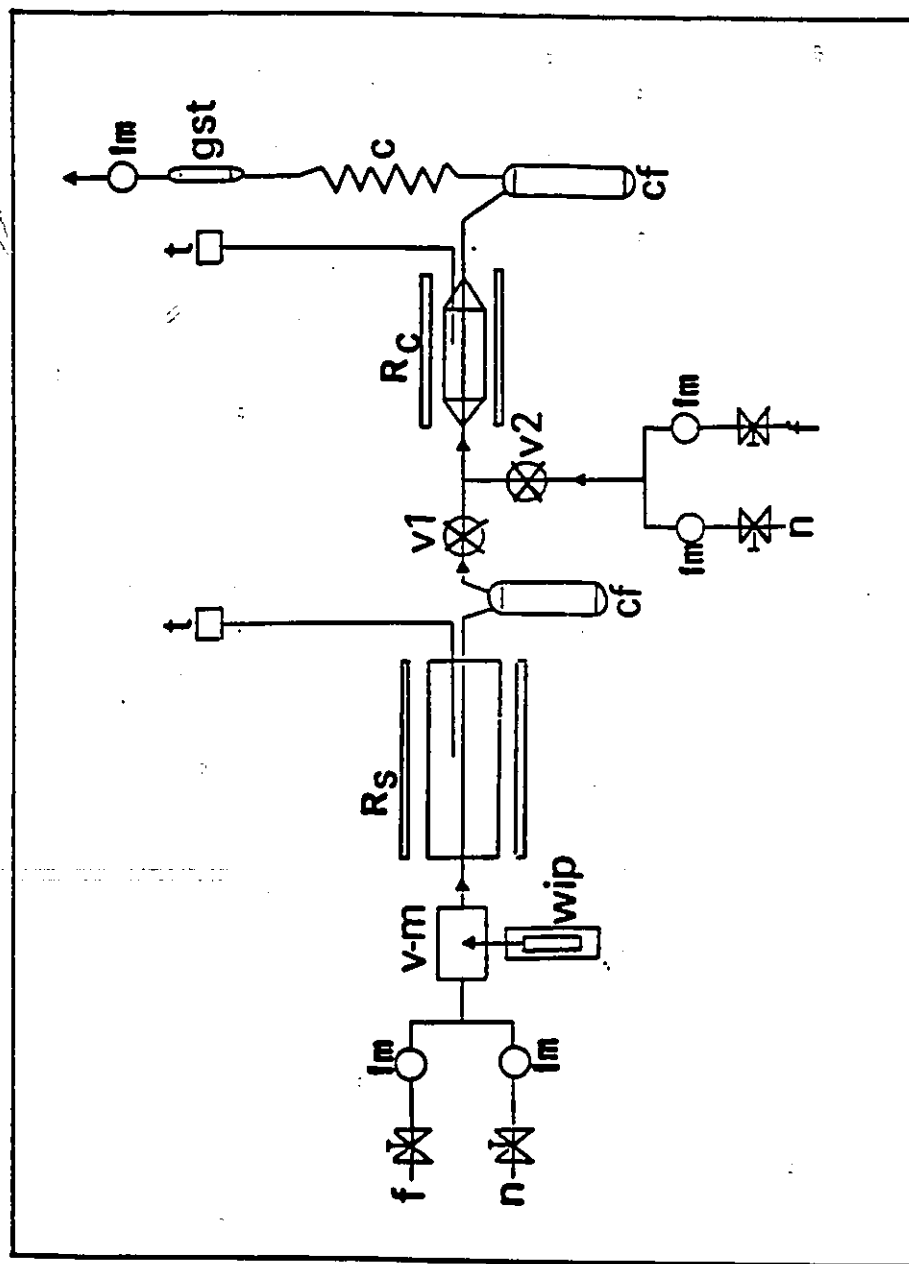


Figure 2.3 Experimental set-up for catalytic testings.

Outstream gases of steam-cracking obtained when V1 is open and V2 is closed. C, condensers; cf, collecting flasks; f, feed (propane, n-butane etc.); fm, flow meters; gst, gas sampling tube; n, nitrogen (carrier gas); Rc, catalytic reactor; Rs, steam-cracker; t, thermocouples (chromel-alumel); v-m, vaporizer-mixer; V1, valve 1 (steam-cracking gases to Rc); V2, valve 2 (pure feeds to Rc); wip, water infusion pump.

The normal operating parameters of the horizontal steam-cracker unit were as follows: feed: propane, temperature R_g : 820°C or 840°C, residence time: 0.85s and 0.75s respectively, water-to-propane molar ratio: 1.1. For runs conducted with pure feedstocks, the usual reaction parameters were as follows: temperature R_c : 400-540 \pm 0.5°C, WHSV: weight feed (gh^{-1})/ weight catalyst (g)= 1.5-1.7 h^{-1} V1 or 0.6 h^{-1} V2, weight catalyst: 4g, duration of a run: 4h.

In the case of mixed feed experiments, after condensing and collecting the water and heavier hydrocarbons (generated in R_g) in the cooling flask, the resulting gaseous stream was sent to the catalytic reactor (thru V1). Columns denoted **Total** in Table 2.3 report the total product distribution of the steam-cracking process at a temperature slightly less than 820°C, at 820°C and at 840°C respectively. Columns denoted **Gas** are the compositions of the gaseous streams entering R_c . Table 2.3 also reports the product distribution obtained when the extruded bentonite binder was loaded in the reactor. It is shown that bentonite has no aromatization activity, however it provides a greater surface area for cracking reactions.

The liquid hydrocarbons formed by the steam-cracking and catalytic reactions were collected in condensing flasks kept at -15°C. The gases were analyzed throughout the run using a Shimadzu GC (Model Mini 3, FID) equipped with a 2.5-m stainless steel column (15wt.-% squalane on chromosorb P) with 2,2-dimethylbutane as internal standard. The collected liquid phases were subsequently analyzed with a Hewlett Packard GC (Model 5790A, FID) equipped with a 50-m PONA type capillary column. When required, n-octane was used to extract the organic phase prior to chromatographic analysis. The n-octane peak was considered as solvent in the chromatogram and was excluded from the product distribution.

2.2.6 Product calculations

All calculations were made on a carbon atom basis. Chromatographic results were converted to C. atoms using an internal standard (2,2DMB) for the gaseous effluent and correction factors for the columns.

Table 2.3 Total product distribution of a propane steam-cracker and resulting gaseous mixture. Test reaction with bentonite binder (blank).

Temperature (°C)	820(*)		820		840		Bento- nite ^a
	Total	Gas	Total	Gas	Total	Gas	Blank
Total Product Distribution (% C. atoms)							
Methane	16.1	16.5	18.2	19.0	21.7	23.3	20.4
Ethylene	29.7	30.5	33.3	34.8	38.3	41.1	37.7
Ethane	1.8	1.8	2.0	2.2	2.4	2.6	2.3
Propylene	17.8	18.3	17.1	17.8	14.8	15.9	2.1
Propane	28.5	29.3	21.9	22.8	13.0	13.9	30.3
Butanes	0.8	0.8	0.5	0.5	0.1	0.1	0.7
Butenes(+ Diene)	2.6	2.7	2.8	2.9	2.9	3.1	3.2
C ₅ ⁺ Aliphatics	1.2	0.0	1.6	0.0	2.0	0.0	1.7
Total Aromatics	1.6	0.0	2.6	0.0	4.8	0.0	1.7
Total	100.1	99.9	100.0	100.0	100.0	100.0	100.1
BTX/ Aromatics	0.72		0.62		0.65		1.00
BTX Aromatics Composition (wt.%)							
Benzene	92.2		89.9		84.0		100.0
Toluene	1.7		2.8		5.3		0.0
Ethylbenzene	0.9		0.6		0.9		0.0
Xylenes	0.9		1.1		1.5		0.0
Styrene	4.3		5.6		8.3		0.0
Total	100.0		100.0		100.0		100.0

820(*): Temperature of steam-cracker slightly lower than 820°C.

C₅⁺ Aliphatics: Aliphatic molecules having C5- C10 C. atoms.

(a) Feed: 820- Gas; Temperature R_c: 500°C.

In the following data, the total conversion of feed is defined as:

$$C_t(C.atom\%) = \frac{(NC)_F - (NC)_P}{(NC)_F} * 100 = \frac{(NC)_R}{(NC)_F} * 100 \quad (2-1)$$

where $(NC)_F$, $(NC)_P$ and $(NC)_R$ refer to the number of C. atoms of hydrocarbon source fed to the reactor, in the gaseous effluent and reacted, respectively.

The selectivity for product i is defined as:

$$S_i(C.atom\%) = \frac{(NC)_i}{(NC)_R} * 100 \quad (2-2)$$

where $(NC)_i$ is the number of C. atoms of product i in the outstream gases.

The yield for product i is defined as:

$$Y_i(C.atom\%) = S_i * C_t * \frac{1}{100} \quad (2-3)$$

2.3 Results and discussion

There have been several reports of enhanced aromatization activity when part or all of the aluminium ions in the ZSM-5 framework are replaced by gallium ions (97,104-108). Fig. 2.4 compares BTX aromatic yields and propane conversions for galloaluminosilicate, gallosilicate and pure H-ZSM-5 zeolite catalysts. In Fig. 2.4, a 20wt.-% increase in BTX yield is observed on gallium modified catalysts when compared with the parent zeolite. Propane conversion also is increased (Fig. 2.4 B) but less significantly. According to Bournonville *et al.* (104), extraframework gallium species formed under the reaction conditions improve the dehydrogenation ability of the catalyst, thus promoting the formation of aromatic molecules as well as propylene from propane. The gallium species are believed to be partial reduction products of Ga_2O_3 ($\text{Ga}_2\text{O}_3 \dots \text{Ga}_2\text{O}$) formed by hydrogen species produced during the reaction. In temperature programmed reduction (TPR) studies (104) of gallosilicate, 53.3% of Ga_2O_3 was reduced to Ga_2O . Gallium is extracted from the framework even under very mild steaming conditions. Therefore, considering the catalysts of this study, extraframework Ga_2O_3 may have been formed as a result of the pretreatment or during gel-synthesis. The slow formation of extraframework gallium is also reported as the reason for an extended induction period, or why the catalyst becomes more active after the first oxidative regeneration. Catalysts with dispersed extraframework gallium species also exhibit high stability (114).

Zinc cations exchanged in the zeolite lattice also have been shown to increase aromatics production from lower alkanes and alkenes (94,109-113). Table 2.4 reports product distributions obtained using catalyst containing 40wt.-% of the individual catalytic components, either zeolite based and ZnO based. When compared to the feed composition (no catalyst column), it is seen that the catalytic activity of those catalysts for aromatization or other product formation is very low. When these components are mixed to form hybrid catalysts (40wt.-% zeolite based + 40wt.-% ZnO based) aromatization activity is improved. The results are shown in Fig. 2.5. Catalysts A and B are the pure and Zn^{2+} ion-exchanged zeolite-based components respectively (included as reference). Catalysts C, D, E represent the mixed samples. It can be observed that when zeolite and oxide functions are mechanically mixed and immobilized in a clay matrix, the resulting catalytic activity toward aromatic formation is enhanced (C,D,E vs A,B). Furthermore, if the oxide function is prepared by heterogeneous co-precipitation,

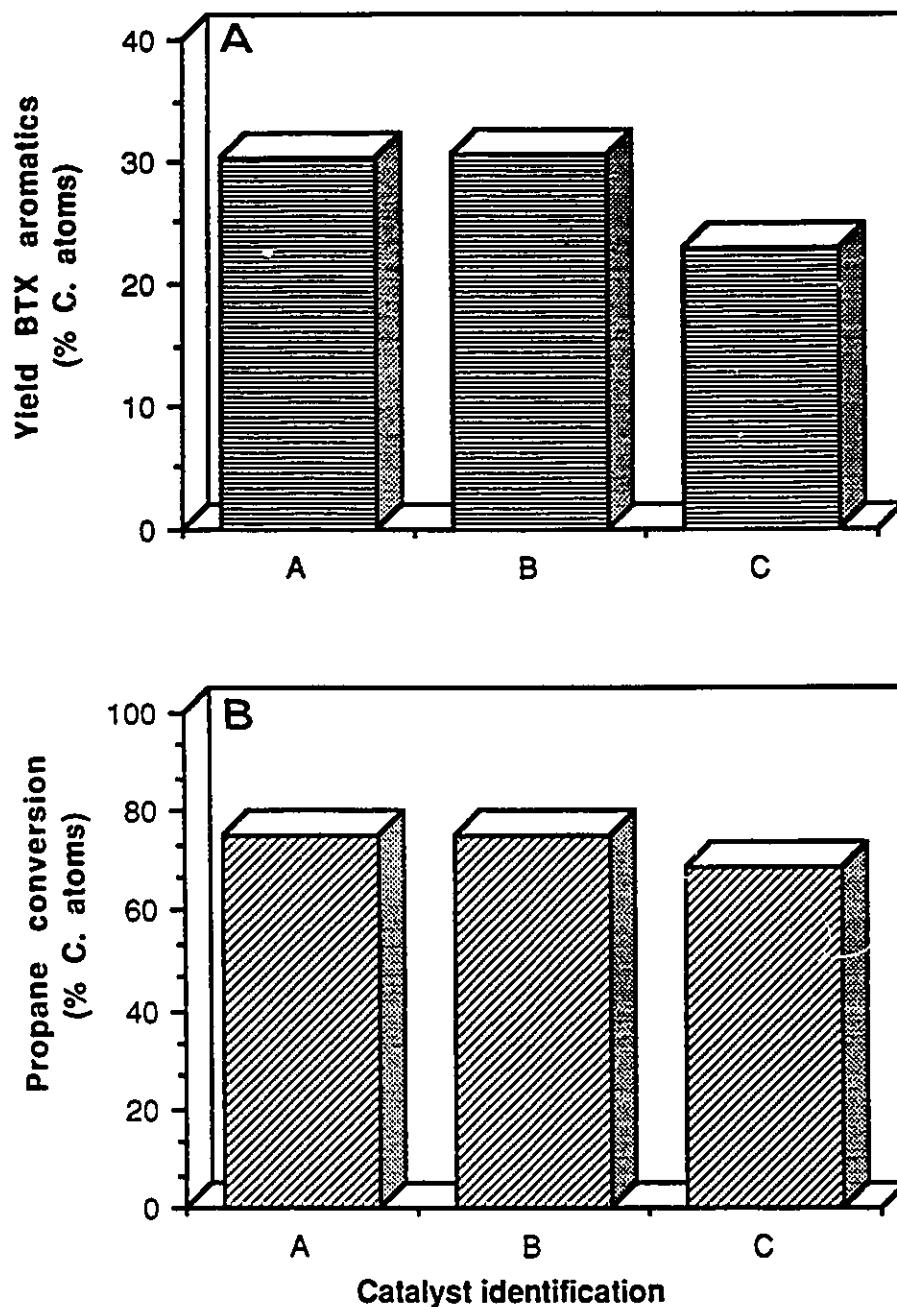


Figure 2.4 Comparison of catalytic activity between pure and chemically modified ZSM-5 catalysts: (A) BTX aromatic yields; (B) Propane conversion. Parameters: Feed: 820- Gas (table 2.3); Temperature R_c : 500°C; WHSV: 1.5h⁻¹. Catalyst composition: 80wt.-% zeolite + 20wt.-% bentonite binder. Catalyst identification:

A H-GaAl-ZSM-5 ($Si/(Ga + Al) = 8.1$)
 B H-Ga-ZSM-5 ($Si/Ga = 5.2$)
 C H-ZSM-5(10.6)

Table 2.4 Catalytic activity of the pure catalytic components.

	No Catalyst	Catalyst Identification			
		A	B	C	D
		Total Product Distribution (% C. atoms)			
C1-C4 Paraffins/ Ethane	44.5/ 2.2	42.0/ 2.0	45.6/ 2.5	41.4/ 2.3	41.5/ 1.9
C2-C4 Olefins	55.5	49.7	46.3	53.2	52.4
C ₅ ⁺ Aliphatics	-	4.7	2.1	1.5	1.9
Total Aromatics	-	4.7	6.0	3.9	4.2
BTX/ Aromatics	-	0.82	0.87	0.48	0.63

C₅⁺ Aliphatics: Aliphatic molecules having C5- C10 C. atoms.

Parameters: Feed: 820- Gas (Table 2.3); Temperature R_c: 500°C; WHSV: 1.5h⁻¹.

Catalyst Composition: 40wt.-% active phase + 60wt.-% bentonite binder.

Catalyst Identification:

A H-ZSM-5(37)

B H-ZSM-5(20) + 0.63wt.-% Zn²⁺ introduced by ion-exchange

C ZnO/γ-Al₂O₃ acidic deposited by wet impregnation (Zn/Al = 1.0)

D ZnO/Al₂O₃ co-precipitate (Zn/Al = 0.39)

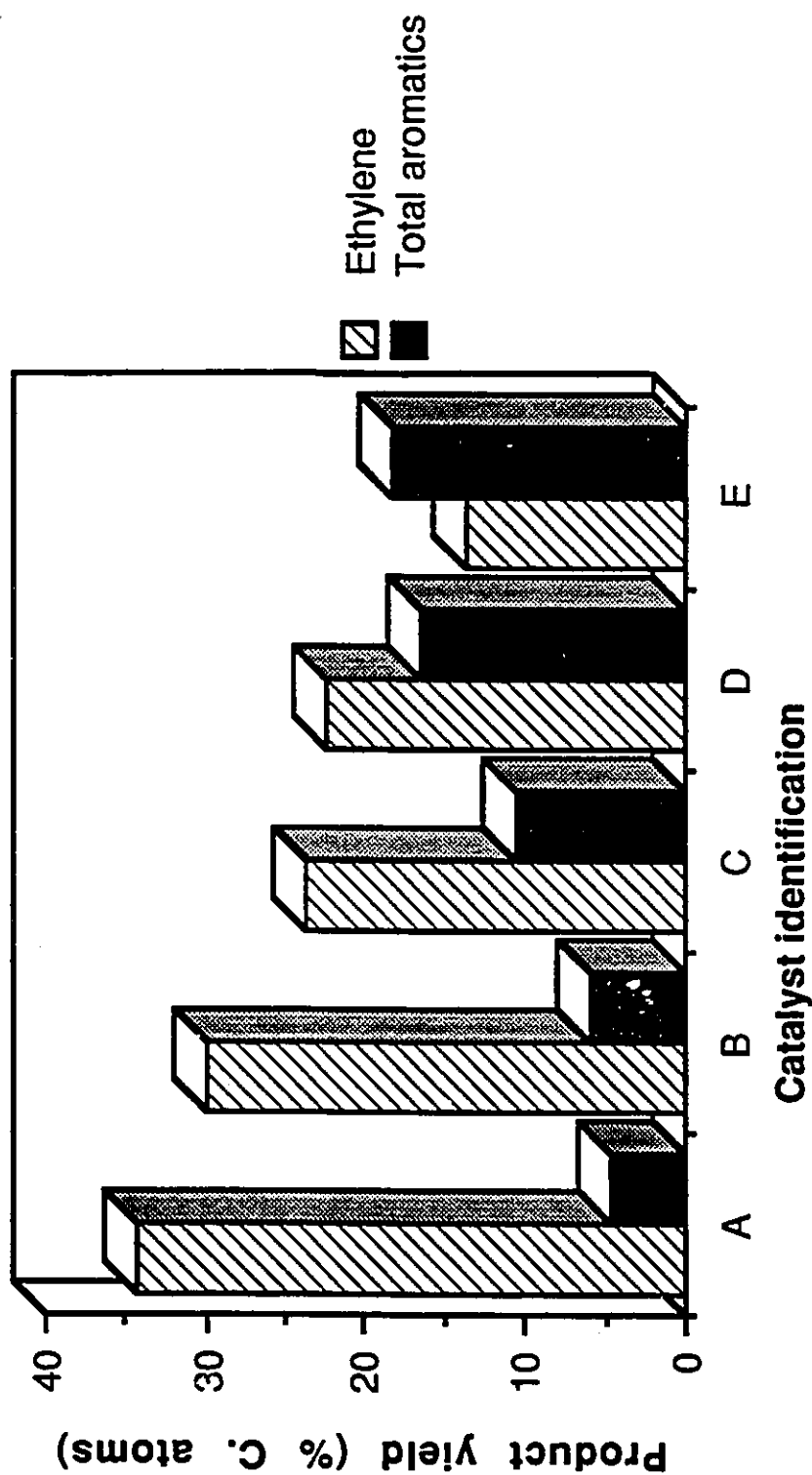


Figure 2.5 Variation of ethylene and total aromatic yields as a function of the catalyst (pure and hybrid).

Parameters: Feed: 820- Gas (Table 2.3); Temperature R_c : 500 °C; WHSV: 1.5h⁻¹.

Catalyst composition:

Pure: 40wt.-% zeolite + 60wt.-% bentonite binder.

Hybrid: 40wt.-% zeolite + 40wt.-% co-catalyst + 20wt.-% bentonite binder.

Catalyst Identification:

(A) H-ZSM-5(37)

(C) H-ZSM-5(37) + ZnO/ γ -Al₂O₃ acidic wet impregnation (Zn/Al = 1.0)

(D) H-ZSM-5(37) + ZnO/ γ -Al₂O₃ co-precipitate (Zn/Al = 0.39)

(E) Catalyst (B) + ZnO/ γ -Al₂O₃ co-precipitate (Zn/Al = 0.39)

the performance is further improved (D,E vs C). As seen in Fig. 2.5, the increased aromatic production is paralleled by a sharp decrease in the ethylene content of the gaseous effluent. This indicates that ethylene is a target molecule in the aromatization sequence of the feedstock mixture, on this type of bicomponent catalyst.

In this series (Fig. 2.5), the highest performance toward aromatics is obtained when the zeolite component is modified by zinc ions introduced by ion-exchange and the oxide component is composed of a $\text{ZnO}/\text{Al}_2\text{O}_3$ co-precipitate having a Zn/Al atomic ratio equal to 0.39. The increased aromatic production is most likely due to the presence of zinc species (109) inside the zeolite channels, which can act as activation and dehydrogenation centers and participate in bifunctional catalysis with the zeolite acid sites. However, this catalyst did not recover its complete catalytic activity after oxidative regeneration. Therefore, further optimization of the catalyst has been focused on a pure zeolite component, with different ZnO based co-catalysts.

Table 2.5 reports the product yields obtained using as feedstock the outstream gases of the steam-cracker operated at 820°C. This series of tests was conducted to investigate the influence of the co-precipitate composition on the performance of hybrid catalysts. All samples were made up of 40wt.-% H-ZSM-5(37) + 40wt.-% oxide component + 20wt.-% bentonite clay. Columns A to D report the product distributions obtained for the mixed-oxide precipitates having a Zn/Al atomic ratio ranging between 0.16 (14mol.-% Zn) and 2.4 (71mol.-% Zn). Columns E and F report boundary product distributions at 500°C, when the co-catalysts are ZnO precipitate and ZnO(BAKER) respectively. High selectivity to aromatics, especially in the BTX range, is observed when compared with the pure H-ZSM-5 (Table 2.4, catalyst A, 4.7wt.-% total aromatics). More specifically, upon examination of Table 2.5 and Fig. 2.6, the highest aromatic yields are achieved when the Zn/Al ratio is equal or greater than 1.0 ($\geq 50\text{mol.-% ZnO}$).

In Fig. 2.7 A and B, a series of tests was undertaken to determine the nature of the aromatizing component. In A, the catalyst formulation consisted of a constant amount of ZnO(BAKER) (40wt.-%) while the weight of the zeolite was varied between 0-40wt.-%. In B, the H-ZSM-5 weight portion was kept constant and ZnO was varied in the same manner. It can be observed that the zeolite component is responsible for aromatization of feed molecules because the aromatic yield is very low if the H-ZSM-5 component is

Table 2.5 Effect of co-catalyst composition on catalytic activity of hybrid catalysts.

Catalyst Identification						
A	B	C	D	E	F	
Zn/Al molar ratio						
0.16	0.39	1.0	2.4			
Total Product Distribution (% C. atoms)						
C1-C4 Paraffins/ Ethane	51.0/ 3.2	45.0/ 3.4	53.2/ 8.1	53.6/ 8.5	54.8/ 11.3	52.5/ 9.3
C2-C4 Olefins	33.9	34.8	25.5	26.7	27.7	28.8
C ₅ + Aliphatics	3.3	3.7	2.3	2.7	2.2	2.3
Total Aromatics	11.9	16.5	19.0	17.1	15.3	16.4
BTX/ Aromatics	0.87	0.87	0.88	0.88	0.89	0.88
BTX Aromatics Composition (wt.-%)						
Benzene	30.0	22.9	30.1	25.1	31.1	30.8
Toluene	36.3	35.0	33.7	35.0	33.1	33.8
Ethylbenzene	6.9	9.7	7.6	8.4	7.5	7.5
Xylenes	26.5	26.0	28.2	31.2	27.7	27.3
Styrene	0.3	0.4	0.4	0.4	0.6	0.5

C₅+ Aliphatics: Aliphatic molecules having C5- C10 C. atoms.

Parameters: Feed: 820- Gas; Temperature R_c: 500°C; WHSV: 1.5h⁻¹.

Catalyst Composition: 40wt.-% H-ZSM-5(37) + 40wt.-% Co-catalyst + 20wt.-% bentonite binder.

Catalyst Identification:

- A H-ZSM-5(37) + Zn/Al=0.16 co-precipitate
- B H-ZSM-5(37) + Zn/Al=0.39 co-precipitate
- C H-ZSM-5(37) + Zn/Al=1.0 co-precipitate
- D H-ZSM-5(37) + Zn/Al=2.4 co-precipitate
- E H-ZSM-5(37) + ZnO precipitate
- F H-ZSM-5(37) + ZnO(BAKER)

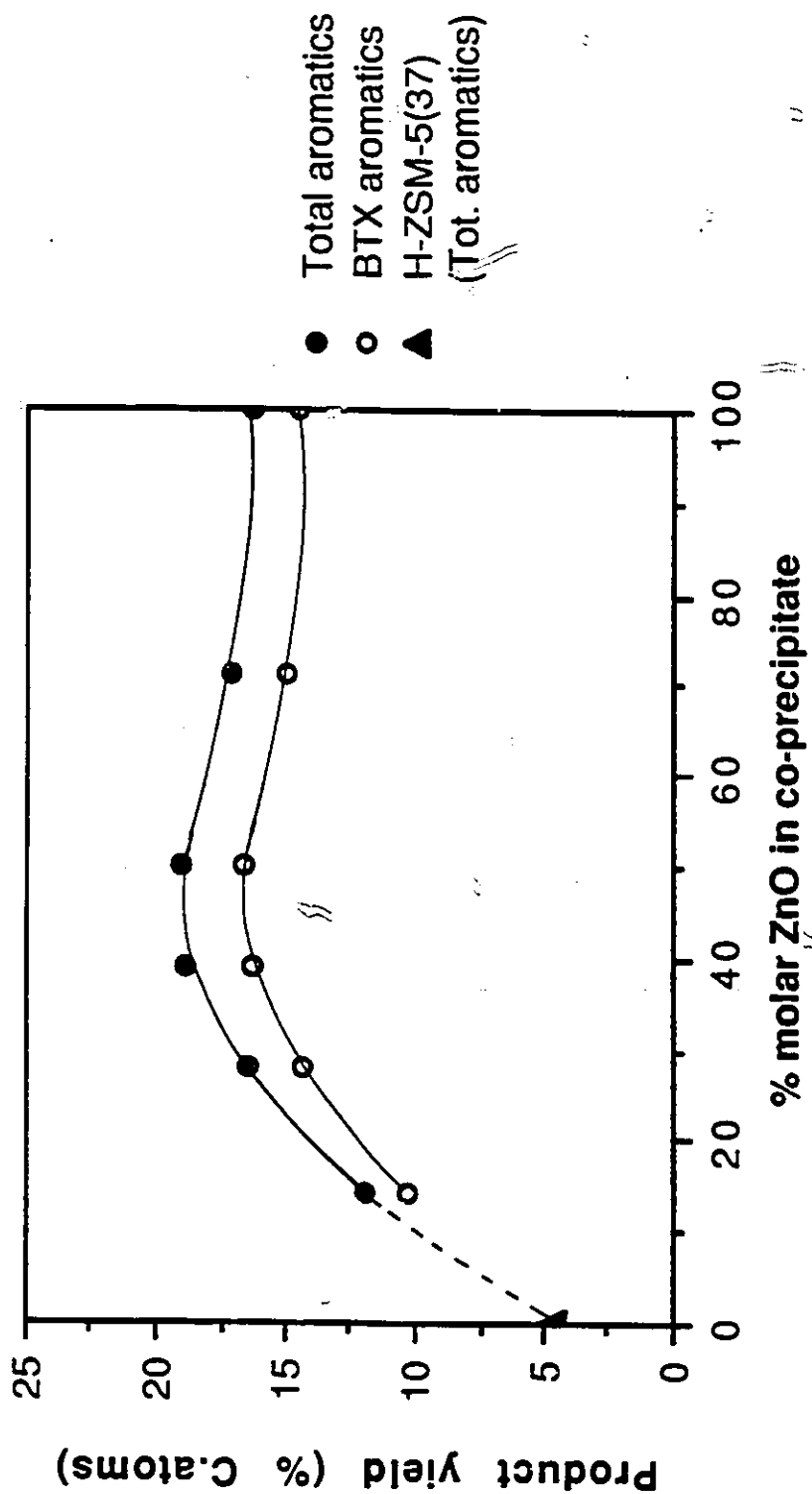


Figure 2.6 Effect of ZnO content of co precipitate on the total and BTX aromatic yields.
Parameters: Feed: 820-Gas (Table 2.3); Temperature R_c : 500 °C; WHSV: 1.5h⁻¹.
Catalyst composition: 40wt.-% H-ZSM-5(37) + 40wt.-% co-precipitate + 20wt.-% bentonite binder.

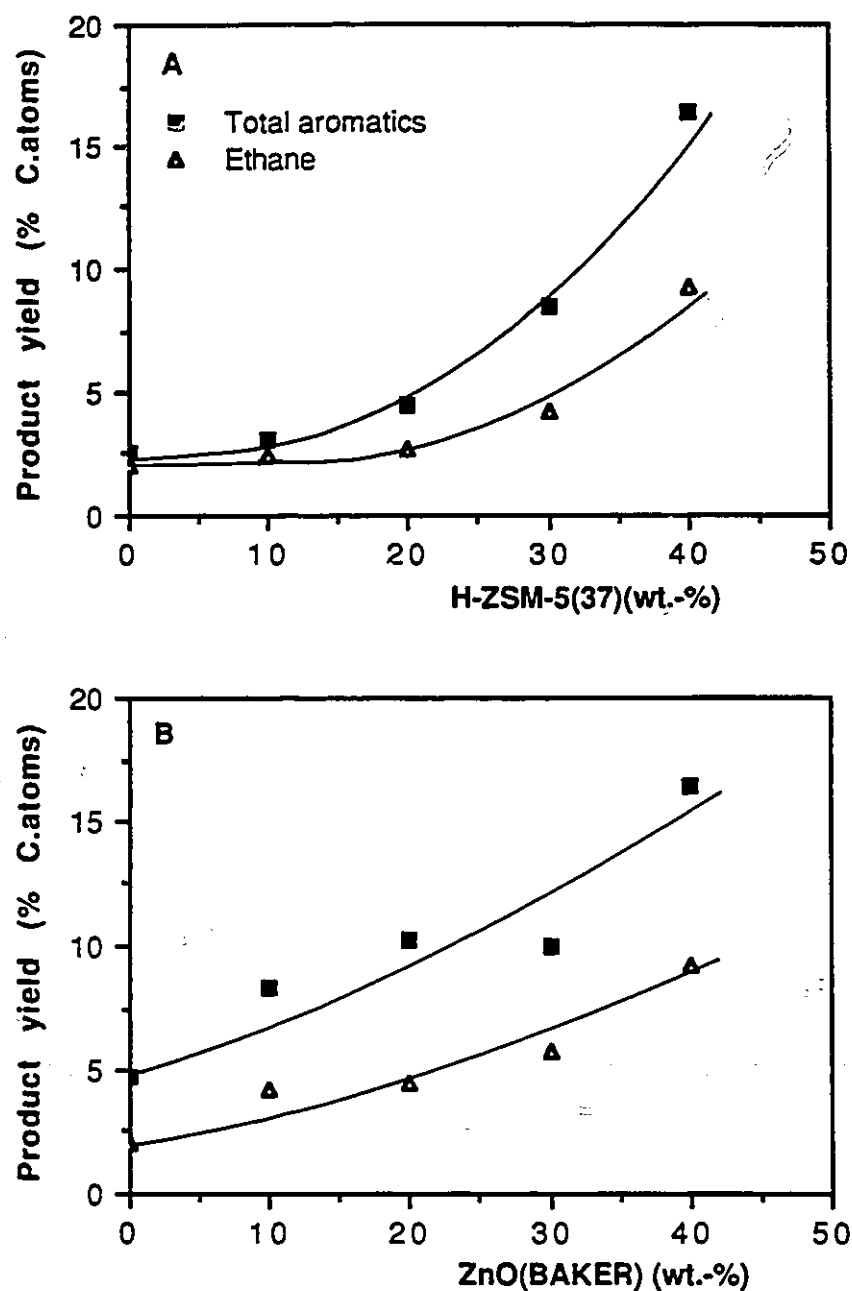


Figure 2.7 Identification of aromatizing and hydrogenating components: (A) Variation of H-ZSM-5(37) weight/ ZnO(BAKER) kept constant; (B) Variation of ZnO (BAKER) weight/ H-ZSM-5(37) kept constant.


Parameters: Feed: 820- Gas (table 2.3); Temperature R_c : 500°C; WHSV: 1.5h⁻¹.

Catalyst composition: 80wt.-% active phase (0-40wt.-% H-ZSM-5(37) + 0-40wt.-% ZnO(BAKER)) + 20wt.-% bentonite binder.

completely absent (A). Another feature to be observed is that ethane yield increases with increasing aromatic formation. An additional hydrogenation ability may then be ascribed to zinc oxide containing hybrid catalysts. In fact, ZnO has long been recognized as a hydrogenation/ dehydrogenation catalyst (116-120).

As a rule with pure H-ZSM-5 zeolite, the increased formation of aromatics is paralleled by two phenomena: increased conversion to ethylene and propylene and increased yield of ethane (mostly) and other paraffins (121-122). Therefore, the aromatics originate from the light olefins (C_2-C_3). Hydrogen is produced during the cyclo dehydroaromatization step (Fig. 2.8) by a series of deprotonations and hydride abstractions, as described by Mole *et al.* (111) and Poutsma (123). The paraffins are produced as a result of hydrogen redistribution reactions associated with the mechanism of aromatic formation, or by cracking on the zeolite acid sites.

In order to investigate the extent of hydrogen transfer between the two components and to determine the optimal catalyst formulation, a series of tests was carried out using commercial ZnO. Although ZnO has a lower promotional effect toward aromatic formation than the co-precipitate (Fig. 2.6 and Table 2.5), it was selected as co-catalyst because it is a known hydrogen adsorbent (124-125) and was readily available at the time. Figure 2.9 A and B report the aromatic and ethane yields respectively. In this sequence, the H-ZSM-5(37) (0-80wt.-%) component was mixed with commercial ZnO(BAKER) (80-0wt.-%) in various weight proportions. The solid mixtures were then extruded with 20wt.-% bentonite binder. As seen in Fig. 2.9 A, a very small amount of ZnO is required to achieve the highest aromatic selectivity. Using a zeolite/ ZnO weight ratio of 15/1, it is possible to increase the aromatic yield from 16wt.-% using 80wt.-% H-ZSM-5(37) to 31wt.-% using the hybrid. Furthermore, it is observed that the addition of total aromatic yields for the pure components (zeolite and ZnO), results in a much smaller amount than when the components are mechanically mixed with optimal catalyst formulation. Therefore, it is reasonable to assume that a synergy exists between the zeolite and the co-catalyst. Fig. 2.9 B further emphasizes that hydrogen transfer is most efficient for the optimal catalyst composition, as evidenced by the increased production of ethane.



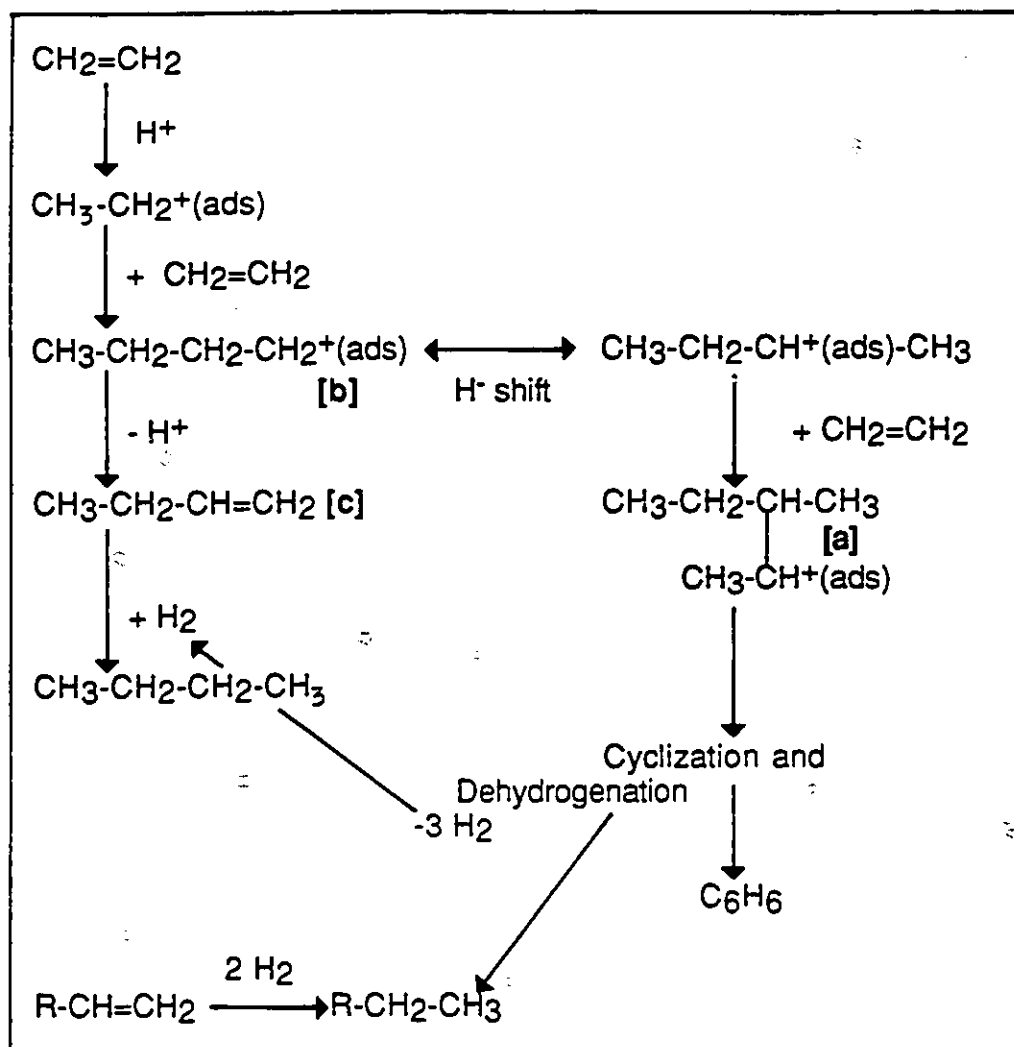


Figure 2.8 Proposed mechanism for olefin (ex: ethylene) aromatization in H-ZSM-5 zeolite. [a] Olefinic oligomer (2°); [b] Adsorbed carbenium ion; [c] Olefin.

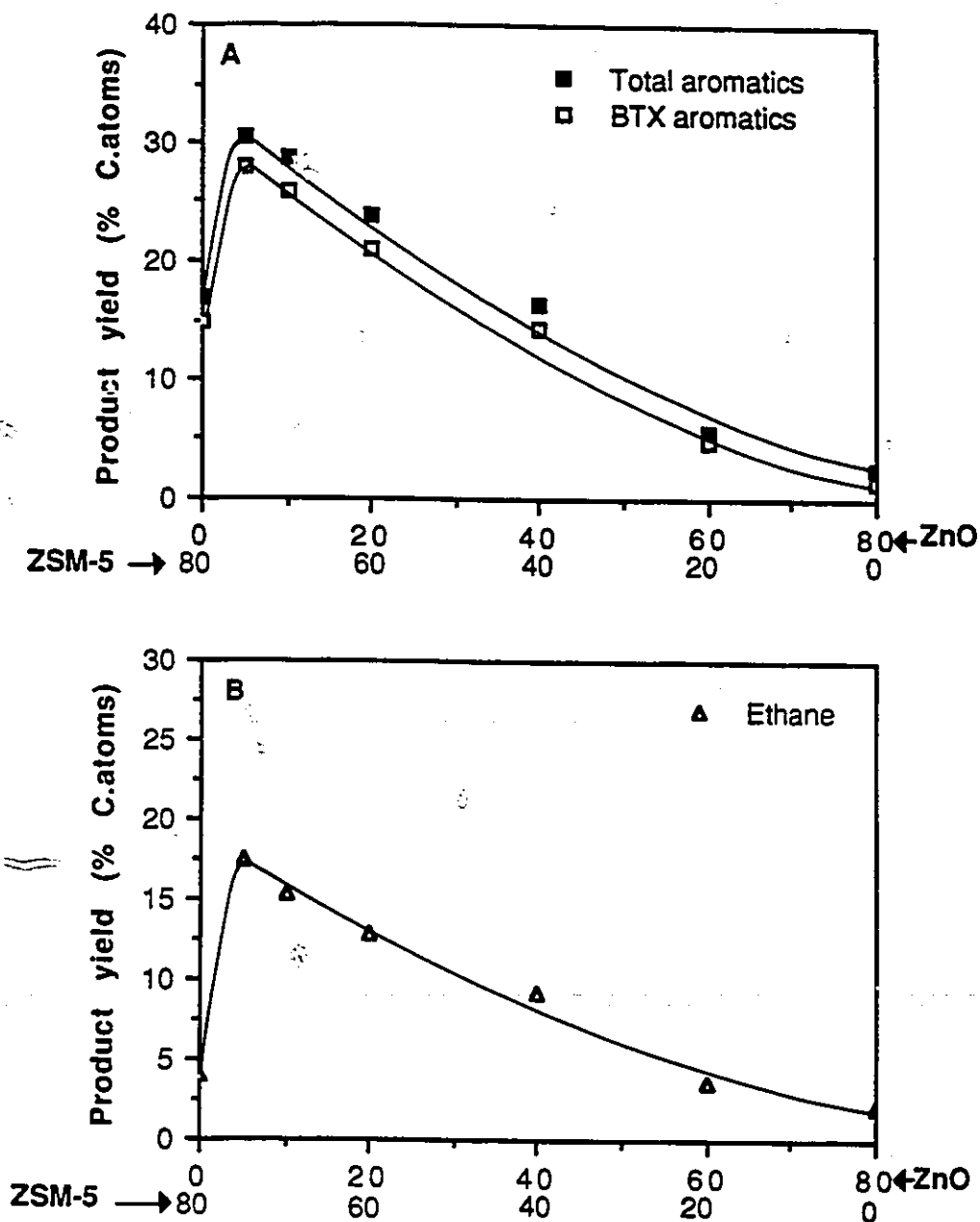


Figure 2.9 Optimization of catalyst composition: (A) Total and BTX aromatic yields; (B) Yield of ethane formed.

Parameters: Feed: 820- Gas (table 2.3); Temperature R_c : 500°C; WHSV: 1.5h⁻¹.

Catalyst composition: 80wt.-% active phase (0-75wt.-% H-ZSM-5(37) + 0-75wt.-% ZnO(BAKER)) + 20wt.-% bentonite binder.

A difference in aromatization reaction rates on pure and hybrid catalysts may exist and be involved in explaining the observed synergy. Although the aromatization component remains the zeolite lattice which is not modified by any metal cations, it is possible that the presence of the oxide function, even in very small amount (5wt-%), has an effect on the rate of hydrogen removal from the reaction loci, as suggested by Inui *et al.* (107-108) and Mole *et al.* (111). These workers found that co-feeding hydrogen with a paraffin resulted in a sharp decrease of aromatization activity on Zn-ZSM-5 and Pt-gallosilicate. Pure H-ZSM-5 remained almost unaffected by such a treatment (107-108, 111). Therefore, the evacuation of hydrogen species from the zeolite channel network may be slow in H-ZSM-5, whereas when a hydrogen accepting surface is present, as is the case for the hybrid catalyst, this step may be in quasi-equilibrium (111), thus explaining the poisoning effect of added hydrogen gas on bifunctional systems.

Species that migrate on the surface and cross particle boundaries are called spillover species. Hydrogen has been claimed to spillover (91). Usually, this phenomenon is invoked when a second surface is activated by migratory species. For the hybrid catalyst, the oxide surface known for its hydrogen adsorption properties acts as a porthole for the hydrogen species formed during the cyclo dehydroaromatization step (Fig. 2.8). In this case, back-spillover or reverse spillover becomes more appropriate when referring to the promotion effect of the co-catalyst (130-131, 138).

Fig. 2.10 shows a hypothetical catalytic cycle explaining the reaction sequence on a hybrid catalyst, using ethylene as a practical example of feed molecule. A portion of the reactant can enter the zeolite channel network and be dimerized and oligomerized by acid catalysis to form the non-aromatic products, path a. Cyclization and dehydrogenation of the oligomers result in the formation of aromatics and hydrogen, path b. At this point, some hydrogen can escape the zeolite crystallite as molecular hydrogen gas, but it is believed (72-73, 114-115) that a major portion migrates across the particle boundaries of ZSM-5 and oxide functions. These migrating species, referred to as spillover hydrogen species (H_{sp}), are then adsorbed by the co-catalyst (ZnO or ZnO/ Al_2O_3 co-precipitate). In path c, H_2 is desorbed and the co-catalyst acts as a sink for the H_{ads} species exiting the zeolite. In path d, the portion of ethylene adsorbed on the co-catalyst reacts with the adsorbed spillover species to form ethane by a reduction mechanism (called scavenging action).

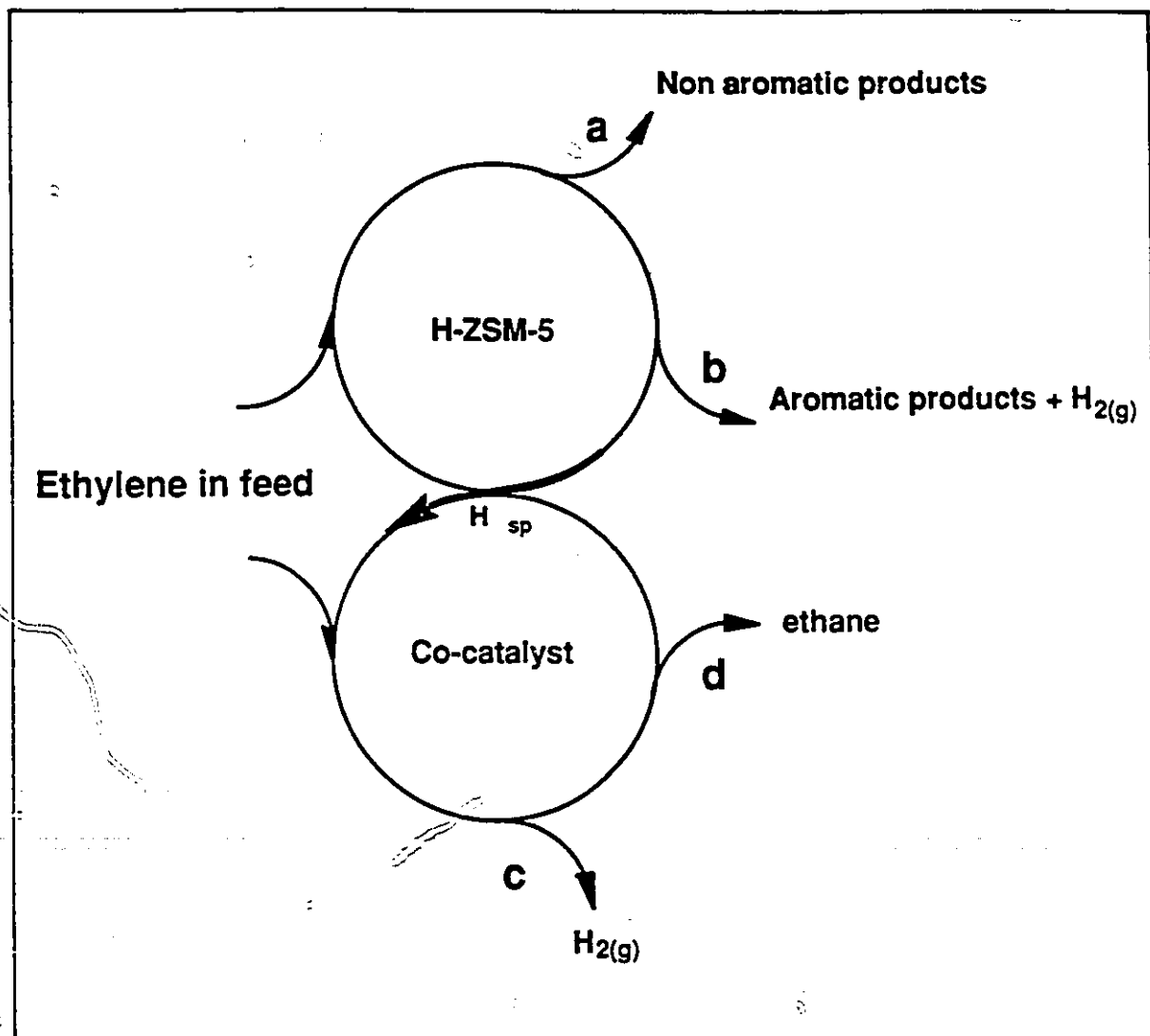


Figure 2.10 Advanced catalytic cycle on hybrid catalyst: aromatizable fraction, ethylene; (a) Oligomerization products; (b) Cyclization/ dehydrogenation products; (c) Sink effect of co-catalyst/ desorption of $H_{2(g)}$; (d) Scavenging effect of co-catalyst/ reduction of ethylene; H_{sp} , Spillover hydrogen species/ surface migration across particle boundaries.

As discussed by Poutsma (123), olefinic and paraffinic molecules can undergo a range of chemical transformations in acid zeolites: positional and geometrical double bond isomerization, skeletal isomerization, condensation, hydrogen redistribution, cracking to smaller fragments. The balance among these reactions is a function of reaction conditions: temperature and pressure. The behavior of a ZnO/alumina hybrid catalyst is shown in Fig. 2.11. For these experiments, the temperature of the catalytic reactor was varied between 400-550°C. In that range it can be observed that the portion of liquid hydrocarbons (total aromatics + C₅-C₁₀ aliphatics) decreases as temperature increases. Conversely, the amount of ethane formed by reduction of ethylene adsorbed on the co-catalyst, increases with temperature. Therefore, since a greater portion of the aromatizable ethylene is sacrificed by the scavenging action of the co-catalyst at high temperature, aromatic propensity is decreased.

Fig. 2.12 compares the aromatic yields for ZnO/Al₂O₃ co-precipitate (Zn/Al=1.0) and commercial ZnO hybrids with the pure zeolite analog for a mixed feed. It can be observed that total aromatic yields of 33wt.-% and 25wt.-% can be achieved on hybrids, while H-ZSM-5(37) yields 20wt.-%. The differences can be rationalized if two parameters are considered: the amount of ZnO present and the surface area of the co-catalysts. BET surface area measurements of 4.2m²/g and 27.4m²/g were obtained for commercial ZnO and the co-precipitate respectively. It is reasonable to assume that the greater surface area provided by the co-precipitate favors a more efficient adsorption of hydrogen species exiting the zeolite crystallites. Considering the ethane yields of 16wt.-% vs 6wt.-% (Table 2.6) for pure ZnO and the co-precipitate respectively, predominance of hydrogenation activity on ZnO is indicated over hydrogen chemisorption/ desorption. ZnO adsorbs ethylene (116-120) from the feed thus decreasing the amount of olefins that enter the zeolite to undergo aromatization.

It is interesting to point out differences in the BTX aromatic product spectrum when the two co-catalysts are used. High selectivity for toluene is characteristic of the ZSM-5 zeolite and can be verified in Table 2.6. Upon comparison of the hybrids, a change in the nature of methyl substituted aromatics is observed. In the case of commercial ZnO, the effects of a more active dealkylating co-catalyst are observed. ZnO favors the production of more benzene by a secondary demethylation reaction compared with the co-precipitate, as also observed by Mole *et al.* (111).

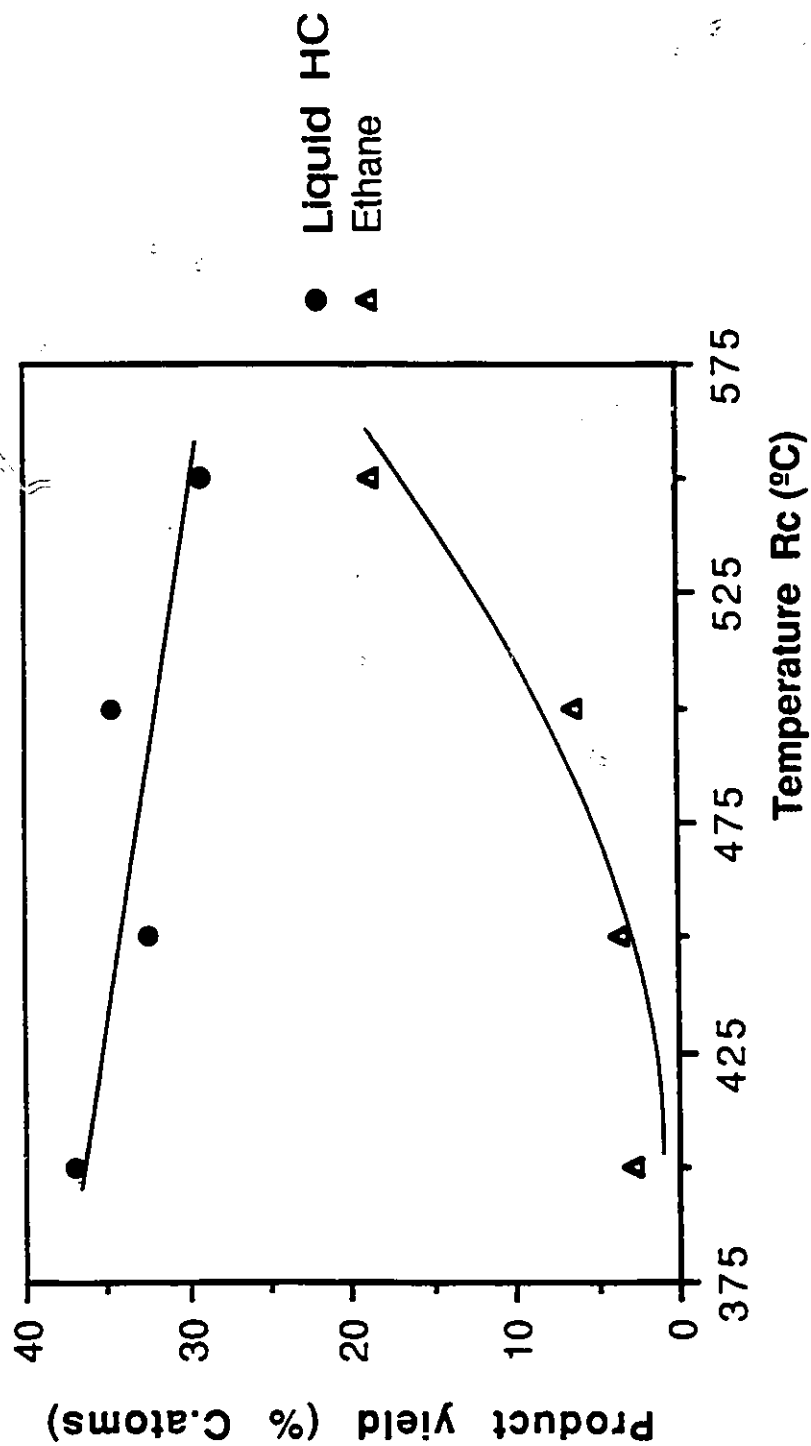


Figure 2.11 Effect of R_c temperature on product yields.
 Parameters: Feed: 840- Gas (Table 2.3); Temperature R_c : 400-550°C; WHSV: $1.7h^{-1}$.
 Catalyst composition: 75wt.-% H-ZSM-5(37) + 5wt.-% ZnO/Al_2O_3 co-precipitate ($Zn/Al = 1.0$) + 20wt.-% bentonite binder.

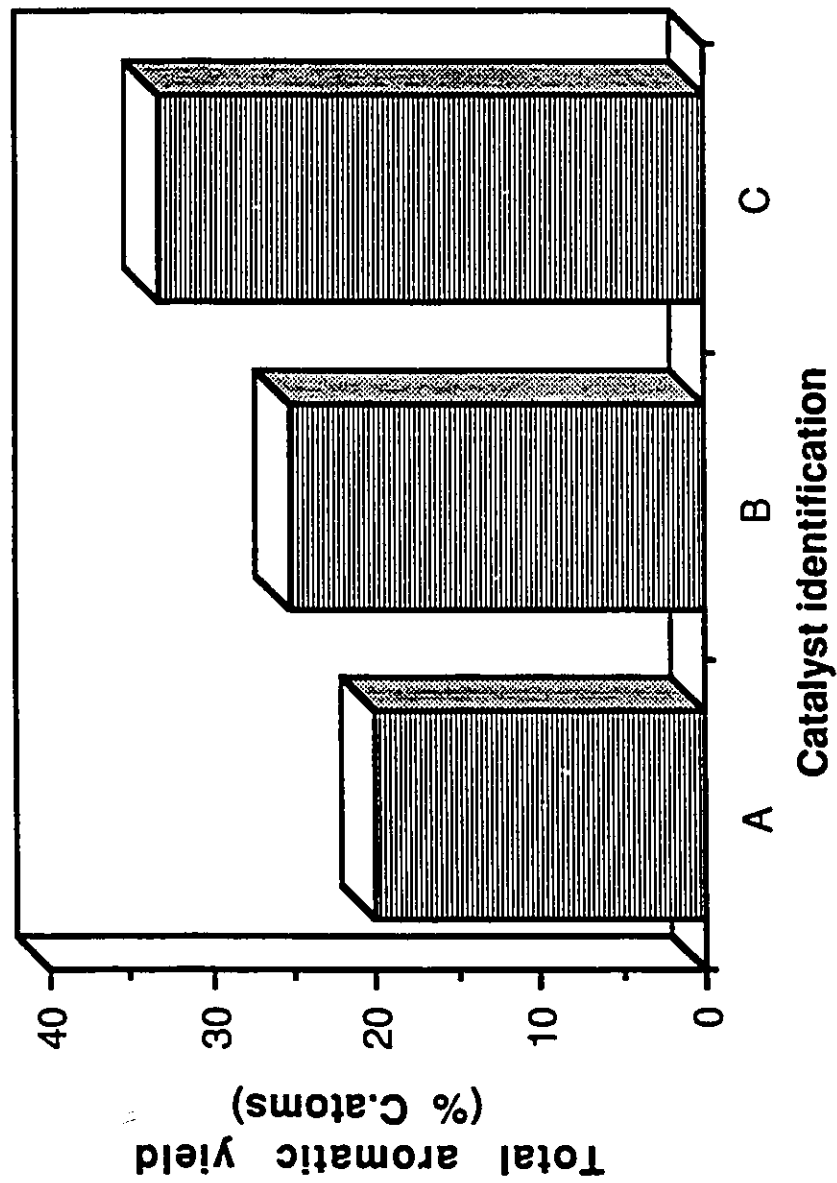


Figure 2.12 Comparison of total aromatic yields for pure ZSM-5 and hybrid catalysts of optimal composition.
Parameters: Feed: 840- Gas (Table 2.3); Temperature R_c : 500°C; WHSV: 1.7h⁻¹.
Catalyst composition: 80wt.-% active phase (75-80wt.-% H-ZSM-5(37) + 0-5wt.-% co-catalyst) + 20wt.-% bentonite binder.

Catalyst identification: (A) H-ZSM-5(37) (B) H-ZSM-5(37) + ZnO(BAKER)
 (C) H-ZSM-5(37) + ZnO/Al₂O₃ co-precipitate (Zn/Al = 1.0)

Table 2.6 Comparison of product distribution between the pure H-ZSM-5(37) (80wt.-%) zeolite and the hybrid catalysts of ZnO(BAKER) or ZnO/Al₂O₃ co-precipitate (Zn/Al = 1.0).

	Catalyst Identification		
	H-ZSM-5(37)	H-ZSM-5(37) + ZnO(BAKER)	H-ZSM-5(37) + Zn/Al = 1.0
Total Product Distribution (% C. atoms)			
C1-C4 Paraffins/ Ethane	54.7/ 4.1	56.1/ 16.2	51.2/ 6.4
C2-C4 Olefins	21.6	17.6	14.1
C₅⁺ Aliphatics	3.5	1.1	1.5
Total Aromatics	20.3	25.4	33.2
BTX/ Aromatics	0.88	0.89	0.91
BTX Aromatics Composition (wt.%)			
Benzene	28.7	38.8	31.7
Toluene	37.7	33.9	38.5
Ethylbenzene	4.9	4.9	5.5
Xylenes	28.5	22.0	24.1
Styrene	0.2	0.5	0.2

C₅⁺ Aliphatics: Aliphatic molecules having C5- C10 C. atoms.

Parameters: Feed: 840- Gas (table 2.3); Temperature R_c: 500°C; WHSV: 1.7h⁻¹.

Fig. 2.13 A and B show the aromatic yields of ZnO/Al₂O₃ based hybrid catalysts for pure propane and n-butane feeds respectively. At 540°C (R_J), comparison of aromatic product yields show an increase of almost 40wt.-% for ZnO/alumina hybrid over the parent zeolite when propane is fed to the catalytic reactor, and nearly 76wt.-% for n-butane. Fig. 2.14 A and B show that the optimal catalyst formulation using pure paraffinic feedstock is between 5wt.-% and 20wt.-%. The increased proportion of oxide component needed in the case of paraffin aromatization can be correlated with the reactant conversion (Fig. 2.14 B). As discussed by several authors (104-112), initial activation of paraffinic molecules can be enhanced when zinc or gallium ions are exchanged in the zeolite framework. Their presence increases the activity of the zeolite by C-H bond polarization (238) in the initial step of the reaction. The co-catalyst is thought to behave in a similar fashion to the exchanged cations, in that it contributes to activation of the feed (see increased conversion Fig. 2.14 B) without itself being an active dehydrogenation component in the initial hydride abstraction (115).

Table 2.7 reports product distributions with pure feedstocks at 500°C. The catalysts evaluated are the pure H-ZSM-5(34) and hybrids (15/1: zeolite/co-catalyst) of Al₂O₃-S, ZnO/Al₂O₃ co-precipitate with Zn/Al ratio equal to 1.0 and ZnO precipitate respectively. For all feeds, the addition of 5wt.-% of Al₂O₃-S slightly promotes aromatization. The ZnO function is necessary to induce significant migration of hydrogen species with concomitant aromatic yield enhancement. When light olefins are used as feeds, the reactant conversion is nearly complete. The selectivity to aromatic hydrocarbons is greatly enhanced at the expense of other reaction products formed inside the zeolite. The presence of the co-catalyst displaces the equilibrium toward aromatic formation. When propane feed is used, the hybrid systems induce increased conversion and increase aromatic yield, although conversion is relatively low because of temperature conditions.

In all cases, there is a clear hydrogen transfer effect between the zeolite and co-precipitate particles. The latter act as hydrogen-accepting surfaces for the species produced during the dehydrocyclization step within the zeolite framework (Fig. 2.8). Since the zeolite crystallites have an average particle size of 2-3µm, and they are mechanically admixed with the co-precipitate particles, the hydrogen transfer mechanism involves distances that may be as large as a few µm. Such a phenomenon invokes hydrogen

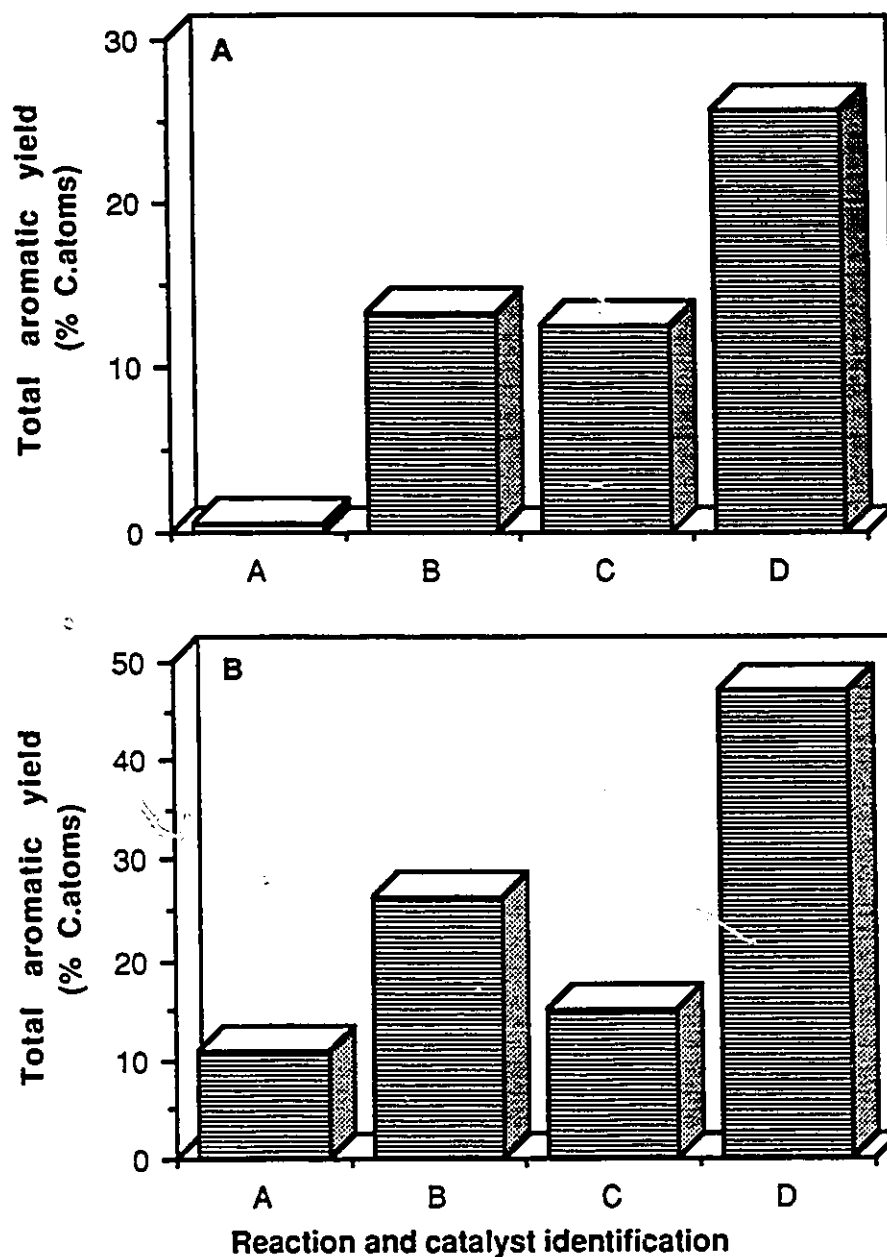


Figure 2.13 Comparison of aromatization activity between pure and hybrid ZSM-5 catalysts: (A) Propane feed; (B) n-Butane feed.

Parameters: Temperature R_c : 500°C and 540°C; WHSV: 0.6h⁻¹.

Catalyst composition: 80wt.-% active phase + 20wt.-% bentonite binder.

Pure catalyst: 80wt.-% H-ZSM-5(37)

Hybrid catalyst: 75wt.-% H-ZSM-5(37) + 5wt.-% ZnO/Al₂O₃ co-precipitate (Zn/Al = 1.0)

Reaction and catalyst identification:

(A) Pure catalyst, Temperature R_c : 500°C

(B) Hybrid catalyst, Temperature R_c : 500°C

(C) Pure catalyst, Temperature R_c : 540°C

(D) Hybrid catalyst, Temperature R_c : 540°C

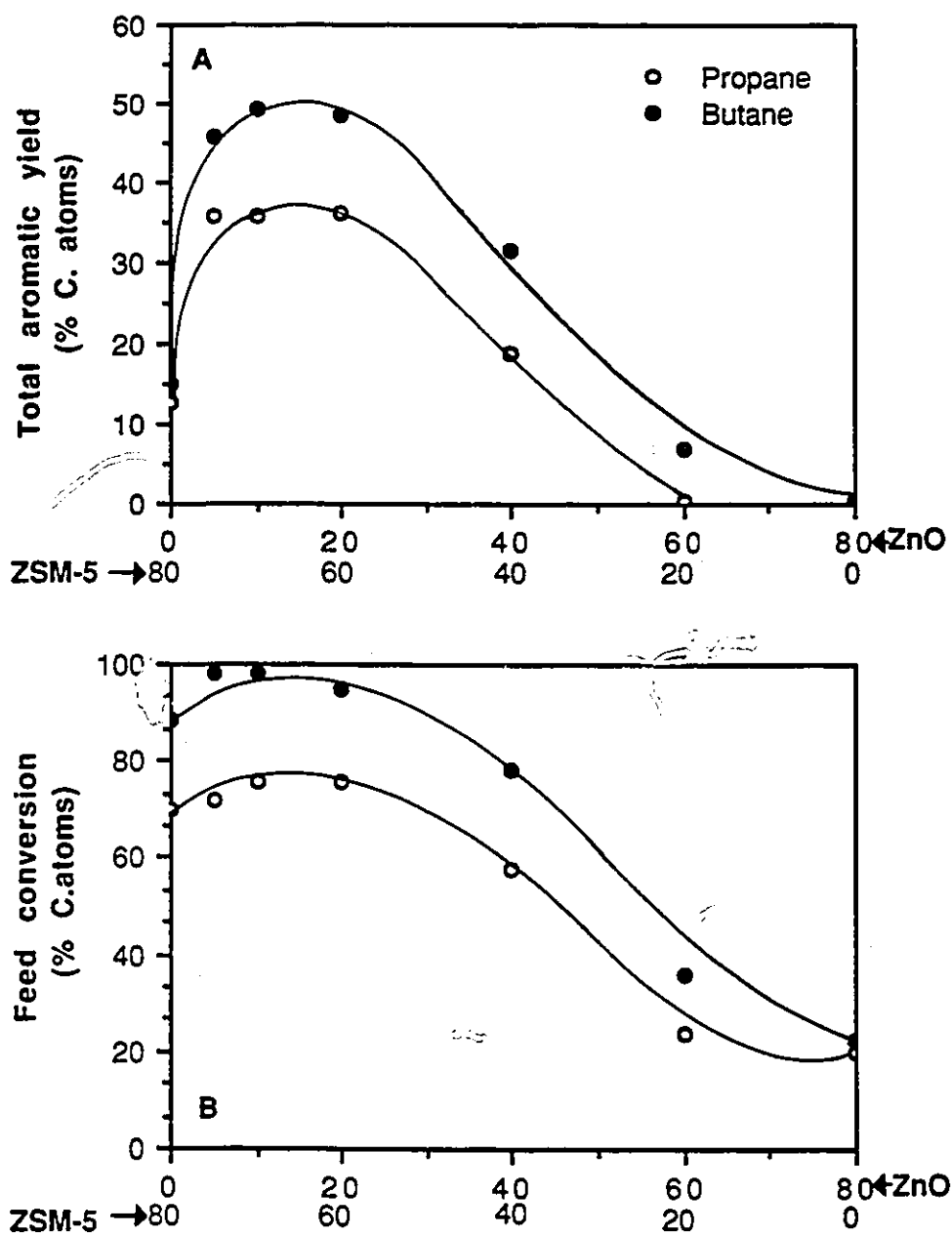


Figure 2.14 Optimization of catalyst composition for pure paraffinic feed: (A) Total aromatic yields; (B) Feed conversion.

Parameters: Temperature R_c : 540°C; WHSV: 0.6h⁻¹.

Catalyst composition: 80wt.-% active phase (0-75wt.-% H-ZSM-5(37) + 0-75wt.-% ZnO(BAKER)) + 20wt.-% bentonite binder.

Table 2.7 Comparison of product distributions using pure feedstocks.

	H-ZSM-5 (34)	H-ZSM-5 (34) + Al ₂ O ₃ -S	H-ZSM-5 (34) + Zn/Al = 1.0	H-ZSM-5 (34) + ZnO prec.
Product Distribution (% C. atoms)				
Ethylene Feed				
Methane	2.8	2.8	2.9	3.2
Ethylene	4.4	4.6	8.5	3.4
Ethane	5.1	5.5	11.5	21.0
Propylene	5.6	6.0	4.0	1.7
Propane	26.9	25.6	5.3	4.2
Butanes	7.5	6.9	2.0	0.8
Butenes	2.1	2.3	1.2	0.4
C ₅ ⁺ Aliphatics	3.4	2.4	1.9	3.6
Total aromatics	42.2	44.0	62.8	61.8
BTX/ Aromatics	0.84	0.82	0.85	0.83
Ethylene Conversion	96.6	96.7	93.5	97.3
Propylene Feed				
Methane	2.5	2.5	3.0	4.1
Ethylene	4.4	4.0	2.8	1.3
Ethane	3.8	3.9	5.3	11.6
Propylene	6.2	5.3	4.5	3.5
Propane	28.6	29.5	10.0	13.5
Butanes	7.9	8.1	3.2	2.0
Butenes	2.4	1.9	1.5	0.9
C ₅ ⁺ Aliphatics	3.8	3.2	4.2	0.8
Total aromatics	40.4	41.6	65.5	62.2
BTX/ Aromatics	0.84	0.84	0.91	0.88
Propylene Conversion	95.3	95.6	96.2	97.4
Propane Feed				
Methane	3.3	2.6	1.7	2.4
Ethylene	2.9	2.5	1.4	1.6
Ethane	1.9	1.4	1.8	2.7
Propylene	2.8	2.2	2.3	2.3
Propane	81.4	81.2	80.4	79.6
Butanes	3.3	3.1	2.2	1.9
Butenes	0.9	0.6	0.5	0.5
C ₅ ⁺ Aliphatics	1.4	3.5	0.9	0.2
Total aromatics	2.1	3.0	8.7	8.9
BTX/ Aromatics	0.82	0.8	0.91	0.91
Propane Conversion	23.4	27.9	29.4	28.2

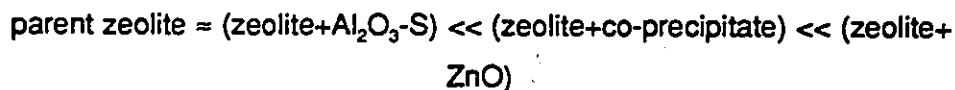
C₅⁺ Aliphatics: Aliphatic molecules having C5- C10 C. atoms.Parameters: Temperature R_c: 500°C; WHSV: 0.5h⁻¹.

spillover occurring in the reverse direction (91). In fact, the presence of an external pressure of hydrogen significantly reduces the aromatization promotion action of the co-catalyst (115), probably by saturating the surface of the co-catalyst which chemisorbs hydrogen.

The sequence of relative selectivity to aromatics in the presence of olefinic feeds is:



In the presence of paraffinic feeds, this sequence is modified to:



Aromatization of a light paraffin requires a preliminary dehydrogenating step with respect to an olefinic feed. From the above activity trends, this prerequisite is better fulfilled with pure ZnO.

SEM photographs (Fig. 2.15) show the textural properties of three co-precipitate surfaces and commercial ZnO. Two distinct phases are discernable: one similar to a sponge, the other smoother and more like a block. It is possible to envisage a co-penetration of the two textures, maximized when $\text{Zn/Al} \geq 1.0$, that may be involved in explaining the co-catalyst's activity.

To ascertain the importance of the co-precipitates acidic properties, the co-catalyst was neutralized with Na_2O (72). Catalytic comparison between hybrid and doped hybrid catalysts showed a much lower aromatic formation in the latter case. Acidity measurements obtained by ammonia TPD yielded a decreased acid density.

The aromatization reaction involves the participation of olefinic oligomers (intermediate [a], Fig. 2.8), and they can be used as a starting point for explaining the HBS mechanism. This step leads to the evolution of three hydrogen molecules. Via hydrogen redistribution reactions discussed by Poutsma (123), they can react with an

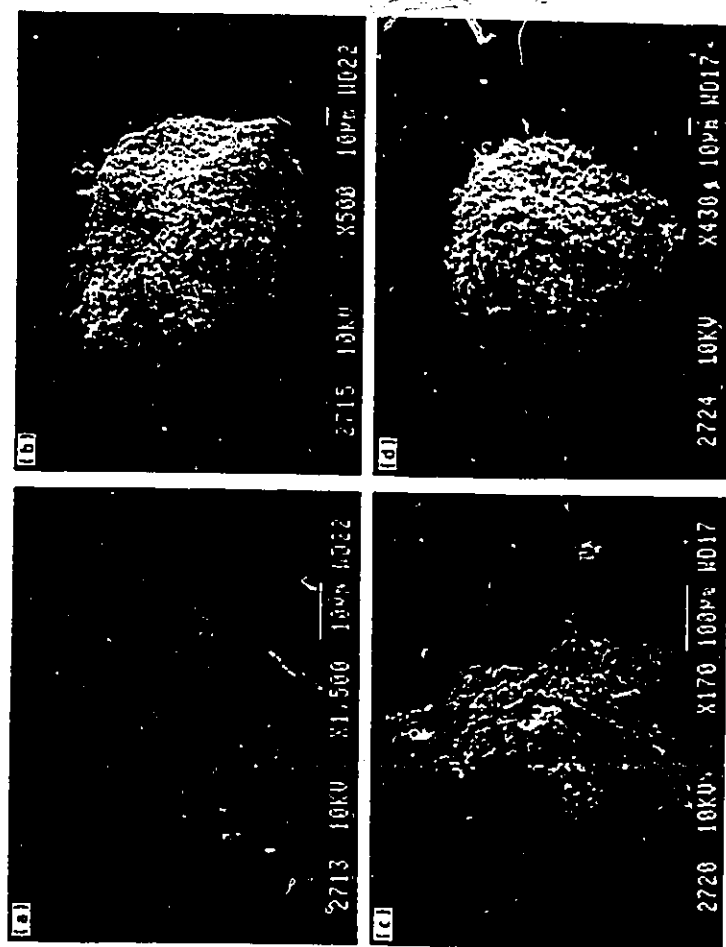
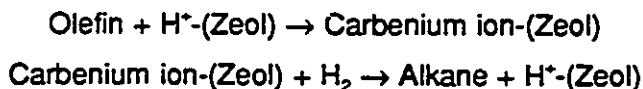


Figure 2.15 Scanning electron microscopy photographs: (A) Zn/Al = 0.14; (B) Zn/Al = 0.14; (C) ZnO precipitate; (D) ZnO (BAKER)

adsorbed carbenium ion (intermediate [b], Fig. 2.8) to generate an alkane which desorbs from the zeolite, restoring the free acid site. The following scheme can be used:



The reverse reaction of the second step is identical to the formation of a carbenium ion by hydride (H^-) abstraction. This mode of activation occurs when an alkane adsorbs on a strong Brønsted acid site, with the resulting evolution of hydrogen.

However, the situation where three carbenium ions are adsorbed on three adjacent sites and are also very close to an aromatizing site, is quite demanding in terms of reaction geometry. Therefore, aromatization occurs as a sequence of condensation and rearrangement steps while the intermediates migrate in the zeolite channels. Furthermore, the adsorbed hydrogen species must also migrate on the surface (on the acid sites (84)) in order to be released at the outside of the zeolite particles. This induces a disturbance of the efficiency for aromatic formation within the channels and the resulting localized hydrogen partial pressure may affect the equilibrium position.

Considering the surface of the oxide component, alkenyl-type species must be adsorbed on the co-catalyst to further react with hydrogen to form the corresponding alkane. Active sites must be present which have the capacity to trap hydrogen species (sink) and to enable them to react with hydrocarbons (scavenging). Modification of their catalytic behavior by Na_2O doping, have indicated (72) that neutralization of the co-precipitate's acidity or at least alteration of the electron density distribution must be considered when trying to describe the intrinsic properties of the co-catalyst which explain the hydrogen back-spillover mode of action.

The role of ZnO within the co-precipitate must be considered. In fact, hydrogen adsorption is thought to occur on the ZnO surface having Zn^0 and Zn^+ defects (116), which can act as active sites for hydrogen species migrating on the surface of the co-catalyst. The presence of zinc oxide reduction species has been confirmed using ESR by Spinicci and Tofanari (116). Therefore, the maximum activity observed for mixed oxide hybrids ($\text{Zn}/\text{Al} \geq 1.0$), is probably due to a combined redox/acido-basic effects.

2.4 Conclusions

Pure H-ZSM-5 zeolites have a definite advantage in the synthesis of aromatics from light olefins and paraffins. The medium pore size (5.5\AA) and tridimensional intersecting channel network, provides steric and geometrical constraints that favor the production of commercially valuable BTX hydrocarbons.

It has been shown that chemical modification of ZSM-5 zeolites by isomorphous substitution (gallium) or ion-exchange (zinc), can result in increased aromatic yields. By admixing a small quantity of oxide function (ZnO or $\text{ZnO}/\text{Al}_2\text{O}_3$ co-precipitate) with the H-ZSM-5, a synergistic effect for aromatization of light olefins and paraffins has been observed. It has been shown experimentally that the presence of the co-catalyst promotes hydrogen evacuation from the zeolite lattice. The result is a long distance ($\geq 1\mu\text{m}$) hydrogen back-spillover action where $\text{H}_{2(g)}$ migrate from the zeolite internal acid sites to the acido-basic/ redox co-catalyst surface.

The development of novel hybrid catalysts is of scientific and applied interest because it opens the way to the preparation of catalysts with improved catalytic activity and selectivity. Furthermore, it allows modification of the components individually.

In this chapter, hydrogen back-spillover has been claimed as the promoting effect of aromatization on hybrid catalysts. The next section will examine the established model of spillover, illustrate its incidence and action in other catalytic reactions and provide more probing experimental evidence for the studied reaction. Monitoring of $\text{H}_{2(g)}$ in the gaseous effluent will be used to provide more information about sink/scavenging actions.

**3.0 Evidence for the Involvement of Hydrogen Back-Spillover
In the aromatization of light olefins and paraffins
on hybrid zeolite catalysts**

Partly presented in references 115, 126-129 (232).

3.1 Introduction

BTX aromatic hydrocarbons have a high commercial value. They can be used as octane boosters in gasoline, as feedstock for plastics, as commodity chemicals, etc. Great efforts have been devoted in the last decade for the development of new upgrading processes, focused on the selective production of these monoaromatics from lower value fractions (80-83, 85-86, 90, 94-95).

In the M2-Forming process (80-82) developed by Mobil Oil, light olefins and paraffins are converted to BTX aromatics on a pure H-ZSM-5 catalyst, having a $\text{SiO}_2/\text{Al}_2\text{O}_3$ ratio equal to 70. It is reported that on this catalyst, the aromatic yield is limited by a hydrogen constraint, since the hydrogen content in the products is lower than in the feed (8.7wt.-% vs 18.3wt.-% respectively). At the reaction temperature (538°C), cracking is important and the excess hydrogen is expelled in the form of methane, ethane as well as a small amount of molecular H_2 . The result is a limited aromatic yield because of hydrocarbon loss.

In the CYCLAR process developed jointly by BP/UOP (86), gallium is added by a reflux procedure to the ZSM-5. A certain quantity of Ga^{3+} ions are inserted in the zeolite framework, while some Ga_2O_3 remains on the surface. It is observed that propane and n-butane are selectively converted to aromatics and a significant amount of hydrogen is co-produced. An additional dehydrogenation activity has been attributed to gallium species formed during the reaction (88, 107).

In the preceding chapter, it was shown that hybrid catalysts obtained by mechanically admixing the H-ZSM-5 zeolite ($\text{Si}/\text{Al}=40$) with a small amount of ZnO based co-catalyst (ZnO precipitate or commercial; $\text{ZnO}/\text{Al}_2\text{O}_3$ co-precipitate), could result in a selective conversion of short chain hydrocarbons to BTX compounds. The synergistic aromatic production observed when a metal oxide was placed at the pore openings, was explained by long-distance hydrogen back spillover. The involvement of HBS in aromatization of light paraffins on hybrid ZSM-5, has recently been confirmed by Fujimoto *et al.* (130-131) using alumina-supported Ga_2O_3 or pure gallia co-catalysts.

Mole *et al.* (111) have discussed the effects of zinc in the ZSM-5. The increased selectivity for propane aromatization has been ascribed to the presence of zinc ions in the lattice, which enable the catalyst to reject hydrogen species as H_2 molecules rather than as light alkanes. In a model describing the aromatization reaction sequence, the rate of hydrogen diffusion in the zeolite was shown to increase in the presence of metal ions. The dehydrogenation of alicyclic intermediates was said to be in quasi-equilibrium, thus shifting the selectivity toward BTX formation (111).

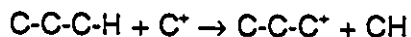
Recent results by Le Van Mao *et al.* (114-115, 132-133) have shown that α -quartz, used without the addition of any metal, is also an effective co-catalyst in n-butane aromatization on ZSM-5 hybrids. Alone, quartz does not chemisorb any gaseous hydrogen at the reaction temperature. The effects of α -quartz particle sizes were investigated (132). It was demonstrated that when the average particle size of the co-catalyst is small (90 μm , BET surface area 0.7m²/g vs 675 μm), n-butane conversion is increased. The aromatic yields (32.8 vs 29.1wt.-%) and H_2 productions (0.101 vs 0.079mole H_2 /C.atom) are also affected. A HBS action/ sink effect for the co-catalyst in the absence of metal function, has been related to a decreased surface energy barrier at the ZSM-5 crystallite pore openings (114-115, 127, 129, 132-133), a sort of tunnel effect by hydrogen species across particle boundaries (134-135).

The aim of this chapter is to define the role of the metal oxide co-catalyst in the various steps of the aromatization sequence for pure and mixed olefinic/paraffinic feedstocks. Differences due to co-catalyst compositions (ZnO or ZnO/Al₂O₃ co-precipitate with Zn/Al ratio equal to 1.0) will be pointed out. From a series of experiments designed specifically to probe certain properties of the catalyst, the importance of hydrogen transfer will be demonstrated. A proposal will be made to explain the mode of action of HBS in aromatization on hybrids.

3.2 Hydrogen effects In catalysis and hydrogen spillover

On solid acid catalysts such as zeolites, hydrocarbons are adsorbed as carbocations or carbenium ions. The hydrogen transfer reactions associated with positively charged adspecies, are hydride transfer reactions (111, 123, 136). Hydride transfer by carbenium ions is of great importance in many reactions such as catalytic cracking, alkylation, isomerization and hydrocracking of paraffins, as well as the aromatization of olefins and paraffins. On bifunctional catalysts that have acid sites and hydrogenation/ dehydrogenation functions close by, the increased activity of hydrogen transfer reactions is used to explain the catalytic performance.

Acid catalyzed cracking of paraffins generally involves a bimolecular hydrogen transfer step between the reactant molecule and a product carbenium ion (36,123, 136):



As a result of hydride transfer between olefinic products, hydrogen rich paraffins and hydrogen poor polyolefins, aromatics and coke precursors are co-produced. Successive hydrogen transfer activity eventually leads to the formation of coke, the major cause of deactivation in cracking catalysts.

In medium pore zeolites such as the ZSM-5, low hydride transfer activity is observed because of steric constraints in the channels and reaction loci (136). At low temperature, light olefins undergo rapid isomerization, oligomerization and interconversion reactions with remarkable selectivity and catalyst stability. At longer contact time or increased temperature, a shift in product distribution toward BTX aromatics and light paraffins occurs because the conversion or the rates of hydrogen transfer and cracking reactions increase respectively. In ZSM-5 zeolites, coking is minimized because of transition state shape selectivity. Hydrogen transfer reactions are involved in controlling product selectivity. Adsorbed hydride species can migrate on acid sites in the zeolite lattice (84), to eventually be released as $\text{H}_{2(g)}$, or they can react with an adsorbed hydrocarbon fragment to form the corresponding paraffin. The contact time and the temperature determine the incidence of paraffin formation.

The mobilization of a adsorbed species from one phase onto another where it does not directly adsorb from the gas phase, is called spillover (137-138, 151). The spillover species can react with another adsorbing gas on the second phase or can activate it. Spillover depends on at least two prerequisites: a source for the spilling species and an acceptor. Reverse or back-spillover is observed to proceed by surface migration of the spilt over species from the accepting phase to the metal, where they can desorb as H_2 molecules or react with another hydrogen acceptor such as O_2 or ethylene. The second phase acts as a porthole for the hydrogen species produced by the reaction.

Hydrogen spillover can result in partial reduction of semiconductors or insulating oxides, and cause a modification in the global catalytic properties of a solid. Common to each proposal of spillover explanation, is the dissociative adsorption of H_2 onto a metal (Pt, Ni) or metal oxide (ZnO , Cr_2O_3). Three possible H_{sp} species can be created: ionic (H^+ or H^-), radical (H^\cdot) or bonded ($H-$). Studies (137) suggest that atomic hydrogen (as radical or ion) is involved in the creation of active sites on various oxides.

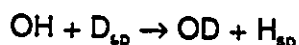
Catalytic hydrogenation of ethylene, acetylene and C_6 -cycles has been studied on SiO_2 activated by hydrogen spillover prior to the reaction (139-143). NH_3 and O_2 poisoning experiments showed no effect on the hydrogenation ability of the activated surface, suggesting the creation of new sites on SiO_2 which are not acidic in nature (139). Proton NMR studies by Lenz *et al.* (149) have shown that H_{sp} is radical like on silica and that the active site is electron-rich: metallic or basic. According to Candau *et al.* (150), spillover and diffusion of hydrogen species on SiO_2 occurs by a chain reaction which is mediated by the hydroxyl groups of the surface. Using *in situ* FTIR, surface diffusion coefficients ranging between 10^{-3} and $10^{-6} \text{ cm}^2 \text{ s}^{-1}$ have been measured, faster than previously estimated and not rate limiting.

The alumina surface has also been activated toward CO or ethylene hydrogenation by hydrogen spillover above 400°C (144-147) or by oxygen spillover (148). These activated SiO_2 and Al_2O_3 surfaces have shown induction periods when the first dose of ethylene was introduced in the closed system, but not the second. The induction period disappeared if activation was followed by a vacuum treatment prior to the reaction. These results indicate that new surface sites are created on insulating oxides by the spillover hydrogen species during the activation step. H_{sp} must be removed from the activated

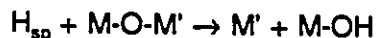
surfaces to obtain high hydrogenation activities.

In two recent reviews by Teichner (151) and Pajonk (138), the impact on catalysis by hydrogen and oxygen spillover phenomena, as well as the types of Spillover Assisted Catalytic Reactions (SACR) are discussed.

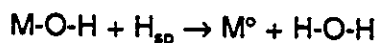
Teichner (151) describes how spillover hydrogen may produce various changes in the non-metallic phase onto which it migrates. It can be a simple exchange:



or in a stronger interaction, the spilled species may react with the oxide leading to the creation of surface defects or active sites:



The oxide may even be reduced with the production of water (surface or bulk effect):



In many cases, the oxide phase can be activated by the creation of new catalytic centers by the spillover species (e.g., Al_2O_3 (144-147) and SiO_2 (139-143)).

Synergy between two phases can have the following origins:

- (1) Bifunctional catalysis
- (2) Creation of new active sites at the interface
- (3) Spillover- remote control
- (4) Spillover- reaction

As described by Weisz (152), bifunctional catalysis refers to a class of catalysts where sites responsible for distinctly different reactions or reaction steps, are components of the solid catalyst. Paraffin isomerization on silica-alumina supported-Pt is a typical example. A general prerequisite for bifunctional catalysis requires physical conditions of

intimacy between the components so that mass transfer limitations are eliminated. Mixed catalytic components are described by Weisz as capable of exhibiting bifunctional catalysis. The second surface acts in the interception of the reaction products formed on the first phase, thus diverting the reaction selectivity (152). The important properties of the catalyst components are:

- (1) the particle sizes of each component in the mixed catalyst composite;
- (2) the maximum degree of heterogeneity allowed in the catalyst mass, with regards to the distribution of regions or patches for each type of catalytic activity.

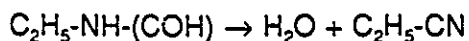
The creation of new active sites at the interface refers to the modification of intrinsic catalytic properties by Metal-Support Interactions (MSI) (153). They can be weak (e.g., $\text{ZnO} + \text{Al}_2\text{O}_3 \rightarrow \text{ZnAl}_2\text{O}_4$ at high temperature (154)-WMSI), medium (metal on zeolite (153)-MMSI) or strong (Pt on TiO_2 (155)-SMSI). According to Bond (153), the principle behind MSI induced changes deals with the effect a support can have on the electronic properties of a metal or vice versa.

Remote control spillover refers to a situation where the activator phase is separated from the acceptor prior to the reaction. The surface of a usually inert oxide can be activated by the spillover species and result in the creation of new active sites (e.g., Al_2O_3 and SiO_2 in the hydrogenation of ethylene after $\text{Pt}/\text{Al}_2\text{O}_3$ pretreatment in the presence of hydrogen gas).

Reaction spillover occurs when the activator and acceptor are not separated. The spillover species then participate in the reaction because of their suitable diffusion coefficients ($10^{-3} \text{ cm}^2 \text{ s}^{-1}$ on SiO_2 (150)) and activation energies ($\approx 1 \text{ kcal/mol}$) (151).

Pajonk (138) separates Spillover Assisted Catalytic Reactions (SACR) in three categories:

- (I) Spilled over species as co-catalysts can be exemplified by the catalytic (redox/acidic) dehydration of n-ethylformamide in propionitrile on $\text{Sb}_2\text{O}_4/\text{MoO}_3$ in the presence of oxygen gas.



Oxygen does not directly react with the reactant, but its presence is necessary to maintain a high selectivity and avoid catalyst deactivation. O_2 adsorbs on Sb_2O_4 and spills over to the MoO_3 surface where dehydration takes place. The action of O_{sp} is to prevent deactivation by preventing MoO_3 partial reduction.

(II) Spillover species as poison (coke) scavengers can be exemplified by Pt/alumina vs Pt-Sn/alumina catalysts in coking experiments. Under reaction conditions, hydrogen is not co-fed with the hydrocarbon stream. Although the amount of carbonaceous deposit on both catalysts is equal after the coking treatment, when Sn is present the Pt surface remains free from coke. The effect of Sn is to keep the coke precursors (olefins and aromatics) less strongly adsorbed and more able to migrate on the support. A longer catalyst lifetime is obtained.

(III) Spillover with kinetically active species is exemplified by the dehydrocyclization of small paraffins and olefins on hybrid ZSM-5 catalysts (reverse spillover). The importance of SACR is well established.

3.3 Experimental

3.3.1 ZSM-5 zeolite synthesis

Several zeolites were synthesized according to the method of Argauer and Landolt (100). The composition of the synthesis gel and the parameters were selected so the resulting zeolites had a Si/Al atomic ratio ranging between 19 and 95. Silicalite was obtained commercially from Linde. The procedure used to obtain the final form of the zeolites, as well as characterization techniques used on the zeolite powders in their acid form, are as described in section 2.2.1. Table 3.1 reports the results of characterization experiments.

Prior to using a new zeolite, standard catalytic tests for pure and hybrid catalysts were conducted to ensure uniformity and reproducibility with previously synthesized batches.

3.3.2 Synthesis of the co-catalysts

The co-catalysts were synthesized by heterogeneous co-precipitation according to the preparation method described in section 2.2.2. In this chapter, only pure ZnO and ZnO/alumina co-precipitate (from aluminium sulphate salt) ($\text{Zn/Al}=1.0$) were used. The co-catalysts were crushed and sieved. The oxide powders were characterized by atomic absorption, X-ray powder diffraction, BET surface area, SEM, hydrogen chemisorption and ammonia TPD. Table 3.1 reports the results of the characterization experiments.

3.3.3 Acidity measurements

For the zeolite and co-precipitate surfaces, the technique of temperature programmed desorption (TPD) of ammonia was used to determine the acid site density and relative acid strengths. The operative procedure is as outlined in section 2.2.3.

Table 3.1 Physico-chemical properties of the various hybrid catalyst components.

Zeolite⁽¹⁾	Si/Al ratio	Na₂O (wt.-%)	DC	BET surface area (m²/g)	Total acid density⁽²⁾ (x10⁴ mol/g)
H-ZSM-5(20)	19.9	0.10	100	361	13.5
H-ZSM-5(32)	31.5	0.09	98	436	8.0
H-ZSM-5(36)	36.0	0.08	102	408	3.4
H-ZSM-5(95)	94.5	0.02	97	361	1.4
H-ZSM-5(125)	124.9	0.06	110	420	0.8

Co-catalyst⁽³⁾	Zn/Al ratio	BET surface area (m²/g)	Average pore size (Å)
(Treated at 550 C for 12h.)			
ZnO(Baker)	∞	4.2	104
ZnO/Al ₂ O ₃ co-precipitate	1.0	27.4	98

Matrix			
Bentonite clay (extrudate)	-	2.3	169

DC: Degree of crystallinity with respect to H-ZSM-5(20).

(1) Zeolite average particle size (SEM) 2-3μm.

(2) Total acid density measured by NH₃-TPD.

(3) Co-catalyst average particle size (SEM) 80-100μm.

3.3.4 Hydrogen chemisorption measurements

To measure the hydrogen adsorption capacity of the co-catalyst powders, extrudates (0.8g) were loaded in a quartz reactor and pretreated at 550°C under flowing He overnight. Using a volumetrically calibrated loop (1ml), hydrogen gas was pulsed at 500°C. The effluent was monitored using a SRI student GC equipped with a thermal conductivity detector (TCD) and set on-line with the furnace. The amount of nonadsorbed hydrogen gas was estimated by integration of the chromatographic trace obtained for every pulse. Known amounts of H₂ were injected into the GC as a volumetric calibration procedure, so TCD responses could be reported as moles H₂/ pulse. The difference between total moles H₂ pulsed and the recorded non-adsorbed fraction indicated the capacity for adsorption of the co-catalyst surface at 500°C, a temperature used for catalytic reactions.

3.3.5 Preparation of the catalysts

To prepare the final catalysts, the H-ZSM-5 powders (mesh size higher than 60) and zinc oxide based precipitate powders (mesh size higher than 60) were mechanically mixed at room temperature. The required amounts varied between 0 and 80wt.-%. Bentonite clay (20wt.-%) was then incorporated and intimately mixed with the solid catalyst. Deionized water was added dropwise until a malleable paste was obtained. The latter was extruded into 1.5mm O.D. *spaghettis*. The final extrudates were dried at 120°C overnight and activated in air at 550°C for about 10h. The final length of the catalyst extrudates was 5 ± 0.5 mm.

For the samples where the co-catalyst was introduced by dry impregnation, instead of using deionized water to obtain a malleable paste, an aqueous solution containing the required amount of zinc nitrate and/or aluminium sulphate was used. The principle of this incorporation method is that as the aqueous solution is added, it is preferentially absorbed by the bentonite clay binder which acts as a sponge. Upon extrusion, the force causes the zinc or aluminium hydroxyls to migrate onto the exterior of the zeolite crystallites.

3.3.6 Catalytic testing

Catalytic testing was as described in section 2.2.5. Figure 2.3 shows the schematic experimental set-up. The feed was composed of gaseous olefinic and paraffinic hydrocarbons (reference: Table 2.3), as generated in a bench scale steam-cracker (R_s and V1), or pure feedstocks (R_s and V2 introduction).

The normal operating parameters of the horizontal steam-cracker unit were as follows: feed: propane, temperature R_s : 820°C or 840°C, temperature R_c : 500°C, residence time: 0.85s and 0.75s respectively, water-to-propane molar ratio: 1.1, resulting WHSV: weight feed (gh^{-1})/ weight catalyst (g) = 1.5-1.7 h^{-1} V1. For the runs conducted with pure feedstocks (ethylene, propane and n-butane), the usual reaction parameters were as follows: temperature R_c : 500-540 \pm 0.5°C, WHSV: weight feed (gh^{-1})/ weight catalyst (g) = 0.6 h^{-1} V2, weight catalyst: 4g, duration of a run: 4h.

For experiments where the catalyst was reduced prior to the reaction, a mixture of H_2 in N_2 was introduced by V2, while the catalytic reactor temperature was maintained at 400°C for 3.5h.

For experiments in which H_2 or air were co-fed, the carrier gas/co-feed mixtures in required amounts, were mixed prior to contact with the hydrocarbon feed and introduced by V2.

The liquid hydrocarbons formed by the steam-cracking and catalytic reactions were collected in condensing flasks kept at -15°C. The gases were analyzed throughout the run using a Shimadzu GC (Model Mini 3, FID) equipped with a 2.5-m stainless steel column (15wt.-% squalane on Chromosorb P) with 2,2-dimethylbutane as internal standard. The amount of hydrogen in the effluent was measured chromatographically using a 30-m HayeSep DB column from Chromatographic Specialties (HP Model 5890-TCD/ N_2 carrier gas). Prior to analysis, a volumetric calibration was performed using pure hydrogen gas. The collected liquid phases were subsequently analyzed with a Hewlett Packard GC (Model 5790A, FID) equipped with a 50-m PONA type capillary column. When required, n-octane was used to extract the organic phase prior to chromatographic analysis. The n-octane peak was considered as solvent in the chromatogram and was

excluded from the product distribution.

3.3.7 Product calculations

All calculations were made on a carbon atom basis. Chromatographic results were converted to C. atoms using an internal standard (2,2DMB) for the gaseous effluent and correction factors for the columns.

The definitions of total feed conversion, selectivity and yield for product *i* can be found in section 2.2.6.

3.4 Results and discussion

Si/Al atomic ratio variations in zeolites, induce acid density and acid strength distribution changes. As discussed in section 1.3.3, increasing the Si/Al ratio or decreasing the aluminium content, results in driving up the ionicity of the Al-O bonds (20) and acid strength increases progressively. On pentasils, changes in the acidity when Si/Al ratios vary, cause changes in the activity and selectivity for cracking and aromatization reactions.

Cracking studies (156-157) have shown that only the strongest acid sites are selective for cracking paraffin molecules. In cracking of n-hexane, the intrinsic activity for the formation of both paraffins and aromatics decreased at higher $\text{SiO}_2/\text{Al}_2\text{O}_3$ ratios. The relative concentration of acid sites on which hydrogen transfer reactions occur, was singled out as an important factor in determining the activity and selectivity of the zeolite framework.

Aromatization reactions dominate at low Si/Al ratios, since oligomerization/cyclization are favored when carbenium ions exist in high concentration. Cyclodehydroaromatization by a series of hydride abstractions (111, 123), depends on effective acid mediated hydrogen transfer reactions, enhanced by high acid densities (84, 136).

Table 3.2 reports the influence of the Si/Al ratio in a H-ZSM-5 for n-butane aromatization. It is observed that the total catalytic activity, expressed as n-butane conversion, decreases as the Si/Al ratio increases. The highest aromatic selectivity is achieved when the Si/Al ratio is low. The cracking tendency, given by the aromatics to methane yields ratio, increases with acid strength (increasing Si/Al) as expected.

Hydrogen is co-produced during aromatization, coking and cracking (158-159), as a result of hydrogen rearrangement reactions. It can be eliminated as molecular hydrogen or react with other adsorbed species, forming methane and other light paraffins. The formation of saturated molecules competes with the aromatization reaction. If an adequate hydrogen sink was provided, it is possible to imagine the removal of more hydrogen as H_2 from the reaction loci. This would limit the hydrocracking tendency of the adspecies in the zeolite channel network and increase the aromatic production.

Table 3.2 Effect of zeolite Si/Al ratio in n-butane aromatization.

H-ZSM-5 Si/Al ratio	(19)	(32)	(36)	(95)	(125)
Total Product Distribution (% C. atoms)					
C1-C3 Paraffins	50.5	55.4	49.9	5.6	4.9
Butanes ⁽¹⁾	5.0	5.7	14.3	87.3	87.7
C2-C4 Olefins	11.9	16.8	19.6	6.6	7.1
C ₅ ⁺ Aliphatics	1.7	1.0	1.2	0.1	-
Total Aromatics	31.1	21.2	15.2	0.4	0.3
BTX/Aromatics	0.92	0.91	0.93	1.0	1.0
n-Butane conversion (% C. atoms)	96.2	96.0	88.5	36.2	32.0
Aromatics/Methane ⁽²⁾	3.7	1.8	1.7	0.3	0.2

(1) iso-Butane almost absent (< 2wt.-%).

(2) $Y_{\text{aromatics}}/Y_{\text{methane}}$ = Cracking or hydrocracking tendency of the zeolite.

C₅⁺ Aliphatics: Aliphatic molecules having C5- C10 C. atoms.

Feed: n-Butane; Temperature R_g: 550°C; WHSV: 0.6h⁻¹.

Catalyst composition: 80wt.-% H-ZSM-5 + 20wt.-% bentonite binder.

Table 3.3 Hydrocracking tendency of hybrid catalysts used in n-butane aromatization.

Catalysts	Aromatics/Methane
H-ZSM-5(32)+Co-precipitate	5.7
H-ZSM-5(36)+Co-precipitate	7.1
H-ZSM-5(95)+Co-precipitate	2.4
H-ZSM-5(125)+Co-precipitate	1.0

Feed: n-Butane; **Temperature** R_c : 550°C; **WHSV**: 0.6h⁻¹.

Catalyst composition: 75wt.-% H-ZSM-5 + 5wt.-% ZnO/Al₂O₃ co-precipitate (Zn/Al=1.0) + 20wt.-% bentonite binder.

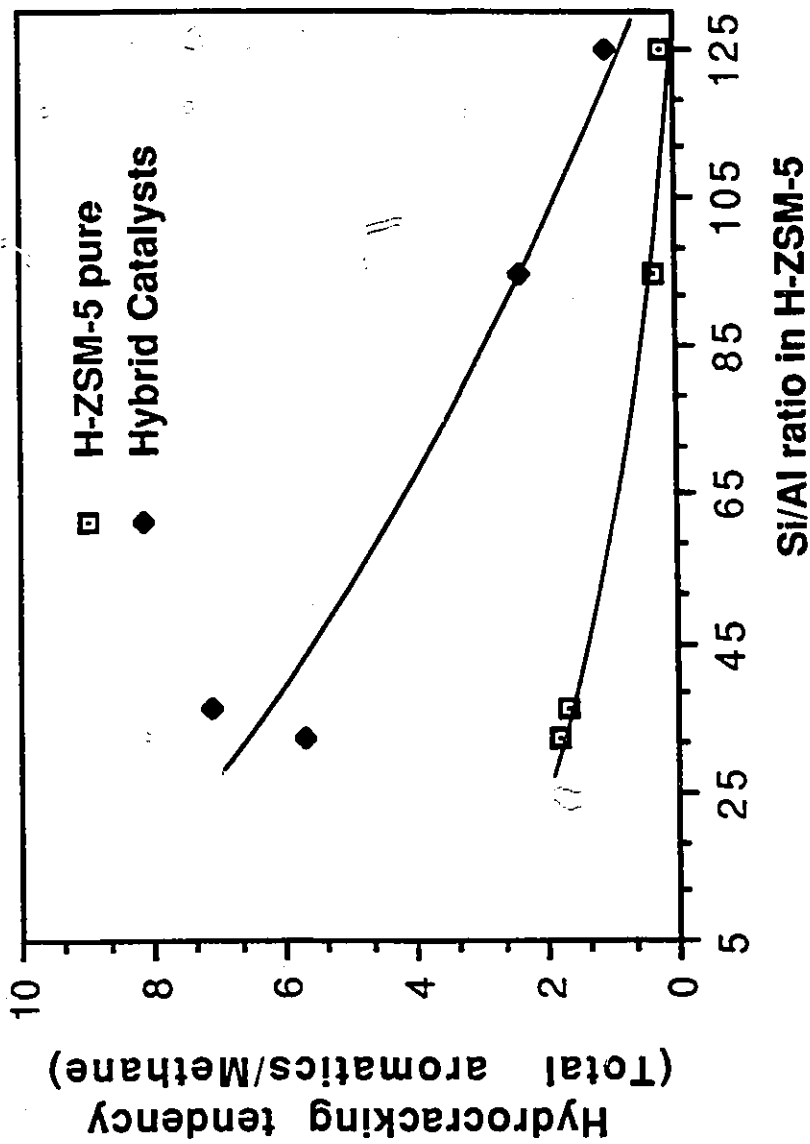


Figure 3.1 Hydrocracking tendency for pure H-ZSM-5 and $\text{ZnO}/\text{Al}_2\text{O}_3$ ($\text{Zn}/\text{Al} = 1.0$) co-precipitate hybrid catalysts as a function of the Si/Al ratio in the H-ZSM-5 zeolite.

Feed: n-Butane; Temperature R_c : 550°C ; WHSV: 0.6h^{-1} .

Catalyst composition: (Pure) 80wt.-% H-ZSM-5 + 20wt.-% bentonite binder
(Hybrids) 75wt.-% H-ZSM-5 + 5wt.-% $\text{ZnO}/\text{Al}_2\text{O}_3$ ($\text{Zn}/\text{Al} = 1.0$) co-precipitate + 20wt.-% bentonite binder.

Table 3.4 Conversion of n-butane on 'pure' ZnO catalyst (adapted from reference 126).

Catalyst	Bentonite (blank)	ZnO	ZnO reduced in H ₂	ZnO
Feed	n-butane	n-butane	n-butane	n-butane + 55% H ₂ /N ₂
Conversion (% C. atoms)				
	21.0	31.4	22.4	30.1
Total Product Yield (% C. atoms)				
C1-C4 Paraffins	96.7	97.4	96.7	96.8
C2-C4 Olefins	3.3	2.6	3.2	3.0
C ₅ * Aliphatics	0.0	0.0	0.0	0.0
Total Aromatics	0.0	0.0	0.1	0.2

C₅* Aliphatics: Aliphatic molecules having C5- C10 C. atoms.

Temperature: 540°C; **WHSV:** 0.6h⁻¹.

According to Mole *et al.* (111), the presence of Zn^{2+} in the ZSM-5 lattice increases H_2 out diffusion, resulting in lower cracking activity and higher formation of oligomers and aromatics. Similarly, Table 3.3 reports that hybrid catalysts also provide a hydrogen adsorbent. The ratio of aromatics to methane yields for all Si/Al hybrids, are higher than those obtained for pure H-ZSM-5 analogs (Table 3.2). Suppression of the secondary formation of paraffins, especially methane, can be inferred upon addition of the second oxide surface. Results show that in speeding up hydrogen removal from the zeolite, the co-catalyst enables the zeolite to become more active in aromatization. Fig. 3.1 depicts hydrocracking tendencies as a function of Si/Al ratios for pure and hybrid catalysts.

In the case of paraffinic feeds, more hydrogen species need to be removed than for an olefin based source (4 moles vs 3 moles). As seen in Table 3.4 and discussed by Fujimoto *et al.* (130-131) and Gnep *et al.* (88), ZnO alone is not capable of directly dehydrogenating propane or n-butane. However, the presence of this component in a hybrid catalyst may promote the activation of paraffin molecules by a polarization effect of H-H and C-H bonds (109, 238). The polarization is thought to be responsible for the easier adsorption inside the zeolite framework (109, 238).

Two alternative pathways can be envisaged for the adsorption of a paraffin molecule (110, 126):

(I) cracking on the zeolite acidic sites:



The ethylene produced could then undergo oligomerization and aromatization. However, this pathway is unlikely since an appreciable increase in methane production was not recorded on hybrid catalysts (Table 3.3).

(II) Hydride abstraction on the zeolite acid sites (88), probably Lewis in nature (160):



(a): 1 mole hydrogen generated.

After the initial activation step according to scheme (II), adsorbed propyl cations can undergo oligomerization on the acid sites of the zeolite, followed by aromatization to benzene. It is suggested that the hydride species produced are submitted to an external pull exerted by the co-catalyst surface. Once adsorbed on this second oxide, they can be released to the stream as H_2 or ethane.

Data from Table 3.5 show two effects for pure ZnO in the hybrid using propane feed. To facilitate the initial activation of the reactant by hydride abstraction, as seen by a greater consumption of propane and low methane yield, and to beneficially use the scavenging action to promote aromatization, as seen by increased yields of both ethane and total aromatics.

The BTX aromatics product spectrum in Table 3.5, is significantly modified when ZnO is used as co-catalyst. The formation of benzene is favored at the expense of alkylated monoaromatics. Increased formation of benzene may be caused by dealkylation reactions assuming identical oligomeric reaction intermediates as proposed by Mole *et al.* (111).

Monitoring the amounts of molecular hydrogen in the outstream gases during the reactions, has provided direct evidence for the involvement of the co-catalyst in hydrogen removal during ethylene aromatization. Table 3.6 reports the obtained values for pure and hybrid catalysts based on ZnO or ZnO/alumina co-precipitate (Zn/Al=1.0). Column A shows a typical product spectrum obtained with a pure H-ZSM-5, with the associated total hydrogen production and the rate of hydrogen production normalized in time. Columns B and D show the product selectivities and associated hydrogen productions for fresh ZnO/Al₂O₃ co-precipitate and ZnO hybrids respectively. The results in columns C and E were obtained using catalysts B and D respectively, that had been reduced prior to reaction in a 30% H_2 / N_2 mixture for 3.5h at 400°C. It can be seen that within experimental error, ethylene conversions are constant for all catalysts. Therefore, differences in selectivity can be attributed to variations in catalyst chemical composition or pretreatment. Upon comparing columns A vs B and D, it can be observed that the addition of a co-catalyst surface favors the out migration of hydrogen species (30.5 and 16.2mmol H_2 /h vs 5.8mmol H_2 /h). The jump in H_2 production is paralleled by increased conversions of C_3 - C_4 olefins and C_5^+ aliphatics to total aromatics. Removal of hydrogen

Table 3.5 Comparative study of product yields between pure and hybrid catalysts in propane aromatization.

Catalysts	H-ZSM-5(38)	Zn/Al=1. Hybrid ⁽¹⁾		ZnO Hybrid ⁽²⁾	
		$\Delta^{(3)}$		$\Delta^{(3)}$	
Total Product Yield (% C. atoms)					
Methane	11.3	4.6	-6.7	8.1	-3.2
Ethane	5.5	10.9	+5.4	19.7	+14.2
Propane	49.1	47.4	-1.7	28.3	-20.8
Butanes	2.6	1.0	-1.6	0.6	-2.0
Ethylene	9.0	1.6	-7.4	1.1	-7.9
Propylene	7.2	7.8	+0.6	5.8	-1.4
Butenes	1.7	0.8	-0.9	0.6	-1.1
C ₅ ⁺ Aliphatics	1.2	0.2	-1.0	0.2	-1.0
Total Aromatics	12.6	25.7	+13.1	35.8	+23.2
BTX/Aromatics	0.90	0.94	-	0.90	-
BTX Aromatics Composition (wt.-%)					
Benzene	24.4	41.8	+17.4	46.7	+22.3
Toluene	43.7	40.2	-3.5	38.6	-5.1
Ethylbenzene	3.6	1.1	-2.5	0.7	-2.9
Xylenes	28.2	16.6	-11.6	13.7	-14.5
Styrene	0.2	0.3	+0.1	0.2	0

C₅⁺ Aliphatics: Aliphatic molecules having C5- C10 C. atoms.

(1) Hybrid catalyst: 75wt.-% H-ZSM-5(38) + 5wt.-% ZnO/Al₂O₃ co-precipitate (Zn/Al=1.0).

(2) Hybrid catalyst: 75wt.-% H-ZSM-5(38) + 5wt.-% ZnO(Baker).

(3) Percent variation with respect to yields obtained with parent H-ZSM-5(38).

Feed: propane; **Temperature R_c:** 540°C; **WHSV:** 0.6h⁻¹.

Catalyst composition: 80wt.-% Active phase + 20wt.-% bentonite binder.

Table 3.6 Aromatization activity and corresponding H₂ evolution on pure and hybrid catalysts. Effect of reduction on catalytic activity of the hybrids.

Catalyst	A	B	C	D	E
Total Product Selectivity (% C. atoms)					
C1-C4 Paraffins (Ethane)	39.5 (4.3)	26.3 (16.5)	20.3 (8.9)	40.0 (33.4)	37.0 (29.0)
C3-C4 Olefins	18.4	6.4	8.8	4.6	3.4
C₅⁺ Aliphatics	6.8	1.9	2.5	1.0	0.9
Total Aromatics	35.4	65.4	67.9	54.4	58.7
BTX/Aromatics	0.83	0.86	0.85	0.83	0.79
Ethylene Conversion (% C. atoms)	92.3	92.2	91.1	89.0	93.7
Total H₂ Produced (mmol)	5.4	29.5	44.6	19.8	26.4
Rate H₂ Production (mmol/h)	5.8	30.5	31.1	16.2	18.9
H₂/Aromatics (molar ratio)	0.4	1.3	1.7	1.2	1.0

C₅⁺ Aliphatics: Aliphatic molecules having C5- C10 C.atoms.

Feed: Ethylene; **Temperature** R_c: 500°C; **WHSV:** 0.6h⁻¹.

Catalyst Identification:(including 20wt.-% bentonite binder)

A 80wt.-% H-ZSM-5(43)

B 75wt.-% H-ZSM-5(43) + 5wt.-% ZnO/Al₂O₃ co-precipitate (Zn/Al=1.0)

C 75wt.-% H-ZSM-5(43) + 5wt.-% ZnO/Al₂O₃ co-precipitate (Zn/Al=1.0) reduced 30% H₂/N₂ 3.5h. at 400°C

D 75wt.-% H-ZSM-5(43) + 5wt.-% ZnO precipitate

E 75wt.-% H-ZSM-5(43) + 5wt.-% ZnO precipitate reduced 30% H₂/N₂ 3.5h. at 400°C

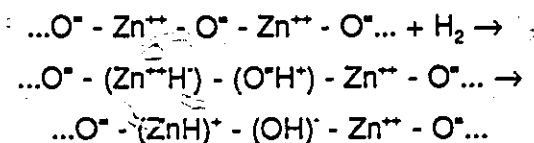
adspecies from the internal zeolite acid sites, results in a higher efficiency of the lattice for aromatization. 84.4wt.-% and 53.7wt.-% more aromatics respectively have been obtained under identical reaction conditions for B and D hybrids with respect to the pure ZSM-5 parent.

Upon comparison of ethane selectivities recorded for hybrids of mixed oxides and pure oxide co-catalysts (B vs D), as well as the rates of H_2 production for the same catalysts, it is found that:

- (1) the sink action, resulting in lower ethane production and higher $H_{2(g)}$ release, is predominant on ZnO/Al_2O_3 co-precipitate;
- (2) the scavenging action resulting, in lower hydrogen production and higher ethane formation, predominates on ZnO. The net effect of the scavenging action is the loss of potentially aromatizable ethylene by a side reaction on the co-catalyst surface.

Reduced catalysts in columns C and E show the same trends as their fresh analog, but H_2 productions are increased. Usually, for a fresh or oxidatively regenerated hybrid, an induction period characterized by low H_2 and ethane fractions in the gaseous effluent is observed. A 'steady-state' product distribution, is only attained 40-50 minutes after the start of the reaction. Hydrogen gas pretreatment submits the catalyst to a reductive atmosphere prior to the reaction and it is reasonable to believe that the changes occurring on the ZnO based components during that time, are similar to the modifications caused by H_{2p} during the induction period.

ZnO acid-base pairs are known to chemisorb H_2 . Heterolytic cleavage of molecular hydrogen on a ZnO surface yields (165):



Migration of H^+ to the next oxygen yields two hydroxyls and the production of metallic zinc:



In the above scheme, Zn-O is reduced by hydrogen chemisorption and a Zn(0) defect site is created in the lattice. ZnO, a typical n-semiconductor, also loses some of its lattice oxygens upon thermal treatment (around 500°C) (116, 194). Non-stoichiometric excess of zinc, as Zn(I) and Zn(0), are produced on the surface and are associated with localized electron excess concentrations. These defect sites could be the active sites responsible for dissociative adsorption of H_{sp} exiting the zeolite channels. This conclusion was also put forth by Spinicci and Tofanari (116) in ESR spectroscopy studies of ZnO based propylene dehydroaromatization catalysts.

The presence of alumina in the co-precipitate can be viewed as a third surface component that helps to free Zn-O active sites from adspecies, by promoting molecular hydrogen desorption from the surface (enhanced sink effect on ZnO/ Al_2O_3) (161). IR spectroscopic studies (162) have shown that hydrogen can be dissociatively adsorbed on η - and γ -alumina. Temperature programmed desorption studies (163) have shown that for alumina-supported metals, dissociatively adsorbed hydrogen is able to spillover until the surface is equilibrated. The reactivity of spillover hydrogen species toward hydrogenation of unsaturated molecules on alumina is low (144-147, 164).

Fig. 3.2 depicts the results of hydrogen chemisorption studies conducted at 500°C on fresh ZnO and ZnO/ Al_2O_3 co-precipitate (Zn/Al=1.0) samples. It can be seen that the adsorption capacity of fresh zinc oxide is smaller than that of ZnO/alumina. Table 3.7 shows that if the hydrogen adsorption capacity is reported per unit surface area, ZnO possesses twice the capacity of ZnO/ Al_2O_3 . Since the co-precipitate has a Zn/Al atomic ratio equal to 1.0 or 50mol.-% Zn in its chemical composition, only ZnO acid-base sites can directly adsorb H_2 from the gas phase. Therefore, at the onset of reaction alumina does not adsorb H_{sp} . However, since ZnO/alumina hybrids show a higher hydrogen desorption ability than ZnO hybrids after the initial induction period, it is reasonable to believe that the alumina surface becomes activated by a second migration of adsorbed hydrogen species from ZnO.

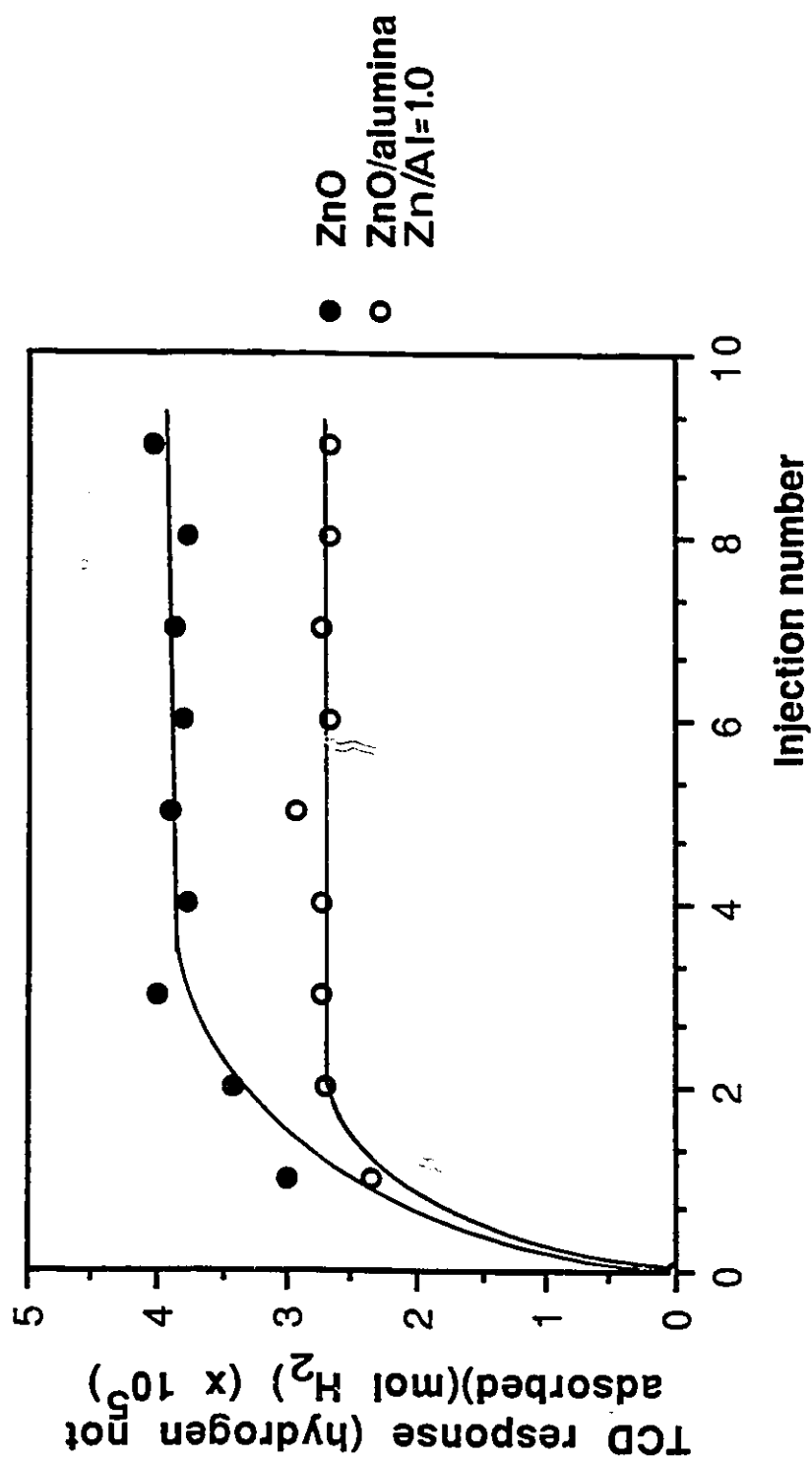


Figure 3.2 Hydrogen chemisorption studies of co-catalysts performed at 500°C.

Table 3.7 Results of hydrogen chemisorption experiments for the co-catalysts performed at 500°C.

Catalyst	ZnO precipitate	ZnO/Al₂O₃ co-precipitate (Zn/Al=1.0)
Hydrogen Adsorption Capacity per Unit Weight (mol/g)	4.249x10⁻⁵	16.02x10⁻⁵
Hydrogen Adsorption Capacity per Unit Surface Area (mol/m²)	1.180x10⁻⁵	0.5857x10⁻⁵

In summary:

- (1) the active sites on Zn-O responsible for H_{sp} adsorption, could be partial reduction sites or defects also created by H_{sp} during the induction period;
- (2) a greater amount of ethane is formed with pure ZnO because the most efficient method of removing H_{ads} is by reaction with ethylene (scavenging on ZnO);
- (3) in the case of ZnO/ Al_2O_3 co-precipitate, the amount of ethane is considerably reduced because of the role alumina plays in H_2 recombination (sink on ZnO/alumina);
- (4) the production of BTX aromatics is more important of ZnO/alumina co-precipitate because the scavenging action is not as important.

The HBS sequence on a co-precipitate hybrid catalyst can be suggested to be: the interception of hydrogen adspecies exiting the ZSM-5 channels by Zn-O active sites (partially reduced after time t) and subsequent migration to the activated Al_2O_3 surface with $H_{2(g)}$ release. Some ethane is formed by the reaction of H_{ads} and ethylene $_{ads}$.

The HBS sequence on ZnO hybrid catalyst can be suggested to be: the interception of hydrogen adspecies exiting the ZSM-5 channels by Zn-O active sites (partially reduced after time t) and the formation of ethane by $H_{ads} + \text{ethylene}_{ads}$ reaction on ZnO. Some $H_{2(g)}$ is also released.

The importance of physical contact between the zeolite and the co-catalyst can be assessed in Fig. 3.3. Catalyst A represents the standard catalytic activity for H-ZSM-5(36) and shows the lowest aromatic yield. Catalysts C and E are hybrids of ZnO/ Al_2O_3 co-precipitate and ZnO precipitate respectively. As expected for the aromatization of mostly olefins from a steam-cracker, catalyst C is more active. Catalysts D is a ZnO hybrid, where the co-catalyst was introduced by dry impregnation. In hybrid F, commercial ZnO powder of lower density than the precipitated ZnO was used. It is expected that for these latter catalysts, the surface at the interface between zeolite particles and oxide phase is more important. Results show a promotion of the scavenging action on the co-catalyst, enhanced by conditions of intimacy.

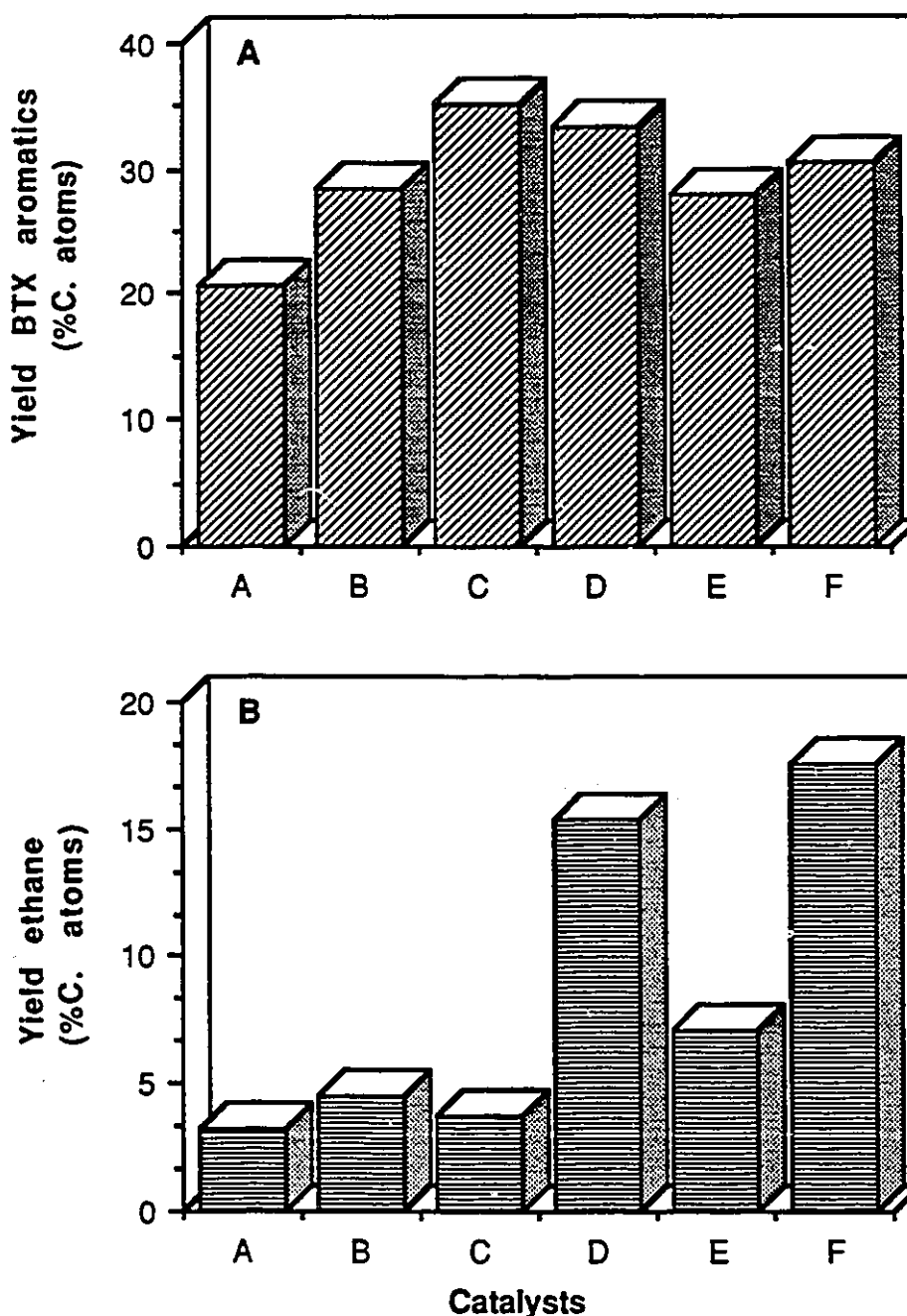


Figure 3.3 Studies of the effect of distance between the co-catalyst and the zeolite.
Feed: Table 2.3 820-Gas; Temperature R_c : 500 °C; WHSV: 1.5h⁻¹.

Catalyst composition: (Pure) 80wt.-% H-ZSM-5 + 20wt.-% bentonite binder
 (Hybrids) 75wt.-% H-ZSM-5 + 5wt.-% ZnO based co-catalyst + 20wt.-% bentonite binder.

Catalyst identification:

- A H-ZSM-5(36)
- B H-ZSM-5(36) + Zn/Al = 1.0 mixture (dry impregnation)
- C H-ZSM-5(36) + Zn/Al = 1.0 co-precipitate
- D H-ZSM-5(36) + ZnO (dry impregnation)
- E H-ZSM-5(36) + ZnO precipitate
- F H-ZSM-5(36) + ZnO Baker

Table 3.8 Influence of distance between zeolite and ZnO particles in n-butane aromatization (adapted from references 115 and 126).

Catalyst/Condition	A	B	C	D	E	F
Conversion (% C. atoms)	81.4	78.8	75.4	70.9	78.3	88.8
Total Product Yield (% C. atoms)						
C1-C4 Paraffins	63.0	65.5	63.8	62.7	67.2	46.0
C2-C4 Olefins	17.2	18.0	16.8	13.5	14.6	8.9
C ₅ ⁺ Aliphatics	3.2	2.6	3.2	2.8	2.2	1.3
Total Aromatics	16.6	13.9	16.2	21.1	16.0	43.8
BTX/Aromatics	0.92	0.93	0.92	0.93	0.94	0.92

C₅⁺ Aliphatics: Aliphatic molecules having C5- C10 C. atoms.

Temperature R_g: 540°C; WHSV: 0.6h⁻¹

Catalyst Composition: Pure H-ZSM-5(36) (80wt.-%) + 20wt.-% bentonite binder .

Bicomponent experiments: 75wt.-% H-ZSM-5(36) + 5wt.-% ZnO(Baker) + 20wt.-% bentonite binder.

Catalyst Identification and Catalytic Bed Conditions:

A H-ZSM-5(36)

B ZnO(Baker) --> H-ZSM-5(36) 2 beds separated by a porous disk

C H-ZSM-5(36) --> ZnO(Baker) 2 beds separated by a porous disk

D H-ZSM-5(36) + ZnO(Baker) mixed extrudates

E H-ZSM-5(36) extrudates of zeolite sorted out from mixture of experiment D .

F Hybrid H-ZSM-5(36) + ZnO(Baker)

Further evidence of the effects of distance between the two components for n-butane aromatization is shown in Table 3.8. In this series of tests pure extrudates were studied, mixed or in different catalyst bed configurations. Results show that the ZnO co-catalyst exerts its influence at rather large distances (column D), estimated to a few μm . This table also indicates that contamination of the zeolite framework by Zn^{2+} migration is excluded because enhancement of aromatic activity was not observed in reaction E (a catalyst previously used in the presence of mixed ZnO extrudates).

The significance of Zn^{2+} and Ga^{3+} solid-state ion exchange reactions with the zeolite, has been discussed thoroughly by Le Van Mao *et al.* (114-115, 132-133). It was shown for n-butane feed that even small amounts of inert oxides were effective co-catalysts. For alumina, silica gel, colloidal silica or α -quartz in their pure form, without the addition of any metallic ions, a 2-fold or more increase in aromatic formation was recorded. Alone, solid state ion exchange processes cannot justify the substantially modified catalytic selectivity observed in bicomponent systems. It is however possible, as discussed by Mériaudeau and Naccache (166), for $\text{Ga}_2\text{O}_3/\text{ZSM-5}$ catalysts after a redox treatment.

As proposed by several authors (130, 167-170), the addition of gaseous oxygen co-feed in paraffin conversions on pure ZSM-5, can increase aromatization propensity. The oxygen molecules act as a sink, able to react with hydrogen species adsorbed on the zeolite surface and removing them as water. Table 3.9 reports the influence of an added air partial pressure for n-butane aromatization on pure H-ZSM-5(36). The formation of water is observed as predicted, paralleled by an increased aromatic yield. Oxygen removes hydrogen by chemical reaction. In a similar fashion, the co-catalyst is active because it provides a porthole for the desorption of hydrogen species. Co-feeding hydrogen gas results in a slightly depressed aromatization activity for pure ZSM-5.

With regards to the importance of hydrogen in the explanation of enhanced aromatic selectivity, the effects of an added hydrogen partial pressure were systematically studied for ethylene aromatization. They are depicted in Fig. 3.4 A (aromatic yields), B (ethane yields) and C (H_2 production). The catalysts compared were: pure H-ZSM-5(42), $\text{ZnO}/\text{Al}_2\text{O}_3$ co-precipitate ($\text{Zn}/\text{Al}=1.0$) and ZnO precipitate hybrids. It can be observed that for the parent zeolite, the aromatic production decreases slowly, ethane yields are

Table 3.9 Influence of oxygen (air) and hydrogen on the aromatization performance of pure H-ZSM-5(36) (adapted from reference 126).

Feed	n-butane + N ₂ ⁽¹⁾	n-butane + air ⁽²⁾	n-butane + N ₂ + H ₂ ⁽³⁾
Conversion (% C. atoms)	81.4	85.3	75.2
Total Product Yield (% C. atoms)			
C1-C4 Paraffins	63.0	54.7	64.0
C2-C4 Olefins	17.2	19.4	18.3
C ₅ + Aliphatics	3.2	3.6	2.9
Total Aromatics	16.6	22.3	14.8
Water	-	0.5 (g)	-
BTX/Aromatics	0.92	0.91	0.95

C₅+ Aliphatics: Aliphatic molecules having C5- C10 C. atoms.

Temperature R_c: 540°C; **WHSV:** 0.6h⁻¹.

(1) n-butane: 14ml/min; N₂: 10ml/min

(2) n-butane: 14ml/min; air: 12.5ml/min

(3) n-butane: 14ml/min; N₂: 10ml/min; H₂: 5ml/min

Catalyst: 80wt.-% H-ZSM-5(36) + 20wt.-% bentonite binder.

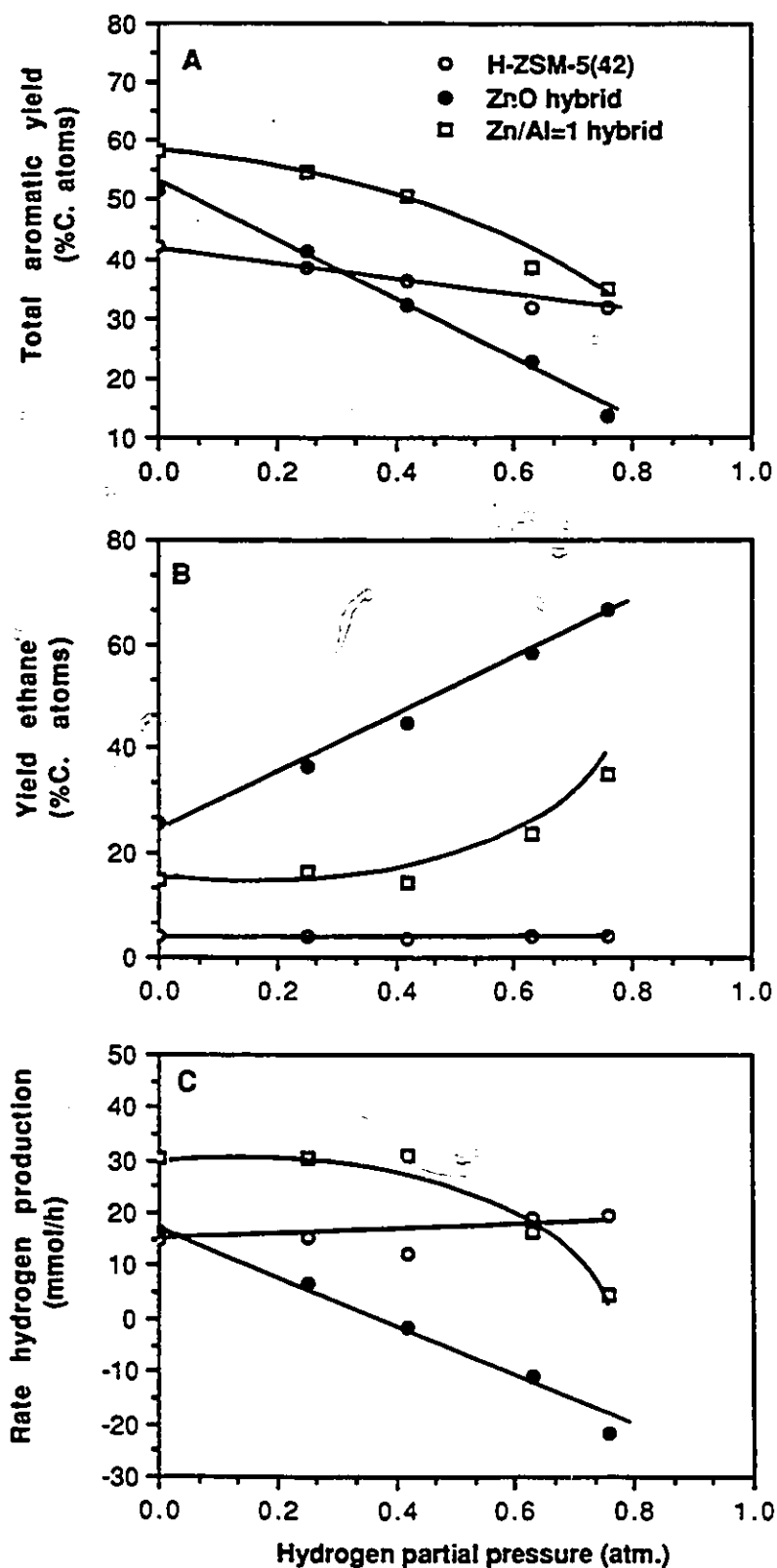


Figure 3.4 Effect of added feed hydrogen on catalytic activity of pure and hybrid catalysts in the aromatization of ethylene.

Feed: Ethylene; Temperature R_g : 500°C; WHSV: 0.6h⁻¹.

Catalyst composition:

(Pure) 80wt.-% H-ZSM-5 + 20wt.-% bentonite binder
 (Hybrids) 75wt.-% H-ZSM-5 + 5wt.-% ZnO/Al₂O₃
 (Zn/Al = 1.0) co-precipitate or ZnO + 20wt.-% bentonite binder.

invariable, while the production of hydrogen is almost constant. The progressive addition of $H_{2(g)}$ may be to shift the reaction mechanism to a new pathway, reflected in a slow drop in aromatic formation.

Comparing Fig. 3.4 A,B,C for both hybrid catalysts, the same trends can be observed, although they are more dramatic for the ZnO system. Sharp decreases in aromatic yields and hydrogen productions, reflect the inability of the co-catalyst surfaces to keep up as effective hydrogen adsorbents (for H_{sp}). The addition of hydrogen gas acts as a poison, blocking the available sites to adspecies exiting the zeolite channels. The decreasing aromatic yields are counterbalanced by increased formation of ethane. Particularly for the ZnO hybrid, although the co-catalyst accounts for only 5wt.-% of the total composition, a clear shift from aromatization to hydrogenation is seen upon increasing the amounts of co-fed H_2 . Ethane formation on the co-catalyst acquires such driving force, that even the hydrogen gas supplied with the feed, is consumed in the reduction process. At high P_{H_2} , ethylene adsorption by the internal zeolite acid sites is almost completely suppressed, even if the zeolite lattice accounts for 75wt.-% of the total catalyst weight. The severe poisoning by an added hydrogen partial pressure on hybrid systems leave little doubts about the importance of hydrogen transfer reactions and the involvement of HBS in explaining the enhanced aromatization propensity. Unanswered questions such as how does HBS work? or what are the physico-chemical properties of the co-catalyst which drive HBS? remain.

Fig. 3.5 shows SEM photographs of the configurational arrangement in fresh and used ZnO/ Al_2O_3 co-precipitate (Zn/Al=1.0) hybrid systems. On the fresh sample (A), the different dimensions of zeolite particles and sieved co-catalyst particles can be observed (2-3 μm vs $\approx 80\mu m$). Since the co-catalyst accounts for a much smaller weight percentage of the catalyst composition, the particles are not homogeneously distributed and so the majority of zeolite particles do not share an interface with the co-catalyst. Furthermore, since the global performance of the zeolite is modified by addition of only a small amount of co-catalyst, the effects are suggested to operate on large distances (confirmed in Table 3.8).

On the used sample (B), it can be observed that the co-precipitate particle is broken. Compared with its fresh analog, the zeolite particles have somehow become

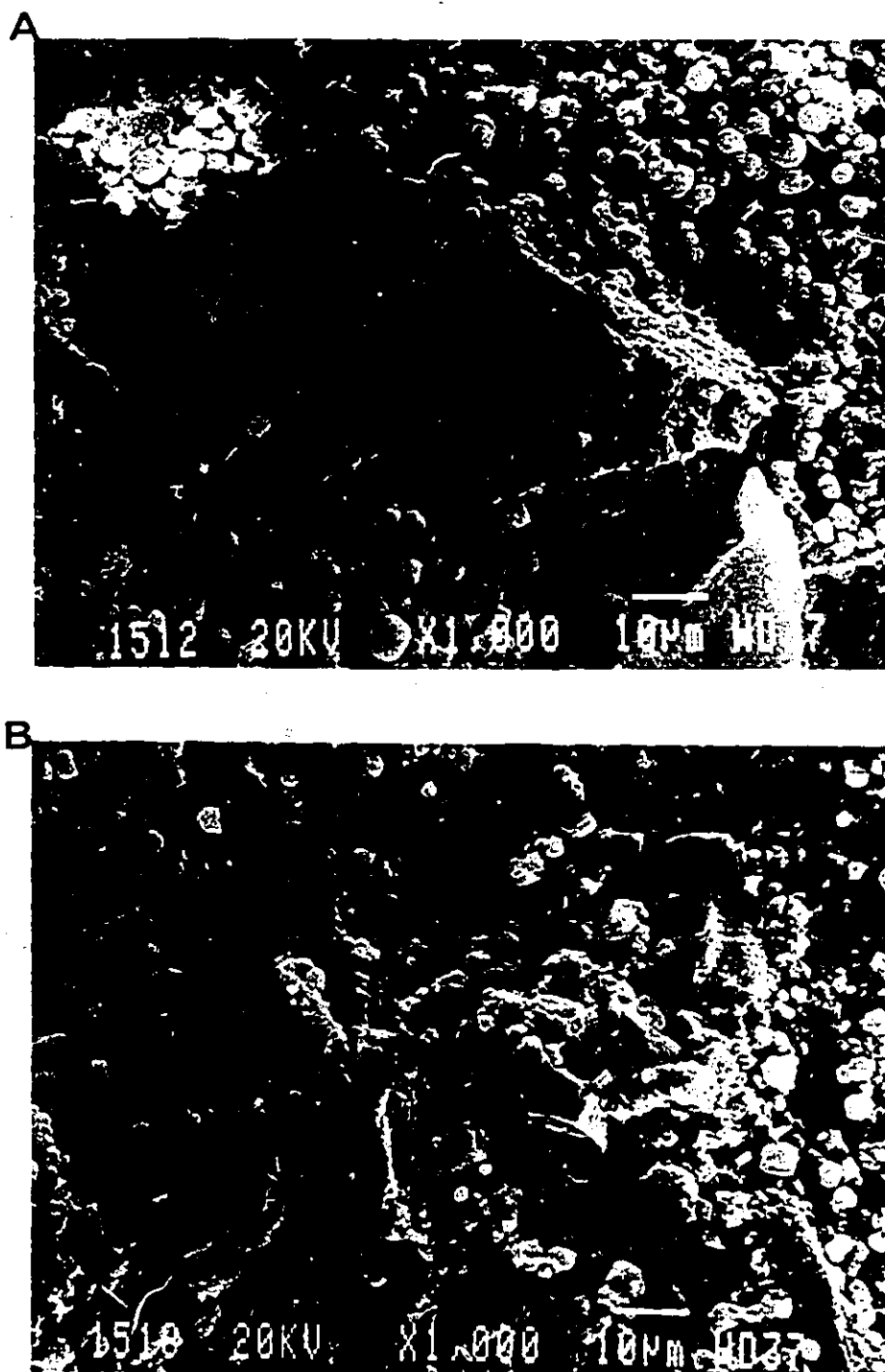


Figure 3.5 S.E.M. photographs of hybrid catalysts in the extrudate form.

(A) Fresh $\text{ZnO}/\text{Al}_2\text{O}_3$ co-precipitate ($\text{Zn}/\text{Al} = 1.0$) hybrid;

(B) Used $\text{ZnO}/\text{Al}_2\text{O}_3$ co-precipitate ($\text{Zn}/\text{Al} = 1.0$) hybrid.

intertwined after the reaction. H_{2p} adsorption on Zn-O acid-base pairs of the co-precipitate particle, may have caused a partial reduction of the lattice and since Zn^0 becomes volatile around 500°C (reaction temperature), lability or complete removal of metallic zinc atoms, could have resulted in co-catalyst structure collapse with the rearrangement of zeolite particles. EDAX chemical analysis of the peripheral environment did not indicate migration of zinc to the zeolite framework. Reduction and loss of zinc metal from the catalyst is believed to be one reason for particle collapse. The same effects explain the gradual catalytic activity decay with time and zinc deposits along reactor walls.

Partial reduction of the co-catalyst is seen as a prerequisite for efficient removal of hydrogen adspecies from the zeolite channels, as shown by the beneficial effects of prior reduction (Table 3.6). The creation of surface defect sites such as: partially reduced zinc (Zn^+) (116, 165) or oxygen vacancies are believed to be the adsorption sites for H_{2p} and co-adsorbed ethylene. In studies of ethylene hydrogenation on zinc oxide catalysts, it was observed that no activity was recorded much below 500°C (165) although adsorption occurred at lower temperature.

Zinc oxide, the initial hydrogen adsorbent found by chemisorption studies (Table 3.7), is a n-type semiconductor. In the electronic theory of catalysis (177-178), changes occurring in semiconductors as a result of chemisorption are examined. There have been several studies on the electronic interpretation of zinc oxide's catalytic activity (165, 171-176). In short, for n-type ionic crystals, conduction of the surface layers is modified by the electrons associated with anion vacancies in the lattice (O^{2-}), or free electrons balancing interstitial cations (Zn^{2+}). On ZnO, heterolytic hydrogen chemisorption results in crystal defects that cause inherent surface heterogeneity (Boudart, 171) or surface potential effects (de Boer, 176). In other words, changes occur in the work function of the metal oxide lattice due to the chemisorbed gas. The variation of surface potentials upon adsorption is documented and established (175).

For zeolites, as discussed by Clément (39), the activity and selectivity depends on the interaction between the diffusing molecule and the electric field at the pore opening. Barthomeuf and Mirodatos (40-41) describe an internal energy field gradient as a determinant force of product spectrum.

Inside the framework, a simple model describing the zeolite-sorbate system is related to a periodic array of interconnected sorption sites (179). Molecular migrations of sorbed species through the array is assumed to proceed by thermally activated *jumps* from one site to an adjacent site (179). Inside the channel, free gas molecules do not exist (180).

Diffusion in ZSM-5 zeolites falls in the configurational regime. The pore dimensions are in the same order as the diffusing molecules. Intracrystalline diffusivity studies of aromatic hydrocarbons (181) have shown the effect of preadsorbed molecules on the counter diffusivity values of substituted benzene molecules. Using 2 μm zeolite particles, reduction of the apparent diffusivity coefficients of the molecules by 1 to 2 orders of magnitude were observed. The authors suggest (181) that the diffusing species can only occupy vacant or vacated sites from preadsorbed molecules. They conclude that unidirectional, highly constrained molecular traffic prevails in ZSM-type zeolites. In studies of the microdynamics of methane, ethane and propane (182) in ZSM-5, mobility of molecules was suggested to be the limiting step in the overall kinetics. Decreased intracrystalline diffusivities with increasing sorbate concentration was explained in terms of mutual molecular interference (182).

Kärger, Pfeifer *et al.* (183-188) have examined intracrystalline self-diffusion coefficients using the technique of pulsed field gradient Xe^{129} -NMR. Upon comparison of *in situ* intracrystalline diffusivity coefficients with values from uptake and desorption kinetics (tracer desorption technique) experiments, substantial differences have been observed. For kinetically determined diffusion coefficients ($D_{d,app}$), a striking crystallite radius dependence was observed. $D_{d,app}$ drastically decreased with decreasing crystallite size whereas self-diffusion coefficients were invariable. For sufficiently large crystallites, quantitative agreement between sorption and NMR experiments was recorded. The discrepancies on small crystallites were taken as evidence for the existence of surface barriers on several zeolites. It was reported that contact with hydrocarbons at high temperature, could also dramatically enhance the surface barrier (187) leading to a steep decrease in the dynamic adsorption-desorption capacity of molecular sieves. Obstacles at the surface that cause pore blocking (e.g., coke), can also be promoters of surface resistances.

Structural surface barrier properties have been studied by Bülow and co-workers (189-190). A model describing mass transfer resistances at the surface of zeolites was developed. The model is based on potential-energy distributions in the force field of a zeolite crystal (mathematical modelization taken as a function of distance from the pore opening).

Derouane and co-workers (193) have examined the effects of surface curvature. Large divergences between intracrystalline (self-diffusion) and non-equilibrium diffusion coefficients observed, were also explained by the existence of a barrier. In this explanation, the surface barrier was caused by different surface curvatures at the exterior of the zeolite particle, with respect to the pore wall. In the cracking of C_{23} , differences in surface and molecule curvatures were used to explain the *window effect* which allows product maxima of C_{3-4} , C_{11-12} molecules with minima at C_{7-9} to desorb from erionite.

The principle of diffusion barrier (191) was applied in the elaboration of a performing catalyst for CO/NO reaction on Ni_3N . The added gas-to-surface diffusion resistances (glass powder) were suggested to protect the catalyst from oxidative deactivation. In another example, inert solids were used to enhance the extent and rate of solid conversion (e.g., CO_2 capture on lime and SO_2 capture on Mn ore) (192). The effects of pellet porosity, inert oxide concentration and particle size were found important in determining catalytic activity. Similar results were found by Le Van Mao *et al.* (132) using α -quartz in hybrids for the aromatization of n-butane.

The importance of surface barriers to diffusion on zeolites has been outlined. Examples of energy barrier modifications to tailor catalytic selectivity have been given. On ZnO at high temperature, defect sites and electronic variations have been claimed by Morrison (194) to be related to surface barrier effects. The barrier results from the creation of a space charge layer caused by electron transfer between the interior and surface states. Variation in the capacity and rate of oxygen and hydrogen adsorption with temperature is explained (194) in terms of changing electrostatic potential at the surface. It is possible to think that the driving force behind HBS is closely associated with the existence of surface barriers. At this moment the evidence is not sufficient. However, the idea merits further study consideration. A surface potential modification between zeolite and co-catalyst particles could result in increased rates of hydrogen removal (maybe

even products) from the zeolite lattice, with a net effect being an enhanced aromatization propensity on hybrid catalysts.

3.5 Conclusions

In this chapter, the importance of hydrogen transfer activity within the zeolite lattice was demonstrated. It was related to the balance between aromatization propensity and cracking ability of the hybrids. Evacuation of adsorbed hydrogen species from the zeolite in the form of spilt over species, was promoted by admixing another surface. Severe poisoning by co-feeding H_2 on hybrids was taken as clear evidence for the involvement of HBS.

The actions of ZnO and ZnO/alumina (Zn/Al=1.0) co-catalysts were scrutinized. ZnO was established as a promoter for ethylene reduction, especially under conditions of intimacy (scavenging). Zn-O pairs were suggested to be the initial adsorbents for H_{sp} by chemisorption studies. Partially reduced zinc species were postulated as active sites on ZnO based surfaces. The activated alumina surface of ZnO/ Al_2O_3 co-precipitate was proposed to be responsible for the increased hydrogen desorption.

Fig. 3.6 is a schematic representation of the proposed HBS model. It contains representations of different surface curvatures, simplified reaction network in the zeolite particles for olefins and paraffins, and sink/scavenging actions on the surface of the co-catalyst. The interface between the two components is considered to be chiefly responsible for the postulated modification of energy barriers invoked as driving force behind HBS. However, a more global approach should be considered since it operates on large distances.

In the next chapter, the physico-chemical characterization of the pure components and the hybrid catalysts will be presented. Correlations will be made between the activity/selectivity/stability and the physico-chemical properties of the solids, including the influence of preparation reagents and pretreatment.

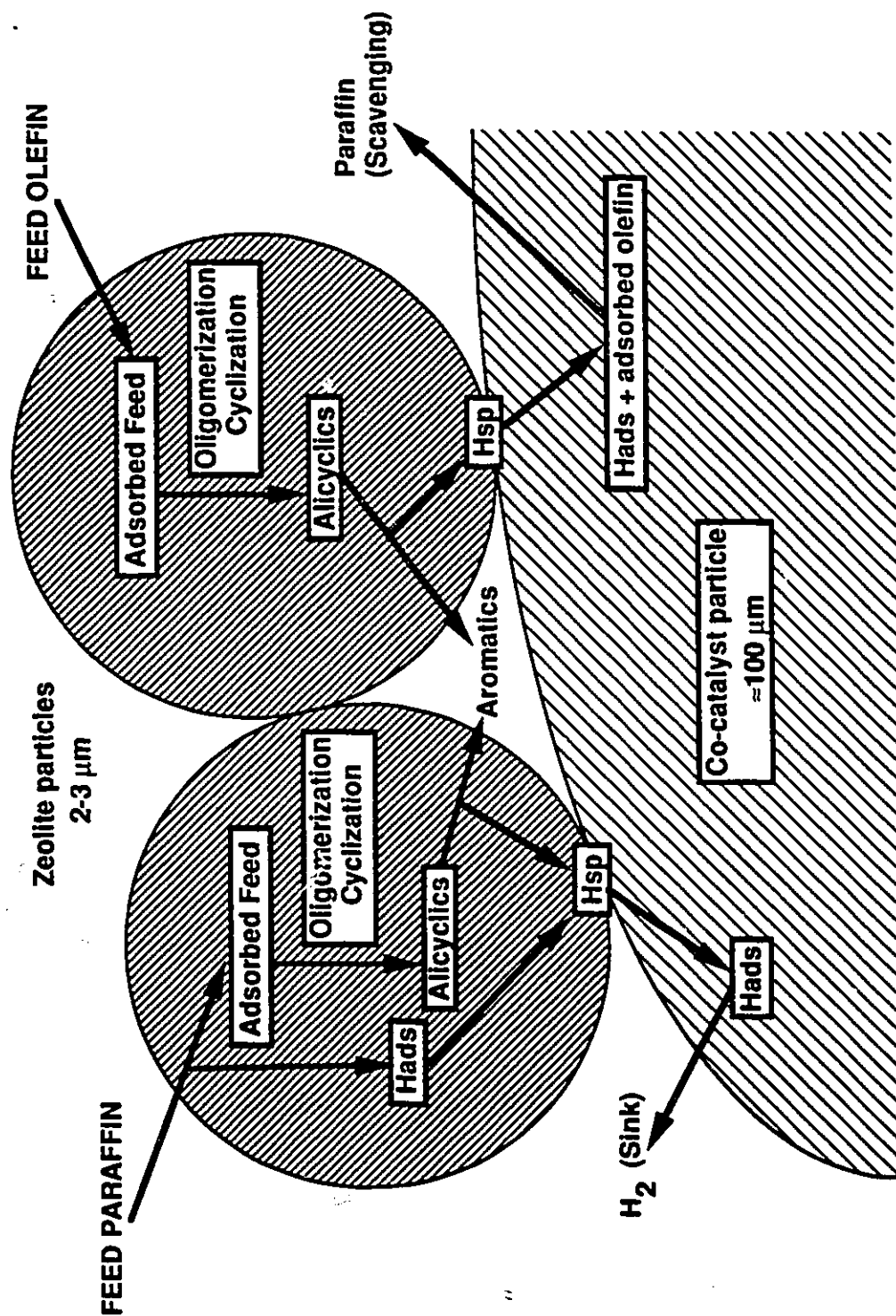


Figure 3.6 Schematic representation of the interface and mode of interaction between the zeolite and co-catalyst particles.

4.0 Physico-chemical characterization of catalytic components and correlation with the chemical reactivity of pure and hybrid systems

4.1 Introduction

The reasons underlying the development of new catalytic technologies are the socio-economic pressures for change (195). The goal of most catalysis research programs is to select a catalyst that drives a desired reaction with a minimum amount of side products, economically (196). In other words, at high rates and with a long lifetime. The methodology is the use of ideas, hypotheses, previous empirical knowledge, experience and surface materials science (196). The scientific aim is to elucidate the *structure-function* relationships that govern specific reaction paths. *Structure* implies a knowledge of the chemical nature and the local geometric arrangement of the atoms at the active site. *Function* refers to the electronic structure determined by the energy levels and the distribution/ symmetry of valence electrons. Furthermore, details of bulk, surface and active site similarities and differences are desirable.

Catalyst characterization has multiple aims that must be interrelated to understand why catalysts are active and selective (197). During the past ten years, substantial progress has been made in the development of physical techniques to characterize heterogeneous catalysts. Especially notable are *in-situ* techniques, that allow data acquisition under dynamic conditions. Examples of elemental surface analysis techniques include: Auger spectroscopy, XPS, SIMS and STEM. Molecular species on the surface can be analyzed by TPD/MS or FTIR. Selective chemisorption methods are used for the determination of metal surface area, particle size, as well as to obtain acidity-basicity information. Geometric structural analysis can be performed by XRD and MAS-SSNMR. Textural parameters are studied by sorption techniques such as BET and mercury porosimetry. Klier (196) gives a more comprehensive review of these characterization tools.

In all catalyst characterization techniques, a central role is played by reactor studies. They determine whether a catalyst or a class of catalysts are worthy of detailed structural and surface analyses. An interdisciplinary approach is the key to a successful research and development research program (198). Most branches of chemistry, surface science, chemical engineering and chemical physics should be involved simultaneously and work in tandem.

Characterization and preparation must also be carefully combined (199) since the preparation method of a catalyst ultimately determines its properties. Although chemical composition is a major factor directing catalytic behavior, depending on the preparation method, the conditions and reagents used, changes may occur in the nature of the interactions between the catalytic components. Variations in metal dispersion, pore structure, surface area, or crystallochemical changes can be at the origin of catalytic behavior differences. Boreskov (200) discusses the tasks involved in developing a theory of catalyst preparation. The aims are to find out (200):

- (1) which properties of a catalyst other than chemical composition influence the basic characteristics. These are: activity, selectivity, stability (thermal, resistance to poisoning), mechanical strength and hydrodynamic character (particle size, shape, density);
- (2) which are the optimum values of these combined properties that will provide a high quality catalyst for a particular reaction;
- (3) how these properties can be manipulated during the catalyst preparation to achieve optimum values.

Tanabe *et al.* (201) studied the effects of preparation on the acidity of mixed oxides. $\text{TiO}_2\text{-SiO}_2$ and $\text{TiO}_2\text{-ZnO}$ prepared by heterogeneous co-precipitation showed a higher acid strength than analogs prepared by the homogeneous method. Trimm *et al.* (202) have studied the effects of preparation conditions on the porosity and surface area of alumina. They found that variations in precipitation and aging steps were more determinant of textural properties than washing and drying. In studies of nickel systems, Cardew *et al.* (203) and Lansink Rotgerink *et al.* (204) confirmed that preparation influences the texture of the catalysts. However, the catalytic activity for CO-methanation and toluene hydrogenation were identical in all cases. In contrast, Mizukami *et al.* (205) showed that chemically mixed ruthenium catalysts for partial benzene dehydrogenation to cyclohexene, were much more effective than co-precipitated analogs. Textural properties and component intimacy were said to be different.

Aromatization of light olefins and paraffins is a reaction that has attracted much industrial interest (80-83, 85-86, 90, 94-95, 206). The intensive research activity has been fuelled by the economic rewards anticipated for up-grading a low value feed such as

natural gas derived LPG. As a result a new class of more efficient catalysts has been developed. These catalysts are bifunctional ZSM-5 zeolites containing platinum, gallium or zinc. It has been suggested that the metal or metal oxide function confers an additional dehydrogenation ability to the catalysts, that can favorably shift the equilibrium toward BTX formation (111).

In the present work, bicomponent catalysts have been prepared by mechanical admixing (72-73, 114, 126-127). Enhanced aromatic selectivity for light olefinic and paraffinic feedstocks was observed when ZnO or ZnO/Al₂O₃ co-precipitate components were added to a H-ZSM-5. This chapter investigates the influence of preparation on some basic properties (200). Correlations will be made between the physico-chemical characterization results and reaction studies.

4.2 Experimental

4.2.1 ZSM-5 zeolite synthesis

Several zeolites were synthesized according to the method of Argauer and Landolt (100). The composition of the synthesis gel and the parameters were selected so that the resulting zeolites had a Si/Al atomic ratio around 40. The procedure used to obtain the final form of the zeolites, as well as characterization techniques used on the zeolite powders, are as described in section 2.2.1.

Prior to using a new zeolite, standard catalytic tests for pure and hybrid catalysts were conducted to ensure uniformity and reproducibility with previously synthesized batches.

4.2.2 Synthesis of the co-catalysts

The co-catalysts were prepared by heterogeneous co-precipitation. A liquid mixture of soluble $\text{Zn}(\text{NO}_3)_2 \cdot 6\text{H}_2\text{O}$ with $\text{Al}_2(\text{SO}_4)_3 \cdot n\text{H}_2\text{O}$ ($n=12-14$) or $\text{Al}(\text{NO}_3)_3 \cdot 9\text{H}_2\text{O}$ salts was used for ZnO/alumina co-precipitates. Pure soluble salts yielded the corresponding pure oxides. The complete preparation method is described in section 2.2.2. Commercial ZnO (BAKER) and acidic $\gamma\text{-Al}_2\text{O}_3$ (STREM Chemicals) were used for comparison. A calibration graph predicting the final oxide concentrations was established. Table 4.1 reports the results obtained from atomic absorption chemical analysis.

Identification of the co-precipitates with respect to the reagents used, is based on the addition of an extra character to define aluminium sulphate or nitrate salt. For example, a ZnO/ Al_2O_3 co-precipitate from aluminium sulphate having a molar ratio equal to 1.0 or 50mol.-%Zn, is described as: Zn/Al-S=1.0. From the nitrate salt it is: Zn/Al-N=1.0. Pure oxides are $\text{Al}_2\text{O}_3\text{-S}$ and $\text{Al}_2\text{O}_3\text{-N}$ respectively.

The co-catalysts were crushed and sieved (80-100 mesh size). The samples were examined by X-ray powder diffraction. BET surface areas and pore size distributions were obtained on an ASAP 2000 apparatus from Micromeritics. Residual sulphate was measured by potentiometric titration according to an ASTM E 395-70 method (S.I.R.U.,

Table 4.1 Results of co-catalyst calibration obtained by atomic absorption.

mol.-% Zn Content (Theoretical)⁽¹⁾	mol.-% Zn Content (Experimental)⁽²⁾
0	0
25	14
50	28
75	50
100	96

(1) mol.-% Zn compound used for co-catalyst synthesis.

(2) mol.-% Zn compound present in co-catalyst powders as measured by atomic absorption.

Concordia University, Montreal). SEM/EDAX was performed on a JEOL JSM-840 instrument ((CM)² Polytechnique, Montreal)). Results of acidity characterization using ammonia TPD can be found in Table 2.2 and Fig. 2.2. Thermogravimetric (TGA) analysis was performed on a STA 1500 apparatus from PL Thermal Sciences. Thermograms were obtained in flowing N₂ or H₂ gases and using the following temperature program: T_i: 25°C; ramp: 5°C/min.; T_f: 800°C. A uniform particle size, a small sample weight (18.00mg) and a slow heating rate were selected to avoid problems of reproducibility and heat transfer within the sample pans.

4.2.3 Preparation of the catalysts

To prepare the final catalysts, the H-ZSM-5 powder and alumina, zinc oxide-aluminium oxide or zinc oxide powders were mechanically mixed at room temperature. The required amounts varied between 0- 90wt.-%. Bentonite clay (10- 60wt.-%) was then incorporated and intimately mixed with the solid catalyst. Deionized water was added dropwise until a malleable paste was obtained. The latter was extruded into 1.5mm O.D. *spaghettis*. They were dried at 120°C overnight and activated in air at 550°C for about 10h. The final length of the catalyst extrudates was 5 ± 0.5 mm.

For some experiments, the zinc oxide component was introduced by incipient wet impregnation technique on an alumina support. An aqueous solution containing the required amount of zinc nitrate was prepared. The alumina support was allowed to bath in the liquid for 12h at room temperature. The solution was then evaporated to dryness. The resulting powder was stored at 120°C overnight and during the activation step conducted at 550°C, the oxide was formed on the surface of alumina.

4.2.4 Catalytic testing

Catalytic testing was as described in section 2.2.5. Fig. 2.3 shows the schematic experimental set-up. The feed was composed of gaseous olefinic and paraffinic hydrocarbons (see Table 2.3), as generated in a bench scale steam- cracker (R_s and V1), or pure feedstocks (R_c and V2 introduction).

The normal operating parameters of the horizontal steam-cracker unit were as follows: feed: propane, temperature R_c : 820°C or 840°C, temperature R_c : 500°C, residence time: 0.85s and 0.75s respectively, water-to-propane molar ratio: 1.1, resulting WHSV: weight feed (gh^{-1})/weight catalyst (g)= 1.5-1.7 h^{-1} V1. For the runs conducted with pure feedstock (ethylene) the usual reaction parameters were as follows: temperature R_c : 500-540 \pm 0.5°C, introduction by V2, weight catalyst: 4g, duration of a run: 4-5h. Regeneration *in-situ* used in stability studies, consisted in flushing the catalyst with air at 550°C for 4h. For induction period experiments, equimolar amounts of ethylene and hydrogen gases were used along with the nitrogen carrier gas. Pretreatment consisted of flushing the catalyst at the reaction temperature with pure hydrogen or ethylene for 15min. The ethane to ethylene ratios were obtained chromatographically using a 1m packed silica gel column. For experiments where the catalysts were reduced prior to the reaction, a mixture of H_2 in N_2 was introduced by V2, while the catalytic reactor temperature was maintained at 400°C for 3.5h.

The liquid hydrocarbons formed by the steam-cracking and catalytic reactions were collected in condensing flasks kept at -15°C. The gases were analyzed throughout the run using a Shimadzu GC (Model Mini 3, FID) equipped with a 2.5-m stainless steel column (15wt.-% squalane on Chromosorb P) with 2,2-dimethylbutane as internal standard. The amount of hydrogen in the effluent was measured chromatographically using a 30-m HayeSep DB column from Chromatographic Specialties (HP Model 5890-TCD/ N_2 carrier gas). Prior to analysis, a volumetric calibration was performed using pure hydrogen gas. The collected liquid phases were subsequently analyzed with a Hewlett Packard GC (Model 5790A, FID) equipped with a 50-m PONA type capillary column. When required, n-octane was used to extract the organic phase prior to chromatographic analysis. The n-octane peak was considered as solvent in the chromatogram and was excluded from the product distribution.

4.2.5 Product calculations

All calculations were made on a carbon atom basis. Chromatographic results were converted to C. atoms using an internal standard (2,2DMB) for the gaseous effluent and correction factors for the columns. The definitions of total feed conversion, selectivity and yield for product i can be found in section 2.2.6.

4.4 Results and discussion

The texture of a catalyst refers to the detailed geometry of the void space in the particles and the agglomerates (207). The external surface, the pore shape, the extent of accessible internal surface area and the pore size distribution are all textural features. They are strongly dependent on the way a catalyst has been prepared and subsequently treated. Mercury porosimetry and physical adsorption isotherms analysis (e.g., BET) are the two principal means to get reasonably good textural descriptions (27, 207-209).

The adsorption isotherm is obtained as a function of the adsorptive pressure in the gas phase and records the amounts of substance adsorbed at equilibrium while the temperature is kept constant. The adsorbed amount is usually calculated from the relative pressure, i.e., pressure in the gas phase divided by the saturation pressure ($v = f(p/p_s)_T$). The BET method is a volumetric method that relates the volume of adsorbed species to pressure.

Table 4.2 reports the measured BET total surface areas of the co-catalysts precipitated from different reagent salts. Fig. 4.1 A shows a typical BET isotherm. Comparing the oxides obtained from aluminium nitrate and sulphate precursors, it can be observed that the accessible surface areas of the first group are more important. For mixed oxides, trends indicate a surface area decrease with increasing zinc oxide content. Pure $\text{Al}_2\text{O}_3\text{-N}$ is characterized by 52.3% times the surface of $\text{Al}_2\text{O}_3\text{-S}$. Precipitated and commercial ZnO have similar surface areas, however on the average they possess 85.5% and 91.5% less accessible surface than Zn/Al-S=1.0 and Zn/Al-N=1.0 respectively.

Physical adsorption isotherms can be classified in five different groups numbered I to V. This classification relates the shapes of the isotherms to the mean pore sizes (207). *Type II* isotherms are observed for macroporous adsorbents having pore sizes $>100\text{\AA}$, while *Type IV* isotherms are characteristic of mesoporous adsorbents ($50\text{-}100\text{\AA}$) (207, 209). The isotherm shape is a good first approximation of the mean pore sizes present in the solid. 'Mixed' isotherms are also indicative of the general porosity.

Table 4.3 reports the isotherm types and pore shapes of the co-catalysts. It can be observed that as the amount of ZnO increases, so does the macroporosity of the co-

Table 4.2 BET total surface areas for co-catalysts prepared from different reagent sources.

Catalyst Identification	mol.-% Zn Content	BET Total Surface Area (m ² /g).
Preparation from Al(NO₃)₃ Salt		
Al ₂ O ₃ -N	-	214.
Zn/Al-N= 1.0	50	45.6
Zn/Al-N= 1.9	65	41.5
Preparation from Al₂(SO₄)₃ Salt		
Al ₂ O ₃ -S	-	102.
Zn/Al-S= 1.0	50	27.4
Zn/Al-S= 2.4	71	23.0
Pure Zinc Oxide		
ZnO-N	100	3.62
ZnO (BAKER)	100	4.16

Degassing temperature: 350°C.

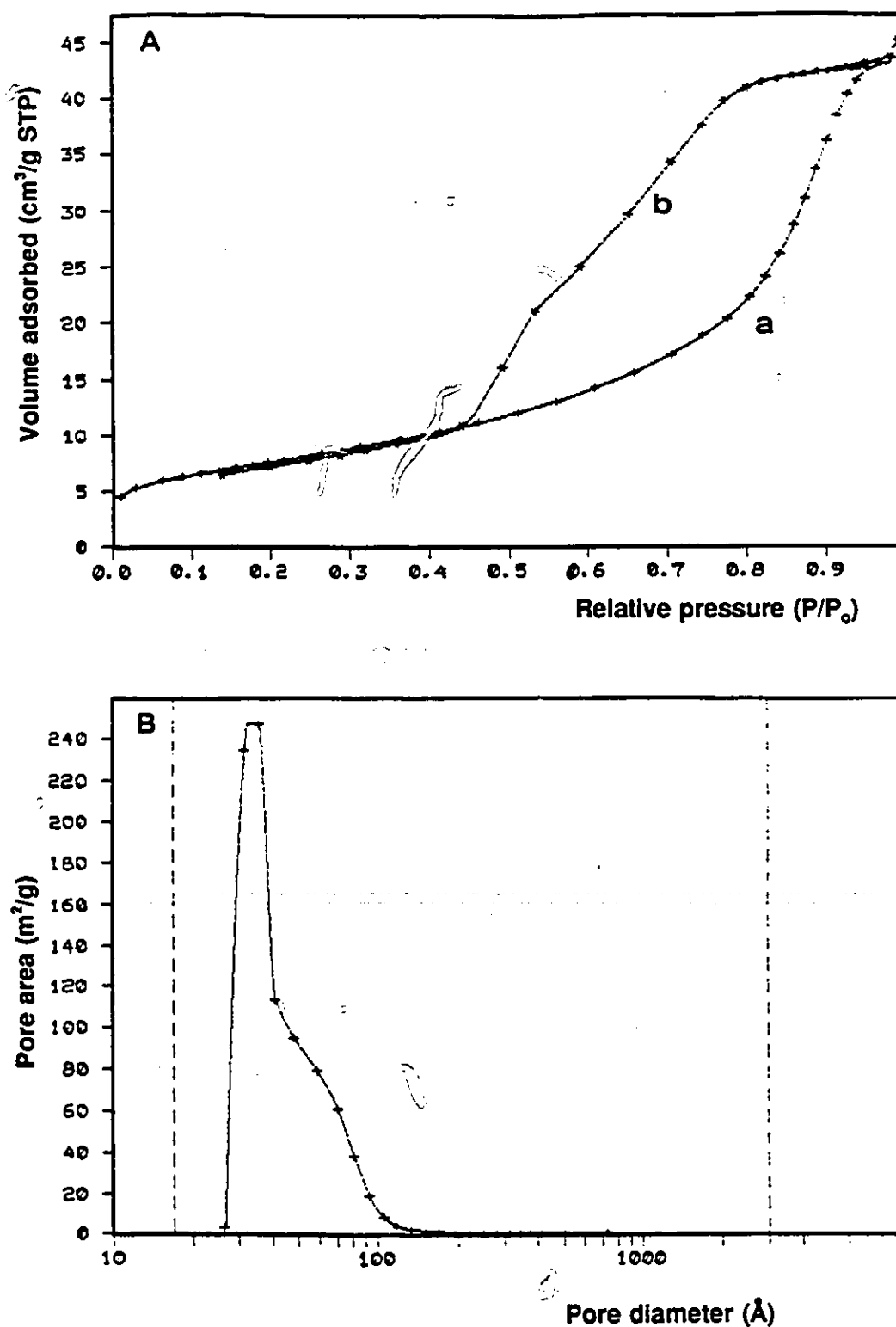


Figure 4.1 BET plots. (A) BET isotherm with **a** branch: adsorption and **b** branch: desorption; (B) Pore size distribution plot ($dA/d\log(D)$ desorption plot).
Sample Identification: Zn/Al-S=1.0.

Table 4.3 Porosity for co-catalysts prepared from different reagent sources; Isotherm types and pore shapes.

Catalyst Identification	Isotherm Type	Type of Hysteresis Loop	Pore Shape
Preparation from $\text{Al}(\text{NO}_3)_3$ Salt			
$\text{Al}_2\text{O}_3\text{-N}$	IV	E	ink bottle
Zn/Al-N= 1.0	IV \rightarrow II	almost none	almost cylindrical
Zn/Al-N= 1.9	II		cylindrical
Preparation from $\text{Al}_2(\text{SO}_4)_3$ Salt			
$\text{Al}_2\text{O}_3\text{-S}$	IV	E	ink bottle
Zn/Al-S= 1.0	IV	E	ink bottle
Zn/Al-S= 2.4	II	E	ink bottle
Pure Zinc Oxide			
ZnO-N	II	-	cylindrical
ZnO (BAKER)	II	-	cylindrical

Degassing temperature: 350°C.

Hysteresis: resistance to desorption indicative of capillary condensation.

E shape: indicative of a *wide* pore size distribution which extends from the micropore into the macropore range. A unique solution for the pore sizes cannot be obtained from the nitrogen isotherm at 77 K.

catalyst (IV \rightarrow II). Furthermore, mixed oxides from aluminium nitrate seem more macroporous than their sulphate analogs. The enlarged pores of alumina prepared from a nitrate salt have also been reported by Trimm *et al.* (202). Le Van Mao *et al.* (114) have observed that a $\text{Ga}_2\text{O}_3/\text{SiO}_2$ Ludox co-catalyst prepared from gallium nitrate, exhibited a very regular pore size range centered at 200\AA .

A hysteresis loop is sometimes observed upon measurement of the desorption isotherm ($p/p_s: 1 \rightarrow 0$) (Fig. 4.1 B). Hysteresis is a resistance to desorption indicative of a capillary condensation in the pores (209). The shape of the hysteresis loop can provide additional information on the porous texture. Five types of hysteresis loops corresponding to five pore shapes are proposed (207-209). Type E hysteresis is broad and indicates *ink-bottle* pores, having $\text{radius}_{\text{internal pore}}$ much greater than $\text{radius}_{\text{neck}}$ (207). Type E is further indicative of a wide distribution of pore sizes that extend from micropores into the macropore range (208). The absence of hysteresis may be taken to indicate that the pores are nearly perfect cylinders (207, 209) closed at one end. In Table 4.3, the shape or the absence of hysteresis indicate that ZnO and nitrate-based co-precipitates are characterized by more regular (cylindrical) pores, while the oxides obtained from sulphate precursors possess irregular pore shapes.

Table 4.4 assesses the pore size distributions of the solids. The data treatment method and the set of assumptions used separate the two methods that provide pore size distribution estimates. It can be observed that ZnO is macroporous, while the oxides obtained from nitrate precursors have wider average pore sizes than sulphate analogs, as also seen by Trimm *et al.* (202) and Le Van Mao *et al.* (114). The percent differences calculated between adsorption and desorption values obtained with the Barrett, Joyner and Halenda approach, reflect pore size heterogeneities. Oxides from aluminium sulphate show the most disordered surfaces which can be characterized by low surface areas, irregular pore shapes and broad pore size distributions. It is expected that the sulphate-based heterogeneous co-precipitates have a higher surface entropy and undergo a more facile surface restructuration during the reaction.

Fig. 4.2 depicts the total aromatic yields obtained with pure and hybrid catalysts. In this series of tests the precursor salts were varied in the co-catalysts precipitation step. Textural properties of the resulting pure or mixed oxides have been shown to be modified

**Table 4.4 Porosity for co-catalysts prepared from different reagent sources;
Pore size distribution.**

Catalyst Identification	Method Used			% Δ BJH ⁽ⁿ⁾
	BET Average	BJH _{ads.}	BJH _{des.}	
	Pore Diameter (Å)	Average Pore Diameter (Å)	Average Pore Diameter (Å)	
Preparation from Al(NO ₃) ₃ Salt				
Al ₂ O ₃ -N	53.4	53.1	43.2	0.23
Zn/Al-N= 1.0	159.	140.	121.	0.16
Zn/Al-N= 1.9	150.	162.	160.	0.01
Preparation from Al ₂ (SO ₄) ₃ Salt				
Al ₂ O ₃ -S	51.1	74.8	46.5	0.61
Zn/Al-S= 1.0	98.4	89.2	47.9	0.86
Zn/Al-S= 2.4	118.	129.	59.2	1.18
Pure Zinc Oxide				
ZnO-N	69.8	110.	106.	0.04
ZnO (BAKER)	104.	103.	116.	0.11

Degassing temperature: 350°C.

(1): % Δ BJH = $|(BJH_{ads.} - BJH_{des.}) / BJH_{des.}|$

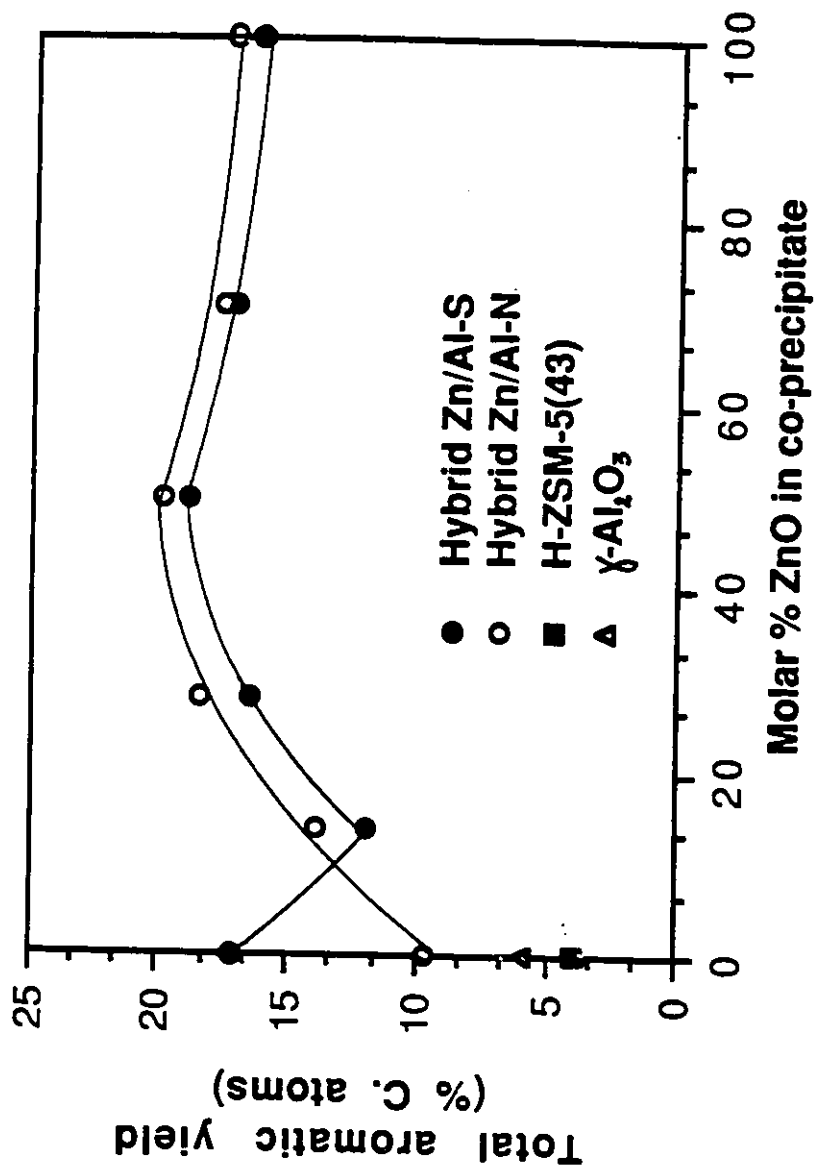


Figure 4.2 Influence of preparation reagents on resulting catalytic activity.
 Parameters: Feed: 820- Gas (Table 2.3); Temperature P_c : 500°C; WHSV: 1.5h⁻¹.
 Catalyst composition: 40wt.-% H-ZSM-5(37) + 40wt.-% co-precipitate + 20wt.-% bentonite binder.

by this procedure. It can be observed that for 20-100% ZnO content in the co-catalyst, the aromatization propensity of the different hybrid systems is very similar. In other words, for 20-100% ZnO content in the co-catalyst the chemical composition rather than the textural properties, seem to determine the catalytic activity.

Differences in aromatic yields can also be observed for pure alumina co-catalysts as a function of preparation (Fig. 4.2). Surface areas of acidic γ - Al_2O_3 , Al_2O_3 -N and Al_2O_3 -S are $225\text{m}^2/\text{g}$, $214\text{m}^2/\text{g}$ and $102\text{m}^2/\text{g}$ respectively. In heterogeneous catalysis, it is usual to correlate the extent of surface area with catalytic activity. However, for these hybrid catalysts composed of a pure oxide, surface area and catalytic activity trends are reversed. Furthermore, acidic γ - Al_2O_3 and Al_2O_3 -S show opposite catalytic activities although both possess similar acid densities and acid strength distributions. Therefore, surface area and acidity can be considered to be secondary properties in the explanation of aromatic formation when pure inert oxide hybrids are used. Alumina powder XRD studies have shown that γ -alumina exhibits the diffraction pattern expected for its spinel structure, while Al_2O_3 -N and Al_2O_3 -S are partly and completely amorphous respectively. Because it is amorphous or microcrystalline, the disordered texture and structure of the alumina-S co-catalyst may be partly responsible for the enhanced catalytic activity of this hybrid.

Acidity measurements of mixed oxides from different reagent sources have been made using the technique of ammonia TPD. In Fig. 2.1 it was seen that acid density seemed correlated with the catalytic activities of hybrids. Identical measurements of Zn/Al-N co-precipitates were performed but no acidity was recorded in all cases. Table 4.5 reports the amounts of sulphate present in a series of co-catalysts. SO_4^{2-} anions in a solid catalyst are superacid promoters (201, 210). The generation of acidity has been attributed by Yamaguchi (210) to the presence of covalent S=O bonds in sulphur complexes, that are formed on the metal oxide surfaces. From Fig. 4.2, acidity does not appear to be primordial in determining the catalytic properties of mixed oxides, since the hybrids composed of Zn/Al-S and Zn/Al-N co-precipitates show almost identical aromatic forming tendencies. From Table 4.5, it further can be observed that the amounts of sulphate remaining in the co-precipitates are almost invariable with respect to the ZnO content or thermal pretreatment.

Table 4.5 Residual sulphate content as determined by potentiometric titration (ASTM E 395-70)⁽¹⁾.

Catalyst Identification Zn/Al Ratio	mol.-% Zn Content	wt.-% SO₄²⁻
Al ₂ O ₃ -S	0	18.5
Zn/Al-S= 0.16	14	26.6
Zn/Al-S= 0.39	28	25.2
Zn/Al-S= 1.0 ⁽²⁾	50	20.0
Zn/Al-S= 1.0 ⁽³⁾	50	20.4
Zn/Al-S= 1.0 ⁽⁴⁾	50	16.5
Zn/Al-S= 2.4	71	19.0

(1) Analysis performed by S.I.R.U., Concordia University, Montreal Qc.

(2) Co-precipitate activated in air at 550°C.

(3) Co-precipitate activated under nitrogen at 550°C.

(4) Co-precipitate not activated.

According to Willard *et al.* (211-212), the proportion of sulphate in a precipitate is a function of the precipitation pH rather than the sulphate concentration in the mother liquor. The presence of SO_4^{2-} anions also influences the density of the polymeric hydroxides composing the gel. Experiments have revealed (211) that sulphate ions cannot be removed from the gel after aging, even by excessive washing. A TGA study of zinc sulphate decomposition by Narayan *et al.* (213) has shown that sulphate anions can remain trapped in a solid structure up to a temperature of 1113 K (840°C). In an oxidative atmosphere, SO_3 , SO_2 and O_2 decomposition products have been identified by EGA (213). It can be concluded that the temperature of activation used for the co-precipitate powders (550°C) was not high enough to remove all SO_4^{2-} impurities.

Srinivasan *et al.* (214) have studied the effects of sulphate ions on a zirconia crystal structure. They showed using DTA/TGA, that the addition of SO_4^{2-} anions during the preparation step led to the formation of tetragonal zirconia. One phase monoclinic zirconia was obtained by a fast precipitation method in the absence of any impurities. The presence of sulphate ions encapsulated in zinc oxide- alumina co-precipitates, could act as impurities promoting disorder and XRD amorphous structures.

Fig. 4.3 shows SEM photographs of the co-precipitates at high magnification. Differences in the textural properties can be observed. Block-like rather smooth surfaces and sponge-like features can be seen. As the zinc oxide content increases in the co-precipitates, there is a progression of the sponge-like phase. Powder XRD studies of the co-catalysts have revealed the presence of progressively more intense ZnO diffraction lines with increasing zinc contents. In a surface spectroscopic investigation by Strohmeier and Hercules (215), ZnO segregation was observed in solids containing more than 22wt.-% of zinc cations impregnated on γ -alumina. A similar chemical composition segregation was recorded for the co-precipitates using EDAX (Table 4.6).

Another feature to be observed when examining co-catalyst SEM photographs is the spatial organization of block- and sponge-like phases. As the amount of zinc increases, the interface or degree of intimacy between the two textures becomes more important. XRD studies (215-216) have identified the formation of ZnAl_2O_4 and NiAl_2O_4 spinels after calcination of $\text{ZnO}/\text{Al}_2\text{O}_3$ mixtures or after reduction of $\text{Ni}^{2+}/\text{Al}_2\text{O}_3$ respectively. The existence of Weak Metal Support Interactions (WMSI) was invoked to explain the

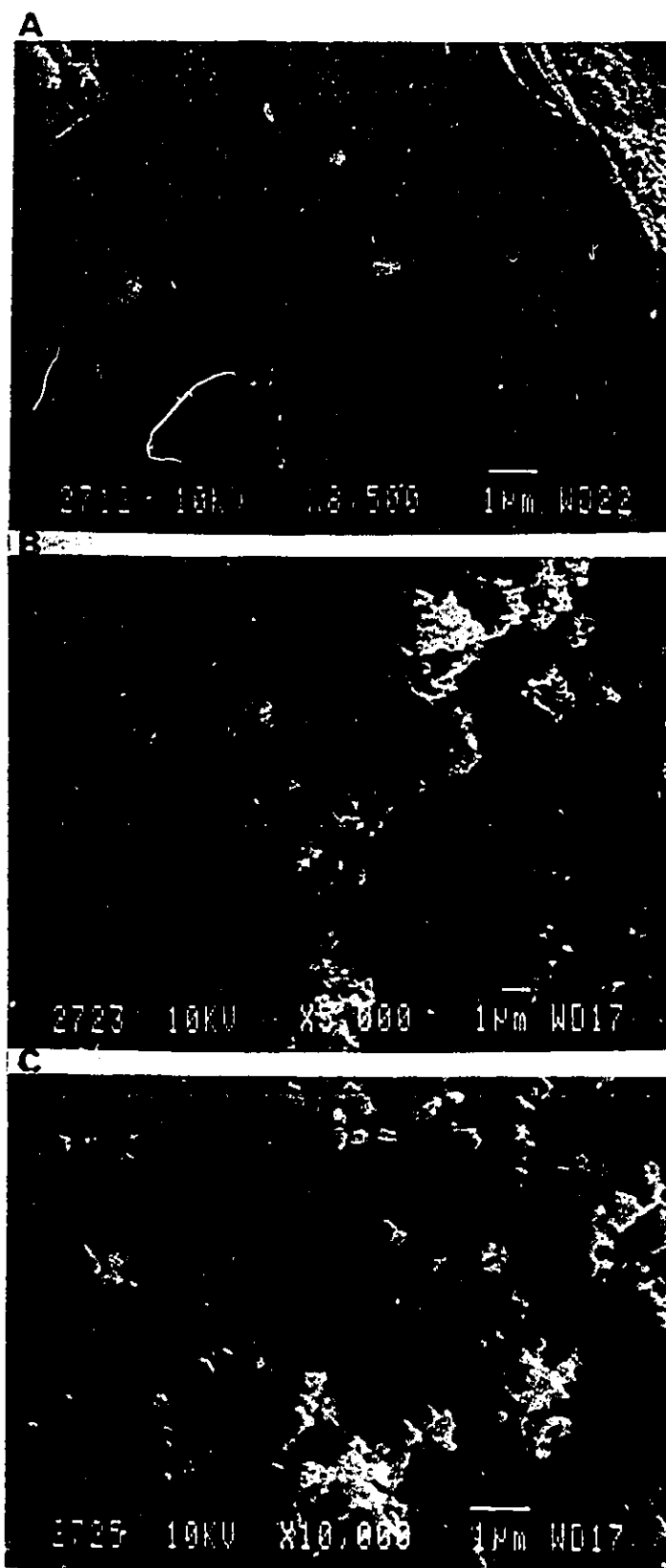


Figure 4.3 SEM photographs of co-precipitates; **A** Zn/Al-S=0.16; **B** Zn/Al-S=1.0; **C** ZnO precipitate.

formation of ZnAl_2O_4 from mechanically admixed ZnO and alumina (154). For cations supported on $\gamma\text{-Al}_2\text{O}_3$, the formation of an aluminate phase was explained by the diffusion of Zn^{2+} or Ni^{2+} ions into vacant T_d sites of the defect γ -alumina spinel (215). Evidence of spinel formation was not found in the co-precipitates by powder XRD. However, ZnAl_2O_4 crystallite sizes may have been too small to be detected ($<30\text{\AA}$).

In Table 4.6 it can be seen that sulphur is not evenly distributed between the two phases. The open porosity of the sponge-like phase seems to promote a better oxidation of SO_4^{2-} impurities during the calcination step at 550°C . The oxygen content also varies between the two textures. There is an indication of sponge oxygen enrichment or ZnO textural phase oxygen enrichment. Above 500°C the ZnO lattice can contain defect sites caused by deoxygenation (165, 194). Deoxygenation is also responsible for the canary-yellow color of ZnO at high temperature (217). The increased dispersion and the segregation of a sponge-like phase at higher zinc oxide loadings (50-100mol.-%), coupled with oxygen enrichment/probable deoxygenation ability at high temperature, may be involved in the explanation of active site formation. ZnO defect sites are the primary H_{2p} acceptor sites (chemisorption studies) (Table 3.7). A good dispersion of ZnO-like sponge phase in the co-precipitate is a logic prerequisite to obtain high aromatic propensity in hybrid systems.

Induction period studies can yield information about the activation of a surface with time. In this case, activation may be related to thermal deoxygenation or surface partial reduction with the creation of defect sites. Fig. 4.4 shows the behavior of a ZnO precipitate at different temperatures. It can be observed that the rate and extent of surface activation increases with temperature, while deactivation is more pronounced at 540°C .

Fig. 4.5 depicts the influence of pretreatment on the activation of ZnO. Curve A represents the catalytic activity toward ethylene hydrogenation at 540°C . Curves B and C represent surface activations after H_2 and ethylene pretreatments respectively. It can be observed that reduction prior to the reaction favorably enhances the rate of activation. The first point observed in curve B is most likely due to the reaction of ethylene with preadsorbed hydrogen species on the ZnO surface. Deactivation of fresh and reduced catalysts is identical after 30 min. The ethylene pretreated catalyst exhibits a curve which

Table 4.6 EDAX chemical analysis results for the co-precipitates.

Phase	Element	Net Integral	Zn/Al Ratio	(Zn+Al)/O Ratio
Zn/Al-S = 0.16				
Block	Zn	1328	3.33X10 ⁻²	2.01
	Al	39923		
	O	20524		
	S	9150		
Zn/Al-S = 1.0				
Block	Zn	7129	4.51X10 ⁻¹	1.21
	Al	15800		
	O	18992		
	S	10247		
Sponge	Zn	4405	9.25X10 ⁻²	2.03
	Al	47643		
	O	25640		
	S	1497		
Zn/Al-S = 2.4				
Block	Zn	10057	1.66	1.22
	Al	6051		
	O	13200		
	S	7372		
Sponge	Zn	5472	1.81X10 ⁻¹	1.83
	Al	30223		
	O	19456		
	S	1736		
ZnO Precipitate				
Sponge	Zn	15141	-	-
	Al	781		
	O	93141		
	S	226		
ZnO (BAKER)				
Sponge	Zn	14271	-	-
	Al	299		
	O	3020		
	S	83		

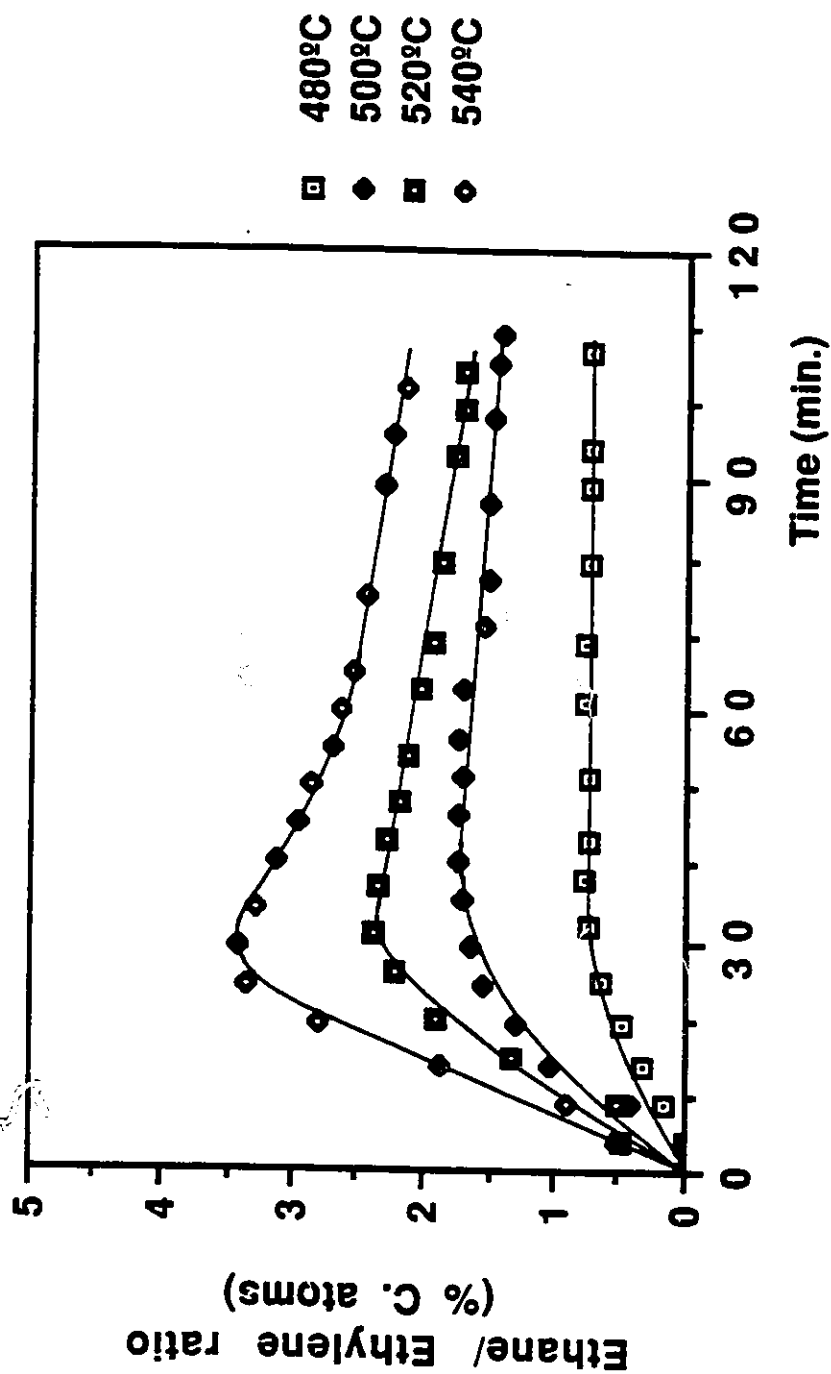


Figure 4.4 Study of induction periods on ZnO-N precipitate as a function of temperature.
 Parameters: C_2H_4/H_2 molar ratio: 1.0; Partial pressure C_2H_4 : 0.17 atm.; WHSV: $1.2h^{-1}$.
 Catalyst composition: 90wt.-% ZnO-N precipitate + 10wt.-% bentonite binder.

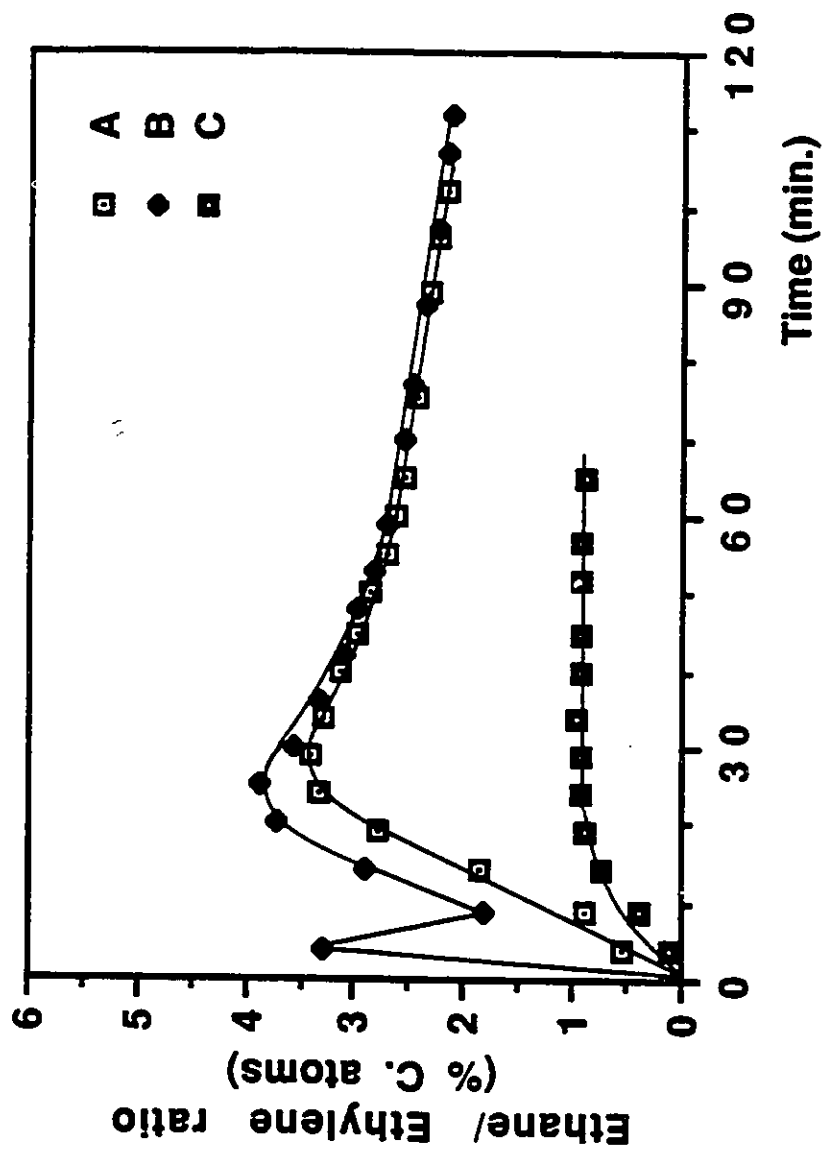


Figure 4.5 Study of induction periods on ZnO-N precipitate as a function of pretreatment.
 Parameters: Temperature P_c : 540°C; C_2H_4/H_2 molar ratio: 1.0; Partial pressure C_2H_4 : 0.17 atm.; WHSV: 1.2 h⁻¹.
 Catalyst composition: 90wt.-% ZnO-N precipitate + 10wt.-% bentonite binder.
 Catalyst Identification: (A) ZnO-N; (B) ZnO-N/ H_2 pretreatment 15 min.; (C) ZnO-N/ C_2H_4 pretreatment 15 min.

is typical of pre-poisoned catalytic activity.

Fig. 4.6 represents the activation of a Zn/Al-S=1.0 co-precipitate at different temperatures. The rates and extent of activation increase with temperature, but the major differences are seen by the absence of deactivation. In fact it appears that two activation mechanisms take place. In a first step, the ZnO phase activation is fast and similar to that of the pure ZnO precipitates. The absence of deactivation and the slow increase in catalytic activity observed with time, can be associated with the activation of alumina. The mechanism is thought to be based on activation by spillover hydrogen species, from ZnO defect sites to the alumina surface (Table 3.6). Pre-reduction of the catalyst increases the rate of activation (Fig. 4.7).

Fig. 4.8 examines the effects co-precipitate preparation reagents and preparation methods have on activation. Curves A and B represent the induction periods obtained for aluminium sulphate and nitrate-based co-precipitates respectively. The initially greater activity of Zn/Al-N=1.0 with respect to its analog, can be explained by the extent of surface area since Zn/Al-N possesses about 40% more surface than Zn/Al-S. Catalysts prepared by incipient wet impregnation show depressed activation rates (C and D) when compared with the co-precipitates. It can be deduced that the degree of intimacy between zinc and aluminium complexes throughout the co-precipitate particles, is an important factor that is involved in orienting the catalytic properties of the hybrid at the beginning of the reaction. After 90 min., all catalysts exhibit similar catalytic activities independently of the nature of salt precursors or the preparation methods used. These results indicate that the chemical composition is the most important characteristic of the co-precipitate.

Fig 4.9 reports the stability of hybrid catalysts while they are being submitted to a series of reaction-regeneration cycles. It is observed that the deactivation rate of the ZnO is slower than that of the co-precipitate hybrid. It has been observed by hydrogen chemisorption that the primary acceptors of H_{sp} are ZnO defect sites. Because of H_{sp} chemisorption, Zn^{2+} partial reduction of the oxide lattice can occur with some Zn^0 volatilization at 500°C. Since the Zn/Al-S=1.0 co-precipitate has 50mol.-% less zinc content than ZnO, it is reasonable to expect that after several reaction-regeneration cycles, the activity of the co-precipitate hybrid falls below that of the ZnO hybrid.

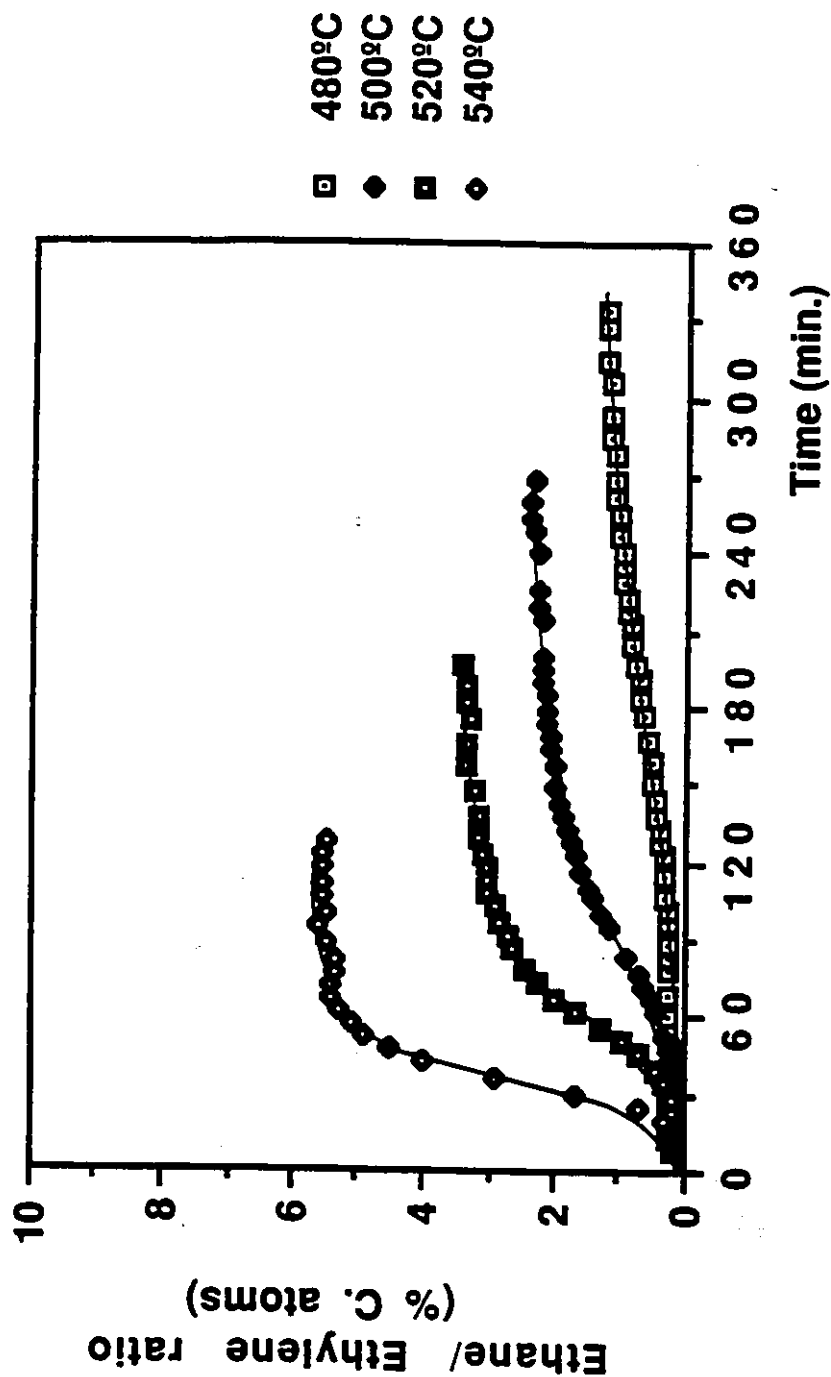


Figure 4.6 Study of induction periods on Zn/Al-S=1.0 co-precipitate as a function of temperature.
 Parameters: C_2H_4/H_2 molar ratio: 1.0; Partial pressure C_2H_4 : 0.17atm.; WHSV: $1.2h^{-1}$.
 Catalyst composition: 90wt.-% Zn/Al-S=1.0 co-precipitate + 10wt.-% bentonite binder.

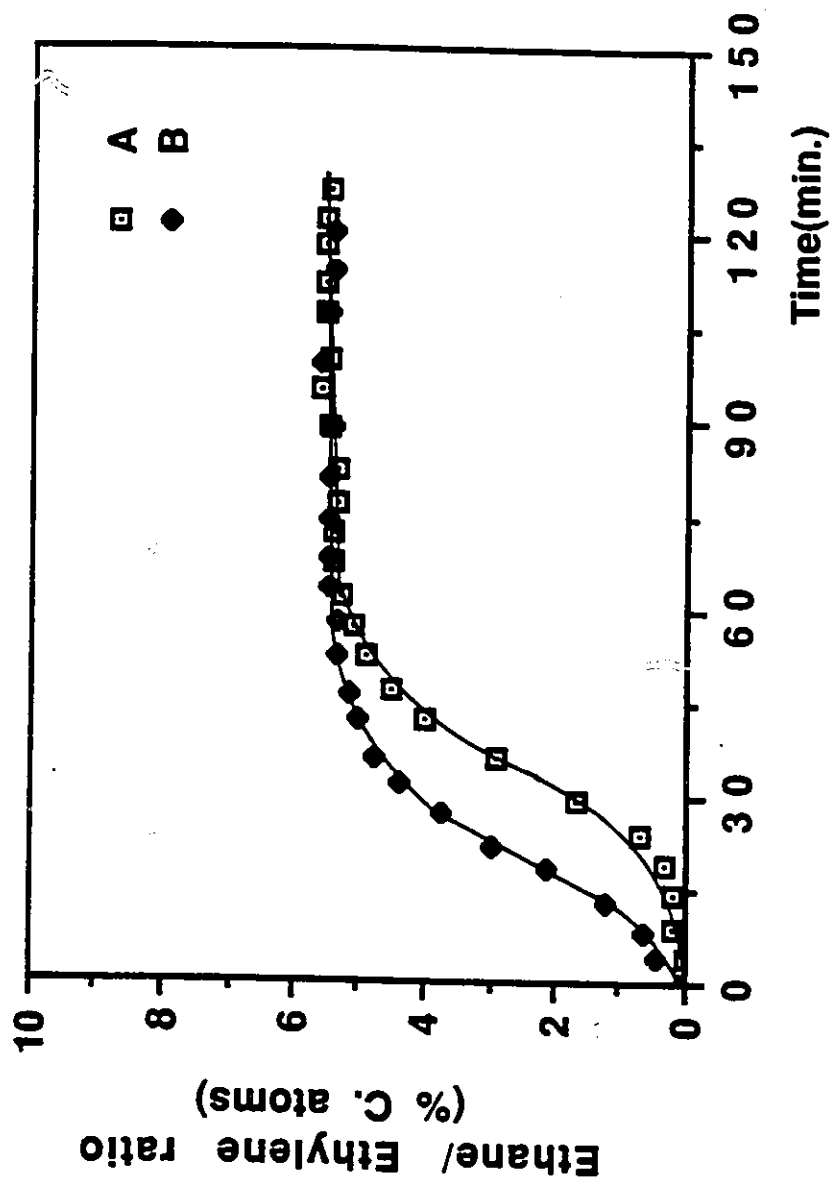


Figure 4.7 Study of induction periods on Zn/Al-S=1.0 co-precipitate as a function of pretreatment.
Parameters: Temperature R_c : 540°C; C_2H_4/H_2 molar ratio: 1.0; Partial pressure C_2H_4 : 0.17 atm.; WHSV: 1.2 h⁻¹.
Catalyst composition: 90wt.-% Zn/Al-S=1.0 co-precipitate + 10wt.-% bentonite binder.
Catalyst Identification: (A) Zn/Al-S=1.0; (B) Zn/Al-S=1.0 / H_2 pretreatment 15 min.

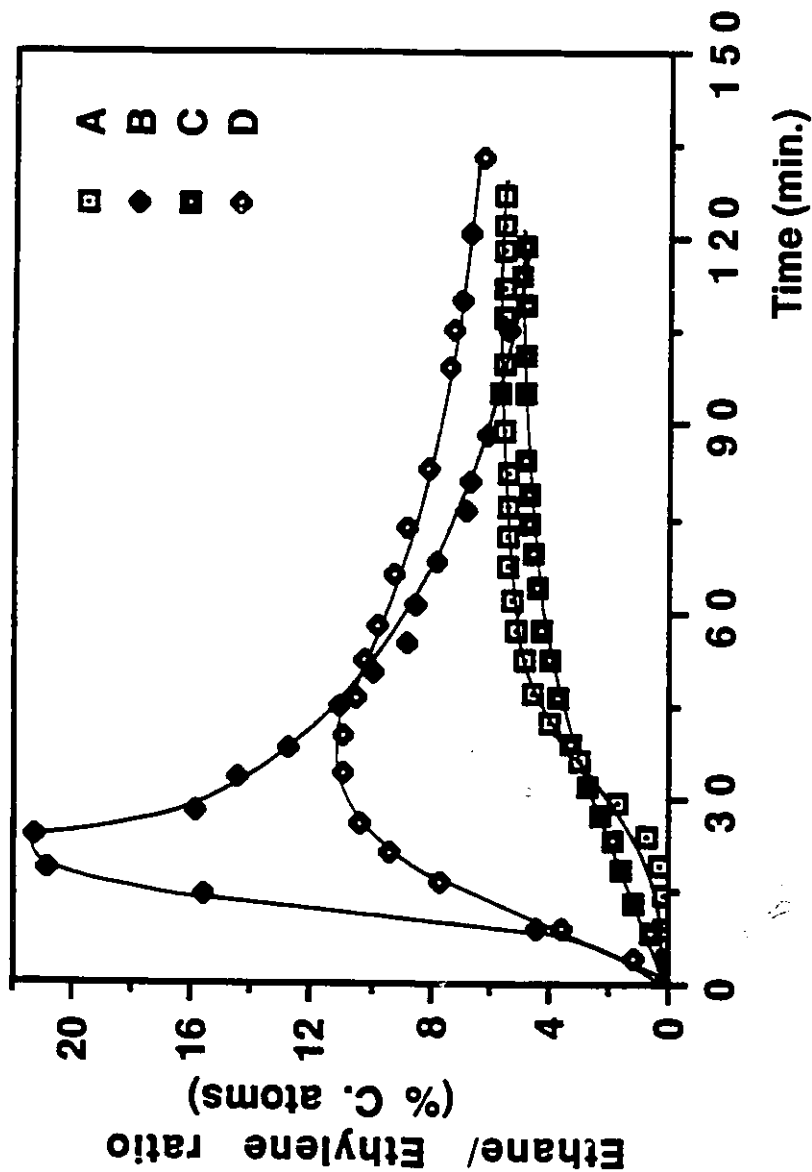


Figure 4.8 Study of induction periods on $\text{Zn}/\text{Al}=1.0$ as a function of preparation method.
Parameters: Temperature P_c : 540°C ; $\text{C}_2\text{H}_4/\text{H}_2$ molar ratio: 1.0; Partial pressure C_2H_4 : 0.17 atm. ; WHSV: 1.2 h^{-1} .
Catalyst composition: 90wt.-% $\text{Zn}/\text{Al}-\text{S}=1.0$ co-precipitate + 10wt.-% bentonite binder.

Catalyst Identification: (A) $\text{Zn}/\text{Al}-\text{S}=1.0$; (B) $\text{Zn}/\text{Al}-\text{N}=1.0$;
 (C) ZnO incipient wet impregnation on $\text{Al}_2\text{O}_3-\text{S}$ precipitate ($\text{Zn}/\text{Al}=1.0$);
 (D) ZnO incipient wet impregnation on $\text{Al}_2\text{O}_3-\text{N}$ precipitate ($\text{Zn}/\text{Al}=1.0$).

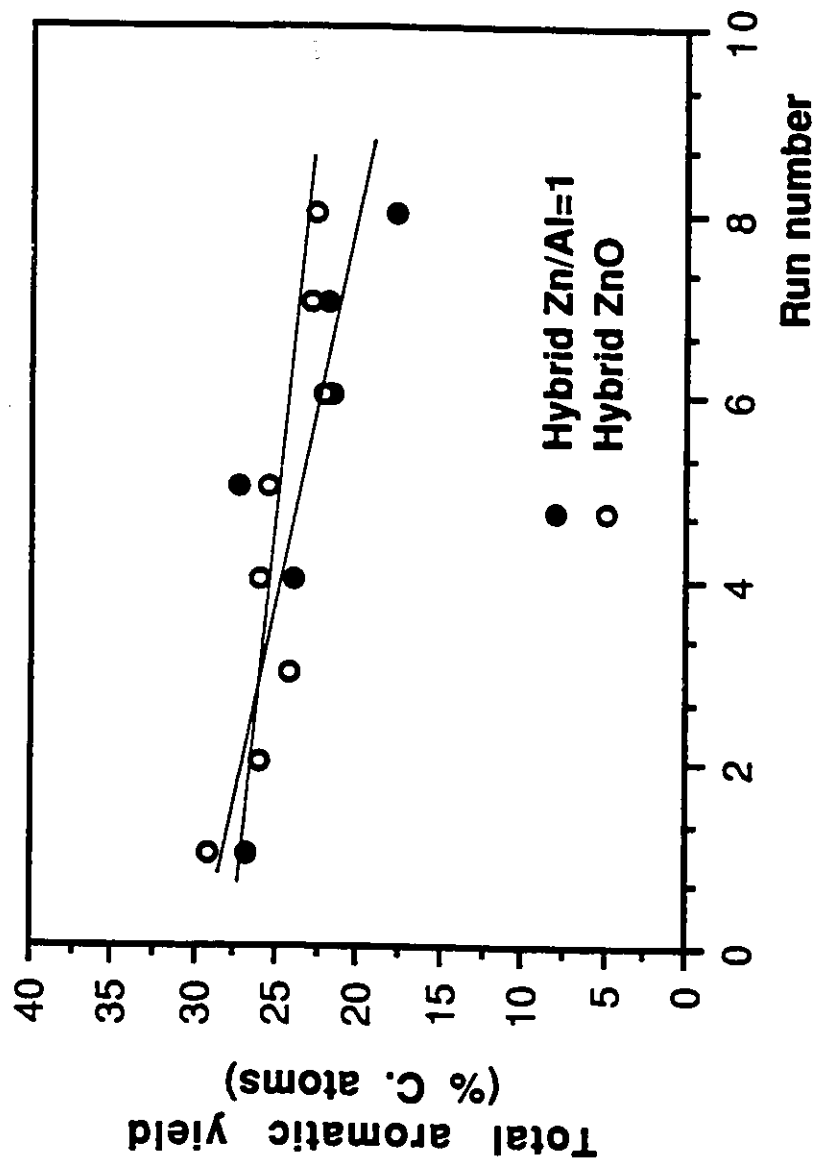


Figure 4.9 Study on the stability of hybrid catalysts as a function of run number.
Parameters: Feed: 820- Gas (Table 2.3); Temperature P_c : 500°C; WHSV: 1.5h⁻¹; Reaction time: 5hrs;
 Regeneration *in-situ*: 550°C/4hrs.
Catalyst composition: 75wt.-% H-ZSM-5(34) + 5wt.-% co-catalyst + 20wt.-% bentonite binder.

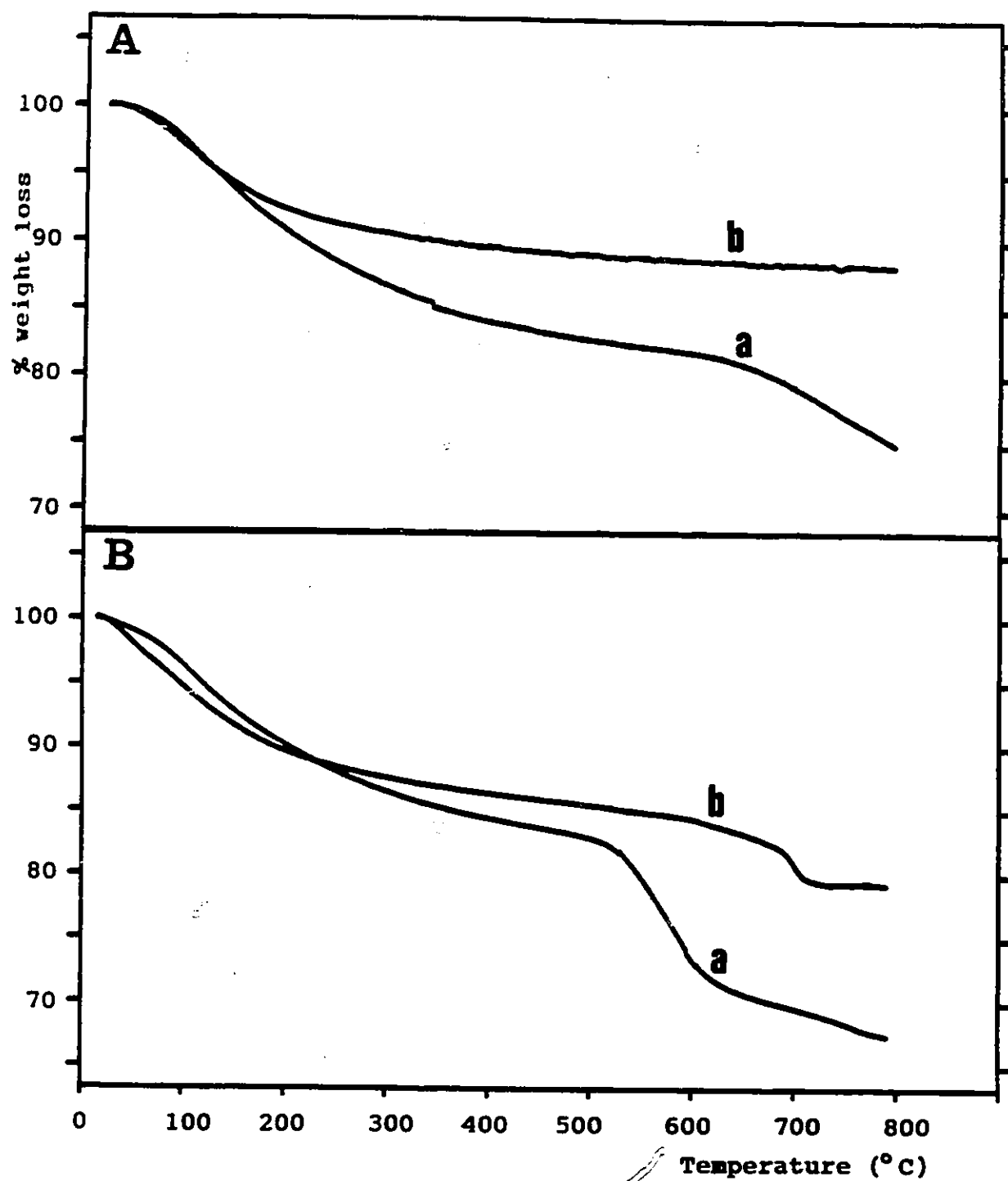


Figure 4.10 Thermograms of alumina precipitates. (A) N₂ atmosphere; (B) H₂ atmosphere.
Catalyst Identification: a Al₂O₃-S; b Al₂O₃-N.

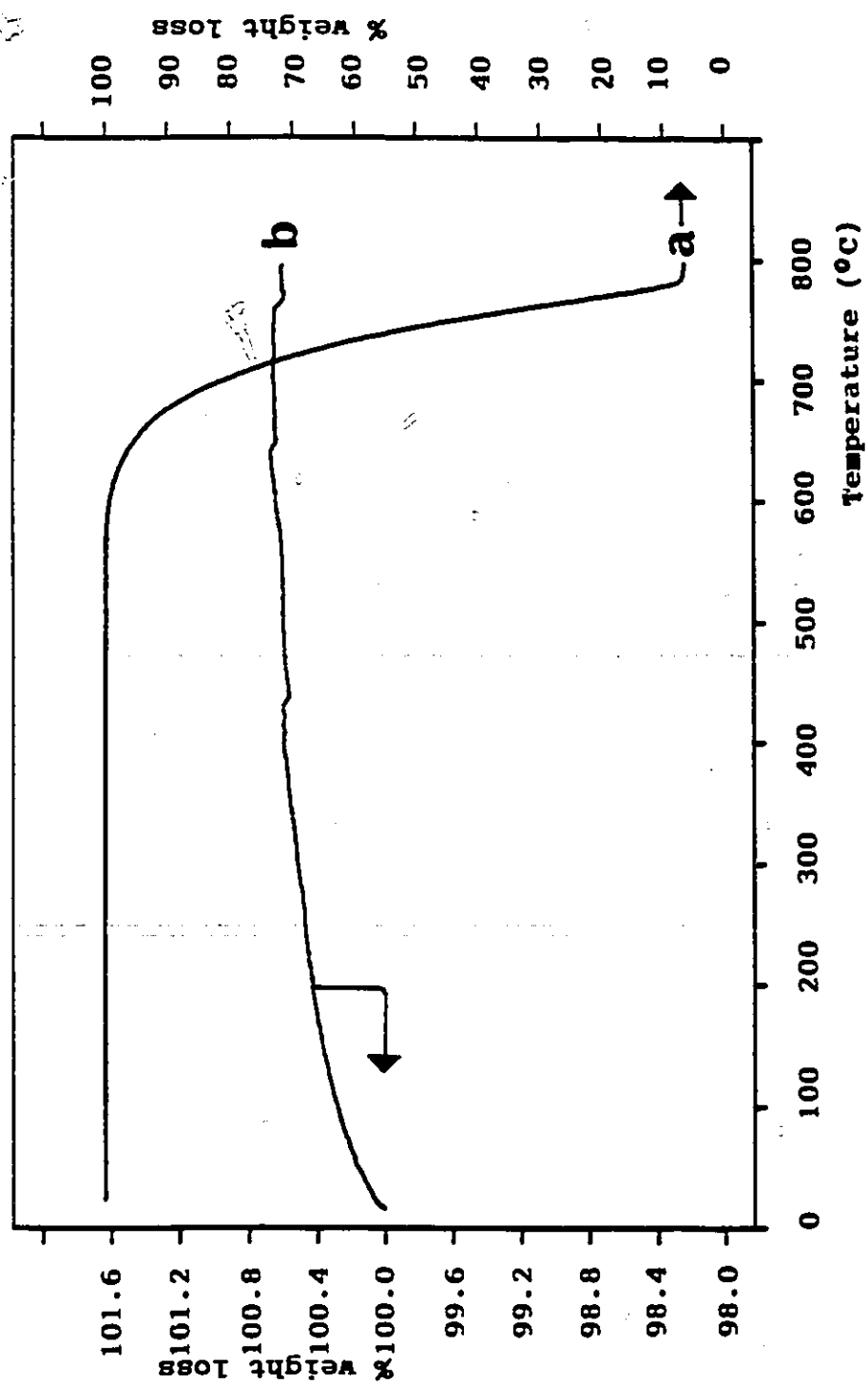


Figure 4.11 Thermograms of ZnO-N precipitate; a H₂ atmosphere; b N₂ atmosphere.

Thermogravimetric (TGA) investigations of the co-precipitates obtained from different reagent sources have been performed. TGA analyses can record changes in mass as a function of temperature on a thermobalance (218-219). Dynamic thermogravimetric studies examine mass changes with a linear increase in temperature. The resulting thermograms provide information regarding thermal stability, the composition of the initial sample and the reaction intermediates. Although some solid samples have the same chemical composition, there may be considerable differences in their behavior upon heating. Differences in defects, porosity, surface properties can be recorded and correlated with the preparation method and the catalytic activity in order to obtain additional information.

Fig. 4.10 reports the thermograms recorded for $\text{Al}_2\text{O}_3\text{-S}$ and $\text{Al}_2\text{O}_3\text{-N}$, in inert and reducing atmospheres respectively. The first weight decrease recorded for a and b in N_2 and H_2 below 250-300°C, is due to surface dehydration. It can be observed that the nature of the gas (A vs B), does not drastically influence the behavior of each alumina upon heating. This implies that pure alumina is not substantially reduced or activated. If we compare the behavior of the sulphate-based alumina to that of its nitrate analog at high temperature, it shows more a important mass loss above 500°C. This loss can be attributed to the volatilization of SO_4^{2-} impurities from the alumina matrix, which have not been removed during the activation step (220). Comparing the behaviors of $\text{Al}_2\text{O}_3\text{-S}$ in inert and reducing atmospheres, it is observed that the rate of sulphur-based compounds release is increased in the presence of H_2 . The onset temperature for impurity removal in N_2 is close to 600°C and proceeds gradually until 800°C. In hydrogen, SO_4^{2-} reduction products start to escape the alumina matrix around 525°C and the major portion is freed before 650°C. The facile evolution of sulphate reduction products at lower temperature in a reducing atmosphere is mentioned by Yamaguchi (215) and by Tanabe *et al.* (221) for sulphate-promoted Fe_2O_3 catalysts.

Fig 4.11 shows the thermograms obtained for ZnO precipitates in reducing and inert atmospheres. Curve a represents the behavior of ZnO in hydrogen and it can be observed that in the temperature interval 600-800°C, the oxide lattice is reduced to metallic zinc. Curve b shows the behavior of ZnO in flowing nitrogen. The apparent mass gain recorded is due to gas density changes upon heating with the resulting variations in buoyancy exerted on the sample (219). Since no dehydration or weight changes are

observed between 25°C and 800°C in an inert atmosphere, the zinc oxide lattice is suggested to be stable in the absence of reducing species. Deoxygenation of the ZnO lattice and the creation of the active sites responsible for H_{2p} interception, is induced by the presence of a reducing atmosphere such as in aromatization.

Fig. 4.12 shows the thermograms obtained for Zn/Al=1.0 co-precipitates in inert (A) and reducing (B) atmospheres. The features observed in flowing nitrogen are:

- (1) dehydroxylation/dehydration of Zn/Al-S=1.0 at low temperature. Loss of sulphate impurities is observed above 550°C;
- (2) high stability of Zn/Al-N=1.0. The absence of any dehydration weight loss may be related to the absence of acidity or better ZnO phase coverage since ZnO does not exhibit any dehydration features (Fig. 4.11 b).

In a hydrogen atmosphere, Zn/Al-N=1.0 reveals a similar curve to that of pure ZnO (Fig. 4.11 a), but the onset temperature for mass loss is higher (650°C) and the percent weight loss restricted to about 60wt.-%. For Zn/Al-S=1.0, dehydration, low temperature sulphate reduction product release and 50wt.-% weight loss attributed to the reduction of the ZnO phase are recorded.

Wise and Oudar (222) give a comprehensive explanation of surface energy and entropy effects. Catalysis by oxides is examined by Kung (223) and Kiselev and Krylov (224). In summary, under reaction conditions the surface of a solid catalyst can undergo rearrangement or be modified by reactant chemisorption. Chemisorption or the reaction conditions (temperature, pressure, concentration) can affect the geometric or electronic structure of surface layers. In catalysis by oxides, surface deoxygenation and conductivity changes upon chemisorption are frequent. The creation of such defect sites is often related to enhanced catalytic activity. The apparent independence of preparation reagents on catalytic activity at steady-state, as well as the different induction period behaviors point toward surface restructuring. New active sites are created that promote hydrogen migration by the restructuring process taking place during the induction step of the reaction.

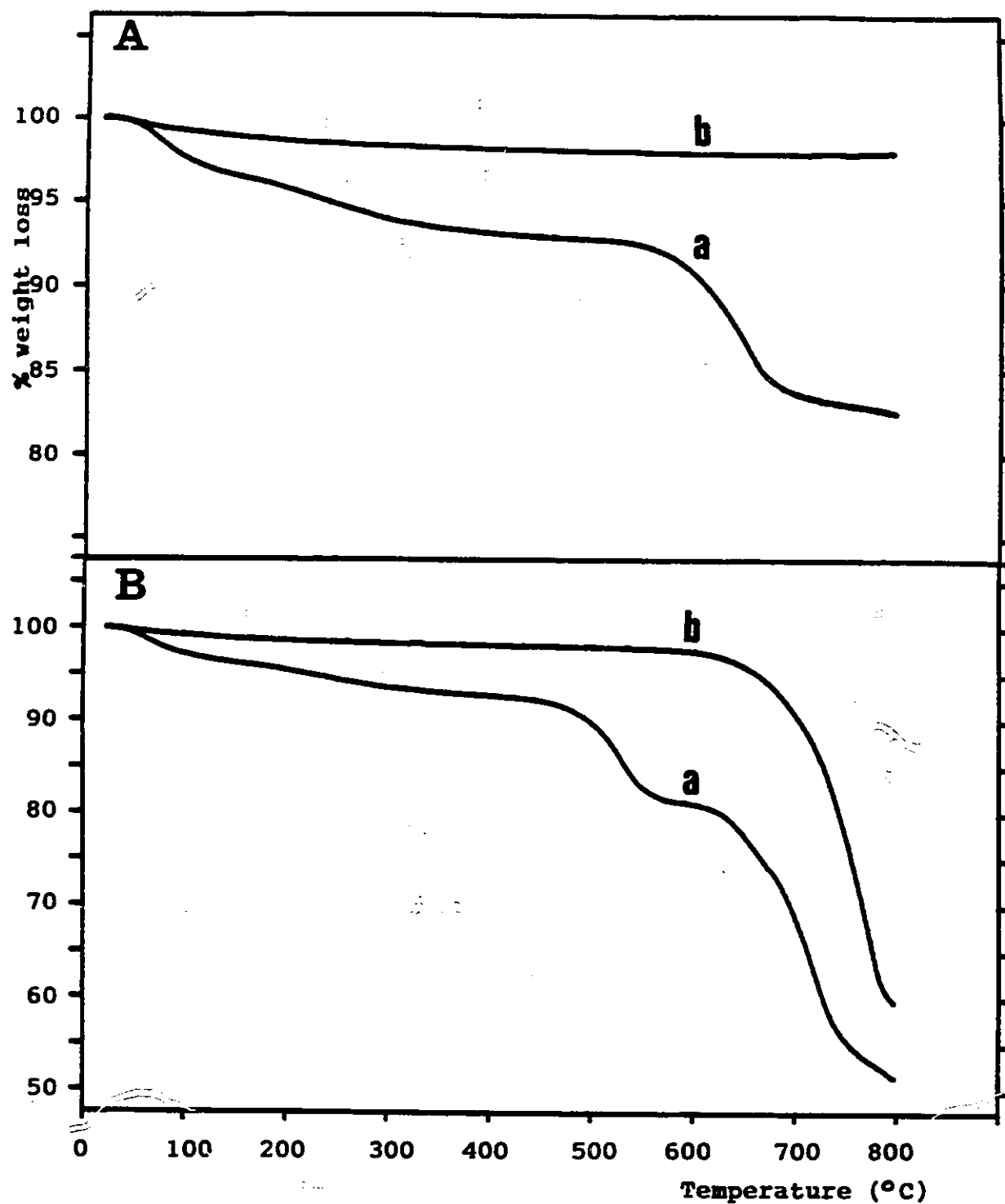


Figure 4.12 Thermograms of zinc oxide alumina co-precipitates. (A) N₂ atmosphere; (B) H₂ atmosphere.

Catalyst Identification: a Zn/Al-S=1.0;
 b Zn/Al-N=1.0.

4.4 Conclusions

In this chapter, results of physico-chemical characterization have been correlated with catalytic activity.

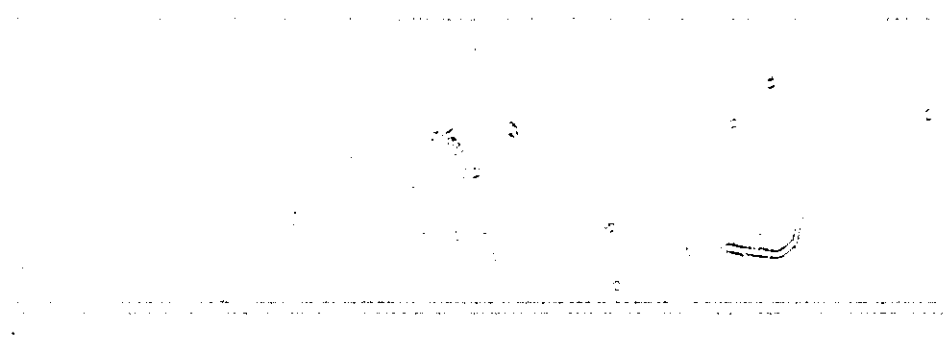
A more comprehensive picture of active site characteristics has been compiled. It was found that differences in surface area and porosity were not as determinant of catalytic activity as chemical composition. Also, acidity and zinc aluminate formation were not identified as primary factors orienting chemical reactivity. The sulphate content of the co-catalysts was related to pH and found independent of temperature treatment.

Induction period studies at different temperatures and as a function of pretreatment and preparation methods have revealed information about the activation step. Activation was related to deoxygenation of the ZnO lattice and partial reduction of both ZnO and alumina phases.

Stability studies coupled with thermogravimetric studies in inert and reductive atmospheres, have indicated the importance of surface restructuring and have been related to active site formation.

In the next chapter, dynamic characterization of the catalyst will be pursued in a kinetic investigation. Using the information contained in product selectivities, synergy toward aromatic formation on hybrid catalysts will be explained.

5.0 Kinetic study of ethylene aromatization on pure and hybrid catalysts



5.1 Introduction

Aromatics are high commercial value commodity chemicals. Their formation from cheap and abundant feedstocks such as LPG, have attracted much industrial and academic interests in the last decade. The current advances in aromatization processes and catalysts have been reviewed by Seddon (225).

BTX aromatics have been produced from C_2 - C_4 light paraffins on pure ZSM-5 zeolites in their acid form (78-83). The limitations observed in aromatic yields have been ascribed to the formation of light paraffins (C_1 - C_3), that act as hydrogen sink molecules. Hydrogen is produced primarily during the cyclodehydrogenation step of aromatization (Fig. 2.8).

Enhanced aromatic selectivity is achieved on bifunctional catalysts. These catalysts are made up of an acid component (H-ZSM-5 zeolite) and a dehydrogenation component. The acid component is responsible for oligomerization, isomerization, condensation and cracking reactions. The dehydrogenation component can be incorporated in the lattice during gel synthesis (Ga) to form gallosilicate or galloaluminosilicate. It can also be introduced by ion-exchange/reflux (Ga, Zn or Pt) or by mechanical admixing with the zeolite powder (Ga_2O_3 , ZnO). Atomic, ionic or oxide forms of the dehydrogenation component are efficient in the promotion of aromatization selectivity. Location inside the zeolite framework, extraframework or at a certain distance from zeolite crystallites all result in a synergistic behavior toward BTX compounds formation.

Acid mediated hydrogen transfer reactions (84, 136) are slow in the ZSM-5 lattice (136) and may even be rate limiting (111). The effects of the dehydrogenating component are to help in the activation of paraffin molecules, to promote the dehydrogenation of reaction intermediates leading to enhanced aromatic formation and to assist in hydrogen out migration from the zeolite lattice.

The most important inconvenience of having acid and dehydrogenation functions located inside the zeolite framework, is a rapid deactivation of the catalyst under reaction conditions. Highly dispersed Pt in H-ZSM-5 was found to promote coke formation in

ethane aromatization (226). The higher stability of the chemisorption Pt-ethylene complexes and the increased rate of olefinic intermediate consecutive reactions, were invoked to explain the increased coke formation. In propane aromatization, gallosilicate experienced deactivation much faster than its aluminium analog (227) with coking selectivities calculated by TGA of 0.38C.-% vs 0.06C.-% respectively. It was postulated that in gallosilicate, dehydrogenation was favored by the proximity of Lewis/Brønsted acid sites (227) and the higher formation of hydrogen deficient compounds in the zeolite was seen as a coke precursor (228). NiZSM-5 in ethylene oligomerization (229), gallo-aluminosilicate in the conversion of light naphtha into aromatics (230), or ZnZSM-5 in the transformation of heavy hydrocarbons to BTX compounds (231) all showed high coking tendencies.

Bifunctional catalysts where the second component is located outside the zeolite channel system, are called hybrid catalysts. ZnO and Ga₂O₃-based hybrids have been developed and studied by Le Van Mao *et al.* (72-73, 114-115, 126-128, 132, 232-233) and Tofanari *et al.* (116). Ga₂O₃ hybrids by Fujimoto *et al.* (130-131), Kanazirev *et al.* (234-236) and Mériaudeau *et al.* (166, 237) were also found selective in the aromatization of C₃-C₄ paraffins. The action of the ZnO (or Ga₂O₃)-based co-catalyst is to speed up the removal of hydrogen species from the zeolite internal surface. Increased aromatization selectivity has been related to Hydrogen Back-Spillover (HBS) and confirmed by Fujimoto *et al.* (130-131) and Pajonk (138). Kanazirev *et al.* propose that the development in aromatization activity is related to the formation of gallium suboxide (234) although the increased rate of hydrogen transfer reactions on hybrids was mentioned (235). A dual site dehydrogenation mechanism on Ga₂O₃/ZSM-5 has been proposed (236-238), based on the formation of active centers via solid state reaction and subsequent cooperation between Ga and Brønsted acid sites. The migration of Ga₂O₃ on the zeolite lattice has been observed (166).

An important advantage of having acid and dehydrogenating functions that are separated such as in the hybrid configuration, is a slower deactivation. For example, in ethylene and propylene oligomerization studies over composite catalysts (239-240) (ZSM-5/SiO₂-Al₂O₃ matrix) at high temperature, coke migration to the external surface was observed using TPO measurements. Similarly, the acetylene-water reaction over Ni/ZSM-5/Al₂O₃ catalysts (241) showed a slower deactivation with respect to pure H-ZSM-5.

Introduction of Pt in gallosilicate reduced catalyst decay and helped oxidative regeneration (96, 108). Addition of NiS to ZnZSM-5 showed less carbon deposit and a sustained aromatic selectivity (231).

One of the main ambitions of surface science is to provide an increased understanding of heterogeneous catalysis. The goal is a detailed microscopic description of a chemical reaction in terms of individual atom motions. This description is called *reaction dynamics* (242). *Macroscopic kinetics* can be measured in a catalytic reactor and apparent activation energies can be obtained for each catalyst under reaction conditions. Information is acquired on the interaction of feed molecules with the catalyst under different conditions of temperature, concentration and time. When the knowledge obtained by *macroscopic kinetic* studies is related to a suitable *micro-kinetic model*, information about the *reaction dynamics* is available. The *micro-kinetic model* is based on binding energies and reaction rate constants deduced from surface science experiments on well-defined single crystal surfaces (242).

The *macroscopic kinetic* study presented in this chapter for ethylene aromatization, probes behavioral differences between pure (H-ZSM-5, ZnO or ZnO/alumina) and hybrid catalysts (ZnO hybrid or ZnO/alumina hybrid). Activation energies and pre-exponential factors will be calculated using the Arrhenius equation. Comparison of reaction product selectivities taken in conjunction with TGA analyses of spent catalysts will be used to provide further evidence for the mode of action on hybrid catalysts.

5.2 Theoretical principles of kinetic studies

5.2.1 Mechanism of contact catalysis

On a solid heterogeneous catalyst, chemical reactions occur between the adsorbed compounds found on the surface. The entire cycle contains five consecutive steps, each of which can influence the overall reaction rate. These steps are (9):

- (1) Diffusion of the reactant over the catalyst particle;
- (2) Adsorption;
- (3) Reaction;
- (4) Desorption;
- (5) Diffusion of the reaction products into the surrounding medium.

Steps (1) and (5) correspond to the physical processes of mass transfer to and from the catalyst particle, and into and out of its pores (Fig. 5.1). For an active surface to achieve its full conversion potential, reactants and products must be able to reach and leave the surface quickly.

Fick's laws of diffusion describe the movement of molecules through the stationary external layer of adsorbed fluid ($A \leftrightarrow B$, Fig. 5.1). Fick's first law expresses in statistical terms the net displacement rate (net flux, F), as the difference between the concentration of mobile species, dc , across a volume element, dx , with a proportionality constant, D (243):

$$\text{Flow rate} = -D \frac{dc}{dx} \quad (5-1)$$

Fick's second equation is the mass balance difference between the in- and out- flux of molecules for each volume element (243):

$$D \frac{\partial^2 c}{\partial x^2} = \frac{\partial c}{\partial t} \quad (5-2)$$

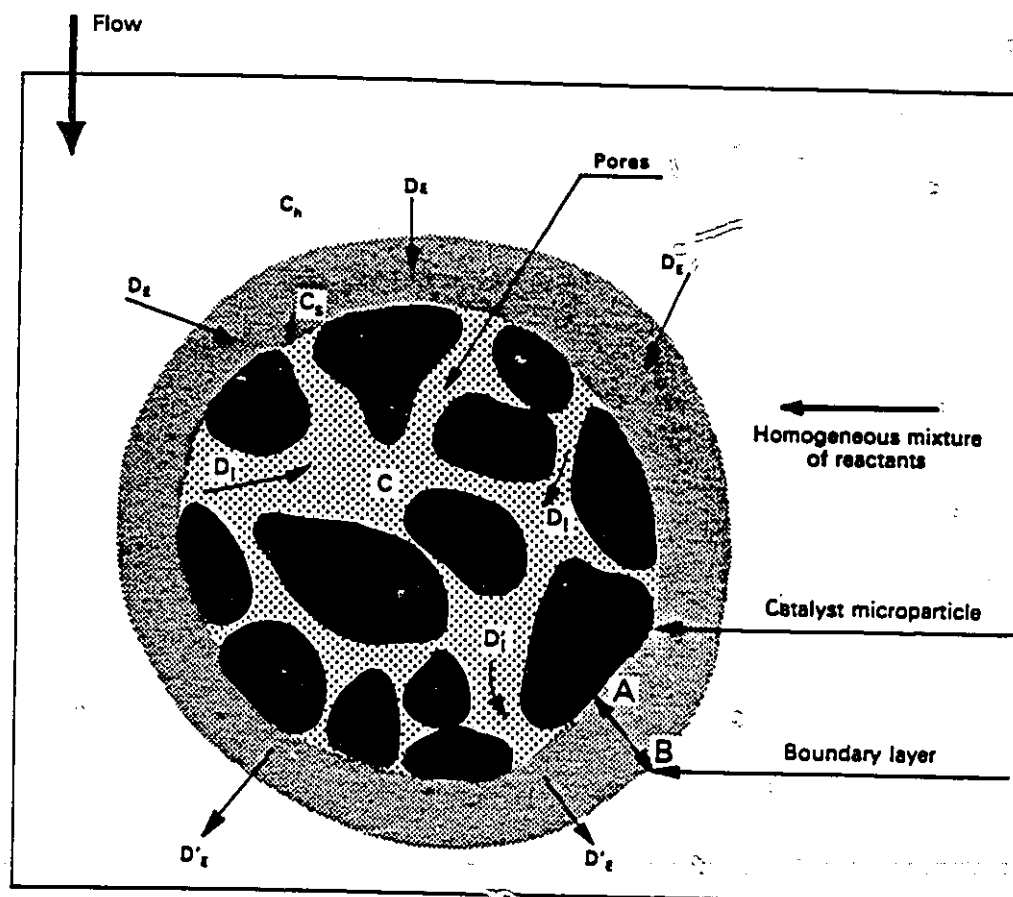


Figure 5.1 Features of the diffusion process that occurs during heterogeneous catalysis. D_i : intragranular diffusion of reactants; D'_i : intragranular diffusion of products; D_e : extragranular diffusion of reactants; D'_e : extragranular diffusion of products; C_h : concentration of a reactant in the external homogeneous phase; C_s : concentration of a reactant in the external surface of the particle; C_p : concentration of a reactant inside the particle's pores; $A \leftrightarrow B$: stationary external layer of adsorbed fluid. (From reference 9).

The physical processes of diffusion tend to equalize the concentrations (9).

Diffusion proceeds in two steps: external diffusion, D_E , and internal diffusion, D_I . These diffusion regimes exist because the catalyst particles have internal pores that are accessible to the reactant molecules. D_E is related to the concentration gradient in the stationary $A \leftrightarrow B$ layer or $D_E \sim (C_h - C_s)$ in Fig. 5.1. D_I is a function of the concentration gradient between the surface and at any interior point inside the pore or $D_I \sim (C_s - C)$ in Fig. 5.1.

A reaction can experience diffusional limitations that can be either intragranular ($D_I \neq D_I$) or extragranular ($D_E \neq D_E$). Interparticulate diffusion limitations also are possible as a result of coke formation during the reaction (244). For these cases, the measured reaction rates will be slower than the intrinsic activity of the surface.

Steps (2) to (4) involve chemical phenomena, including the surface mediated reaction between adsorbed reactants to form the products (Fig. 5.2).

5.2.2 Catalyst evaluation

A catalyst evaluation study must include the estimation of intrinsic rate parameters from experimental data (245). Knowledge of reaction rates and adsorption constants can be related to catalyst structure and composition, while conversion and selectivities can give information about the mechanism.

The primary objective of all kinetic studies is to express reaction rates in terms of parameters that can be measured experimentally and that correspond to the properties of the reactant, the catalyst and the reactor. A correct interpretation of the experimental results can lead to the identification of the step or steps that limit the overall reaction rate. Identification of the rate determining step of a single catalytic cycle at quasi-steady state, contributes an interesting and useful detail of the reaction mechanism. Examples are given by Boudart and Tamaru (246).

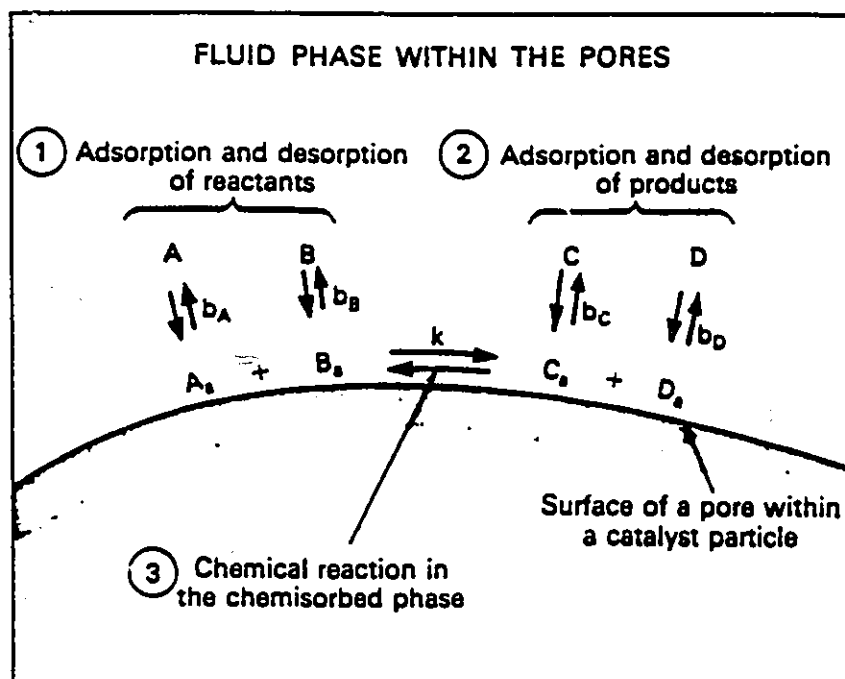


Figure 5.2 Features of the chemical reactions occurring within the adsorbed fluid phase during heterogeneous catalysis.

(1) Chemisorption equilibrium, b_A and b_B , of reactants A and B to and from the catalytic surface; (2) Desorption equilibrium, b_C and b_D , of products C and D to and from the catalytic surface; (3) Chemisorbed-phase reaction between reactants A and B, giving products C and D (from reference 9).

The selective acceleration of a desired reaction can become possible after the specific effects of each parameter have been investigated and related to the catalytic selectivity. Chemical kinetics govern mechanisms of catalytic action and chemisorption. Physical kinetics are related to intra- and extragranular diffusion processes (9) or in other words they describe the movement of mobile species across the catalyst bed.

5.2.3 Measuring the properties of catalysts: catalytic reactors

Activity, selectivity and stability are properties that can only be determined by studying the catalyst under reaction conditions (9, 247). Various types of experimental reactors with associated advantages and disadvantages exist. Selection of an isothermal reactor, evaluation of the best operating conditions and investigation of diffusional limitations constitute the first stages of a chemical kinetic study.

Reactors where data is acquired under dynamic conditions and unchanging concentrations include the differential fixed bed reactor. Reactors where data is acquired under dynamic conditions in the presence of a concentration gradient, include the integral fixed bed reactor (or piston-flow, plug-flow reactor).

A fixed bed reactor operates in differential mode when the reaction rate is constant at every given point throughout the catalytic mass (9, 245). Therefore, the rate is directly obtained as a function of conversion as in equation 5-3:

$$V_A = \frac{\bar{N}_{A0}}{m} [(x_A)_{outlet} - (x_A)_{inlet}] \quad (5-3)$$

where

V_A : intrinsic rate

\bar{N}_{A0} : molar flow of reactant A at inlet of reactor

m : catalyst mass

$(x_A)_{outlet}$: concentration of reactant A at outlet

$(x_A)_{inlet}$: concentration of reactant A at inlet

The slope of the curve obtained when $\ln V_A$ vs \ln conversion are plotted, yields the order of reaction (245). A disadvantage associated with using a differential reactor is the difficulty involved in precisely measuring the very low conversion rates required (9).

An integral reactor is one where the concentration of reactants and therefore the specific rate is no longer constant along the catalyst bed (9). Conducting a reaction at a higher conversion results in such an axial concentration gradient. The intrinsic rate is then related to each mass element of the catalyst bed, dm (Fig. 5.3 and equation 5-4).

$$\bar{N}_{A_0} dx = V_A dm \quad (5-4)$$

where dx : differential in the rate of conversion of the reactant A
 dm : mass element

Since the intrinsic rate, V_A , varies along the reactor axis as the concentration progressively changes, integration of equation 5-4 gives:

$$\frac{m}{\bar{N}_{A_0}} = \int_0^x \frac{dx}{V_A} \quad (5-5)$$

where m/\bar{N}_{A_0} : space velocity.

The curve obtained when conversion is plotted against contact time (space velocity⁻¹) yields the specific reaction rate. The tangent at any point on the curve is equal to the specific reaction rate at the corresponding conversion level. The initial slope is related to the intrinsic activity of the catalyst. The advantage of using an integral reactor is the considerable simplification in data acquisition. A disadvantage is that experiments are imprecise and accurate reaction rates cannot be obtained. When possible, integral

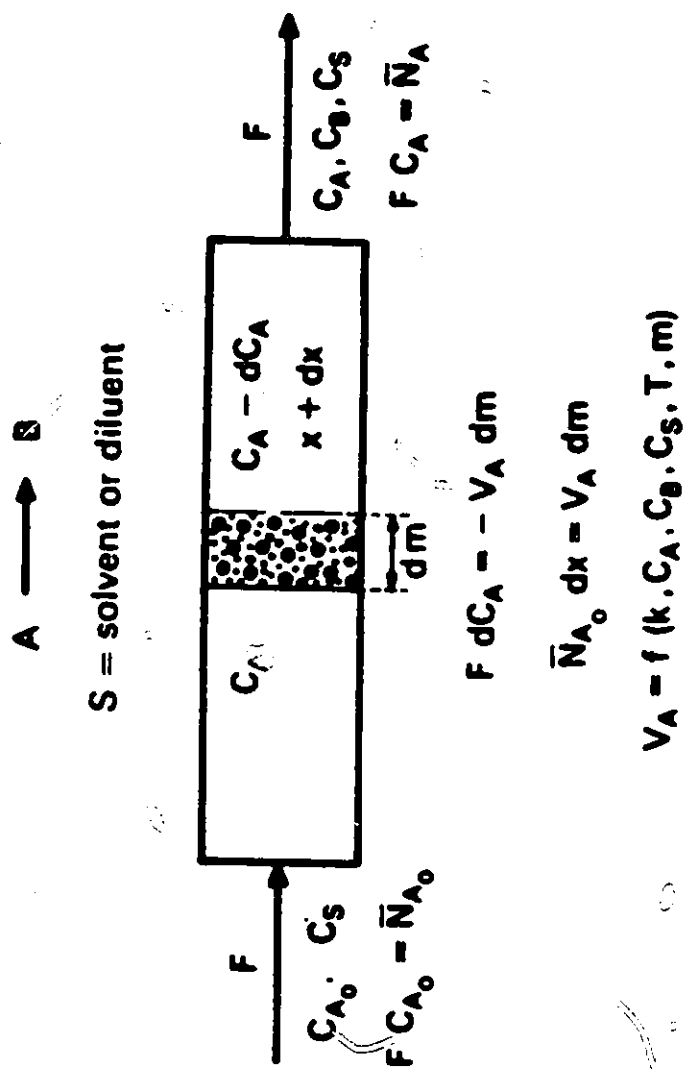


Figure 5.3 The system for reactions over a concentration gradient through piston-type flow reactor (from reference 9).

reactors are not used in kinetic studies.

5.2.4 Arrhenius equation

$$k = Ae^{-\frac{E_{\text{exp}}}{RT}} \quad (5-6)$$

The main theories of chemical kinetics arise as a result of Arrhenius' formulation of the rate constant (248). Although originally empirical and macroscopic, the Arrhenius law is remarkably satisfactory (248-249) by virtue of its simplicity.

One of the various theories of reaction rates is the theory which examines the passage of species over potential-energy surfaces, or hypersurfaces. These energy surfaces are potential energy maps that relate the surface potential energy to the geometries of the reactant molecules and the reactions intermediates. If it is assumed that the activated complexes or transition states formed are in equilibrium with the reactants, chemical kinetic properties can be described by the activated complex theory (248-249). In this theory, the thermodynamic formulation of the rate constants is based on the premise that equilibrium between reactants and the activated complex may be expressed in terms of thermodynamic functions or partition functions (248). The resulting expression for the reaction rate is:

$$k = e^2 \frac{kT}{h} e^{\frac{\Delta S_a}{R}} e^{-\frac{E_{a,\text{exp}}}{RT}} \quad (5-7)$$

where $e^2(kT/h)$: frequency component for crossing a barrier in one direction
 $e^{\Delta S_a/R}$: entropy component
 $e^2(kT/h) e^{\Delta S_a/R}$: A, pre-exponential factor
 $E_{a,\text{exp}}$: activation energy measured experimentally
 (Derivation in references 248-249)

The pre-exponential factor, A, includes frequency and entropy contributions which account for the structures of the reacting molecules and the manner in which they come together in the collision act (248).

The experimental activation energy measured in heterogeneous catalysis, $E_{a,exp}$, represents all the processes that occur simultaneously on the surface. It is therefore referred to as an apparent activation energy, $E_{a,app}$ and defined as:

$$E_{a,app} = E_{D_F} + \sum E_{reaction} + E_{D_T} \quad (5-8)$$

If the external and internal diffusion contributions are assumed to be negligible, these steps are not rate limiting and the measured rates then reflect the energies contributed by the individual reactions. In this case, $E_{a,app}$ can be assumed to be closely related to the intrinsic properties of the surface.

In zeolites, it has been observed that when intragranular limitations exist and if reactant heats of adsorption are high, $E_{a,app}$ can sometimes be negative (180, 250). An example of this phenomenon is the alkylation of toluene with ethanol (250) on a ZSM-5 zeolite having a crystallite size distribution between 2-5 μ m. It has been observed that the catalytic activity for alkylation decreases as temperature is increased.

In the interaction of light olefins and paraffins on zeolites at high temperature, several reactions take place on the surface at any given time. The individual contributions of reactions such as oligomerization, isomerization, condensation (conjunct polymerization), cyclization, dehydrogenation/hydrogenation, hydrogen transfer/redistribution, cracking, alkylation, disproportionation etc (80-83, 121-123, 252) are incorporated $E_{a,app}$. The value of $E_{a,app}$ depends on the balance between endothermicity-exothermicity for all catalytic actions. Values for A and $E_{a,app}$ can be obtained by plotting $\ln k$ vs $1/T(K)$. Curvature in the Arrhenius plot as a result of the passage between a chemically controlled regime to an intracrystalline diffusion controlled regime ($f(T,p)$), can be observed. In that case the measured apparent activation energy can be significantly decreased ($E_{a,app} < E_{a,intrinsic}/2$) (180, 245, 249).

Since in order to have a reaction it is necessary to overcome a free energy barrier ($\Delta G_a = \Delta H_a - T\Delta S_a$), both the activation energy and the pre-exponential factor must be favorable. If the energy barrier is low the reaction may still be improbable if ΔS_a is largely negative. Conversely, $E_{a,app}$ may be high but if the entropy of activation is large and positive, the reaction may be helped (249).

The compensation effect (249, 251) shows a parallelism between the energy and the entropy contributions in a process and shows that the catalytic reactivity of a surface is not only a matter of active sites. Due to the compensation effect, comparison of similar reactions on one catalyst or of one reaction on similar catalysts are found not to be independent of each other (251).

5.3 Experimental

5.3.1 ZSM-5 zeolite synthesis

The ZSM-5 zeolite used during the kinetic studies was synthesized according to the method of Argauer and Landolt (100). The composition of the synthesis gel and the parameters were selected so the resulting solid had a Si/Al atomic ratio of about 40. Procedure to obtain the final form of the zeolite, as well as characterization techniques used are as described in section 2.2.1. SEM photographs indicated an average particle size of 2-3 μ m. The acid zeolite powder was carefully sieved to obtain 80-100 mesh size agglomerates. Table 5.1 reports the results of characterization experiments.

Two zeolite batches of 100g each were prepared and characterized separately. Prior to being used, each batch underwent standard catalytic tests to ensure uniformity and reproducibility with previously synthesized zeolites and between themselves. Once catalytic activity was verified, the two batches were mixed and reserved exclusively for the kinetic studies.

5.3.2 Synthesis of the co-catalysts

The co-catalysts were synthesized by heterogeneous co-precipitation according to the preparation method described in section 2.2.2. In this chapter, only pure ZnO precipitate and Zn/Al-S=1.0 co-precipitate were used. The co-catalysts were crushed and sieved (80-100 mesh size). SEM photographs indicated an average particle size of 80-100 μ m. The oxide powders were characterized by atomic absorption, X-ray powder diffraction, BET surface area, SEM, hydrogen chemisorption and ammonia TPD.

5.3.3 Preparation of the catalysts

To prepare the final catalysts, the H-ZSM-5(43) and co-catalyst powders were mechanically mixed at room temperature. Bentonite clay was then incorporated and intimately mixed with the solid catalyst. Deionized water was added dropwise until a malleable paste was obtained. The latter was extruded into 1.5mm O.D. *spaghettis* and was dried at 120°C overnight and activated in air at 550°C for about 10h. The final length

TABLE 5.1 Physico-chemical characterization of H-ZSM-5(43) zeolite used in kinetic studies.

Si/Al ratio	43.0
Na₂O content (wt%)	0.2
DC (% wt respect to H-ZSM-5(20))	99.5
BET Surface Area (m²/g)	389.5
Acidity measured by NH₃-TPD	
Peak	Temperature (°C)
I	225
II	355
III	555
	Density (mol/g)
	3.37E-04
	1.45E-04
	1.36E-04

DC: Degree of crystallinity.

of the catalyst extrudates was 2 ± 0.5 mm.

Pure H-ZSM-5(43), ZnO and Zn/Al-S=1.0 catalysts were prepared from 90wt.-% active phase and 10wt.-% bentonite clay. Hybrid catalysts were made up of 84.4wt.-% H-ZSM-5(43) powder, 5.6wt.-% co-catalyst powder and 10wt.-% bentonite clay.

All catalysts were used fresh (once only) during the kinetic studies to avoid the acquisition of results influenced by deactivation. Thermogravimetric analyses of spent pure and hybrid catalysts (reactions at 540°C) were conducted on a STA 1500 from PL Thermal Sciences. An oxygen atmosphere was used and a sample weight of 18.0mg. The temperature program was as follows: T_i :25°C, ramp:5°C/min, T_f : 900°C.

5.3.4 Catalytic testing

The experimental set up is as shown in Fig. 5.4. The extruded catalyst was loaded in the tubular reactor (plug-flow reactor, R_c), operating in integral mode. The reactor was made up of a quartz tube (12mm O.D.) having a constant I.D. Ethylene feed (Linde 99.9% purity), hydrogen co-feed when required (C_2H_4/H_2 molar ratio = 1:1) (Linde pre-purified) and nitrogen carrier gas flow rates were controlled by automatic devices. They were introduced in a cyclone-gas mixer (cgm) designed especially to ensure complete mixing of all components and eliminate laminar flows.

The gases were analyzed throughout the run using a Shimadzu GC (Model Mini 3, FID) equipped with a 2.5m stainless steel column (15wt.-% squalane on Chromosorb P) with 2,2-dimethylbutane as internal standard. The amount of hydrogen in the effluent was measured chromatographically using a 30m HayeSep DB column from Chromatographic Specialties (HP Model 5890- TCD/ N_2 carrier gas). Prior to analysis, a volumetric calibration was performed using pure hydrogen gas. The ethane yield was determined from the ethane/ethylene ratio obtained using a calibrated SRI Student GC (TCD detector) equipped with a 1m SiO_2 gel column.

The liquid hydrocarbons formed during the catalytic reactions were collected in a condensing flask kept at -15°C. The amount of liquid was determined by differential weighing of the condensing flask. Hydrocarbons were extracted for chromatographic

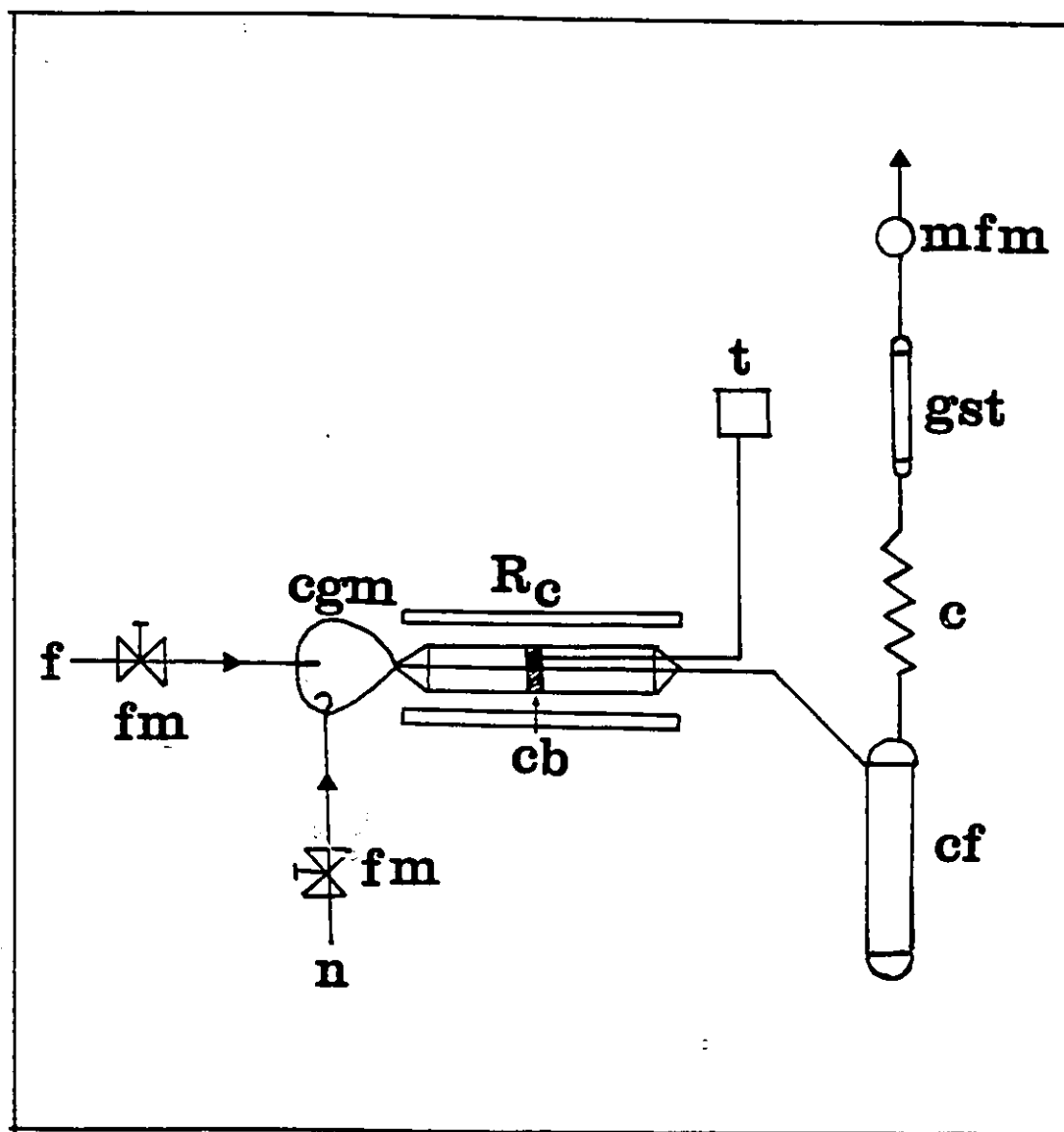


Figure 5.4 Experimental set-up for catalytic testings.
C, condensers; **cb**, catalyst bed; **cf**, collecting flasks; **cgm**, cyclone gas mixer; **f**, feed (propane, n-butane etc.); **fm**, flow meters; **gst**, gas sampling tube; **n**, nitrogen (carrier gas); **R_c**, catalytic reactor; **t**, thermocouple (chromel-alumel).

analysis using n-octane. The collected liquid phases were subsequently analyzed on a Hewlett Packard GC (Model 5790A, FID) equipped with a 50m PONA type capillary column. The n-octane peak was considered as solvent in the chromatogram and was excluded from the product distribution. Product identification in the C_8^+ aromatics fraction was performed by GC-MSD analysis (HP 5970B Mass Selective Detector in tandem with a 5890 HP GC).

5.3.5 Investigation of mass transfer limitations

Prior to the kinetic investigation experiments, mass transfer limitations due to external and internal diffusion processes had to be eliminated so that steps (1) and (5) (Fig. 5.1) were not rate limiting. In this way, it is expected that the apparent initial reaction rate obtained experimentally, will be close to the initial rate for the reaction studied.

The influence of extragranular or interparticulate diffusion limitations was examined while the weight of the catalyst and the temperature were fixed at $0.5 \pm 0.005g$ and $500^\circ C$ respectively. The WHSV was arbitrarily chosen to be $4.3h^{-1}$ and kept constant for all reactions, so that the variable was the flow rate of carrier gas. Nitrogen flow rate variations change the ethylene/nitrogen ratios and the time needed for the gas mixture to travel from one end of the reactor, over the catalyst bed, to the other end is also modified. The residence time changes. Fig. 5.5 shows a plot of percent ethylene conversion as a function of residence time. This graph shows that for a residence time, τ , smaller than 10s, the reaction is limited by internal diffusion (9), while when τ is greater than 12.5s, the system tends toward saturation. Therefore, for the catalyst weight selected and the geometry of the reactor used, a total residence time of 10.2s was chosen for all the kinetic experiments. A one pass-thru time of 10.2s corresponds to a total flow rate ($N_2 + C_2H_4$) equal to $50ml\ min^{-1}$ and the total flow rate to catalyst weight ratio is $100ml\ min^{-1}g^{-1}$.

In a second case, the weight of the catalyst was varied while the WHSV and the flow rate feed/total flow rate ratio remained constant. From Table 5.2 it can be seen that the ethylene conversions and the product distributions are very similar, thus suggesting that changes in the catalyst weight do not influence the reaction. Therefore, for the experimental conditions selected, mass transfer limitations were assumed to be

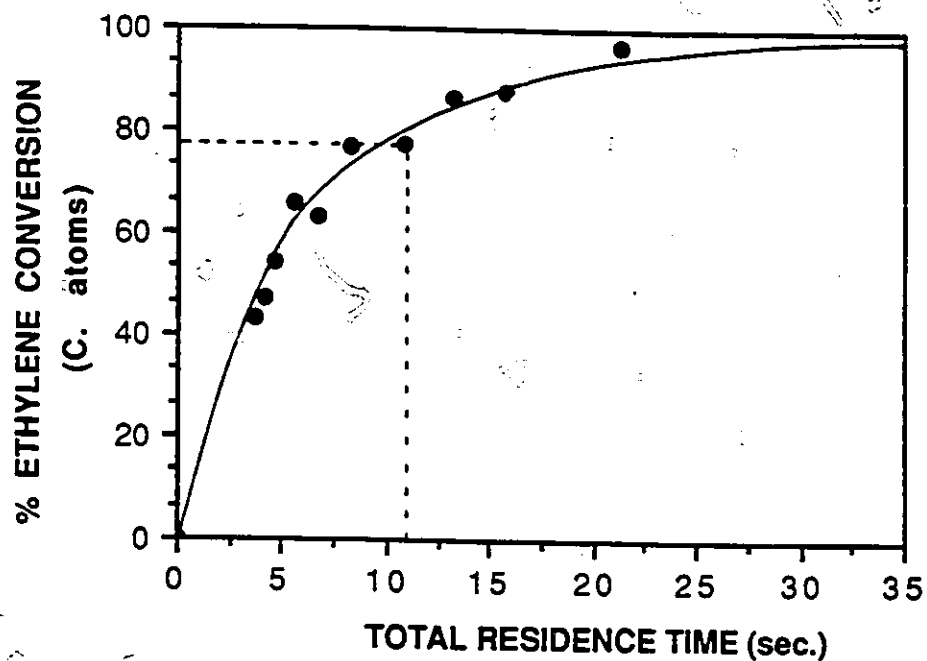


Figure 5.5 Evaluation of external mass transfer limitations. Graph of ethylene conversion as a function of residence time.

Parameters: Temperature R_c : 500°C; WHSV: 4.3h⁻¹.

Catalyst composition: 90wt.-% H-ZSM-5(43) + 10wt.-% bentonite binder.

TABLE 5.2 Effect of catalyst weight on mass transfer.

Weight Cat. (g)	0.50	0.75	1.00
WHSV (hr ⁻¹)	4.24	4.28	4.20
Total Product Distribution (% C. atoms)			
C1-C4 Paraffins	19.2	19.4	21.4
C2-C4 Olefins	47.8	50.7	49.5
C5 ⁺ Aliphatics	11.5	11.3	10.7
Total Aromatics	21.5	18.6	18.6
BTX/Aromatics	0.87	0.88	0.90
Ethylene Conversion (% C. atoms)	85.2	82.0	85.9
Carbon Balance	80.1	85.9	80.2

C5⁺ Aliphatics: Aliphatic molecules having C5- C10 C. atoms.

Temperature R_c: 500°C

Total Flow Rate (ml/min)/ Weight Cat. (g) = 120 ml min⁻¹ g⁻¹

Flow Rate C₂H₄ (ml/min)/ Total Flow Rate (ml/min) = 0.5

eliminated. However, since the zeolite crystallite size was fixed at 2-3 μ m, the possible effects of intragranular diffusion limitations were not verified prior to the kinetic investigations.

5.3.6 Resume of chosen experimental conditions for kinetic studies

Catalyst Composition:	90wt.-% active phase + 10wt.-% bentonite clay
Zeolite crystallite particle size:	2-3 μ m
Co-catalyst particle size:	80-100 μ m
Extrudate Dimensions:	2.0mm X 1.5mm O.D.
Catalyst Weight:	0.5 \pm 0.005g
Total Flow Rate:	50ml min ⁻¹ (τ = 10.2s)
Total Flow Rate/ Catalyst Weight:	100ml min ⁻¹ g ⁻¹
Temperatures:	480°C, 500°C, 520°C and 540°C

5.3.7 Product calculations

All calculations were made on a carbon atom basis. Chromatographic results were converted to C. atoms using an internal standard (2,2DMB) for the gaseous effluent and correction factors for the columns. The definitions of total feed conversion, the selectivity and the yield of product i can be found in section 2.2.6.

5.3.8 Data acquisition for kinetic studies

For all the reactions, special care was taken to monitor all the products and to obtain a good carbon atom recovery. Gaseous samples were taken at regular intervals after the induction period (40-50min) and reproducible product distributions were recorded chromatographically. Runs typically lasted for 180-190min and during that time, no significant catalytic activity decay was observed.

To get reasonably good estimates of the apparent initial reaction rates, it is essential to eliminate diffusion limitations but it is also important to conduct data acquisition when ethylene conversions are as low as possible. Ethylene is extremely reactive on a ZSM-5 zeolite surface and in order to obtain low values of total ethylene

conversion while remaining in the chemically controlled kinetic regime, it was necessary to adopt a procedure based on the variation of ethylene/nitrogen ratios. The total flow rate (50 ml min^{-1}) and the catalyst weight (0.5 g) were kept constant so that the partial pressure of ethylene was varied from one reaction to the next. Since the plug-flow reactor was used at atmospheric pressure ($\approx 1 \text{ atm}$), the total flow rate was taken as equal to 1 atm . The partial pressure of ethylene was consequently smaller than 1 atm .

Justification for the use of partial pressure is as follows (133). An isotherm is formed when the extent of surface coverage (θ) is plotted against partial pressure or relative pressure. As the partial pressure increases, so does θ until a plateau is reached. Similarly, for any one partial pressure, an isotherm exists when θ is plotted against time. As time increases, so does θ until a plateau is reached thus relating the partial pressure to time through surface coverage. Equally true is the event that as the $\text{C}_2\text{H}_4/\text{N}_2$ ratio increases, so does the contact time with respect to the hydrocarbon feed. Therefore, in the present work the ethylene partial pressure can be considered as a time equivalent factor.

Apparent initial rates of reaction (r_o) were obtained when the total ethylene conversion (C_t), or the conversion to product i (C_i) were plotted against feed partial pressures. Curve fitting was done using a Simplex Algorithm and a 3rd order polynomial equation. The first derivative of the equation taken at $\lim x \rightarrow 0$, yielded relative values of r_o for each temperature. The apparent activation energies and pre-exponential factors were evaluated using the Arrhenius plot method (248-249), where $\ln r_o$ is plotted against $1/T$ (K). The straight line obtained has a slope which is equal to $-E_{a,\text{app}}/R$ and an intercept which is equal to $\ln A$.

$$\ln r_o = \ln A - \frac{E_{a,\text{app}}}{R} \frac{1}{T} \quad (5-9)$$

It is to be noted that because of experimental uncertainties inherent to the system and the use of an integral reactor, values of $E_{a,\text{app}}$ and A should be viewed as relatively. They should only be considered as indicative of the different behaviors of pure and hybrid catalysts.

5.4 Results and discussion

Reaction rates are evaluated from feed conversion plots as a function of time or of a time equivalent factor. Fig. 5.6 shows a plot of ethylene conversions as a function of ethylene partial pressures for a pure H-ZSM-5(43) zeolite. Catalytic behaviors have been studied at 480°C, 500°C, 520°C and 540°C and the initial reaction rates were determined at each temperature from the resulting curves. Table 5.3 reports the product selectivity distributions obtained.

Fig. 5.7 and Fig. 5.8 show plots of ethylene conversion variations with partial pressures and at different temperatures, for ZnO and ZnO/alumina hybrid catalysts respectively. Product distributions are reported in Tables 5.4 and 5.5.

Fig. 5.9 and Fig. 5.10 show ethylene conversion plots for pure ZnO precipitate and ZnO/Al₂O₃ co-precipitate (Zn/Al-S=1.0) catalysts respectively. The investigation of ethylene hydrogenation on ZnO-based catalysts using stoichiometric amounts of C₂H₄ and H₂, was undertaken as an attempt to quantify ethylene reduction on hybrids by spillover hydrogen species. It can be observed that even at high ethylene partial pressure (≈ 0.20 atm) and temperature (540°C), the ethylene conversion remains low (< 4% conversion to ethane). This behavior differs from that of ZnO-based co-catalysts in hybrid systems. For the ZnO hybrid and the Zn/alumina hybrid tested under similar conditions, ethane formation reached 35wt.-% and 24wt.-% respectively. In a discussion of IR spectra characteristics for chemisorbed species, Ashmore (171) states that studies on a pair of reactants in some bimolecular reaction, do not always give reliable information about chemisorption from mixtures. The much lower hydrogenation activity of pure ZnO or ZnO/Al₂O₃ co-precipitate catalysts with respect to that of hybrid analogs, seems to belong to that category. The reasons underlying the different catalytic behaviors observed could be related to the nature and the reactivity of the H_{ads} species, that may be different from those of spillover hydrogen species exiting the zeolite lattice. Restructuration of the oxide surface or the presence of other reaction products could also be involved in the explanation.

Fig. 5.11 and Fig. 5.12 depict the Arrhenius plots obtained for all the catalysts studied. Table 5.6 reports the experimentally determined apparent activation energies

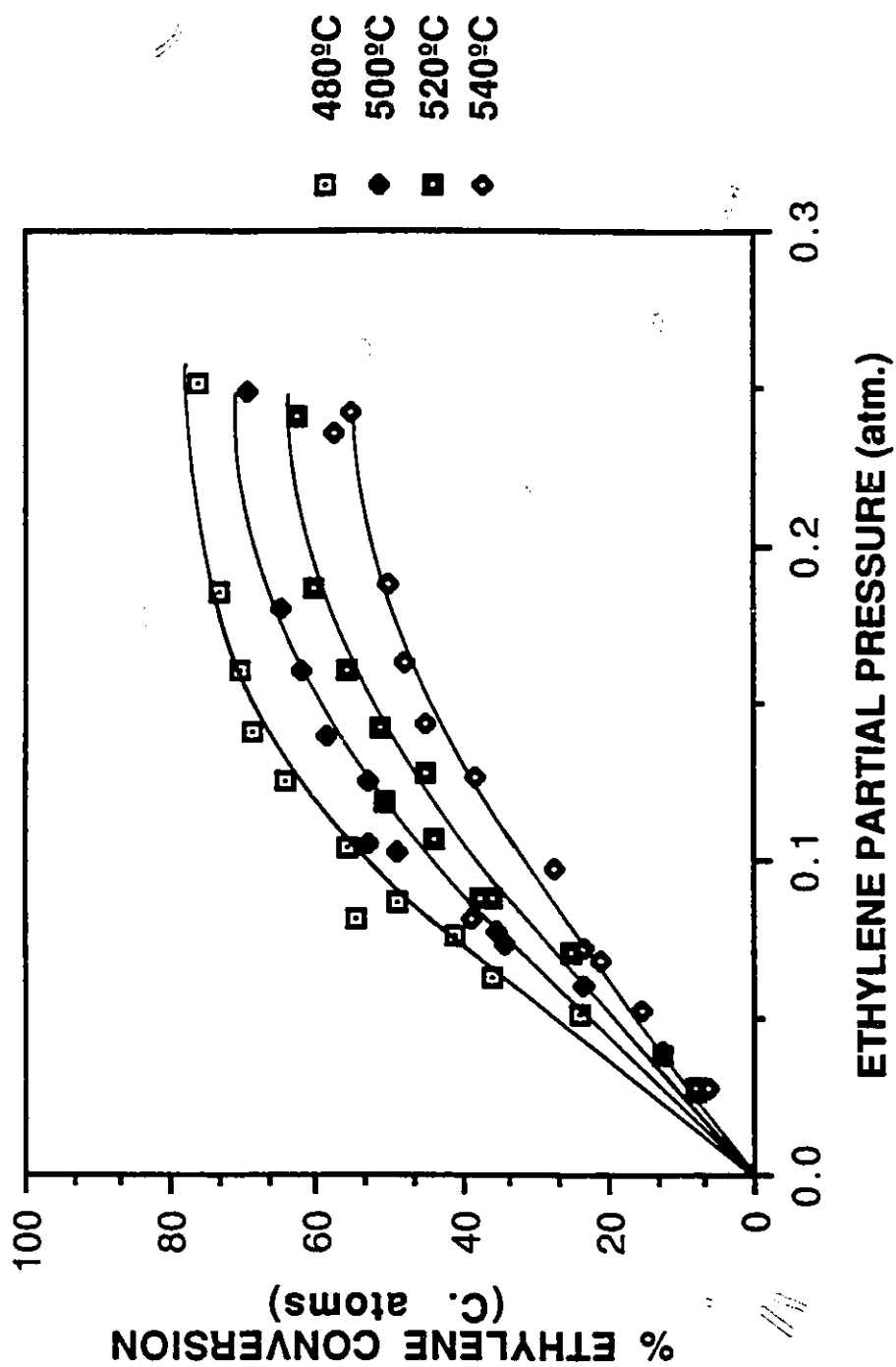


Figure 5.6 Variation of ethylene conversion as a function of feed partial pressure. Data obtained at different temperatures.
Parameters: Feed: ethylene; Temperature P_c : 480-540°C; residence time: 10.2 sec.
Catalyst Composition: 90wt.-% H-ZSM-5(43) + 10wt.-% bentonite binder.

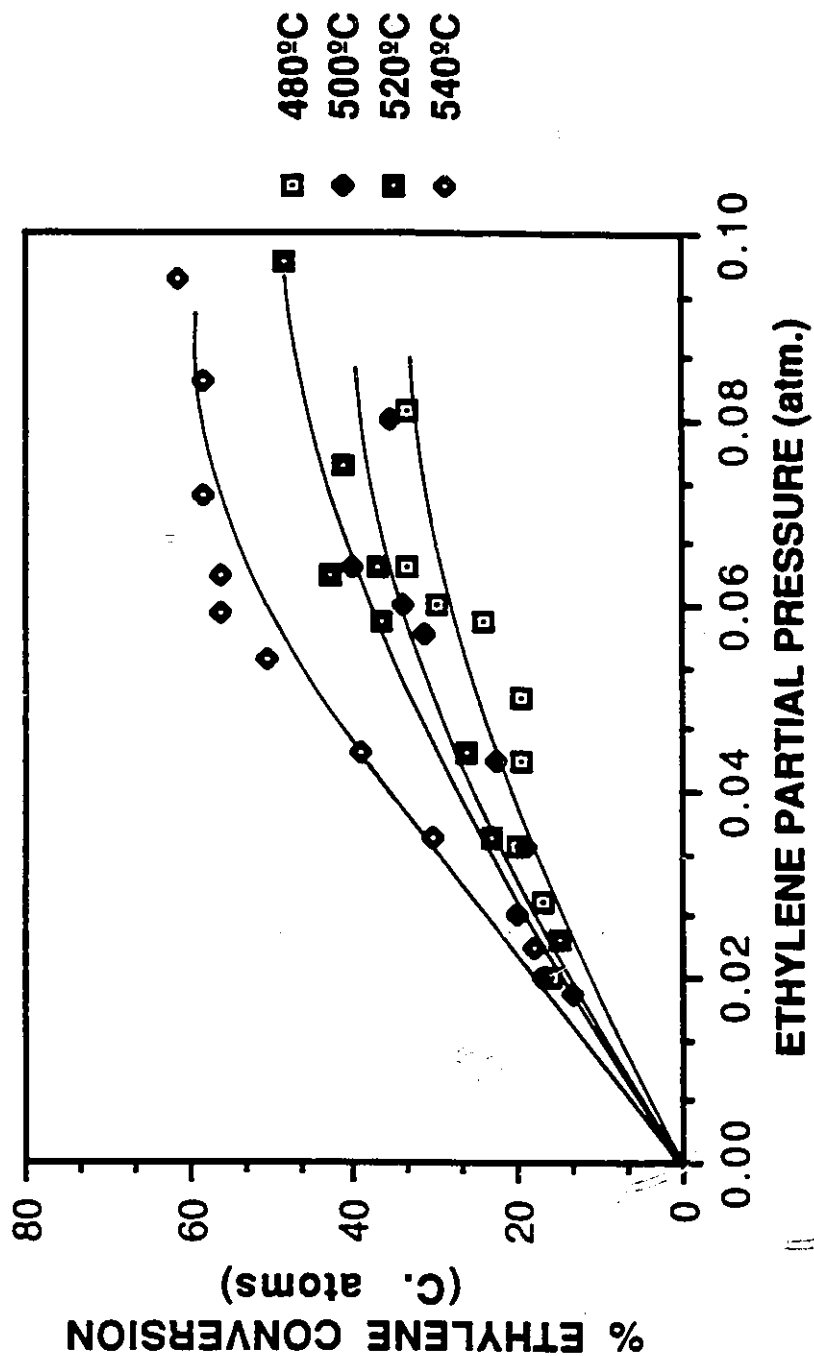


Figure 5.7 Variation of ethylene conversion as a function of feed partial pressure. Data obtained at different temperatures. Parameters: Feed: ethylene; Temperature R_c : 480-540°C; residence time: 10.2 sec. Catalyst Composition: 84.4wt.-% H-ZSM-5(43) + 5.6wt.-% ZnO precipitate + 10wt.-% bentonite binder.

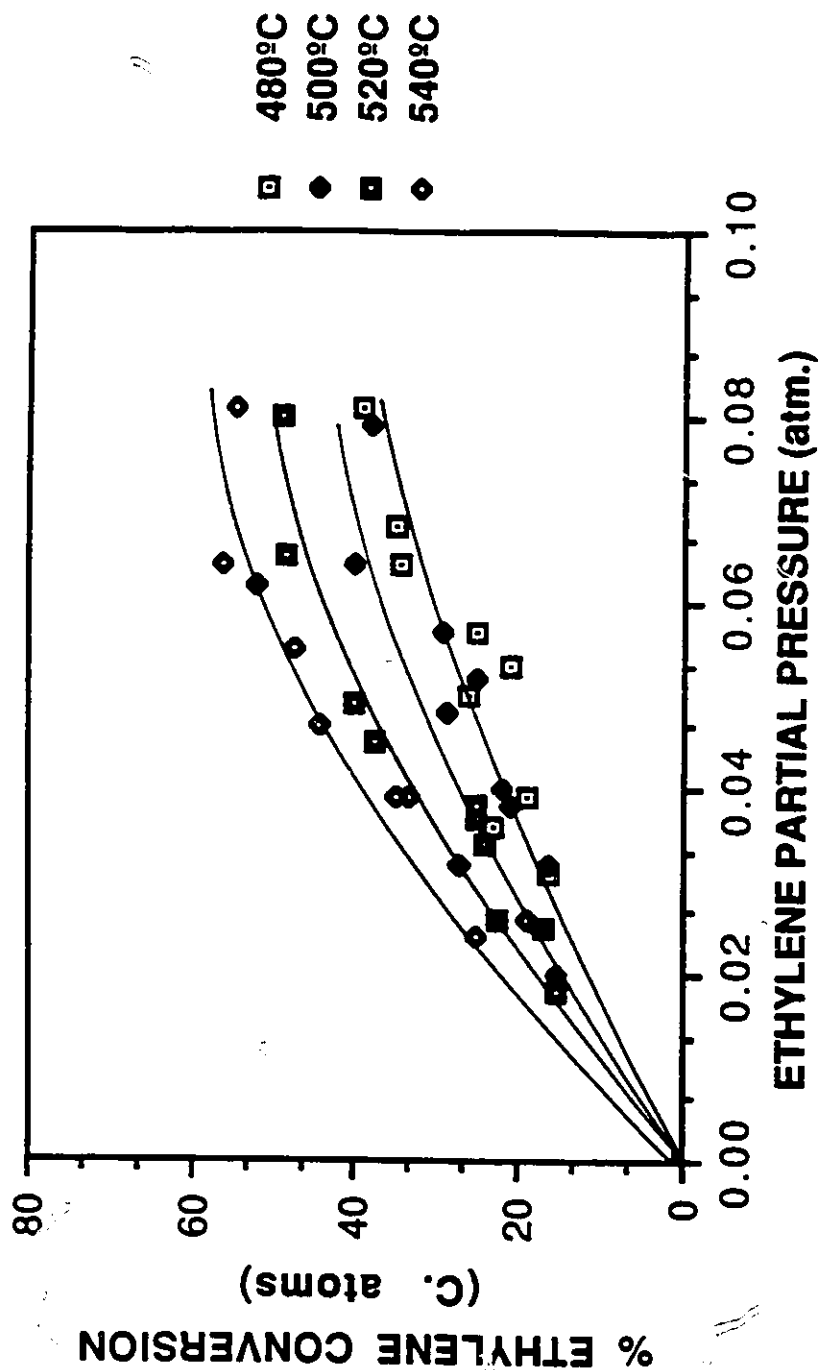


Figure 5.8 Variation of ethylene conversion as a function of feed partial pressure. Data obtained at different temperatures. Parameters: Feed: ethylene; Temperature R_c : 480-540°C; residence time: 10.2 sec. Catalyst Composition: 84.4wt.-% H-ZSM-5(43) + 5.6wt.-% ZnO/Al₂O₃ co-precipitate (Zn/Al-S=1.0) + 10wt.-% bentonite binder.

TABLE 5.3 Product selectivity for H-ZSM-5(43) zeolite catalyst.

T(K)	P _{C₂H₄} (atm.)	C ₂ H ₄ Conversion	Carbon Balance	% Carbon Atoms			Total
				C1	C3-C4 Paraffins	C3-C4 Olefins C5* Aliphatics	
753.5	0.0	0.0		0.0	0.0	0.0	0.0
	0.051	23.9	99	0.2	2.5	93.9	3.9
	0.063	35.8	95	0.3	6.3	89.6	4.0
	0.077	40.7	97	0.3	12.0	85.1	2.8
	0.086	48.8	88	0.2	10.2	79.6	10.1
	0.105	55.6	85	0.2	16.1	74.8	8.9
	0.125	64.1	81	0.2	15.2	77.6	6.9
	0.140	68.5	83	0.3	18.4	68.3	13.0
	0.161	70.6	94	0.4	20.5	65.0	14.2
	0.185	73.1	92	0.4	21.9	63.8	13.8
	0.252	76.0	88	0.4	24.8	56.1	18.7
773.5	0.0	0.0		0.0	0.0	0.0	0.0
	0.061	23.2	99	0.3	2.3	90.4	7.0
	0.074	34.1	99	0.2	3.1	91.0	5.8
	0.078	35.5	96	0.3	3.8	92.1	3.8
	0.103	49.1	89	0.4	10.9	84.4	4.3
	0.105	52.8	89	0.3	10.2	80.7	8.8
	0.125	52.8	84	0.4	13.4	78.3	7.9
	0.139	58.7	92	0.3	15.3	73.1	11.2
	0.161	62.0	90	0.5	19.1	70.8	9.6
	0.181	64.5	98	0.7	18.9	66.8	13.4
	0.249	69.5	91	0.7	21.8	59.1	18.5
793.5	0.0	0.0		0.0	0.0	0.0	0.0
	0.071	25.0	93	0.3	2.0	93.0	4.7
	0.088	35.8	88	0.5	2.6	90.1	6.9
	0.088	37.5	87	0.3	1.8	90.6	7.4
	0.106	44.0	83	0.3	2.2	92.7	4.8
	0.119	50.8	82	0.4	7.4	86.3	5.8
	0.128	44.8	94	0.5	9.5	84.1	6.0
	0.142	51.0	89	0.7	11.7	81.6	6.0
	0.161	55.8	92	0.8	13.2	75.9	10.1
	0.187	60.3	95	0.7	15.3	71.6	12.5
	0.241	62.4	94	1.0	16.2	68.4	14.4
813.5	0.0	0.0		0.0	0.0	0.0	0.0
	0.052	15.5	95	0.3	0.8	93.0	6.0
	0.069	20.9	94	0.5	1.1	90.0	8.5
	0.073	23.5	95	0.5	1.0	93.2	5.3
	0.098	27.4	99	0.6	2.1	85.4	12.0
	0.126	37.9	93	0.7	6.0	87.1	6.2
	0.144	45.1	89	0.9	9.8	81.1	8.2
	0.163	47.9	96	1.0	9.7	81.7	7.5
	0.188	50.0	97	1.1	12.2	73.9	13.0
	0.236	57.6	91	1.4	12.6	67.5	18.5
	0.242	55.2	96	1.5	13.8	69.0	15.7

C5* Aliphatics: Aliphatic molecules having C5- C10 C. atoms.

TABLE 5.4 Product selectivity for Hybrid/ ZnO catalyst.

T(K)	P _{C₂H₄} (atm.)	C ₂ H ₄ Conversion	Carbon Balance	% Carbon Atoms			Total Aromatics
				C1-C4 Paraffins	C3-C4 Olefins	C5+ Aliphatics	
753.5	0.0	0.0		0.0	0.0	0.0	0.0
	0.020	15.9	100	1.4	26.5	4.59	67.6
	0.028	16.8	100	0.9	29.5	5.0	64.7
	0.034	19.9	100	1.0	25.1	5.9	68.0
	0.043	19.7	100	0.6	31.2	3.8	64.5
	0.050	19.9	95	0.7	39.6	4.7	54.9
	0.058	24.4	95	1.3	40.0	4.1	54.3
	0.060	29.9	88	1.1	39.1	4.5	55.4
	0.064	33.4	87	1.1	36.0	4.3	58.6
	0.081	33.4	95	10.8(9.6)	34.0	4.6	50.6
	0.084	48.9	75	10.4(9.3)	26.7	5.0	57.9
773.5	0.0	0.0		0.0	0.0	0.0	0.0
	0.019	13.3	100	0.3	22.6	6.6	70.5
	0.020	17.3	100	1.3	22.5	7.0	69.2
	0.027	19.9	100	0.7	17.7	3.8	77.8
	0.034	19.0	100	0.9	26.2	5.0	69.9
	0.043	22.5	98	0.6	26.5	3.7	69.2
	0.057	31.5	95	11.7(11.2)	24.4	3.1	60.9
	0.060	34.2	91	12.9(12.2)	24.9	2.7	59.6
	0.064	40.4	86	12.6(12.6)	23.9	4.2	59.3
	0.080	35.5	95	15.3(14.4)	27.8	3.1	53.8
793.5	0.0	0.0		0.0	0.0	0.0	0.0
	0.018	17.0	100	0.4	17.0	9.6	73.0
	0.024	14.8	100	0.7	25.0	11.8	62.6
	0.035	23.3	100	1.5	17.9	8.2	72.3
	0.044	26.1	100	11.6(10.8)	21.6	2.9	64.6
	0.058	36.8	87	13.6(12.7)	24.5	1.1	60.8
	0.075	41.4	89	16.7(15.1)	16.8	2.2	64.4
	0.097	48.3	87	29.0(27.1)	14.8	1.5	54.7
813.5	0.0	0.0		0.0	0.0	0.0	0.0
	0.018	13.6	100	1.1	18.4	7.9	72.6
	0.023	17.9	100	0.9	17.0	5.2	76.9
	0.035	30.5	100	2.8	10.9	2.3	84.0
	0.044	39.3	100	23.4(21.6)	9.8	1.1	65.7
	0.054	50.3	78	24.5(22.7)	11.0	0.6	63.9
	0.059	56.4	83	31.3(29.6)	10.3	0.6	57.8
	0.061	63.7	92	31.7(29.1)	6.6	0.6	62.4
	0.063	56.5	91	37.6(36.1)	9.3	0.6	52.6
	0.072	58.1	88	35.8(34.4)	10.3	0.7	53.3
	0.095	61.5	89	42.3(41.0)	7.6	0.8	49.3

C5+ Aliphatics: Aliphatic molecules having C5- C10 C. atoms.

C1-C4 Paraffins: Values placed in parentheses represent the selectivity to ethane.

TABLE 5.5 Product selectivity for Hybrid/ ZnAl-S = 1.0 catalyst.

T(K)	$P_{C_{2H_4}}$ (atm.)	C_2H_4 Conversion	Carbon Balance	% Carbon Atoms			Total Aromatics
				C1-C4 Paraffins	C3-C4 Olefins	C5+ Aliphatics	
753.5	0.0	0.0		0.0	0.0	0.0	0.0
	0.016	13.6	100	1.0	27.7	8.0	63.2
	0.019	16.0	100	0.9	25.9	8.3	64.9
	0.025	17.0	100	0.7	26.2	3.4	69.8
	0.031	16.6	100	0.7	31.9	7.0	60.3
	0.036	23.1	93	0.5	34.1	4.1	61.3
	0.039	19.1	97	0.5	30.5	5.1	63.9
	0.050	26.2	89	0.6	34.2	4.6	60.6
	0.053	21.4	95	1.0	37.9	4.5	56.6
	0.057	25.1	91	10.4(9.6)	36.4	4.4	48.9
	0.064	34.4	85	8.6(7.9)	31.7	4.7	55.0
	0.068	35.2	85	10.5(9.6)	33.1	4.9	51.4
	0.084	39.3	81	5.3(4.2)	36.4	6.1	52.2
773.5	0.0	0.0		0.0	0.0	0.0	0.0
	0.020	15.3	100	1.3	26.3	5.7	66.7
	0.025	17.5	100	1.0	24.1	3.1	71.9
	0.032	16.5	100	0.8	18.2	9.1	62.0
	0.038	21.0	96	1.5	30.7	4.4	63.5
	0.040	22.0	95	0.9	27.0	4.2	67.9
	0.048	29.0	89	0.9	30.1	2.8	66.2
	0.052	25.5	94	14.9(14.0)	29.7	2.6	52.7
	0.057	29.3	93	14.2(13.4)	27.3	2.6	55.9
	0.064	40.2	83	13.3(12.5)	25.0	4.2	57.5
	0.079	38.1	83	13.5(12.5)	25.9	2.9	57.7
793.5	0.0	0.0		0.0	0.0	0.0	0.0
	0.013	16.0	100	2.4	16.7	13.4	67.6
	0.018	15.7	100	2.4	17.8	6.4	73.4
	0.026	22.7	100	1.5	16.4	2.4	79.8
	0.034	24.3	100	1.6	20.0	4.3	74.1
	0.037	25.1	99	1.6	19.4	7.6	71.4
	0.038	25.4	90	1.7	28.0	3.0	67.3
	0.045	37.4	82	7.4(6.2)	19.7	1.5	71.5
	0.049	40.1	85	7.4(6.3)	17.6	1.5	73.5
	0.059	36.8	87	11.0(9.6)	18.3	2.5	68.2
	0.065	48.3	84	14.7(13.3)	14.1	3.7	67.5
	0.080	48.9	87	17.7(16.4)	15.1	3.0	64.2
813.5	0.0	0.0		0.0	0.0	0.0	0.0
	0.014	23.2	100	3.0	9.4	6.8	80.9
	0.024	25.2	100	2.8	12.9	3.6	80.7
	0.026	19.1	100	2.8	17.0	2.0	78.2
	0.032	27.6	100	3.0	12.9	2.7	81.4
	0.039	33.5	91	3.3	16.0	2.1	78.6

Continued

TABLE 5.5 Product selectivity for Hybrid/ ZnAl-S = 1.0 catalyst.

T(K)	$P_{C_2H_4}$ (atm.)	C_2H_4 Conversion	Carbon Balance	% Carbon Atoms			Total Aromatics
				C1-C4 Paraffins	C3-C4 Olefins	C5+ Aliphatics	
	0.039	35.0	89	2.8	14.7	3.5	79.0
	0.047	44.4	95	19.8(18.2)	8.8	0.8	70.6
	0.053	37.9	100	29.4(27.3)	10.2	0.7	59.7
	0.055	47.7	92	30.2(28.4)	15.0	1.1	53.7
	0.062	52.3	87	29.5(27.8)	10.1	1.7	58.7
	0.064	56.4	87	26.0(24.7)	7.3	2.3	64.5
	0.081	54.7	83	25.1(23.6)	10.6	2.0	62.3

C5+ Aliphatics: Aliphatic molecules having C5- C10 C. atoms.

C1-C4 Paraffins: Values placed in parentheses represent the selectivity to ethane.

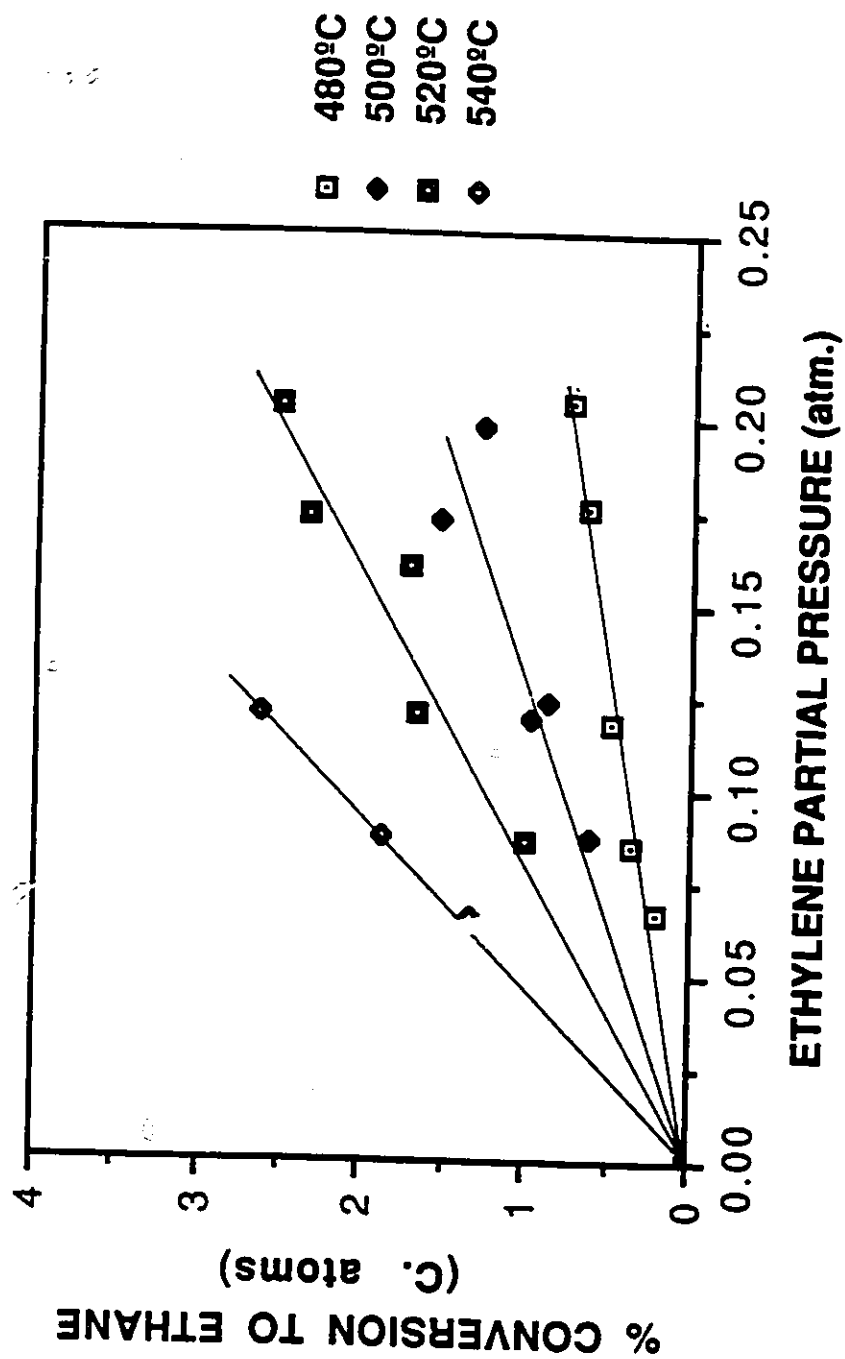


Figure 5.9 Variation of ethylene conversion as a function of feed partial pressure. Data obtained at different temperatures.
Parameters: Feed: ethylene; Temperature P_c : 480-540°C; residence time: 10.2 sec.
Catalyst Composition: 90wt.-% ZnO precipitate + 10wt.-% bentonite binder.

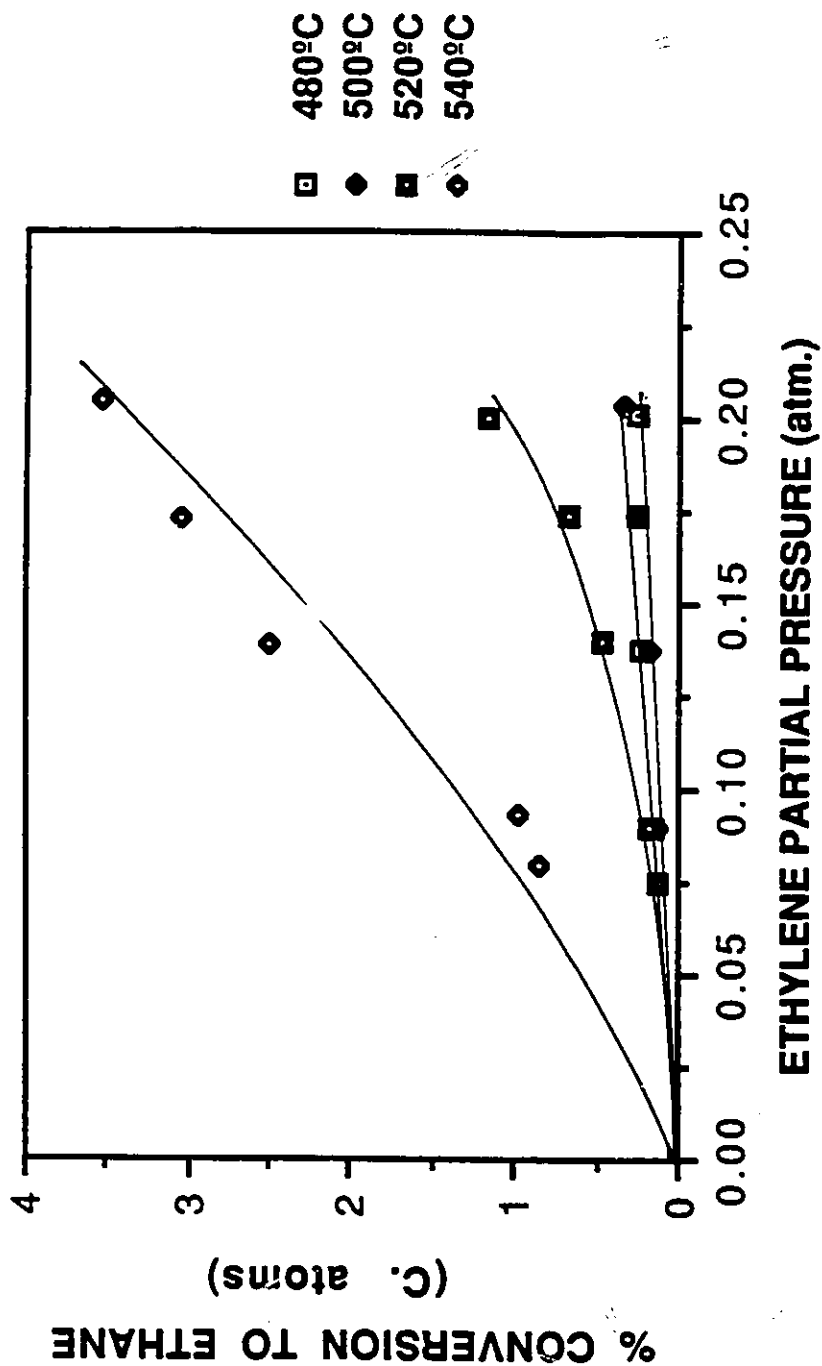


Figure 5.10 Variation of ethylene conversion as a function of feed partial pressure. Data obtained at different temperatures.

Parameters: Feed: ethylene; Temperature R_c : 480-540°C; residence time: 10.2 sec.

Catalyst Composition: 90wt.-% ZnO/Al₂O₃ co-precipitate (Zn/Al-S=1.0) + 10wt.-% bentonite binder.

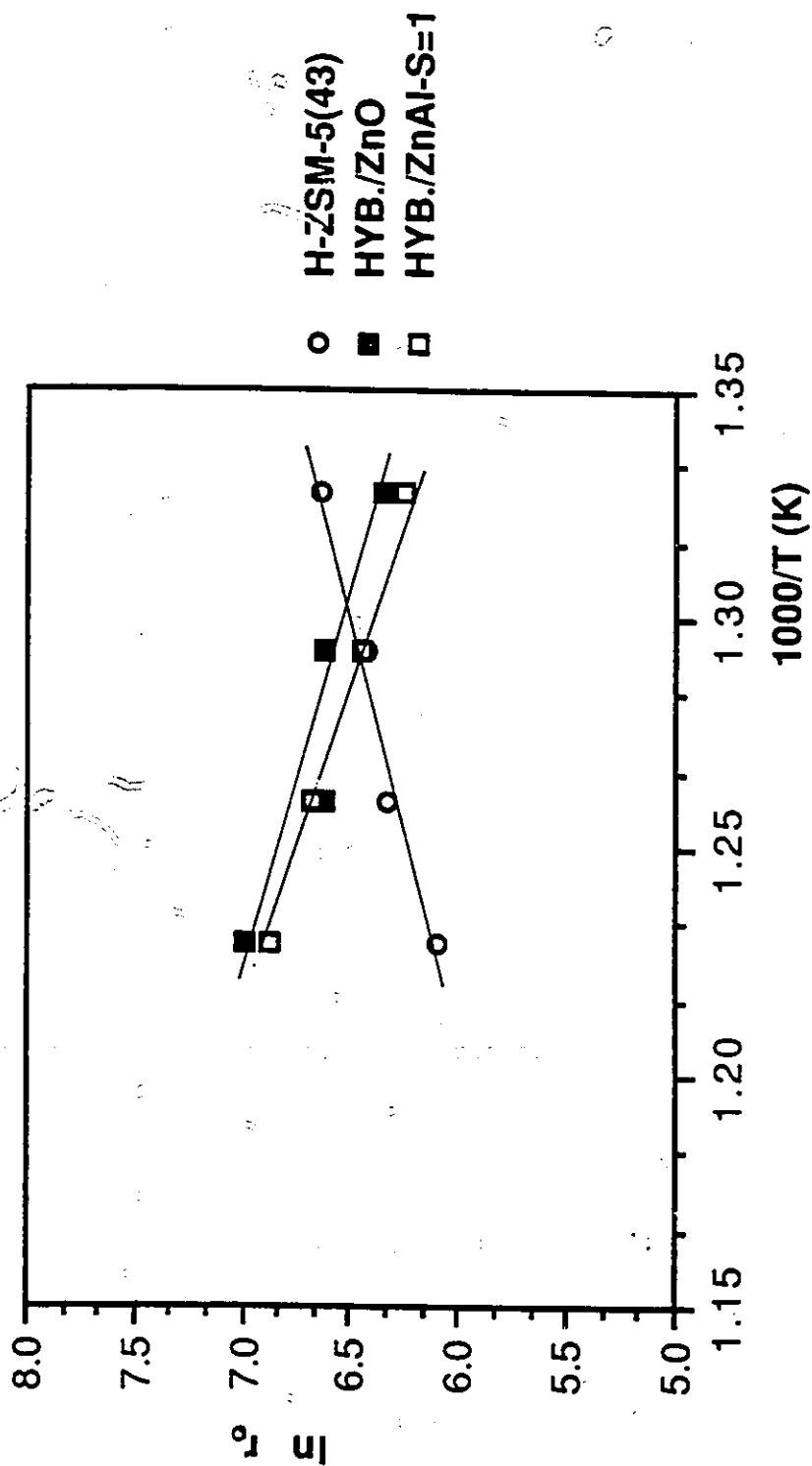


Figure 5.11 Arrhenius plot for pure H-ZSM-5(43) and hybrid catalysts. Rates obtained from total conversion of ethylene.

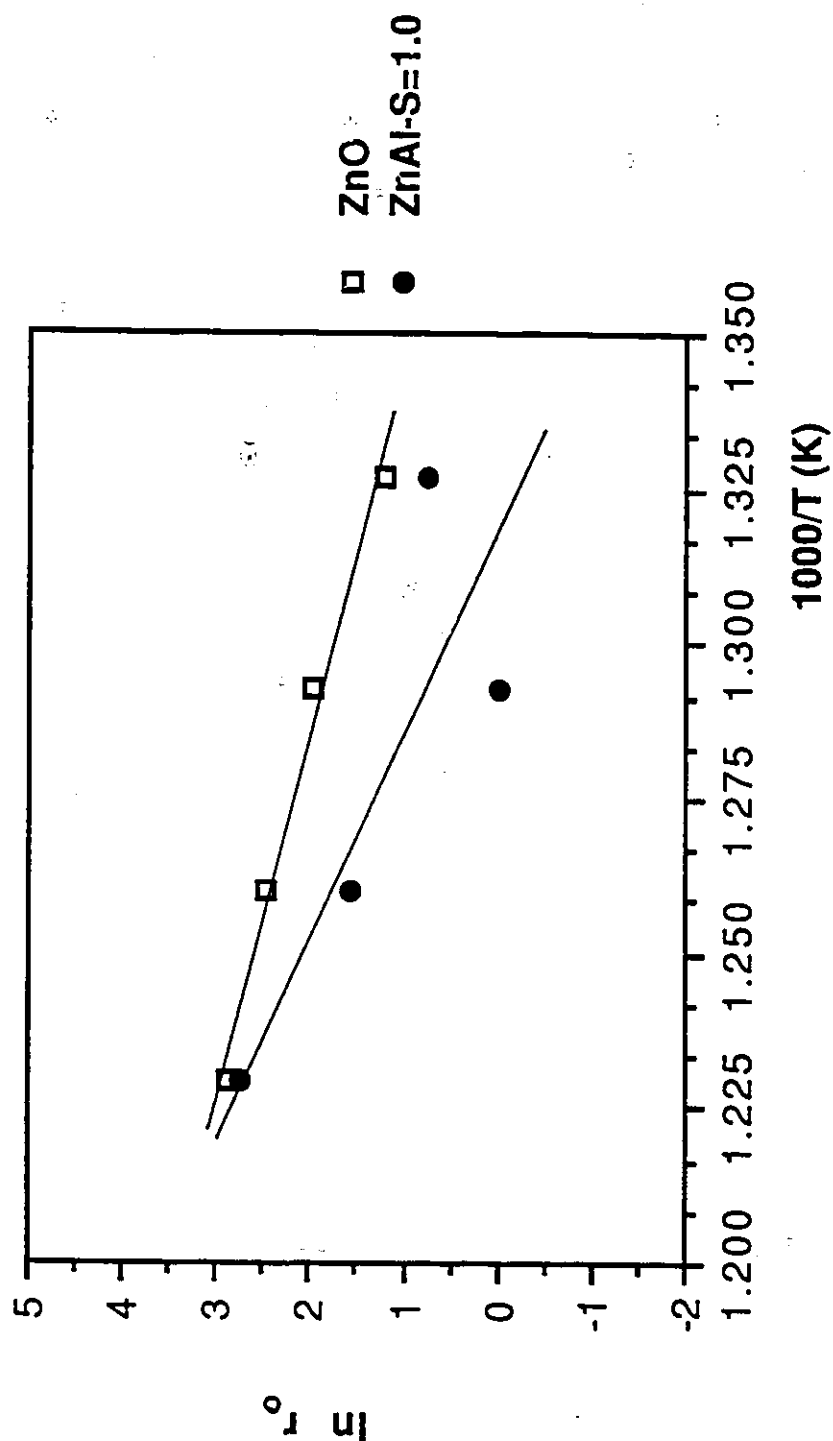


Figure 5.12 Arrhenius plot for pure ZnO precipitate and ZnO/alumina co-precipitate catalysts. Rates obtained from the selective conversion of ethylene to ethane.

TABLE 5.6 Values of apparent activation energies ($E_{a,app}$) and pre-exponential factors (A) as found by the Arrhenius plot method.

Catalyst Identification	Temperature Range (K)	Apparent Activation Energy ($E_{a,app}$)(kJ/mol)	Pre-exponential Factor (A)
Calculations Based on Total Ethylene Conversion			
H-ZSM-5(43)	773-813	-43.5	7.40E-01
Hybrid/ZnO	773-813	48.6	1.34E+06
Hybrid/ZnAl-S=1	773-813	54.2	2.95E+06
Calculations Based on Conversion of Ethylene to Ethane			
ZnO	773-813	140.5	1.99E+10
ZnAl-S=1.0	773-813	190.6	1.82E+13

(*) Oligomers: C3- C4 olefins and C5⁺ aliphatics.

($E_{a,app}$) and the pre-exponential factors (A) in the 773-813K temperature range.

Parent H-ZSM-5(43) exhibits a negative apparent activation energy that indicates reaction inhibition (171, 180, 250) and the pre-exponential factor is small. The magnitude of the pre-exponential factor indicates (249) that the entropy contribution may not be favorable to promote ethylene aromatization in a pure zeolite lattice. The activation energies of the hybrid catalysts are about 50kJ/mol and the pre-exponential factors are large and positive ($\approx \times 10^{+06}$). They indicate a more favorable reaction in free energy terms, promoted by the entropy contribution in bicomponent systems. Activation energies and pre-exponential factors for ethylene hydrogenation on ZnO and ZnO/alumina catalysts are also included, although they do not provide accurate quantitative information about the hydrogenation side reaction found with hybrids, because of the reasons enumerated above.

Similar kinetic studies of n-butane aromatization on pure H-ZSM-5 (Si/Al ratio:36, average particle size: 2-3 μ m), Ga ion-exchange H-ZSM-5 and Ga₂O₃-based hybrid catalysts have been done by Yao *et al.* (232-233). Apparent activation energies approximately equal to 100kJ/mol were determined for all systems. These values are comparable to those obtained by Mole *et al.* (120kJ/mol) (111) for propane aromatization on H-ZSM-5 and ZnZSM-5. Differences in the pre-exponential values were used to explain the aromatization tendencies.

In Fig. 5.6 it can be observed that on a pure H-ZSM-5, ethylene conversion decreases with increasing reaction temperature and a negative apparent activation energy is obtained (Fig. 5.11, Table 5.6). Similar behavior has been observed by Tanabe *et al.* (250) for toluene alkylation with ethanol. Palekar *et al.* (180) report other aromatic alkylation reactions that show a peak in conversion with increasing temperatures. The existence of intragranular diffusion limitations and the increasing amounts of coke formation have been used to explain the observed catalytic activity trends.

To study intragranular diffusion effects in pure zeolites, Doelle *et al.* (253) examined the influence of H-ZSM-5 crystallite sizes on ethylene conversion rates. For crystallite sizes of 0.5 μ m, 2 μ m and 14 μ m, C₂H₄ conversion rates were 5.5 $\times 10^{-7}$, 4.1 $\times 10^{-7}$ and 3.0 $\times 10^{-7}$ mol g⁻¹ sec⁻¹ respectively at 285°C. At 312°C, conversion rates varied

between 7.0×10^{-7} and 3.2×10^{-7} mol g⁻¹ sec⁻¹. It was concluded that crystallites smaller than 1 μ m should be used to eliminate intra- and intercrystalline mass transfer limitations (253). In another study of hexenes cracking on H-ZSM-5 at 538°C, Weisz *et al.* (254) showed mass transport inhibition in large crystallites at high reaction rates. For crystallites having radii of 0.025 μ m and 1.35 μ m respectively, 7530 and 6480 mol sec⁻¹ cm⁻³_{catalyst} were found. Choudhary *et al.* (181) observed a highly constrained molecular traffic of aromatic hydrocarbons in 2 μ m H-ZSM-5 crystallites.

Studies by pulsed field-gradient (PFG) NMR (182-183) have shown a decrease in intracrystalline mobility with increasing adsorbate concentration, due to molecular interference for large enough crystallite sizes ($\leq 30 \mu$ m). It was postulated that the intracrystalline mobility of the molecules was the limiting step in the overall kinetics (182). For small crystallites (2-5 μ m), the discrepancies observed between intracrystalline self-diffusion coefficients obtained by PFG NMR and sorption data, as well as a crystallite radius dependence for uptake measurements have suggested the existence of surface diffusional barriers (183-188). Combined NMR and HREM studies indicated that such surface barriers are caused by a layer of reduced permeability (similar to A \leftrightarrow B in Fig. 5.1) rather than by coke pore blocking on the surface (185). A two dimensional potential energy model for mass transport across an ideal zeolite crystal surface has been developed by Kočířik *et al.* (189-190). In this work, surface resistances were assumed to be analogous to an evaporation barrier. It was shown that especially for small crystals, surface transport resistances could exceed intracrystalline diffusion by several orders of magnitude (189-190). Surface barrier effects in adsorption on ZnO have been discussed by Morrison (194).

In the case of hydrocarbon conversions at high temperature on pure H-ZSM-5, intra- and intercrystalline diffusion limitations have been described if crystallite sizes exceed 1 μ m (253-255) and a surface barrier can also be present (2-5 μ m) (183-190). In contrast, for hybrid catalysts composed of 84.4wt.-% zeolitic component having an identical crystallite size distribution, since the ethylene conversion increases with reaction temperature (Fig. 5.7, 5.8), it is believed that the addition of a small quantity of co-catalyst particles significantly affects the intrinsic diffusion properties of the H-ZSM-5. Modification of surface potential energy barriers using inert solids or co-catalysts in hybrid systems has been demonstrated (191-192, 132-133) and discussed (114-115, 128-129,

232-233).

By examining the product distributions reported in Tables 5.3- 5.5, information can be obtained about the catalytic behaviors of each catalysts at different temperatures. Table 5.7 compares the catalytic selectivities of pure and hybrid catalysts at approximately the same ethylene conversion levels.

In the case of H-ZSM-5(43), it can be observed that C_3 - C_4 olefins and C_5^+ aliphatics make up most of the products exiting the zeolite channel network, and that the production of this fraction increases with temperature. C_3 - C_4 paraffins are formed by secondary oligomer cracking reactions (120-123) and their formation decreases as the temperature increases. A low H_2 /converted ethylene molar ratio reflects slow hydrogen transfer reactions in the zeolite lattice, as expected because of steric constraints (136). According to a kinetic model of light olefin aromatization on H-ZSM-5 zeolites developed by Luk'yanov and Shtral (257), the relative rates of hydrogen transfer reactions are independent of Si/Al ratios. The probability for hydrogen transfer reactions has been related to the intrinsic reactivity/stability of each olefin. For ethylene which forms a primary carbenium ion upon adsorption on a zeolite acid site, the hydrogen transfer rate constant was estimated to be equal to 1 in relative units, while those of C_3^+ and C_4^+ - C_{10}^+ molecules (secondary and tertiary carbenium ions) were 23 and 87 (257) respectively. Therefore, for ethylene aromatization on H-ZSM-5(43), a low $H_2/C_{2H_4 \text{ converted}}$ value equal to 0.10 is not unexpected.

Equilibrium analysis by computer modelization of the product distributions obtained in propene aromatization has been done by Phillips *et al.* (256). The rate determining step in aromatization was established to be cyclization. Coke formation within the channels was inferred due to experimentally higher yields of hydrogen and methane when compared with the values calculated at equilibrium. It was suggested that secondary cracking reactions (forming C_3 - C_4 paraffins) are slow relative to aromatization and alkylation reactions in a pure ZSM-5 lattice.

In the case of hybrid systems, total aromatics account for most of the reaction products (Tables 5.4-5.5, 5.7). The portion of aromatics formed increases with temperature but is limited by the ethane formation on the co-catalyst surface. C_3 - C_4

TABLE 5.7 Product selectivities for pure and hybrid catalysts at 500°C and similar conversion levels.

	H-ZSM-5(43)	Hybrid/ZnO	Hybrid/ZnAl
P_{C_{2H₄}}	0.061	0.043	0.040
Ethylene Conversion	23.2	22.5	22.0
Product Selectivity (% C. atoms)			
Methane	0.29	0.64	0.91
Ethane	0	0	0
Propane	0	0	0
Butanes	2.28	0	0
Propylene	60.55	17.48	16.79
Butenes	19.65	9.00	10.22
C₅* Aliphatics	10.20	3.70	4.18
Total Aromatics	7.02	69.18	67.90
H₂/Ethylene Converted (mol/mol)	0.10	0.55	1.13

C₅* Aliphatics: Aliphatic hydrocarbons having C5- C10 C.atoms.

olefins and C_5^+ aliphatics products decrease with increasing reaction temperatures. H_2 /converted ethylene molar ratios are higher than for the pure zeolite analog, indicating that hybrid catalysts favor hydrogen out-migration. Increased rates of hydrogen removal reflect more efficient hydrogen transfer reactions within the zeolite lattice when hybrid configurations are used.

The higher production of aromatics observed on bifunctional catalysts, is due to the increased dehydrogenation rate of intermediate reaction oligomers by zinc or gallium contained in the ZSM-5 (88, 110-111, 113, 225, 258-266). Mole *et al.* (111) suggest that over ZnZSM-5, the higher rate of hydrogen diffusion in the zeolite channels can result in a depletion of the local hydrogen concentration and can move the equilibrium in the direction of BTX formation. In the model developed for propane aromatization (111), dehydrogenation is said to be kinetically controlled in the ZSM-5 and its rate increases with temperature. This phenomenon is also observed in Table 5.3 by the increase of C_3 - C_4 olefins and C_5^+ aliphatics fractions with temperature. In contrast, for ZnZSM-5 it is claimed that the dehydrogenation step is in quasi-equilibrium and increases with temperature, thus moving the equilibrium toward increased BTX production. Scurrrell (267) proposes that on the ZSM-5 surface, C_6 -cycle hydride abstraction by a carbenium ion to yield the corresponding alkane is preferred, while on ZnZSM-5 hydride abstraction occurs on a Lewis center ($Zn-O$) to form H_2 . These phenomena are also observed in Tables 5.4 and 5.5 for ZnO and ZnO/ Al_2O_3 co-precipitate hybrid catalysts.

Out-migration of hydrogen concentrations is intimately related to the aromatization performance of a ZSM-5 catalyst. Co-feeding of oxygen (air) provides the zeolite with sink molecules that can remove the adsorbed hydrogen species produced during the dehydrocyclization step of aromatization. H_2O is formed and increased aromatic formation is observed (126, 130, 167-170). In hybrid catalysts, the ZnO-based co-catalyst which is at a certain distance from the zeolite crystallites, provides a porthole for the hydrogen produced in the zeolite lattice and is not directly involved in intermediate oligomer dehydrogenation reactions. By inducing hydrogen removal (72-73, 111, 114-115, 126-133, 138, 232-233), the equilibrium position of the rate determining step (cyclization (256)) may also be moved to the right. The increased rates of oligomeric intermediates conversion to alicyclic molecules and fast hydride abstraction reactions (111, 123), which are favored by high rates of hydrogen diffusion in the ZSM-5 zeolite channels, appear to

explain the enhanced aromatic selectivity observed in hybrid catalysts.

H₂/converted ethylene ratio values of 0.55 and 1.13 for the ZnO and the ZnO/alumina hybrids respectively, indicate that the nature of the co-precipitate surface helps molecular hydrogen desorption (Fig. 5.13 A). The presence of an alumina phase which can accept a secondary migration (spillover) of H_{ads} from the ZnO active sites, provides an alternate pathway for hydrogen desorption (144-147). On the ZnO precipitate hybrid H_{sp} desorption is associated with ethane formation (Fig. 5.13 B).

The reaction rate equation of the pure zeolite can be written as:

$$V_{zeolite} = k_{zeolite} P_{ethylene}^{n_1} \quad (5-10)$$

If we consider that the aromatization ability of the zeolite lattice is very similar in the case of pure or hybrid catalysts, the rate equation for the hybrid can be approximated to be:

$$V_{hybrid} = V_{zeolite} + k_{co-catalyst} P_{ethylene}^{n_2} \times P_{hydrogen}^{m_2} \quad (5-11)$$

where the second term represents the sink/scavenging action of the co-catalyst.

If n_2 and m_2 (the orders of reaction) are taken to be equal to 0 and 1 respectively (as for hydrogenation of ethylene on a transition metal (11)), then:

$$V_{hybrid} = V_{zeolite} + k_{co-catalyst} P_{hydrogen} \quad (5-12)$$

and:

$$V_{hybrid} > V_{zeolite} \quad (5-13)$$

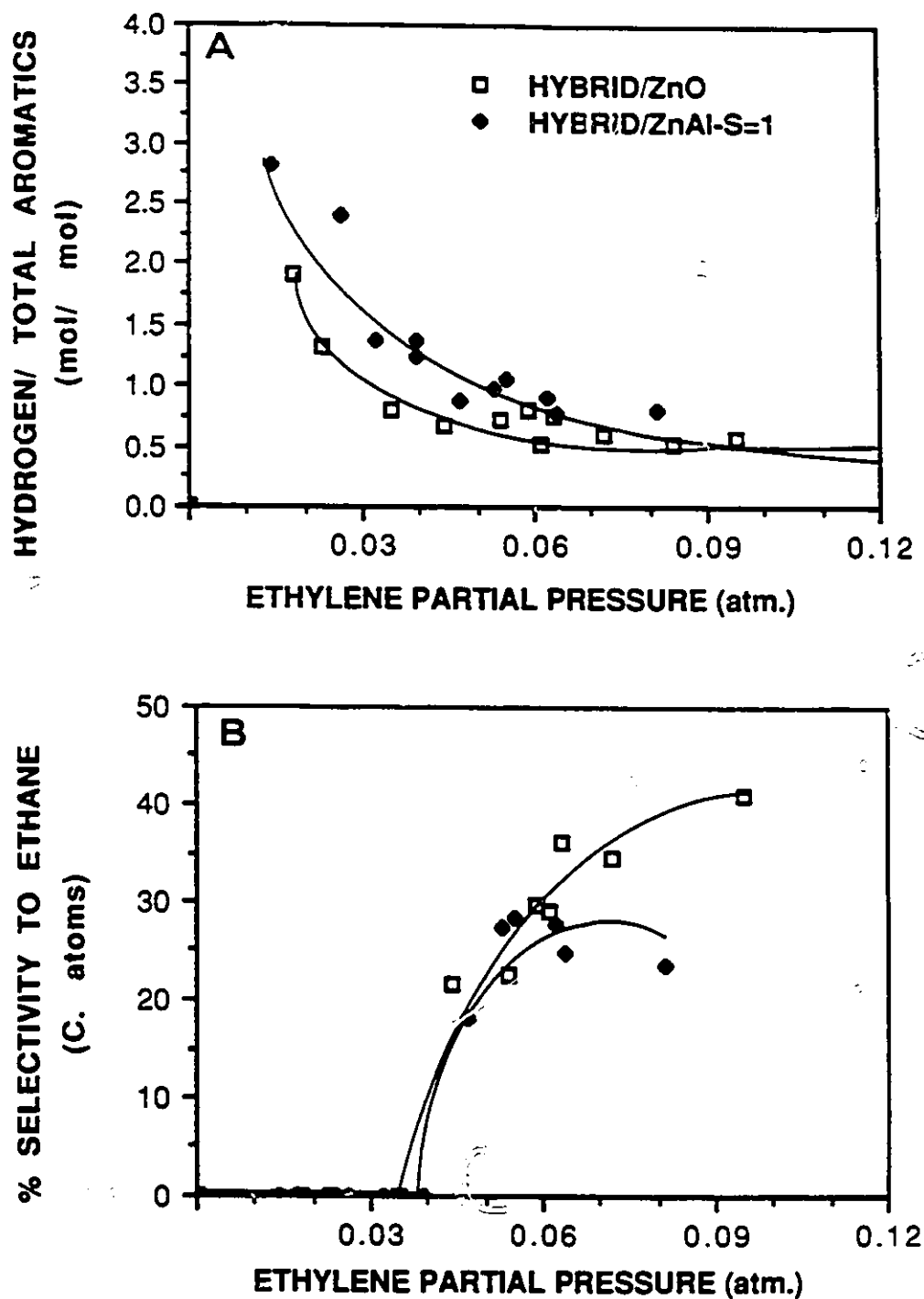


Figure 5.13 Graphs of selectivity as a function of ethylene partial pressure for hybrid catalysts. (A) ratio of molar hydrogen production to total aromatic selectivity; (B) selectivity to ethane.

Parameters: Feed: ethylene; Temperature R_c : 500°C; residence time: 10.2sec.

Catalyst composition: 84.4wt.-% H-ZSM-5(43) + 5.6wt.-% co-catalyst + 10wt.-% bentonite binder.

Since the overall reaction rates of the hybrids are faster than that of the pure zeolite, feed conversions and aromatic selectivities are increased.

Hydrocarbon chemisorption processes and reaction mechanisms of pure ZSM-5 zeolites have been studied extensively. The adsorption of ethylene in the zeolite lattice has been examined by IR spectroscopy. Hydrogen bond formation between the C_2H_4 π -electrons and acidic zeolite hydroxyl groups has been inferred from the disappearance of the 3610cm^{-1} band (268-271) upon hydrocarbon chemisorption. Hydrogen bond strengths have been examined using IR band shifts for the different olefinic molecules (272-273). Due to its lower basicity, hydrogen bond strength between C_2H_4 and acidic OH-groups was found to be weaker than for propylene or pyridine. Hall *et al.* (273) state that a stronger hydrogen bonding ability is generally associated with lower carbenium ion formation activation energies. The ease of carbenium ion formation and the subsequent reactivity of the adsorbed hydrocarbon species, also can be related to stability: $1^\circ C^+ \ll 2^\circ C^+ < 3^\circ C^+$ (123, 252, 257, 274-275). In another approach where *ab initio* quantum chemical calculations were used to model an ethylene interaction with zeolite OH-groups, it was suggested that hydrogen bond formation rearranges in surface alkoxy groups (276-277) rather than carbenium ion, due to the low stability of $1^\circ C^+$. A mechanism for the formation of surface ethoxy groups from ethylene, involving the participation of a 6-membered ring transition state intermediate, was discussed (277).

At room temperature, ethylene oligomerization by a cationic-like polymerization mechanism is observed (239, 274, 278-279). High resolution solid state ^{13}C NMR studies by van Hooff and co-workers (274, 278) have revealed the presence of linear C_{23} - C_{27} oligomeric products from an ethylene feed. Using TGA analysis (268, 275), 70% of the zeolite void volume was shown to be filled by the oligomers formed at room temperature. In the RT-222°C temperature range, light olefin oligomerization rates showed sharp increases which resulted in hindered transport of reactant molecules through the pores due to pore mouth blocking. According to Čejka *et al.* (280), coke blocking in low temperature ethylene oligomerization can be the most important side reaction. At 222°C, linear and branched C_4 - C_6 products were identified by ^{13}C NMR, indicating a cracking activity that also promoted pore mouth opening (229, 239, 278). At 300°C and above, the H-ZSM-5 was said to become a dynamically operational catalytic system in the conversion of small olefins, since on the surface the olefins were immediately

hydrogenated and reoligomerized (278).

At 538°C (80-82, 225, 252, 256) in H-ZSM-5(35), the reactions involved in the conversion of light hydrocarbons to BTX were described as:

- (1) the conversion of olefins and paraffins to small olefins via acid cracking and hydrogen transfer;
- (2) the formation of C_2 - C_{10} olefins via oligomerization, cracking and isomerization;
- (3) aromatic formation via cyclization and hydrogen redistribution.

The significant product selectivity differences between pure and hybrid systems, as well as the inverse catalytic activity trends with temperature, can be taken to indicate a profound modification in the acid component's aromatization ability after the addition of a co-catalyst. Altered internal coking tendencies may contribute to the enhanced activity of hybrid systems, since strong dehydrogenation propensity is often associated with the formation of coke precursors (225-231).

Adsorption and diffusion play important roles in determining the overall reaction rates and product selectivities observed on a catalyst (281-282). Competitive reactions in intrazeolitic media, where strongly adsorbed secondary species may cause diffusional barriers to the transport of reactants or product molecules is discussed by John *et al.* (281). The build up of high molecular weight secondary products that cause severe pore mouth/ fluid phase desorption barriers have been shown to have a strong kinetic influence in benzene alkylation (122). The presence of intrazeolitic diffusional barriers sometimes leads to negative apparent activation energies on pure H-ZSM-5 (180, 250).

On all zeolites (283), coke formation begins with oligomerization, which is followed by cyclization, monoaromatic formation through hydrogen transfer, alkylation and then second cyclization and hydrogen transfer to yield bi-aromatics, tri-aromatics, etc. Due to the transition state shape selectivity, coking tendencies are intrinsic to each zeolite pore structure and in H-ZSM-5, because of lower acid site density and steric constraints in the reaction loci (channel intersection), lower coking tendency is usually observed. In spite of this, ZSM-5 zeolite as well as other acid catalysts eventually deactivate due to the accumulation of coke deposits in the pores and on the external surface (225, 239).

Coking in ZSM-5 is a combination of acid site poisoning and pore blocking. Coke formed on the exterior of the lattice has a polynuclear aromatic (pre-graphitic, coronene like) structure and is insoluble (282-284). Deactivation species or soluble coke formed inside the ZSM-5 lattice, result from small olefin polymerization reactions (282-284). Deactivation by soluble coke occurs in three ways (283):

- (1) limitation of the access of reactant molecules to active sites;
- (2) blockage of the access to the reaction loci by coke molecules;
- (3) blockage of the access to the pores in which there are no coke molecules (out diffusion).

In studies of ethylene coking reactions on a pure ZSM-5, aliphatic and alkylbenzenic coke precursors were identified by CP MAS ^{13}C NMR (283). For C_2H_2 conversions, the observed loss in catalytic activity was said to arise from the rapid polymerization of reactants to polycyclic aromatics, which are precursors to coke formation (241). In contrast, it was shown that when a H-ZSM-5 was embedded in a $\text{SiO}_2/\text{Al}_2\text{O}_3$ matrix (SA), ethylene oligomerization was promoted (239-240) and a temperature decrease for coke decomposition was observed using TPO experiments. More specifically, for a 5wt.-% H-ZSM-5 in a SA matrix, coke oxidation was seen by a sharp peak at about 400°C , while for the ZSM-5 analog a broad peak centered at 520°C characterized the TPO profile. The authors concluded that a broad peak shape reflected the broad nature of coke species and suggested the presence of a highly aromatic coke and/or coke deposits predominantly concentrated inside the zeolite pores. The ease of coke oxidation in the hybrid was taken as an indication of coke formation mainly outside the zeolite and characteristic of synergy (239-240). Fujimoto *et al.* (285) in studies of syn gas conversion to $\text{C}_3\text{-C}_4$ hydrocarbons on hybrid $\text{Pd}/\text{SiO}_2/\text{H-ZSM-5}$ catalysts, attributed the enhanced selectivity to the quick diffusion of methanol and olefins intermediates, in and out of the zeolite channels. When Sn was added to a Pt/alumina catalyst, it was shown that coke precursors migrations (olefins and aromatics) to the support surface were promoted (138).

Table 5.8 reports the aromatic phase detailed product distributions for pure and hybrid catalysts recorded at the same ethylene partial pressures and for identical times on stream. Comparing the results obtained for H-ZSM-5(43) at 480°C and 540°C , it can

TABLE 5.8 Product distribution of the aromatic phase for reactions executed under identical conditions and TGA results obtained with used catalysts. ($P_{C_2H_4}$: 0.08 atm., Time of reaction: 180 min.)

Temperature (°C)	% Carbon Atoms			
	H-ZSM-5(43)		HYBRID/ZnO	HYBRID/ZnAl-S = 1.0
	480	540	540	540
Ethylene Conversion	54.6	38.7	58.4	54.7
Carbon Balance	84	84	83	83
Total Aromatics	10.6	26.9	59.5	62.3
BTX/Aromatics	0.89	0.88	0.88	0.85
H ₂ Production (mmole)	2.3	2.5	8.2	11.3
Benzene	36.2	31.1	52.2	53.1
Toluene	55.4	46.3	32.1	30.0
Ethylbenzene	1.1	4.3	1.4	1.4
Xylenes	5.5	14.8	6.5	6.6
Styrene	0.7	2.9	1.0	1.0
C9 ⁺ Aromatics	1.1	3.2	6.7	8.0
Distribution of C9 ⁺ Aromatics				
C9 Aromatics	36.4	68.3	40.2	41.3
C10 Aromatics	22.9	20.9	13.2	13.3
Naphthalene	15.2	4.9	17.1	17.6
Naphthalene,2-methyl	20.1	5.2	21.2	21.1
Naphthalene,1-methyl	2.3	0.4	1.6	2.6
C11 ⁺ Aromatics	3.0	0.4	6.7	4.1
TGA results of used catalysts				
Weight Sample (mg)	16.4	18.0	18.2	18.1
% wt. Total Loss	3.9	7.2	3.9	3.6
% wt. Loss > 450°C	0.7	0.7	1.3	1.1

be observed that the ethylene conversion is higher at 480°C, the total aromatic yield is more important at higher temperature and the hydrogen production is almost equal. These results indicate that in a pure H-ZSM-5, dehydrogenation is indeed kinetically controlled and increases with temperature, as modelled by Mole *et al.* (111). The similar hydrogen yields indicate that at 540°C hydrogen out-migration is inhibited.

Comparing the aromatic selectivities for pure and hybrid catalysts at 540°C (Table 5.8), it can further be observed that:

- (1) the conversions, aromatic selectivities and hydrogen productions are enhanced in hybrid systems;
- (2) the higher production of benzene in the BTX fraction of hybrid systems indicates a higher dealkylation activity, as noticed by Mole *et al.* (111) and Kanai *et al.* (113) for ZnO containing catalysts;
- (3) the C_9^+ aromatic fractions in hybrid systems are much more important than for the parent zeolite;
- (4) bulky naphthalene and alkylated naphthalene molecules (2- and 1-methyl, C_{11}^+ aromatics) of the C_9^+ aromatics fraction are desorbed more readily in hybrid systems.

Fig. 5.14 shows the thermograms obtained for the used catalysts of Table 5.8, using the TGA technique and an oxygen atmosphere. Prior to oxidation, the color of the crushed H-ZSM-5 was grey while that of the hybrid powders was completely black. Especially in the 50-250°C temperature range, it can be observed that the TGA curves of hybrids differ from that of the pure zeolite analog. In that range, the H-ZSM-5 loses about 5wt.-% in adsorbed species compared to 1-2wt.-% for the hybrids. In Table 5.8, it is observed that the total weight losses for the hybrids are about 3.8wt.-%, while the pure zeolite is characterized by a 7.2wt.-% loss. Weight losses above 450°C are comparable.

The initially different colors of the spent catalysts, coupled with a high weight loss at low temperature for the H-ZSM-5 suggest that:

- (1) catalyst deactivation occurs from the formation of soluble coke inside the zeolite channels in the pure catalyst;

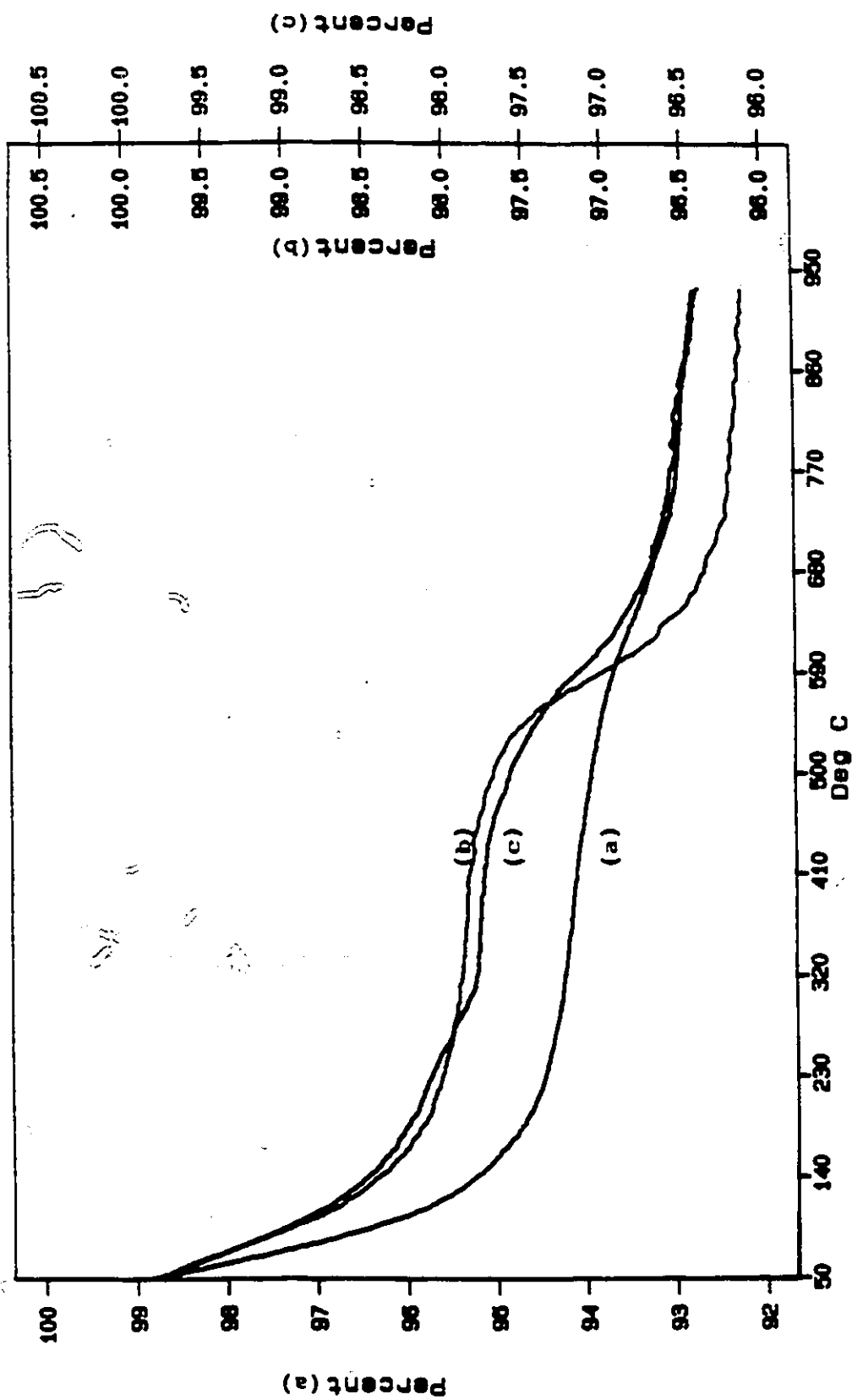


Figure 5.14 Thermograms obtained for used catalysts.
 Parameters: Temperature: 540°C; P_{cat} : 0.08atm.; residence time: 10.2sec.; reaction time: 180min.

Catalyst Identification:
 (a) H-ZSM-5(43)
 (b) Hybrid Zn/Al-S = 1.0 co-precipitate
 (c) Hybrid ZnO precipitate

(2) the presence of the co-catalyst favors the out-migration of bulky species as well as hydrogen.

Bulky species in the zeolite reaction loci can result in deactivation (225, 281-284) or the creation of intra-diffusional limitations (122, 180-183, 250). In an attempt to elucidate the nature of intrazeolitic adsorbed species, diethyl ether was used as the extraction solvent. The distribution of soluble coke precursors with respective boiling points appear in Table 5.9. 49% of the molecules identified belong to the C_9^+ aromatic fraction and their boiling points do not exceed 250°C. It is estimated that the high weight loss recorded for the used H-ZSM-5 below 250°C in Fig. 5.14, is due to the desorption of these bulky naphthalene like species from the internal zeolite pores. These species, which are increasingly formed during ethylene aromatization at 540°C due to thermodynamic considerations, are responsible for the creation of transport barriers within the zeolite channels and result in decreased conversions at higher temperatures and a negative apparent activation energy. High entropy conditions due to the inherent encumbrance of the zeolite channels at higher temperatures, leads to unfavorable pre-exponential factors and ultimately lower performance of the ZSM-5.

Modification of surface energy barriers on the zeolite crystallites, induced by the presence of co-precipitate particles has been suggested. Higher hydrogen out-diffusion in the ZSM-5 channels, as well as an increased formation of H_2 (ethane) have been shown to be promoted by ZnO or ZnO/ Al_2O_3 surface porosities located at the zeolite pore openings. It has been observed that hybrid catalyst configurations also favor the out-migration of C_9^+ aromatics coke precursors, trapped inside the zeolite lattice when the zeolite is used alone at high temperature. The darker color of the hybrid catalysts as well as information contained in the TGA profiles, are similar to the observations of Lund *et al.* (239-240). Synergy for aromatic formation is expressed through hydrogen removal and coke precursors out-migration in hybrids.

TABLE 5.9 Product distribution obtained from used H-ZSM-5(43) zeolite catalyst treated with diethyl ether (Temperature: 540°C, $P_{C_{2H_6}}$: 0.08atm).

	% Peak Area	Boiling Point (°C)
Benzene	5.0	81.1
Toluene	18.6	110.6
C8 Aliphatics	1.4	-
Ethylbenzene	5.0	136.2
p-Xylene	7.1	138.3
m-Xylene	7.5	139.1
o-Xylene	4.3	144.4
Styrene	1.7	145.2
C9 Aromatics	14.4	-
Benzene 1,2-propanedienyl	15.5	-
C10 Aromatics	4.8	-
Naphthalene	13.0	218.9
Naphthalene 1-methyl	1.7	244.6

5.5 Conclusions

Kinetic investigations of pure and hybrid catalysts have clarified the modes of action of the co-catalyst components. From studies of ethylene conversions as a function of time equivalent factors (ethylene partial pressures), initial reaction rates were evaluated for each catalyst in the 480-540°C temperature range. Apparent activation energies were calculated with associated pre-exponential factors.

H-ZSM-5(43) exhibits a negative activation energy and a low pre-exponential factor. The negative $E_{a,app}$ was explained by the presence of transport barriers within the zeolite channels, that result from trapped soluble coke precursors. The coke precursors were identified as C_9^+ aromatic molecules.

Hybrid catalysts were characterized by apparent activation energies equal to about 50kJ/mol, with large and positive pre-exponential factors. The enhanced aromatization selectivity of these catalysts was related to a favorable entropic activation energy, an increased diffusion rate of hydrogen adsorbed species in the zeolite channels and an easier out-migration of coke precursors. The cyclization step, the rate determining step in a pure H-ZSM-5, was found to be increased by the higher hydrogen transfer activity.

Studies of pure ZnO or ZnO/alumina catalysts did not give reliable information on the hydrogenation activity of these components in hybrid configurations.

The greater hydrogen desorption capability of ZnO/Al₂O₃ was related to the presence of an alumina phase able to accept migratory H_{ads} species from ZnO active sites. Reduction of co-adsorbed ethylene on ZnO to form ethane, was the preferred hydrogen desorption mode on this co-catalyst.

6.0 Conclusions

The conversion of light olefins and paraffins (C_2 - C_4) into BTX aromatic hydrocarbons, has attracted much industrial and academic interest because it provides a way to up-grade low value feedstock to commercially valuable products.

The objectives of this work have been the conception, the synthesis, the optimization and the evaluation of a new class of bifunctional catalysts. These catalysts have been shown to possess properties that promote the aromatization of light olefins and paraffins.

It has been discovered that bifunctional catalysts where the second component is separated from H-ZSM-5 crystallites by $1\mu\text{m}$ or more, can induce a synergistic formation of BTX aromatics. The effects of ZnO or ZnO/ Al_2O_3 co-precipitate particle addition to those of zeolite crystallites have been studied in hybrid configurations and the results were compared with the catalytic activity of pure H-ZSM-5 analogs. At least a 2-fold increase in BTX yields were obtained using feed mixtures generated in a propane steam-cracker or pure propane/ n-butane feeds. The optimal Zn/Al compositions of the co-precipitates were established to be equal to or greater than 1.0. The optimal catalyst formulations were experimentally evaluated at 5wt.-% of ZnO precipitate or 5-20wt.-% of ZnO/alumina co-precipitate.

Especially for ZnO hybrids, it was observed that the ethane yields and the aromatic formations were parallel. Ethane production was related to the reduction of co-adsorbed ethylene by the zinc oxide surface using hydrogen produced during the dehydrocyclization step of the reaction.

Due to the large distances between the acid and the ZnO-based components, migration across surface boundaries by adsorbed hydrogen species was described by a hydrogen back-spillover model. Co-catalyst particles were seen as portholes for hydrogen interception and subsequent desorption. The increased formation of hydrogen in the effluent was described by sink/scavenging actions of the co-catalyst.

The importance of hydrogen removal from the zeolite lattice was thoroughly examined, while H_2 productions were monitored during the catalytic reactions. Oxygen and hydrogen co-feeding studies confirmed the involvement of HBS in aromatization

synergy on hybrid systems. A decrease in potential energy barriers was postulated to explain the driving force behind hydrogen removal from the zeolite lattice.

Correlation of the physico-chemical characterization data and the catalytic tests helped to define the important properties of the co-catalyst. Textural or acidity properties were shown to be less important than the chemical composition or the presence of a disordered/ XRD amorphous structure capable of undergoing facile restructuring. Hydrogen chemisorption experiments indicated that ZnO sites are the primary acceptors of H_{sp} exiting the zeolite lattice. The increased sink action observed on the co-precipitate was related to the ability of alumina to accept H_{ads} in a second spillover.

Kinetic studies, based on ethylene aromatization, compared the catalytic behaviors of pure and hybrid systems. A negative apparent activation energy and a low pre-exponential factor for the H-ZSM-5(43), indicated an unfavorable reaction in entropic terms. The presence of intracrystalline diffusion limitations or an increase in the amount of coke formation within the channels at higher temperatures was proposed. For hybrid catalysts, the apparent activation energies were estimated to be close to 50kJ/mol, with large and positive pre-exponential factors. The addition of a small quantity of co-catalyst particles, at a distance and heterogeneously distributed among the zeolite crystallites, dramatically changed the aromatization capability of the acid zeolitic component.

By comparing the product distributions and H_2 productions obtained at different temperatures, it was suggested that the rate determining step for the reaction in H-ZSM-5 (cyclization) was moved to the right in hybrid catalysts. The faster out-diffusion of hydrogen species was related to enhanced BTX production. Examination of the detailed aromatic product distributions for pure and hybrid catalysts tested under identical experimental conditions, showed the presence of a greater C_9^+ aromatics fraction in hybrid systems. The high weight loss observed in TGA analysis for the used H-ZSM-5 indicated the presence of soluble coke in the pores. Extraction with diethyl ether revealed that 49% of the adsorbed products consisted of C_9^+ aromatics coke precursors. The presence of transport barriers within the zeolite channels as well as surface desorption barriers, were used to explain the lower activity of H-ZSM-5 at 540°C. For hybrid catalysts, migration of coke precursors to the zeolite surface was associated to the presence of co-catalyst particles.

Hybrid catalysts where each component can individually be physically or chemically modified to tailor catalytic activity and selectivity, constitute a new class of bifunctional catalysts. The advantages include formulation flexibility and slower deactivation rates.

Future studies should concentrate on the nature of spilt over hydrogen species. The roles played by intra- and intergranular diffusion in H-ZSM-5 and their specific mechanisms in orienting the product selectivity should be investigated. The effects on diffusion by the addition of co-catalyst particles should be quantified. The nature of soluble coke precursors, as well as the reasons underlying a negative activation energy for H-ZSM-5 should attract a special attention.

7.0 References

1. T. Tietenberg; *Environmental and Natural Resource Economics*, Scott, Foresman and Co. Publishers, IL USA Chapter 7 (1984).
2. J.-M. Carpentier; *L'énergie en Héritage: le Pétrole et le Gaz*, Editions du Méridien, Qc Chapter 1 (1989).
3. I. Moukhlenov; *Principes de la Technologie Chimique*, Editions Mir Moscou, Russia Chapter 1 (1986).
4. J. Biswas and I.E. Maxwell; *Appl. Catal.* **63**:197 (1990).
5. L.L. Hegedus; *Catalyst Design: Progress and Perspective*, L.L. Hegedus editor, Wiley-Interscience Publication, JW&S Inc., NY USA Chapter 1 (1987).
6. L.D. Smith; *O&GJ* March 24:83 (1986).
7. S.C. Stinson; *C&EN* Feb. 17:27 (1986).
8. R.A. Corbett; *O&GJ* **83**(46):127 (1985).
9. J.-F. LePage, J. Cosyns, P. Courty *et al.*; *Applied Heterogeneous Catalysis: Design, Manufacture, Use of Solid Catalysts*, Editions Technip, Paris Chapter 1 (1987).
10. R. Pearce and W.R. Patterson; *Catalysis and Chemical Processes*, Wiley-Interscience Publication, JW&S Inc., NY USA Chapter 1 (1981).
11. S.J. Thomson and G. Webb; *Heterogeneous Catalysis*, University Chemical Texts, Oliver & Boyd Publishers, Edinburgh Chapter 1 (1968).
12. J.M. Basset, J.P. Candy, A. Choplin, P. Dufour, P. Louessard and C. Santini; *Heterogeneous Catalysis and Fine Chemicals*, M. Guisnet *et al.* editors, Elsevier Surface Science Series, Elsevier Science Publishers B.V., Amsterdam **V41**:1 (1988).
13. M.G. White; *Heterogeneous Catalysis*, N.R. Amundson series editor, Prentice-Hall International Series in the Physical and Chemical Engineering Sciences, Prentice-Hall Inc., NJ USA Chapter 1 (1990).
14. M.L. Occelli; *Fluid Catalytic Cracking: Role in Modern Refining*, M.L. Occelli editor, ACS Symposium Series, ACS Publishers, USA **V375**:1 (1988).
15. M.E. Davis; *Ind. Eng. Chem. Res.* **30**:1675 (1991).
16. *European Chemical News*, June 16 **46**(1230):21 (1986).
17. A. Corma; *Zeolites: Facts, Figures, Future*, P.A. Jacobs and R.A. van Santen editors, Elsevier Surface Science Series, Elsevier Science Publishers B.V., Amsterdam **V49A**:49 (1989).
18. J.M. Newsam; *Science* **231**(4742):1093 (1986).

19. D.E.W. Vaughan; *The Properties and Applications of Zeolites*, L.V. Rees editor, Proc. 5th Int'l. Zeol. Conf., Heyden Publishers, London April 18-20:294 (1979).
20. T.L. Barr; *Zeolites* 10(11):760 (1990).
21. C. Naccache, Chen Fang Ren and G. Coudurier; *Zeolites: Facts, Figures, Future*, P.A. Jacobs and R.A. van Santen editors, Elsevier Surface Science Series, Elsevier Science Publishers B.V., Amsterdam V49A:661 (1989).
22. C.D. Chang and A.T. Bell; *Catal. Lett.* 8:305 (1991).
23. H. Pfeifer, D. Freude and M. Hunger; *Zeolites* 5(9):274 (1985).
24. J.C. Védrine, A. Auroux and G. Coudurier; *Catalytic Materials: Relationships Between Structure and Reactivity*, T.E. Whyte Jr, R.A. Dalla Betta, E.G. Derouane and R.T.K. Baker editors, ACS Symposium Series, ACS Publishers, USA V248:253 (1984).
25. C. Marcilly; *Pétrole et Techniques* 328:12 (1986).
26. D.W. Breck; *Zeolites Molecular Sieves: Structure, Chemistry and Use*, Wiley-Interscience Publication, JW&S Inc., NY USA Chapter 8 (1974).
27. J. Fripiat, J. Chaussidon and A. Jelli; *Chimie-Physique des Phénomènes de Surface: Applications aux Oxydes et aux Silicates*, Mason & Cie Publishers, Paris (1971).
28. A.G. Pelmenchikov, E.A. Paukshtis *et al.*; Proc. 9th Int'l. Cong. Catal., M.J. Phillips and M. Ternan editors, Calgary Canada, August V1:404 (1988).
29. K.G. Ione, V.G. Stepanov, G.V. Echevskii, A.A. Shubin and E.S. Paukshtis; *Zeolites* 4(4):114 (1984).
30. Z. Gabelica, E.G. Derouane and N. Blom; *Catalytic Materials: Relationships Between Structure and Reactivity*, T.E. Whyte Jr, R.A. Dalla Betta, E.G. Derouane and R.T.K. Baker editors, ACS Symposium Series, ACS Publishers, USA V248:219 (1984).
31. K.F.M.G.J. Scholla, W.S. Veeman, P. Frenken and G.P.M. van der Velden; *Appl. Catal.* 17:233 (1985).
32. D. Barthomeuf; *Molecular Sieves- II*, J.R. Katzer editor, ACS Symposium Series, ACS Publishers, USA V40:453 (1977).
33. V.R. Choudhary and V.S. Nayak; *Zeolites* 5(1):15 (1985).
34. V.R. Choudhary and D.B. Akolekar; *J. Catal.* 119:525 (1989).
35. J.W. Ward; *J. Catal.* 9:225 (1967).

36. B.C. Gates, J.R. Katzer and G.C.A. Schuit; *Chemistry of Catalytic Processes*, McGraw Hill Book Co. Publishers Chapter 1 (1979).
37. G.L. Woolery, L.B. Alemany, R.M. Dessau and A.W. Chester; *Zeolites* 6(1):14 (1986).
38. W.J. Mortier; Proc. 6th Int'l. Zeol. Conf., B. Olson and A. Bisio editors, Butterworths & Co. Publishers Ltd., Reno, USA July 10-15 (1983):734 (1984).
39. C. Clément; *Pétrole et Techniques* 328:32 (1986).
40. C. Mirodatos and D. Barthomeuf; *J. Catal.* 93:246 (1985).
41. C. Mirodatos and D. Barthomeuf; *J. Catal.* 114:121 (1988).
42. Z.-a. Zheng, J.-j. Cai and D.-c. Liu; Proc. 9th Int'l. Cong. Catal., M.J. Phillips and M. Ternan editors, Calgary Canada, August V1:476 (1988).
43. J.-H. Kim, S. Namba and T. Yashima; *Zeolites* 11(1):59 (1991).
44. Cv. Bezouhanova, Chr. Dimitrov, V. Nenova, S. Spassov and H. Lechert; *Appl. Catal.* 21:149 (1986).
45. W.W. Kaeding, L.B. Young and C.-C. Chu; *J. Catal.* 89:267 (1984).
46. Cv. Bezouhanova, Chr. Dimitrov, V. Nenova and H. Lechert; *Appl. Catal.* 49:101 (1989).
47. D. Fraenkel and M. Levy; *J. Catal.* 118:10 (1989).
48. D.H. Olson and W.O. Haag; *Catalytic Materials: Relationships Between Structure and Reactivity*, T.E. Whyte Jr, R.A. Dalla Betta, E.G. Derouane and R.T.K. Baker editors, ACS Symposium Series, ACS Publishers, USA V248:275 (1984).
49. J.A. Martens, J. Perez-Pariente, E. Sastre, A. Corma and P.A. Jacobs; *Appl. Catal.* 45:85 (1988).
50. W.O. Haag; Proc. 6th Int'l. Zeol. Conf., B. Olson and A. Bisio editors, Butterworths & Co. Publishers Ltd., Reno, USA July 10-15 (1983):466 (1984).
51. V. Ducarme and J. Védrine; *Appl. Catal.* 17:175 (1985).
52. J.G. Bendoraitis, A.W. Chester, F.G. Dwyer and W.E. Garwood; *New Developments in Zeolite Science and Technology*, Proc. 7th Int'l. Zeol. Conf., Y. Murakami, A. Lijima and J.W. Ward editors, Elsevier Surface Science Series, Kodansha Ltd. Publishers, Tokyo August 17-22 V28:669 (1986).
53. N.Y. Chen; *J. Catal.* 114:17 (1988).
54. J.C. Védrine, A. Auroux, G. Coudurier, P. Engelhard, J.P. Gallez and G.S. Szabo; Proc. 6th Int'l. Zeol. Conf., B. Olson and A. Bisio editors, Butterworths & Co. Publishers Ltd., Reno, USA July 10-15 (1983):497 (1984).

55. L.B. Young, S.A. Butter and W.W. Kaeding; J. Catal. 76:418 (1982).
56. A. Mol; Hydrocarbon Proc., Int'l. Edition 59(4):233 (1980).
57. A. Mol; Chem. Econ. & Eng. Rev. March 12(3):29 (1980).
58. J. James and R. Boulitrop; Chimie et Industrie- Génie Chimique 104(1):39 (1971).
59. M.Y. Barthel, M.A. Chauvel and M.D. Decroocq; Chimie et Industrie- Génie Chimique 104(9):1087 (1971).
60. S.B. Zdonik and E.C. Meilun; CEP 79(9):56 (1983).
61. F. Billaud, H. Ajot and E. Freund; Revue de l'Institut Français du Pétrole 38(6):763 (1983).
62. F.-D. Kopinke, G. Zimmermann and B. Ondruschka; Ind. Eng. Chem. Res. 26:2393 (1987).
63. D. Depeyre, C. Flicoteaux, F. Arbabzadeh and A. Zabaniotou; Ind. Eng. Chem. Res. 28:967 (1989).
64. F. Billaud, P. Chaverot, M. Berthelin and E. Freund; Ind. Eng. Chem. Res. 27:1529 (1988).
65. A.S. Brown; Chem. Business February:11 (1985).
66. M. Picciotti; Hydrocarbon Proc. Int'l. Edition 59(4):223 (1980).
67. P.M. Plehiers and G.F. Froment; Ind. Eng. Chem. Res. 26:2204 (1987).
68. S. DeHaan; O&GJ 81(39):72 (1983).
69. J.H. Koltz and G.A. Delzer; Science May 9 232:744 (1986).
70. A.A. Lemonidou and I.A. Vasalos; Appl. Catal. 54:119 (1989).
71. R. Le Van Mao; US Patent 4,732,881 (Mar.22 1988).
72. R. Le Van Mao and L. Dufresne; Appl. Catal. 51(1):1 (1989).
73. R. Le Van Mao and L. Dufresne; US Patent 4,975,402 (Dec.4 1990).
74. V.E. Pierce and B.B. Bansal; CEP March:27 (1986).
75. P. Chu and G.H. Kùlh; Ind. Eng. Chem. Res. 26:365 (1987).
76. M. Valais and P. Bonnifay; CEP March:34 (1986).
77. P. Leprince, A. Chauvel, J.-P. Catry and L. Castex; *Procédés de Pétrochimie*, Editions Technip, Paris (1971).
78. C.D. Chang; *Hydrocarbons from Methanol*, Marcel Dekker Publisher, NY USA (1983).
79. W.E. Garwood and W. Lee; US Patent 4,227,992 (Oct.14 1980).
80. N.Y. Chen and T.Y. Yan; Ind. Eng. Chem. Process Des. Dev. 25:151 (1986).
81. N.Y. Chen; Chemical Week 138(10):36 (1986).

82. S.A. Tabak, B.S. Wright and H. Owens; US Patent 4,504,693 (Mar.12 1985).
83. N.Y. Chen, W.E. Garwood and R.H. Heck; Ind. Eng. Chem Res. 26:706 (1987).
84. W.O. Haag and R.M. Dessau; Proc. 8th Int'l. Cong. Catal. Berlin 2:305 (1984).
85. S.C. Che, R.G. Minet, F.W. Tsai, P. Cronin and G.F. Froment; CEP May:45 (1985).
86. J.A. Johnson, J.A. Weizman, G.K. Hiller and A.H.P. Hall; Paper presented at NPRA Annual Meeting, San Antonio TX USA March (1984).
87. A. Mol; O&GJ Report 81(13):78 (1983).
88. N.S. Gnep, J.Y. Doyemet, A.M. Seco, R. Ramoa Ribeiro and M. Guisnet; Appl. Catal. 43:155 (1988).
89. F.M. Brinkmeyer, D.F. Rohr, M.E. Olbrich and L.E. Drehman; O&GJ 81(3):75 (1983).
90. M.E. Olbrich and J.H. Koltz; AIChE Spring Nat'l. Meeting, New Orleans USA, April 6-10 Prepr #30f (1986).
91. A. El Tanany, G.M. Pajonk, K.H. Steinberg and S.J. Teichner; Appl. Catal. 39:89 (1988).
92. C.D. Chang and W.H. Lang; US Patent 3,894,104 (July 8 1975).
93. R. Le Van Mao, P. Levesque, B. Sjiariel and N.T. Do; Can. J. Chem. Eng. 64:462 (1986).
94. P. Chu; US Patent 4,120,910 (Oct.17 1978).
95. A.W. Chester and Y.F. Chu; US Patent 4,350,835 (Sept.21 1982).
96. T. Inui, Y. Makino, F Okazumi, S. Nagano and Y. Miyamoto; Ind. Eng. Chem. Res. 26:647 (1987).
97. T. Inui, Y. Makino, F Okazumi and Y. Miyamoto; J.C.S. Chem. Comm. No7:571 (1986).
98. N.S. Gnep, J.Y. Doyemet, A.M. Seco, R. Ramoa Ribeiro and M. Guisnet; Appl. Catal. 35:93 (1987).
99. K. Tanabe, K. Shimazu, H. Hattori and K. Shimadzu; J. Catal. 57:35 (1979).
100. (a) R.L. Argauer and G.R. Landolt; US Patent 3,702,886 (Nov.14 1972).
(b) R. von Ballmoos and J.B. Higgins; *Zeolites- Collection of Simulated XRD Powder Patterns for Zeolites* 10(5):942S (1990).
101. C.R. Bayense and J.H.C. van Hooff; Appl. Catal. General:A 79:127 (1991).

102. (a) R. Le Van Mao, P. Levesque, B. Sjiariel and P.H. Bird; *Can. J. Chem.* **63**:3464 (1985).
(b) R. Le Van Mao, T.M. Nguyen and J. Yao; *Appl. Catal.* **61**:161 (1990).
103. N.-Y. Topsøe, K. Pedersen and E.G. Derouane; *J. Catal.* **70**:41 (1981).
104. L. Petit, J.P. Bournonville and F. Raatz; *Zeolites: Facts, Figures, Future*, P.A. Jacobs and R.A. van Santen editors, Elsevier Surface Science Series, Elsevier Science Publishers B.V., Amsterdam **V49B**:1163 (1989).
105. J. Kanai and N. Kawata; *Appl. Catal.* **55**:115 (1989).
106. G.P. Handreck and T.D. Smith; *J.C.S. Farad. Trans. 1* **85**(10):3215 (1989).
107. T. Inui, I. Ishihara, K. Kamachi and H. Matsuda; *Zeolites: Facts, Figures, Future*, P.A. Jacobs and R.A. van Santen editors, Elsevier Surface Science Series, Elsevier Science Publishers B.V., Amsterdam **V49B**:1183 (1989).
108. T. Inui, K. Kamachi, Y. Ishibara, Y. Makino and H. Matsuda; *Proc. 2nd Int'l. Conf. Spillover*, K.-H. Steinberg editor, Leipzig June 12-16:167 (1989).
109. V.B. Kazansky, L.M. Kustov and A.Yu Khodakov; *Zeolites: Facts, Figures, Future*, P.A. Jacobs and R.A. van Santen editors, Elsevier Surface Science Series, Elsevier Science Publishers B.V., Amsterdam **V49B**:1173 (1989).
110. Y. Ono, H. Nakatani, H. Kitagawa and E. Suzuki; *Successful Design of Catalysts*, T. Inui editor, Elsevier Surface Science Series, Elsevier Science Publishers B.V., Amsterdam p279 (1989).
111. T. Mole, J.R. Anderson and C. Creer; *Appl. Catal.* **17**:141 (1985).
112. V.I. Yakerson, T.V. Vasina, L.I. Lafer, V.P. Sytnyk, G.L. Dykh, A.V. Mokhov, O.V. Bragin and Kh.M. Minachev; *Catal. Lett.* **3**:339 (1989).
113. J. Kanai and N. Kawata; *J. Catal.* **114**:284 (1988).
114. (a) R. Le Van Mao, J. Yao and B. Sjiariel; *Catal. Lett.* **6**(1):23 (1990).
(b) R. Le Van Mao and J. Yao; *Appl. Catal.* submitted for publication (1992).
115. L. Dufresne, J. Yao and R. Le Van Mao; Paper presented at the 199th ACS Spring Nat'l. Meet., Boston Mass. USA April 22-27 (1990)- L.F. Albright, B.L. Crynes and S. Nowak editors, *Chemical Industries Series* **V46**:509 (1991).
116. R. Spinicci and A. Tofanari; *Appl. Catal.* **44**:179 (1988).
117. R.J. Kokes and A.L. Dent; *Adv. Catal.* **22**:1 (1972).
118. R. Uma, R. Venkatachalam and J.C. Kuriacose; *Proc. 5th Int'l. Cong. Catal.*(1972) **V1**:245 (1973).
119. R.J. Kokes; *Proc. 5th Int'l. Cong. Catal.*(1972) **V1**:1 (1973).

120. R.D. Williams and S.K. Sikdar; *J. Catal.* **38**:147 (1975).
121. P. Dejaifve, J.C. Védrine, V. Bolis, J.H.C. van Hooff and E.G. Derouane; Paper presented at the ACS-JSC Meeting, Honolulu April 1-6:286 (1979).
122. P.B. Venuto; *Catalysis in Organic Syntheses*, Academic Press Inc. Publishers, NY USA p67 (1977).
123. M.L. Poutsma; *Zeolite Chemistry and Catalysis*, J. Rabo editor, ACS Symposium Series, ACS Publishers, USA **V171**:437 (1976).
124. R.J. Kokes, A.L. Dent, C.C. Chang and L.T. Dixon; *J.A.C.S.* **94**(13):4429 (1972).
125. J.J.F. Scholten and A. van Monfoort; *Proc. 5th Int'l. Cong. Catal.*(1972) **V1**:385 (1973).
126. R. Le Van Mao, L. Dufresne and J. Yao; *Appl. Catal.* **65**:143 (1990).
127. J. Yao, R. Le Van Mao and L. Dufresne; *Appl. Catal.* **65**:175 (1990).
128. R. Le Van Mao, J. Yao and L. Dufresne; paper presented at the Eastern Canada Symposium in Catalysis, Toronto Canada June 11 (1991).
129. R. Le Van Mao, J. Yao and L. Dufresne; paper presented at the 4th Chemical Congress of North America, ACS Symposium-Petroleum Chemistry Division, New York NY August 25-30 (1991) (idem 232).
130. (a) K. Fujimoto, I. Nakamura and K. Yokota; *Proc. 2nd Int'l. Conf. Spillover*, K.-H. Steinberg editor, Leipzig June 12-16:176 (1989).
(b) J. Haggins; *C&EN* (Jan. 15 1990):30-31 reporting a paper presented by K. Fujimoto *et al.* at PACIFICHEM (Dec. 1989).
131. K. Fujimoto, I. Nakamura, K. Yokota and K. Aimoto; *Bull. Chem. Soc. Jp.* **64**:2275 (1991).
132. J. Yao and R. Le Van Mao; *Catal. Lett.* **11**:191 (1991).
133. R. Le Van Mao; personal communication.
134. R.P. Bell; *The Tunnel Effect in Chemistry*, Chapman and Hall Publishers, London Chapter 5 (1980).
135. V.M. Belousov, L.V. Lyashenko, I.V. Bacherikova and E.V. Rozhkova; *Proc. 2nd Int'l. Conf. Spillover*, K.-H. Steinberg editor, Leipzig June 12-16:144 (1989).
136. N.Y. Chen and W.O. Haag; *Hydrogen Effects in Catalysis: Fundamentals and Practical Applications*, Z. Paál and P.G. Menon editors, Marcel Dekker Inc Publisher, New York NY:695 (1988).
137. W.C. Conner Jr., G.M. Pajonk and S.J. Teichner; *Adv. Catal.* **34**:1 (1986).

138. G.M. Pajonk; Proc. 2nd Int'l. Conf. Spillover, K.-H. Steinberg editor, Leipzig June 12-16:1 (1989).
139. M. Lacroix, G.M. Pajonk and S.J. Teichner; Bull. Soc. Chim. Fr. N° 2-3:l-87 (1981).
140. M. Lacroix, G.M. Pajonk and S.J. Teichner; Bull. Soc. Chim. Fr. N° 2-3:l-94 (1981).
141. M. Lacroix, G.M. Pajonk and S.J. Teichner; Bull. Soc. Chim. Fr. N° 7-8:l-258 (1981).
142. M. Lacroix, G.M. Pajonk and S.J. Teichner; Bull. Soc. Chim. Fr. N° 7-8:l-265 (1981).
143. D.H. Lenz and W.C. Conner Jr.; J. Catal. 104:288 (1987).
144. M. Lacroix, G.M. Pajonk and S.J. Teichner; Bull. Soc. Chim. Fr. N° 2-3:l-101 (1981).
145. B. Sen, J.L. Falconer, T.-F. Mao, M. Yu and R.L. Flesner; J. Catal. 126:465 (1990).
146. B. Sen and J.L. Falconer; J. Catal. 117:404 (1989).
147. D. Bianchi, G.E.E. Gardes, G.M. Pajonk and S.J. Teichner; J. Catal. 38:135 (1975).
148. D. Maret, G.M. Pajonk and S.J. Teichner; *Catalysis on the Energy Scene*, S. Kaliagine and A. Mahay editors, Elsevier Surface Science Series, Elsevier Science Publishers B.V., Amsterdam V19:347 (1984).
149. D.H. Lenz, W.C. Conner Jr., J.P. Fraissard; J. Catal. 117:281 (1989).
150. F.F.C. Candau and W.C. Conner Jr.; Proc. 2nd Int'l. Conf. Spillover, K.-H. Steinberg editor, Leipzig June 12-16:18 (1989).
151. S.J. Teichner; Appl. Catal. 62:1 (1990).
152. P.B. Weisz; Adv. Catal. XIII:137 (1962).
153. C.C. Bond; *Metal-Support and Metal Additive Effects in Catalysis*, B. Imelik *et al.* editors, Elsevier Surface Science Series, Elsevier Science Publishers B.V., Amsterdam V11:1 (1982).
154. P. Putanov, E. Kiš, G. Lomić and G. Bošković; Proc. 9th Int'l. Cong. Catal., M.J. Phillips and M. Ternan editors, Calgary Canada, August V3:1347 (1988).
155. W. Hongli, T. Sheng, X. Maosong, X. Guoxing and G. Xiexian; *Metal-Support and Metal Additive Effects in Catalysis*, B. Imelik *et al.* editors, Elsevier Surface Science Series, Elsevier Science Publishers B.V., Amsterdam V11:19 (1982).

156. R.B. Borade, S.G. Hegde, S.B. Kulkarni and P. Ratnasamy; *Appl. Catal.* **13**:27 (1984).
157. C.P. Bezouhanova, Chr. Dimitrov, V. Nenova, L. Dimitrov and H. Lechert; *Appl. Catal.* **19**:101 (1985).
158. J. Abbot and B.W. Wojciechowski; *Proc. 9th Int'l. Cong. Catal.*, M.J. Phillips and M. Ternan editors, Calgary Canada, August **V1**:206 (1988).
159. J. Abbot and J.D. Head; *J. Catal.* **125**:187 (1990).
160. T. Yamaguchi; *Appl. Catal.* **61**:1 (1990).
161. E. Baumgarten, C. Lentjes-Wagner and R. Wagner; *J. Catal.* **117**:533 (1989).
162. V.B. Kazansky, V. Yu. Borovkov and A.V. Zaitsev; *Proc. 9th Int'l. Cong. Catal.*, M.J. Phillips and M. Ternan editors, Calgary Canada, August **V3**:1426 (1988).
163. R. Kramer and M. Andre; *J. Catal.* **58**:287 (1979).
164. S.J. Teichner; *J. Catal.* **115**:591 (1989).
165. G. Parravano and M. Boudart; *Adv. Catal.* **VII**:47 (1955).
166. P. Mériaudeau and C. Naccache; *Appl. Catal.* **73**:L13 (1991).
167. G. Centi and G. Golinelli; *J. Catal.* **115**:452 (1989).
168. L.W. Zatorski, G. Centi *et al.*; *Zeolites: Facts, Figures, Future*, P.A. Jacobs and R.A. van Santen editors, Elsevier Surface Science Series, Elsevier Science Publishers B.V., Amsterdam **V49B**:1243 (1989).
169. K. Fujimoto, I. Nakamura and K. Yokota; *Zeolites* **9**:120 (1989).
170. Q.-N. Dong, J.R. Anderson, T. Mole *et al.*; *Appl. Catal.* **72**:99 (1991).
171. P.G. Ashmore; *Catalysis and Inhibition of Chemical Reactions*, Butterworths Publisher, London chapter 6 (1963).
172. P. Mark; *Catal. Rev.* **1**:165 (1968).
173. K. Hauße; *Adv. Catal.* **VII**:213 (1955).
174. M. McD. Baker and G.I. Jenkins; *Adv. Catal.* **VII**:1 (1955).
175. R.V. Culver and F.C. Tompkins; *Adv. Catal.* **XI**:67 (1959).
176. J.H. de Boer; *Adv. Catal.* **VIII**:17 (1956).
177. Th. Wolkenstein; *Adv. Catal.* **XII**:189 (1960).
178. F. Solymosi; *Catal. Rev.* **1**:233 (1968).
179. P.H. Nelson, A.B. Kaiser and D.M. Bibby; *J. Catal.* **127**:101 (1991).
180. M.G. Palekar and R.A. Rajadhyaksha; *Catl. Rev.- Sci. Eng.* **28(4)**:371 (1986).

181. N.V. Choudhary, R.V. Jasra, S.G.T. Bhat and T.S.R. Prasada Rao; *Zeolites: Facts, Figures, Future*, P.A. Jacobs and R.A. van Santen editors, Elsevier Surface Science Series, Elsevier Science Publishers B.V., Amsterdam V49B:867 (1989).
182. J. Caro, M. Bülow, W. Schirmer, J. Kärger *et al.*; J.C.S., Faraday Trans. 1 81:2541 (1985).
183. J. Kärger and J. Caro; J.C.S., Faraday Trans. 1 73:1363 (1977).
184. J. Kärger, W. Heink, H. Pfeifer, M. Rauscher and J. Hoffmann; *Zeolites* 2:275 (1982).
185. J. Kärger and H. Pfeifer; *Zeolites* 7:90 (1987).
186. J. Kärger; *AIChE J.* 28(3):417 (1982).
187. J. Kärger, H. Pfeifer *et al.*; *AIChE J.* 34(7):1185 (1988).
188. J. Kärger, H. Pfeifer, F. Stallmach and H. Spindler; *Zeolites* 10:288 (1990).
189. M. Kočířík, P. Struve, K. Fiedler and M. Bülow; J.C.S., Faraday Trans. 1 84(9):3001 (1988).
190. M. Kočířík, A. Zikánová, P. Struve and M. Bülow; *Zeolites: Facts, Figures, Future*, P.A. Jacobs and R.A. van Santen editors, Elsevier Surface Science Series, Elsevier Science Publishers B.V., Amsterdam V49B:925 (1989).
191. Y. Egashira and H. Komiyama; *Ind. Eng. Chem. Res.* 29:1583 (1990).
192. A.P. Dhupe and A.N. Gokarn; *Ind. Eng. Chem. Res.* 29:784 (1990).
193. E.G. Derouane, J.-M. Andre and A.A. Lucas; *J. Catal.* 110:58 (1988).
194. S.R. Morrison; *Adv. Catal.* VII:259 (1955).
195. J.T. Richardson; *Principles of Catalyst Development*, M.V. Twigg and M.S. Spencer editors, Fundamental and Applied Catalysis Series, Plenum Press, New York and London chapter 3 (1989).
196. K. Klier; *Characterization and Catalyst Development: An Interactive Approach*, S.A. Bradley, M.J. Gattuso and R.J. Bertolacini editors, ACS Monograph Series, ACS Washington DC V411:12 (1989).
197. G.J.K. Acres, A.J. Bird, J.W. Jenkins and F. King; *Characterization of Catalysts*, J.M. Thomas and R.M. Lambert editors, JW&S Ltd. Publishers, Wiley-Interscience Publication, Great Britain p55 (1980).
198. V. Haensel and H.S. Haensel; *Characterization and Catalyst Development: An Interactive Approach*, S.A. Bradley, M.J. Gattuso and R.J. Bertolacini editors, ACS Monograph Series, ACS Washington DC V411:2 (1989).

199. S.D. Griffith; *Characterization and Catalyst Development: An Interactive Approach*, S.A. Bradley, M.J. Gattuso and R.J. Bertolacini editors, ACS Monograph Series, ACS Washington DC V411:17 (1989).
200. G.K. Boreskov; *Preparation of Catalysts III*, B. Delmon, P.A. Jacobs and G. Poncelet editors, Elsevier Science Publishers B.V., Amsterdam p223 (1976).
201. K. Tanabe, M. Itoh, K. Morishige and H. Hattori; *Preparation of Catalysts III*, B. Delmon, P.A. Jacobs and G. Poncelet editors, Elsevier Science Publishers B.V., Amsterdam p65 (1976).
202. Y.Huang, A. White, A. Walpole and D.L. Trimm; *Appl. Catal.* 56:177 (1989).
203. P.T. Cardew, R.J. Davey, P. Elliott, A.W. Nienow and J.M. Winterbottom; *Preparation of Catalysts IV*, B. Delmon, P.A. Jacobs and G. Poncelet editors, Elsevier Science Publishers B.V., Amsterdam V31:15 (1987).
204. H.G.J. Lansink Rotgerink, J.G. Van Ommen and J.R.H. Ross; *Preparation of Catalysts IV*, B. Delmon, P.A. Jacobs and G. Poncelet editors, Elsevier Science Publishers B.V., Amsterdam V31:795 (1987).
205. F. Mizukami, S. Niwa, M. Toba, T.Tsuchiya, K. Shimizu, S. Imai and J. Imamura; *Preparation of Catalysts IV*, B. Delmon, P.A. Jacobs and G. Poncelet editors, Elsevier Science Publishers B.V., Amsterdam V31:45 (1987).
206. J.N. Armor; *Appl. Catal.* 78:141 (1991).
207. A.J. Lecloux; *Catalysis: Science and Technology*, J.R. Anderson and M. Boudart editors, Springer Verlag Berlin GDR, Heidelberg Publishers V2:171 (1981).
208. K.S.W. Sing; *Characterization of Catalysts*, J.M. Thomas and R.M. Lambert editors, JW&S Ltd. Publishers, Wiley-Interscience Publication, Great Britain p12 (1980).
209. A.W. Adamson; *Physical Chemistry of Surfaces*, 4th edition, JW&S Ltd. Publishers, Wiley-Interscience Publication, USA chapt16 (1982).
210. T. Yamaguchi; *Appl. Catal.* 61:1 (1990).
211. H.H. Willard and N.K. Tang; *J.A.C.S.* 59:1190 (1937).
212. H.H. Willard and H.C. Fogg; *J.A.C.S.* 59:1197 (1937).
213. R. Narayan, A. Tabatabaie-Raissi and M.J. Antal Jr.; *Ind. Eng. Chem. Res.* 27:1050 (1988).
214. R. Srinivasan, D. Taulbee and B.H. Davis; *Catal. Lett.* 9:1 (1991).
215. B.R. Strohmeier and D.M. Hercules; *J. Catal.* 86:266 (1984).
216. I. Chen and D.-W. Shiue; *Ind. Eng. Chem. Res.* 27:429 (1988).

217. A.G. Sharpe; *Inorganic Chemistry*, Longman Group Limited Publishers, London (1981).
218. M.E. Brown; *Introduction to Thermal Analysis: Techniques and Applications*, Chapman and Hall Publishers, London (1988).
219. W.W.M. Wendlandt; *Thermal Methods of Analysis*, 2nd edition, JW&S, Chemical Analysis Series V19 (1974).
220. I. Chen, S.-Y. Lin and D.-W. Shiue; *Ind. Eng. Chem. Res.* 27:926 (1988).
221. Y. Nagase, T. Jin, H. Hattori, T. Yamaguchi and K. Tanabe; *Bull. Chem. Soc. Jpn.* 58:916 (1985).
222. H. Wise and J. Oudar; *Material Concepts in Surface Reactivity and Catalysis*, Academic Press Inc., Harcourt Brace Jovanovich Publishers, San Diego (1990).
223. H.H. Kung; *Transition Metal Oxides: Surface Chemistry and Catalysis*, B. Delmon and J.T. Yates editors, Studies in Surface Science And Catalysis Series, Elsevier Science Publishers B.V., Netherlands V45 (1989).
224. V.F. Kiselev and O.V. Krylov; *Adsorption and Catalysis on Transition Metals and their Oxides*, G. Ertl and R. Gomer editors, Springer Series in Surface Sciences, Springer-Verlag Berlin Heidelberg New York V9 (1989).
225. D. Seddon; *Catal. Today* 6:351 (1990).
226. W. Reschetilowski, U. Mroczek, K.-H. Steinberg and K.-P. Wendlandt; *Appl. Catal.* 78:257 (1991).
227. C.R. Bayense, A.J.H.P. van der Pol and J.H.C. van Hooff; *Appl. Catal.* 72:81 (1991).
228. C.R. Bayense, H.A.M. Damen and J.H.C. van Hooff; *Prepr. Petr. Chem. Div.* 36(4):651 (1991).
229. T. Dypvik, A. Holmen and Y. Ben Taarit; *Prepr. Petr. Chem. Div.* 36(4):627 (1991).
230. J. Kanai and N. Kawata; *Appl. Catal.* 62:141 (1990).
231. D. Sun and Z. Zhao; *Ind. Eng. Chem. Res.* 30:2013 (1991).
232. R. Le Van Mao, L. Dufresne, J. Yao and D. Ly; *Prepr. Petr. Chem. Div.* 36(4):716 (1991).
233. R. Le Van Mao and J. Yao, *Appl. Catal. General:A* 79:77 (1991).
234. V. Kanazirev, G.L. Price and K.M. Dooley; *J.C.S., Chem. Commun.* p712 (1990).
235. V. Kanazirev, V. Mavrodinova and L. Kosova; *Catal. Lett.* 9:35 (1991).
236. G.L. Price, V. Kanazirev; *J. Catal.* 126:267 (1990).
237. P. Mériaudeau and C. Naccache; *J. Mol. Catal.* 59:L31 (1990).

238. (a) G. Buckles, G.J. Hutchings and C.D. Williams; *Catal. Lett.* **8**:115 (1991).
(b) G. Buckles, G.J. Hutchings and C.D. Williams; *Catal. Lett.* **11**:89 (1991).
239. P.Yarlagadda, C.R.F. Lund and E. Ruckenstein; *Appl. Catal.* **62**:125 (1990).
240. P.Yarlagadda, C.R.F. Lund and E. Ruckenstein; *Appl. Catal.* **54**:139 (1989).
241. Y. He, W.L. Jang and R.B. Timmons; *Energy & Fuels* **5**:613 (1991).
242. J.K. Nørskov, P. Stoltze and U. Nielsen; *Catal. Lett.* **9**:173 (1991).
243. S.F. Garcia and P.B. Weisz; *J. Catal.* **121**:294 (1990).
244. F.J. Shiring, R. Venkatadri and J.G. Goodwin, Jr.; *Can. J. Chem. Eng.* **61**(2):218 (1983).
245. M.T. Klein; Course notes University of Delaware (1989).
246. M. Boudart and K. Tamaru; *Catal. Lett.* **9**:15 (1991).
247. K. Tamaru; *Future Opportunities in Catalysis and Separation Technology*, Studies in Surface Science And Catalysis Series, Elsevier Science Publishers B.V., Netherlands **V54**:32 (1990).
248. K.J. Laidler; *Theories of Chemical Reaction Rates*, McGraw-Hill Book Company Publishers, McGraw-Hill Series in Advances Chemistry (1969).
249. M. Boudart; *Kinetics of Chemical Processes*, N.R. Amundson editor, Prentice-Hall International Series in the Physical and Chemical Engineering Sciences, Prentice-Hall of Canada Ltd. (1968).
250. S.J. Kulkarni, S.B. Kulkarni, P. Ratnasamy, H. Hattori and K. Tanabe; *Appl. Catal.* **8**:43 (1983).
251. G.-M Schwab; *Catalysis: Science and Technology*, J.R. Anderson and M. Boudart editors, Springer Verlag Berlin GDR, Heidelberg Publishers **V2**:1 (1981).
252. R.J. Quann, L.A. Green, S.A. Tabak and F.J. Krambeck; *Ind. Eng. Chem. Res.* **27**:565 (1988).
253. H.-J. Doelle, J. Heering, L. Riekert and L. Marosi; *J. Catal.* **71**:27 (1981).
254. W.O. Haag, R.M. Lago and P.B. Weisz; *Disc. Farad. Soc. (London)* **72**:317 (1981).
255. V.R. Choudhary and D.B. Akolekar; *J. Catal.* **116**:130 (1989).
256. G.W. Norval, M.J. Phillips, R.W. Missen and W.R. Smith; *Appl. Catal.* **54**:37 (1989).
257. D.B. Luk'yanov and V.I. Shtral; *Prep. Pet. Chem. Div.* **36**(4):693 (1991).
258. H. Kitagawa, Y. Sendoda and Y. Ono; *J. Catal.* **101**:12 (1986).
259. Y. Ono and K. Kanae; *J.C.S. Farad. Trans.* **87**(4):663 (1991).

260. Y. Ono and K. Kanae; J.C.S. Farad. Trans. 87(4):669 (1991).
261. G. Sirokman, Y Sendoda and Y. Ono; Zeolites 6:299 (1986).
262. M.R. Guisnet, D. Aittaleb, J.Y. Doyemet and N.S. Gnep; Prep. Pet. Chem. Div. 36(4):668 (1991).
263. G. Giannetto, J.A. Pérez *et al.*; Prep. Pet. Chem. Div. 36(4):659 (1991).
264. E.S. Shpiro, O.P. Tkachenko and Kh.M. Minachev; Prep. Pet. Chem. Div. 36(4):746 (1991).
265. N.R. Bursian, S.B. Kogan *et al.*; Prep. Pet. Chem. Div. 36(4):738 (1991).
266. P.A. Arroyo, E.F. Sousa-Aguiar and J.L.F. Monteiro; Prep. Pet. Chem. Div. 36(4):685 (1991).
267. M.S. Scurrrell; Appl. Catal. 41:89 (1988).
268. V. Bolis, J. Védrine, J.P. Van de Berg, J.P. Wolthuizen and E.G. Derouane; J.C.S. Farad. Trans. I 76:1606 (1980).
269. L.M. Kustov, V.Y. Borovkov and V.B. Kazansky; *Structure and Reactivity of Modified Zeolites*, P.A. Jacobs *et al.* editors, Elsevier Surface Science Series, Elsevier Science Publishers B.V., Amsterdam V18:241 (1984).
270. L.M. Parker, D.M. Bibby and G.R. Burns; *Zeolites: Facts, Figures, Future*, P.A. Jacobs and R.A. van Santen editors, Elsevier Surface Science Series, Elsevier Science Publishers B.V., Amsterdam V49B:963 (1989).
271. O.V. Bragin *et al.*; Kinetika i Kataliz 26(2):391 (1985).
272. N.W. Cant and W.K. Hall; J. Catal. 25:161 (1972).
273. B.V. Liengme and W.K. Hall; Trans. Farad. Soc. 62:3229 (1966).
274. J.P. Van de Berg, J.P. Wolthuizen, A.D. Clague, G.R. Hays, R. Huis and J.H.C. van Hooff; J. Catal. 80:130 (1983).
275. N.S. Gnep, F. Bouchet and M.R. Guisnet; Prep. Pet. Chem. Div. 36(4):620 (1991).
276. V.B. Kazansky and I.N. Senchenya; J. Catal. 119:108 (1989).
277. I.N. Senchenya and V.B. Kazansky; Catal. Lett. 8:317 (1991).
278. J.P. Van de Berg, J.P. Wolthuizen and J.H.C. van Hooff; J. Catal. 80:139 (1983).
279. T.J. Gricus Kofke and R.J. Gorte; J. Catal. 115:233 (1989).
280. J. Čejka, B. Wichterlová and S. Bednářová; Appl. Catal.A:General 79:215 (1991).
281. J.-k. Chen, A.M. Martin, Y. Gul Kim and V.T. John; Ind. Eng. Chem. Res. 27:401 (1988).
282. S. Bhatia, J. Beltramini and D.D. Do; Catal. Rev.- Sci. Eng. 31(4):431 (1989-90).
283. M. Guisnet and P. Magnoux; Appl. Catal. 54:1 (1989).

284. P. Gallezot, C. Leclercq, M. Guisnet and P. Magnoux; J. Catal. 114:100 (1988).
285. K. Fujimoto, H. Saima and H. Tominaga; *New Developments in Zeolite Science and Technology*, Y. Murakami, A. Lijima and J.W. Ward editors, Elsevier Surface Science Series, Elsevier Science Publishers B.V., Amsterdam V28:875 (1986).